TIRE-PAVEMENT NOISE SIMULATION AND ANALYSIS

YANG JIASHENG

NATIONAL UNIVERSITY OF SINGAPORE

2013

TIRE-PAVEMENT NOISE SIMULATION AND ANALYSIS

YANG JIASHENG

A THESIS SUBMITTED

FOR THE DEGREE OF DOCTOR OF PHILOSOPHY

DEPARTMENT CIVIL AND ENVIRONMENTAL ENGINEERING

NATIONAL UNIVERSITY OF SINGAPORE

2013

DECLARATION

I hereby declare that the thesis is my original work and it has been written by me in its entirety.

I have duly acknowledged all the sources of information which have been used in the thesis.

This thesis has also not been submitted for any degree in any university previously.

YANG JIASHENG

21 January 2013

ACKNOWLEDGEMENTS

Table of Contents

EXECUTIVE SUMMARY

Road agencies nowadays are faced with the challenges of reducing traffic noise in transportation network. Besides engine noise and aerodynamic noise, tire-pavement noise is the other main noise source of traffic noise generated by vehicles at normal driving conditions. The use of innovative pavement technologies is one of the means to control tire-pavement noise generation at the source. Since tire-pavement noise generation is a very complex process combined by many physical mechanisms, to date, most studies on tire-pavement noise are experimental in nature and there are few physical models which are capable of modeling tire-pavement noise. The existing physical models suffer from the problem of either considering too few noise generation/propagation mechanisms or assuming noise radiation to be two-dimensional.

The objective of this research is to propose an analytical simulation model to study tire-pavement noise generation mechanisms and evaluate the factors that affect tire-pavement noise. The simulation model was developed using the three-dimensional finite-element method based on the computer code ADINA. The model is composed of two main components: a dynamic tire-pavement interaction model and a sound propagation model. A rolling-tire Lagrange frame of reference is employed in the three-dimensional tire-pavement interaction model. Tire dynamics is simulated by means of the widely used orthotropic thin shell models. The unknown input parameters in the simplified tire model are determined by a comprehensive identification strategy. The Arbitrary-Lagrange-Euler (ALE) frame of reference is used to describe the three dimensional sound propagation model in the near acoustic field. Large eddy simulation (LES), which has been found to

be a suitable method to research sound propagation problems with air turbulence in the near field, is adopted in the present study.

A parametric analysis is performed in this research to evaluate the impact of surface friction on tire pavement noise generation. The simulated results illustrate that friction coefficient has different effects on tire pavement noise in different frequency bands. It has a significant correlation with noise generation in the high frequency band. However, the correlation was poor in the low frequency band. This means that tire-pavement noise in the low frequency range cannot be directly controlled by changing the tire-pavement friction properties.

An extension of the proposed model is made to study the effect of vehicle cornering on tire-pavement noise. The contact stresses are first simulated and analyzed for different cornering directions. It provides some useful information about tire cornering effect on tire structure dynamics. Tire-pavement noise during cornering of vehicles is then discussed based on simulation results. Compared with the straight driving state, a significant noise increase is found in the cornering state. Finally, the effect of cornering radius on tire-pavement noise is studied. The analysis presented has demonstrated the ability of the proposed simulation model to perform parametric analyses on geometric design that may affect tire-pavement noise.

All illustrated in this research is the application of the simulation model to study the impacts of wheel load, vehicle speed and tire width on tire-pavement noise. The study covered the common range of passenger car wheel loads and vehicle speeds under the normal highway operating conditions. The wheel load range studied varied from 1,000 to

4,000 N, the vehicle speed range was from 30 to 90 km/h, and the tire width ranges from 160 to 210 mm. The computer simulation analysis produced results in good agreement with experimental results measured by past researchers. The analysis presented has demonstrated the ability of the proposed simulation model to perform parametric analyses on factors that may affect tire-pavement noise, and to predict tire-pavement noise likely to be generated under different vehicle operating conditions.

The main contributions of the present approach include: (1) A fully three-dimensional contact model is considered to simulate the interaction between tire and pavement; (2) The mechanical and aerodynamic responses in the tire-pavement interaction problem are simultaneously considered; (3) The model is able to predict the near field tire-pavement noise in close agreement with measured data. Compared with existing models, the proposed model is able to simulate more accurately the tire-pavement noise generation in the high frequency band which mainly is influenced by aerodynamic mechanisms, and study more effectively the tire-pavement interaction effect of tire-pavement noise generation.

LIST OF FIGURES

xvii

xix

LIST OF TABLES

Nomenclature

Symbol	Description	Units
h	Ring thickness	m
R	Ring radius	m
u_r	Ring radial displacement	m
u_θ	Ring tangential displacement	m
E	Young's modulus	N/m^2
k_r	Sidewall radial stiffness	N/m^2
k_θ	Sidewall tangential stiffness	N/m^2
ρ	Ring density	kg/m^3
λ	Damping coefficient	Ns/m
$I = h^3/12$	Area inertia moment per unit width	kg/s
p_0	Air pressure	Pa
f_r	Distributed forces per unit width in the radial direction	N/m
f_θ	Distributed forces per unit width in the radial direction	N/m
A	Constant speed coefficient	NA
B	Constant speed coefficient	NA
L	Sound pressure level	dB(A)
V	vehicle speed	km/h
P_{ref}	reference sound pressure	Pa
P_{rms}	RMS sound pressure	Pa
c	sound speed	m/s
f	frequency of sound	Hz
λ	wavelength	m
$L_A(20^\circ C)$	Corrected sound level	dB(A)
$L_A(T)$	Measured sound level	dB(A)
T	Tested air temperature	Deg
K	Temperature coefficient	NA
p^2_{vibr}	Component that represents the mechanically excited sound source	NA
$p^2_{airflow}$	component which is related to air flow within the tire-pavement contact path	NA
p^2_{cavity}	tire interior cavity resonances	NA
$p^2_{aerodyn}$	residual effects of the air flow noise sources around the car body	NA

a, b, c, d	regression coefficients	NA
$\alpha_1, \alpha_2, \alpha_3, b_1, r_1, \delta_1$	exponents	NA
F_c	tire-pavement contact force	N
Γ	tire pavement contact air flow resistance	Pa s/m
B	tire width	m
S	tire tread stiffness	N/m
$G_{pattern}$	Spectral power of the tread pattern variation	W
u	the fluid velocity of volume	m/s
b	velocity of the control surface	m/s
e	internal energy per unit of mass	N/m^2
T_1	the maximum period of velocity fluctuations	s
T_2	the time scale characteristic of the slow variations in the flow	s
$\bar{p}$	mean stress	N/m^2
v	dynamic viscosity of fluid	Pa·s
Δ	filtered width	m
$\bar{u}_i$	filtered velocity	m/s
τ_{ij}^R	residual stresses	N/m^2
G_{ij}	shear modulus	N/m^2
ν	Poisson's ratio	NA
ε_i	The middle surface strains	NA
x_i	the shell curvatures	Deg
${}^t\boldsymbol{\tau}_i$	stress tensor	NA
$\delta\mathbf{e}_i$	strain	NA
${}^t\mathbf{f}_i^B$	body forces per unit volume	N
${}^t\mathbf{f}_i^S$	surface force per unit area	N
${}^t\mathbf{f}^C$	surface force per unit area	N
u	dynamic frictional coefficient	NA
τ	non-dimensional frictional variable	NA
${}^t\mathbf{R}$	external force vector	N
${}^t\mathbf{F}$	internal nodal force	N
w_i	eigenvalue	NA
$\{\phi\}_i$	modeshape for modal i	NA
ς_i	modal damping ratio	NA
N	the sampling number	NA
Δ	Element size	m
μ	effective viscosity	$m^2 \cdot s^{-1}$

μ_0	laminar viscosity	$m^2 \cdot s^{-1}$
μ_t	eddy viscosity	$m^2 \cdot s^{-1}$
C_{SGS}	the dimensionless model constant	NA
h_{min}	minimum element sizes	m
h_{max}	maximum element sizes	m

CHAPTER 1   INTRODUCTION

1.1   Sound and Noise

1.1.1   Sound

Sound is a travelling wave transmitted through air in the way of air pressure vibration. A sound source oscillates and makes the surrounding air into motion. The compression and tension of the air cause oscillations to be transmitted to listeners' ears. Sound oscillation is physically a pressure deviation from atmospheric pressure, which is called sound pressure. Sound pressure can be measured by microphone. Instantaneous sound pressure is the deviation from the local ambient pressure caused by a sound wave at a given location and instant in time. The effective sound pressure is the root mean square (RMS) of the instantaneous sound pressure over a given interval of time. Scientifically, sound pressure level is used to describe the intensity of sound pressure. It is a logarithmic measure of the effective sound pressure of a sound relative to a reference value, and is measured in decibels (dB) above a standard reference level. The commonly used reference sound pressure in air is 20 μPa RMS, which is usually considered as the threshold of human hearing at 1 kHz. RMS is the abbreviation of root mean square, also known as the quadratic mean, and is a statistical measure of the magnitude of a varying quantity. The RMS for a function $f(t)$ over all time is

$$p_{rms} = \lim_{T \to \infty} \sqrt{\frac{1}{T} \int_{-\frac{T}{2}}^{\frac{T}{2}} [f(t)]^2 \, dt} \qquad (1.1)$$

in which T is a time period and $f(t)$ is a time function.

The sound pressure level L is defined as

$$L = 20\lg(\frac{p_{rms}}{p_{ref}}) = 10\lg(\frac{p_{rms}}{p_{ref}})^2 \qquad\qquad (1.2)$$

where P_{ref} is the reference sound pressure and P_{rms} is the RMS sound pressure being measured. Table 1.1 shows the relationship between sound pressure and sound pressure level.

The advantage of using sound pressure level rather than sound pressure is that it can approximately and comprehensibly illustrate a measure of the perceived loudness. It is noted that the maximum sound pressure 200 N/m^2 is only 1/500 static atmospheric pressure of about 10^5 N/m^2, which is far smaller than static atmospheric pressure. Researchers mainly analyze sound's two distinguishing attributes: loudness and timbre. The physical meaning for loudness is sound pressure and that for timbre is frequency f. Though audible frequency range for human's ears is from 20 Hz to 20 kHz, the most sensitive frequency range for human being is from 1 to 4 kHz.

The sound waves are characterized by the properties of waves like frequency, wavelength, period, amplitude and speed. Sound waves propagate from a sound source at the speed of sound. In the air of standard conditions, the speed of sound is 340 m/s. Wavelength is a distance between repeating pressure pulses of sound at a given frequency, which can be defined as

$$\lambda = \frac{c}{f} \qquad\qquad\qquad \textbf{(1.3)}$$

where c is the sound speed, f is the frequency of sound, and λ is the wavelength. For a frequency of 1000 Hz, the wavelength of sound is 0.34 m.

1.1.2　Noise

Sound could be either wanted or unwanted. Music is an example of wanted sound, and shouting is an unwanted sound. Unwanted sound is called noise. Noise has a health effect for human beings, which usually results in hearing annoyance. Although noise is described as a kind of unpleasant sound, it is very subjective and mainly depends on the sound perception of listeners. In the mid 1980s, the World Health Organization and OECD (Organisation for Economic Co-operation and Development) collected data and developed an assessment standard on effects of exposure to environmental noise, and report the thresholds for noise annoyance in day time as (OECD, 2002)

(1) at 55-60 dB(A) noise creates annoyance;

(2) at 60-65 dB(A) annoyance increases considerably;

(3) above 65 dB(A) noise constrains behaviour patterns, and causes symptomatic of serious damage.

The term dB(A) is an A-weighting sound pressure level. The reason for using A-weighting is because sound is a composition of different frequency waves. People most easily hear sounds with the main sound sources frequency between 1 and 4 kHz. In order to measure sound on a scale that approximates the hearing function of human ears, more weight should be given to the frequencies that people hear more easily.

3

The existing scales of sound measurements include A-, B- and C-weighting sound levels. The characteristics of the three forms of weighting are illustrated in Figure 1.1. The A, B and C weightings have differences in lower frequency weights. The smallest weights to lower frequencies are provided by the A-weighting scale, and the largest by the C-weight scale. It means that A-weighting scale has the least sensitivity to lower frequencies. A-weighting scale is the most commonly used weighting scheme defined in IEC (International Electrotechnical Commission) and various national standards relating to the measurement of sound pressure level. The curve that describes the A-weighting roughly corresponds to the response of the human ear to sounds. The A-weighting correction values to different frequencies are shown in Table 1.2.

People's noise annoyance perception varies with scenario. For example, people have stronger noise endurance in supermarket than in library. When students read books in library, they prefer a quite environment. It would be noisy for them even if the sound is as low as a whisper. On the contrary, in a supermarket, customers even cannot be interrupted by loud speaking. To clarify the noise annoyance differences in different scenario, researchers collected data and developed the approximate noise levels for the typical scenario in Figure 1.2. The World Health Organization has also suggested a standard guideline value for average outdoor noise level of 55 dB(A), applied during normal day time in order to prevent significant interference with normal activities of local communities (OECD, 2002).

1.2   Traffic Noise Influence over Human Being's Life

Nowadays, a complex transportation network has been a symbol of urbanization development. Convenient transportation enriches people's life. However, traffic noise

from transportation network is around everyone in the city, which affects the living condition of urban residents and could result in sleeping disorder. Many people complain that traffic noise has the greatest direct impact on their life (Milne, 2006). It is illustrated in Figure 1.3 that from 1987 to 1998 traffic noise is still the most serious annoyance in Netherland. The Australian state of the environment estimates that more than 70% of environment noise is due to road traffic. To keep city residents away from traffic noise pollution, many measures have been taken to mitigate the traffic noise, which generally include:

(1) Government makes rules to limit car speed.

(2) Transportation network is constructed far from resident zones in urban plan.

(3) Noise technologies are used to decrease noise from tires and engines of cars.

By taking into account legislation and technological progress, significant reductions of noise from individual sources have been achieved. For example, the noise from individual cars has been reduced by 85 % since 1970 (Sandberg, 2001b). However, data covering the past 15 years do not show significant improvements in exposure to environmental noise, especially road traffic noise. The growth and spread of traffic in space and time and the development of leisure activities and tourism have partly offset the technological improvements. Road and air traffic growth and the expansion of high speed rail risk exacerbate the noise problem. In the case of motor vehicles, other factors are also important such as the dominance of tire noise above quite low speeds (50 km/h) and the absence of regular noise inspection and maintenance procedures.

1.3   Research on Tire-Pavement Noise

Traffic noise is mainly composed of three types:

(1) Propulsion noise;

(2) Aerodynamic noise;

(3) Tire-pavement noise;

The propulsion noise includes all noise sources related with the combustion process of the engine and the transfer of the generated power towards the wheels. The noise caused by the turbulent air flow around a driving vehicle is referred to as the aerodynamic noise. For driving speeds below 120 km/h, this noise has a small contribution to the overall vehicle noise. This is mainly due to the effective aerodynamic design of modern vehicles. However, the aerodynamic noise contributes to a large extent in the vehicle interior noise. With the reduction from propulsion and aerodynamic noise, tire-pavement noise has been the major component of the overall road traffic noise generated by the flow of vehicular traffic on the road, as shown in Figure 1.4. Studies have shown that it is the dominant noise source for vehicles traveling at a speed above 50 km/h. Gibbs et al. (2005) reported that, on statistics, tire-pavement noise represented 75 to 90 percent of the total noise generated by passenger vehicles. For these reasons, there is a strong demand to understand the mechanisms of tire-pavement noise.

There exists more than one mechanisms by which noise are generated from dynamic interaction of tire and pavement surface. Sandberg (2001b, 2003) classified the tire pavement noise generation mechanisms into two types: mechanical mechanisms and aerodynamic mechanisms. The mechanisms involved are complex and there are no

6

simple theoretical solutions available for the prediction of tire-pavement noise. As a result, most of the studies related to tire-pavement noise have been experimentally based. An excellent summary of the major experimental work related to tire-pavement noise is found in the work by Sandberg and Ejsmont (2002).

Although experimental studies can generate empirical relationships between the noise generated and various factors of tire-pavement interaction, they do not provide detailed engineering information (such as spatial, temporal and frequency distributions of sound pressure, contours of sound pressure, etc.) for an in-depth understanding of the mechanisms of tire-pavement noise generation. They also cannot be applied to tire and pavement types not covered by the test conditions, nor to operating conditions and circumstances different from the experimental tests. These limitations can be overcome by developing a numerical model based on theory. A numerical solution when available helps to avoid the large amount of costs and resources needed in performing field experiments.

Several contributions by researchers (Brinkmeier et al., 2008; O'Boy and Dowling 2009; Yum and Bolton, 2003) using numerical methods to solve for the noise generated by tire-pavement interaction have been made in the past. However, all of these models are only concerned with tire structure dynamics, and neglect the effect of nonlinear aerodynamics surrounding tire. They could not sufficiently produce tire-pavement noise prediction in close agreement with actual measured values. With the advancement in computational technology, it is now possible to explore the more complex tire-pavement noise model by taking into account different noise generation mechanisms.

1.4 Objectives

The objective of this research is to develop an analytical framework to estimate tire-pavement noise and study how pavement design and vehicle operating conditions influence tire dynamics and tire-pavement noise generation. The development of such an approach and how it alleviates some of the limitations encountered in the existing methods is one of the main contributions of this research. This can be used as a tool to perform parametric analyses on factors that may affect tire-pavement noise, and to predict tire-pavement noise likely to be generated under different vehicle operating conditions or different pavement design and performance conditions.

1.5 Organization of Thesis

This section gives an outline of the organization of this project. Chapter 2 provides a review of the existing literatures on tire-pavement noise research. The major noise generation mechanisms, factors influence noise and tire-pavement noise modeling overview are given in this chapter. This chapter also states the objectives of the research and defines the scope of work.

Chapter 3 illustrates the numerical modeling of dynamic smooth rolling tires. The underlying objective is to develop a contact model between a smooth rolling tire and a smooth pavement using the finite element method.

Chapter 4 elucidates the simulation modeling of dynamic rolling tire-pavement noise. Noise transmission model is developed, which is coupled with the rolling tire model described in Chapter 3 by means of the fluid structure interface (FSI) method. The

validation of the tire-pavement noise model in the frequency domain method is made using experimental data by past researchers.

Chapter 5 focuses on the numerical study of the effect of surface friction on noise generation. A parameteric analysis is performed in this chapter to evaluate the impact of surface friction on tire pavement noise generation based on the numerical model developed in Chapter 4. The tire dynamics and tire noise distribution are further explored in this chapter.

Chapter 6 focuses on the effect of pavement design on tire-pavement noise. The tire-pavement noise model proposed in Chapter 4 is extended to assess road turning radius effect on tire-pavement noise. The model is validated using experimental results.

In Chapter 7, the analytical model developed in Chapter 4 is further extended to investigate the impacts of wheel load and vehicle speed on tire-pavement noise. The study covered the common range of passenger car wheel loads and vehicle speeds under the normal highway operating conditions.

Finally, a summary of the present research and recommendations for future research are presented in Chapter 8.

Table 1.1 Relationship between Sound Pressure and Sound Pressure Level (Bies and Hansen, 2009)

Sound pressure p_{rms} (N/m^2)	Sound Pressure Level L (dB)	Situation
2×10^{-5}	0	Hearing threshold
2×10^{-4}	20	Forest, slow winds
2×10^{-3}	40	Library
2×10^{-2}	60	Office
2×10^{-1}	80	Busy street
2×10^{0}	100	Pneumatic hammer, siren
2×10^{1}	120	Jet plane during take-off
2×10^{2}	140	Threshold of pain, hearing loss

Table 1.2 A-weighting Network Corrections (dB) (Bies and Hansen, 2009)

Frequency (Hz)	A-weighting correction	Frequency (Hz)	A-weighting correction	Frequency (Hz)	A-weighting correction
10	-70.4	160	-13.4	2500	1.3
12.5	-63.4	200	-10.9	3150	1.2
16	-56.7	250	-8.6	4000	1
20	-50.5	315	-6.6	5000	0.5
25	-44.7	400	-4.8	6300	-0.1
31.5	-39.4	500	-3.2	8000	-1.1
40	-34.6	630	-1.9	10000	-2.5
50	-30.2	800	-0.8	12500	-4.3
63	-26.2	1000	0	16000	-6.6
80	-22.5	1250	0.6	20000	-9.3
100	-19.1	1600	1		
125	-16.1	2000	1.2		
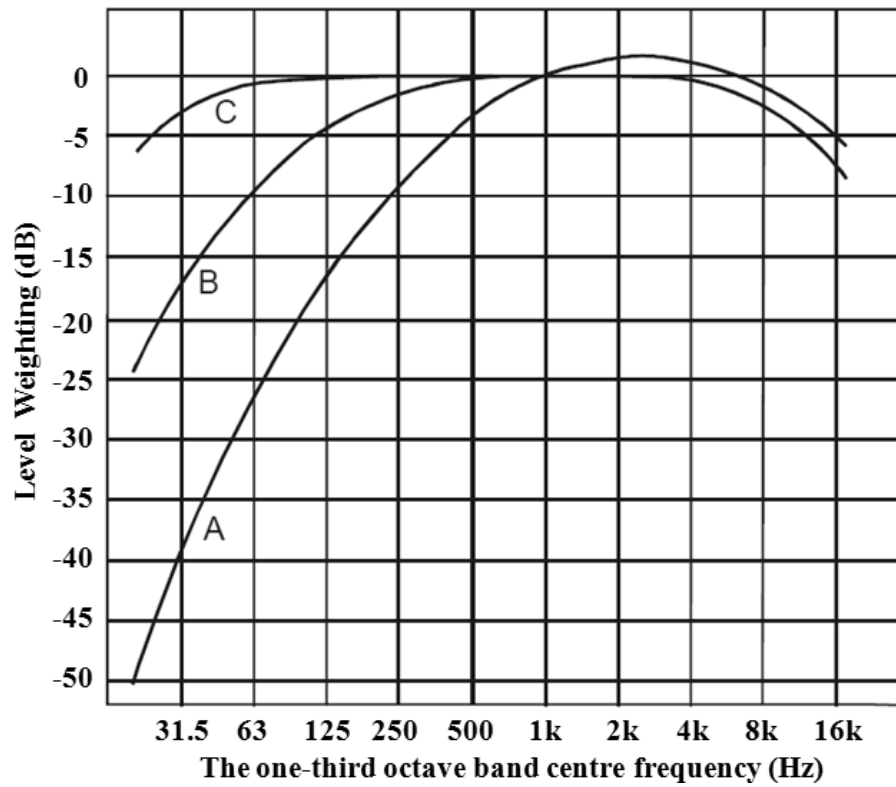
Figure 1.1 A, B and C weighting scheme for sound level calculation (Bies and Hansen, 2009)

Common Indoor and Outdoor Noise Levels

Common Outdoor Noises | Sound Level | Common Indoor Noises

(Decibels)

140 — Threshold of pain

130

120

110 — Rock band (at 15 feet)

Jet Flyover (1,000 feet)

100 — Food blender (at 3 feet)

Gas lawn mower (3 feet)

90 — Garbage disposal (at 3 feet)

Diesel truck (50 feet)

80 — Vacuum cleaner (at 10 feet)

Urban daytime — Normal speech (at 3 feet)

70

Gas lawn mower (100 feet)

60 — Dishwasher (next room)

Heavy traffic (300 feet)

50

Typical urban daytime — Library

40 — Bedroom (at night)

Urban nighttime

30

20 — Whisper

Rural nighttime

10

0 — Threshold of hearing

Figure 1.2 The sound pressure level of typical noise sources (Bernhard and Wayson, 2006)
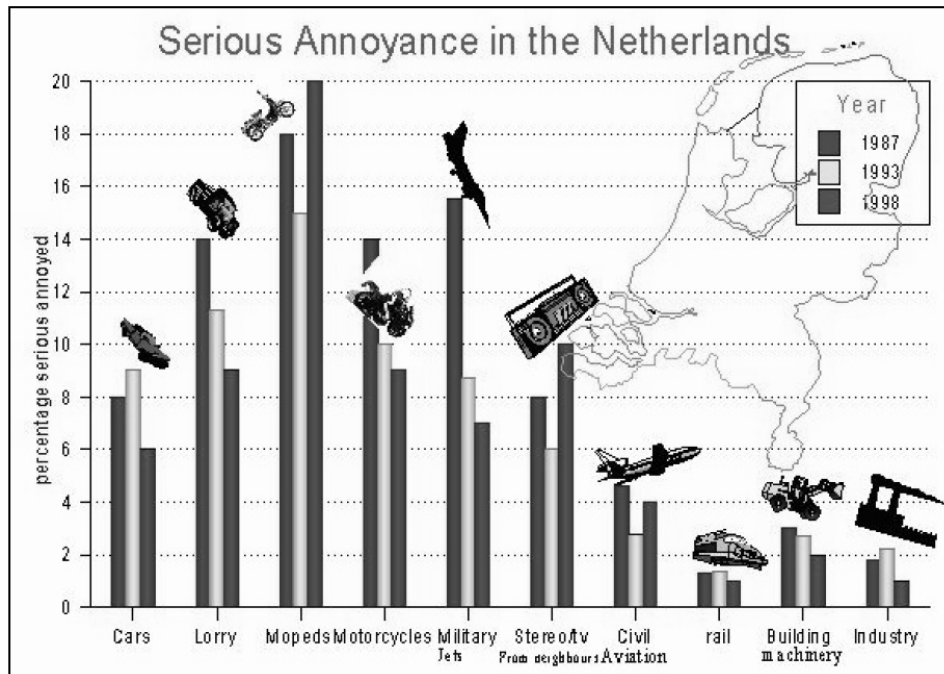
Figure 1.3 Summary of noise annoyance survey in the Netherland (Sandberg, 2001b)
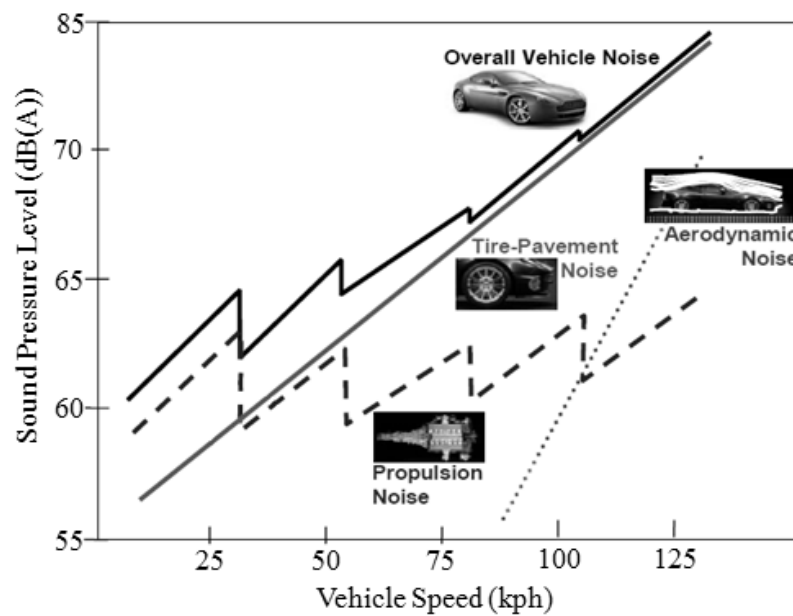
Figure 1.4 Contribution of power unit noise and tire/road noise to the total noise emitted by a vehicle as a function of speed (Rasmussen et al., 2007)

CHAPTER 2   LITERATURE REVIEW

2.1 Introduction

Modeling tire-pavement noise is one of the main challenges in the field of acoustics, covering the structure-borne sound properties of tires, the non-linear contact between tire and road, and horn effects (Sandberg, 2001b; Perisse, 2002; Kindt et al., 2009; O'Boy and Dowling, 2009). Many contributions have been made in this field. This chapter will present a review of the existing literatures about tire-pavement noise researches. Section 2.2 overviews the tire-pavement noise generation mechanisms, including both mechanical and aerodynamic mechanisms. Section 2.3 discusses the main factors influence tire-pavement noise generation. Section 2.4 describes and compares different standard test procedures. In Section 2.5, the existing literatures of tire pavement-noise modeling are discussed. The discussion on the existing models covers tire-pavement interaction dynamics and sound propagation. Section 2.6 identifies the additional work needed and defines the research scope in the present study.

2.2 Overview of Tire-Pavement Noise Generation Mechanisms

Tire-pavement noise generation is a very complex process. Sandberg (2001b) summarized that there are several complex sound generation mechanisms of tire-pavement noise, which are coupled together to generate sound simultaneously. It makes mathematical modeling of tire-pavement noise generation mechanisms a challenging and complex work. To simulate tire-pavement noise, we need to understand the physical principles of noise generations owing to tire-pavement interaction.

The sound producing mechanisms of tire-pavement noise generation are generally classified into two main groups: mechanical and aerodynamic mechanisms.

2.2.1 Mechanical Mechanisms

Noise sources from mechanical mechanisms can be further categorized into radial and tangential vibration of the tire, side wall vibrations, stick-slip, and adhesion stick-snap. These mechanisms mostly occur below 1000 Hz.

2.2.1.1 Radial and Tangential Vibration

Radial vibrations of the tire belt and of profile elements are generated by road roughness elements deforming the tread, or by tread elements hitting or leaving the road surface, which excite the air around the tire to propagate the sound waves away from the vibration source (Sandberg and Ejsmont, 2002). Another impact is the tread vibration in the longitudinal direction (see Figure 2.1). It is attributed to the tangential strain on the tread block due to the friction force interaction between tread blocks and pavement surface. The vibration frequency is related to vehicle speed, and generally occurs at the high frequency range higher than 1 KHz (Brite Euram-3415, 1994).

2.2.1.2 Sidewall Vibrations

Sidewall vibration is generated by sidewall deformation of a rolling tire. The sidewall also acts on a function of sound board to propagate the sound from tread vibrations (see Figure 2.2) (Sandberg and Ejsmont, 2002).

2.2.1.3 Stick-Slip

Stick-slip is caused by the tire and pavement contact surfaces alternating between sticking to each other and sliding over each other with a change of friction force. Since

the static friction coefficient of contact surfaces is larger than the kinetic friction coefficient, if an applied force is large enough beyond the static friction, then the reduction of the friction force to the kinetic friction can cause a sudden acceleration in the velocity of movement. Therefore, the thread blocks of the tire alternately stick and slip on the pavement surface (Sandberg and Ejsmont, 2002). Acceleration, breaking and cornering are all sources of stick-slip mechanism (see Figure 2.3).

2.2.1.4 Adhesion Stick-Snap

Stick-snap is a process that the tread blocks stick to a smooth pavement surface because of both adhesion and vacuum that is created when the air in the tread rib is pushed out. Then, the adhesion is snapped with tire rolling. Noise source is from adhesion forces which make air pushed out and into tread ribs (see Figure 2.4) (Sandberg and Ejsmont, 2002). The friction mechanism is governed by the micro-texture of the pavement surface (Nelson and Phillips, 1994). Andersson and Kropp (2009) experimentally illustrated that the adhesion forces in the tire/road contact interface significantly increased the contact dynamics and resulted in noise generation for certain tire/road combinations. Although the total sound pressure level of noise generated was directly related to the level of the adherence force, the energy distribution in 1/3 octave bands could not be estimated from the adherence force record alone.

2.2.2 Aerodynamic Mechanisms

Tire-pavement noise is also generated by mechanisms related to the movement of air in the cavities of the tread pattern. Noise sources from aerodynamic mechanisms can be classified into air-pumping, air resonant radiation, pipe resonance, and horn effects. These mechanisms mostly occur above 1000 Hz.

2.2.2.1 Air Turbulence

Air turbulences noise is mainly caused by two mechanisms: displacement and rotation. Displacement air turbulence noise is caused by the displacement of tire rolling on a road surface. Rotational air turbulence noise is caused by tire tread dragging air to rotate around tire. Figure 2.5 illustrates these two types of turbulent air flows around tire. This noise is significant at high vehicle speeds (Hayden, 1971).

2.2.2.2 Air-Pumping

Air-pumping is the most common aerodynamic mechanism (see Figure 2.6). The air is filled in the gaps between the tread on a tire and the texture on the pavement surface. Some of the air is squeezed out, and some is trapped and compressed, as the tire rolls on pavement. Subsequently, air is pushed into the gaps between tire tread and pavement as the tire tread returns to the un-deformed state when leaving the contact region. The pumping of air causes sound production and propagation (Sandberg and Ejsmont, 2002).

2.2.2.3 Air Resonant Radiation

Helmholtz resonance is the air resonance phenomenon in a cavity which can amplify the frequency that is distinct to the cavity. It can occur in the wedge between tire and pavement surface (Sandberg and Ejsmont, 2002). The result is an amplification of some frequencies related to the geometry and interaction between tire and pavement (see Figure 2.7).

2.2.2.4 Pipe Resonance

Pipe is a resonator that can amplify sound with frequencies unique to pipe. Grooves and sips on a tire can be regarded as pipe geometries and are pinched off and opened up

frequently on the contact patch. Sound is generated and amplified in these pipes (see Figure 2.8). Their resonant frequencies are dependent on the geometric properties, not on the rolling speed of the tire (Kuijpers and Blokland, 2001).

2.2.2.5 Horn Effects

The wedge shape formed between tire and pavement surface functions like a horn that can amplify sound in the forward and backward directions (Graf et al., 2002; Kuo et al., 2002), as shown in Figure 2.9. This influences the wave propagation and provides considerable amplification of about 10-20 dB (Ronneberger, 1982).

To sum up, all these different mechanisms lead to a complicated combined effect of tire-pavement noise generation. Most researchers generally have no disagreement on the effect of these mechanisms. However, their relative importance is still an issue for further research.

2.3 Factors Affecting Tire-Pavement Noise Interaction

Mechanical and aerodynamic mechanisms play significant roles in the tire-pavement noise generation process. Their relative contributions to noise generation could vary with many factors, which can generally be classified into four types:

(a) Factors related to tire parameters like tire material, tire dimension, tread pattern;

(b) Factors related to road surface characteristics like pavement structure, and pavement texture;

(c) Factors related to tire dynamics like tire speed, tire load and tire pressure;

(d) Environment factors like temperatures and the wetness of pavement surface.

The main components of the tire-pavement noise interaction are composed of the above four groups. The understanding of the interaction of these factors is helpful for researchers to understand the process of the tire-pavement noise interaction. Discussion of the effects of these four groups of factors on noise generation is presented in this section.

2.3.1   Tire Parameters Characteristics

Modern tire technologies have developed rapidly. In the past several decades, many kinds of tires have been designed to improve vehicle performances, like stability, skid resistance and tire wear. Tire structure, tire dimensions and tread pattern are three main factors considered in the process of tire design. Past researches have also recognized that the above three tire properties have great effects on tire-pavement noise generation (Sandberg and Ejsmont, 2002).

(1) Tire structure

Tire structural property is one of the most important factors to influence tire-pavement noise generation. It is generally described by three parameters, namely density, elastic modulus, and Poisson's ratio. Several researchers (Ejsmont, 1982; Doan, 1996; Kropp et al., 1998) have investigated the influence of tire structures on tire-pavement noise. Ejsmont (1982) tested eight tires with a fixed tread pattern but very different belt construction and found that increased tread bending stiffness reduces the tread vibration and the generated sound. Doan (1996) indicated that tire-pavement noise was reduced due to the application of a tire mould profile that gives a high belt tension on the shoulder and a lower belt tension at the centre of the tread band. Kropp et al. (1998) further

19

developed a two-dimensional analytical model to show the effects of the bending stiffness of the belt and the tread band to tire-pavement noise, and found that increasing the mass of the belt could increase its bending stiffness and reduce tire-pavement noise. Recently, some researchers (Brinkmeler et al., 2008) have investigated the relations between tire modes and tire-pavement noise generation, where tire-pavement noise data are transformed from time domain to frequency domain to analyze the effects of tire modes on noise pressure level in frequency domain.

(2) Tire dimensions

Past studies have shown that tire-pavement noise can be improved by optimizing tire dimensions (Walker and Williams, 1979). Walker and Williams (1979) experimentally researched the influence of tire width on tire-pavement noise emission, which shows that there is an obvious increase with tire width increasing. Similar experiments have been done to study the effect of tire diameter (Nilsson, 1979; Ejsmont, 1982), and found that the increase of tire outside diameter resulted in a decrease of tire-pavement noise. Technical University of Gdansk (TUG) (Sandberg and Ejsmont, 2002) tested tire width effect on tire-pavement noise generated on smooth road surface at the speed of 70 km/h. It has found that tire-pavement noise increased by 0.3 dB per 10 mm of width change.

(3) Tread Patterns

Tire tread pattern design deals with trade-off between safety, noise, ride and tire longevity. On statistics, there are about 16,000 different tire patterns used on tires (Sandberg and Ejsmont, 2002). Till now, many tires with different tire patterns have been used in tire-pavement noise measurements (Sandberg and Ejsmont, 2002; Hanson et al.,

2004; Leeuwen et al., 2007). These tire patterns can be classified into: (1) Smooth, slick, bald pattern; (2) Rib pattern; (3) Zig-zag pattern; (4) Block pattern; (5) Lug pattern; (6) Aggressive tread and (7) Pocket type tread;

Tread pattern had been considered as a major effect on tire-pavement noise generation in the past. Based on this initial understanding, it is a reasonable deduction that a smooth tire will be a quiet tire. However, many experiments (Sandberg and Ejsmont, 2002) have proved that the understanding is not correct. On a rough-textured surface, a smooth tire is the noisiest tire type. Although tire pattern is not a dominating factor of tire-pavement noise generation, it can be used to influence noise generation.

A very detailed experiment has been done by Ejsmont and Sandberg (1984) to investigate the effect of simple tread patterns on tire-pavement noise. The results are summarized in Figure 2.10. The increase of groove width from 2 to 9 mm increased A-weighted sound level, but the increase of groove width from 9 to 12 mm decreased A-weighted sound level. A slight decrease of A-weighted levels occurred when tread pattern was randomised.

(4) Tire materials

Studies on the influence of the inner tire structure indicated that an increase of the belt stiffness resulted in a decrease of tire-pavement noise (Kropp, 1989). Moreover, the thread storage modulus had a much larger influence on the exterior tire-pavement noise level than the sidewall storage modulus. On the other hand, the loss tangent of both tread and sidewall had a small effect on the tire-pavement noise. The tread rubber hardness had a substantial effect on the tire-pavement noise. An increase in contact stiffness of the

tread layer caused higher contact forces between tread and road. On the contrary, air pumping noise resulting from local deformation of the tread was found to decrease as a result of higher tread stiffness. A stiffer tread exhibits less local deformation in the contact patch, thus resulting in a weaker volume source. Typical variations in rubber hardness can affect the noise levels by 2-3 dB (Sandberg and Ejsmont, 2002).

2.3.2 Pavement Surface Characteristics

Nowadays, tire-pavement noise is an important consideration in pavement design and construction. This section reviews the effect of road surface characteristics on tire-pavement noise.

2.3.2.1 Pavement Texture

Pavement surface irregularities can be divided into three ranges: microtexture, macrotexture and unevenness (Sandberg and Ejsmont, 2002). Another range of irregularities, megatexture, is also introduced in tire-pavement noise research. The PIARC Technical Committee on surface characteristics developed the following classification of surface irregularities in terms of their wavelengths (Wayson, 1998): microtexture as those with wavelength less than 0.5 mm, macrotexture with wavelength of 0.5 mm - 50 mm, megatexture with wavelength of 50 mm - 500 mm and unevenness with wavelength of 0.5 m - 50 m.

An ISO working group studied the relative importance of the four ranges to tire-pavement noise generation (Wayson, 1998), and found that microtexure is important for skid resistance but it does not have a significant effect on tire-pavement noise generation. Similarly, Sandberg and Ejsmont (2002) concluded that the ranges in microtexture and

unevenness do not have any measurable effect on tire-pavement noise, while ranges in macrotexture and megatexture have considerable influence on tire-pavement noise generation and safety. The surface texture of macrotexture drains water off the pavement surface for safety but causes radial excitation of tires (Wayson, 1998). An European state of the art report (Brite Euram 3415, 1994) reported that low frequency noise is caused by tire vibrations and is a function of megatexture. According to this report, the noise spectra of low frequency in the range of less than 1 kHz are positively correlated with long wavelength texture greater than 10 mm, while high frequency noise spectra are negatively correlated with short wavelength texture. Fujikawa et al. (2005) defined some essential road roughness parameters that govern noise variation and provided information on tire-pavement noise abatement (Fujikawa et al., 2005). The results reveal that pavement asperity height is not an essential parameter, but asperity height unevenness, asperity radius and asperity spacing are important for the abatement of tire vibration noise. The effect of the ranges of pavement texture on tire-pavement noise generation is illustrated in Figure 2.11.

2.3.2.2 Porosity

Porosity refers to air voids within the pavement structure. In addition to water drainage function, the air voids also help the dispersion of the sound that is made between tire and pavement (see Figure 2.12). This noise absorption property significantly reduces the generation of certain forms of tire-pavement noise. Typically, porous surface layer will have 15-25 % void volume (Sandberg and Ejsmont, 2002). A higher porosity could reduce the durability of the road surface.

2.3.2.3   Pavement Surface Discontinuities

Pavement defects and road facilities are the main reason of road surface discontinuities. Furthermore, pavements have a discontinuous nature in the design due to pavement material properties variation with the environment. Kindt et al. (2009) experimentally tested tire-pavement noise variation with pavement surface discontinuities. Tire-pavement noise increases with tire passing cross the discontinuities of road surface due to changes of excitation force on tire. Gagen (1999) also studied the effect of pavement surface discontinuities on cavity resonance in tire tube. These resonances are prominent at discontinuities like bridge transitions and railway crossings. The different types of discontinuities are shown in Figure 2.13.

2.3.3   Tire Dynamics Characteristics

Tire dynamics characteristics are a main factor that influences tire-pavement noise generation. It includes tire speed, load and inflation pressure.

(1) Tire speed

The influence of tire speed on tire-pavement noise is highly dependent upon the properties of pavement surface. Steven and Pauls (1990) experimentally investigated the speed-noise relationship, and found that the sound level of tire-pavement noise is proportionally related to the logarithm of the speed. This finding was later confirmed by Ivannikov et. al. (1998) and Steven et al. (2000). Many experiments (Walker and Williams, 1979; Ejsmont, 1982) suggested the following logarithmic linear relationship between speed and tire-pavement noise for some pavements:

$$L = A + B\log(V)$$

(2.1)

where L is sound pressure level with unit dB(A), A and B are constant speed coefficients and V is vehicle speed with unit km/h.

This kind of logarithmic linear speed-noise relationship has been widely used in the analysis of experimental results (Ejsmont, 1982; Steven and Pauls, 1990; Ivannikov et al., 1998), which is summarized in

Table 2.1. It is observed from the Table that all tests have similar B coefficient values, but different A coefficient values.

(2) Driving and braking forces

Longitudinal slip, which is a result of driving or braking torque on the wheel, increases the tire-pavement noise significantly. In the extreme cases of high slip, it could make a very squeal noise. Steven (1989) shows that the influence may be as high as 12 dB. He also found that the increase of noise due to torque is much higher for low speeds than for high speeds. An increase of 20 -40 dB occurs for a slip of 10-15%.

(3) Tire load and inflation pressure

Based on measurements by Ejsmont (1982), for typical passenger car radial tires, noise increases by 1-2 dB(A) per doubling of load, provided that the inflation pressure is adjusted to the load. If the pressure is not adjusted, the increase is about 0.7 - 1.5 dB(A) per doubling of load. Earlier experimental researches for rib patterned truck tires and lug-patterned tires have been done by RMA (1971) on asphalt and concrete surfaces, where

noise increases by some tenths of a dB per doubling of load for rib patterned truck tires, and 5 dB(A) increase for lug-patterned tires. There are similar results on cement concrete surfaces. These highlight that tire-pavement noise generally will increase with tire load and inflation pressure. In a research in Japan, Konishi and Tomita (1996) tested the influence of passenger car wheel load and found that noise level increased by 2 dB per doubling of load on average. Studies by Wolf et al. (1992) and Iwao and Yamazaki (1996) indicated that the influence of wheel load on tire-pavement noise reduced with increasing vehicle speed. Ejsmont and Taryma (1982) measured tire-pavement noise of passenger car radial tires and reported that noise increased by 1 to 2 dBA per doubling of wheel load when inflation pressure was adjusted to the load; by 0.7 to 1.5 dBA if inflation pressure was not adjusted.

(4) Tire cornering

When a vehicle moves on a horizontal curve, its tires are subject to radial forces due to the cornering movement. Yamazaki and Fujikawa (1989) investigated the lateral acceleration distribution for typical driving conditions, and found that 60% of the driving time the lateral acceleration is $< 0.5 \text{ m/s}^2$, about 30 % of the time it is $0.5\text{-}1.5 \text{ m/s}^2$, and about 10% of the time it is $1.5\text{-}2.5 \text{ m/s}^2$. A valuable experimental research has been done by Ejsmont and Sandberg (1981) who investigated the geometric pavement curve radius effect on tire-pavement noise for car and truck tires. Noise data was collected by CPX methods. It was found that for car tires straight driving makes less noise than cornering driving. The noise level normally decreases as geometric pavement curve radius increases. The results obtained for the truck tires were similar, but the increase of noise during cornering was more noticeable.

26

2.3.4 Environment Factors

The environment factors that influence tire-pavement noise generation and propagation mainly include temperature and wetness.

2.3.4.1 Temperature

In the 1980s, Sandberg and Ejsmont (1985) have investigated the temperature effects on tire-pavement noise by experimental methods. It is illustrated that noise pressure level will decrease as temperature increases. Noise measurements are normally taken when outdoor temperature is between $5 \, ^\circ C$ and $30 \, ^\circ C$. In order to repeat and compare the noise measurements, they should be done at the same temperature. Temperature correction could be done by considering the following three main factors: tire temperature, road surface temperature and air temperature. The correction coefficient is highest for air temperature than for the other two kinds of temperature (Anfosso-Ledee and Pichaud, 2007). It is generally required that measured tire-pavement noise levels be corrected to a reference air temperature of $20 \, ^\circ C$. Correction can be made in the following form (Sandberg and Ejsmont, 2002):

$$L_A(20\, ^\circ C) = L_A(T) - K(T - 20) \tag{2.2}$$

where $L_A(20\, ^\circ C)$ is the corrected sound level at $20 \, ^\circ C$, $L_A(T)$ is a measured sound level, T is the tested air temperature $(^\circ C)$, and K is a temperature coefficient.

2.3.4.2 Wetness

Wetness is another important environment factor that influences tire-pavement noise. Past experimental researches have shown that tire-pavement noise will change with

wetness on the road. On a very wet pavement, a tire produces more high frequency noise above 1,600 Hz, and less low frequency noise. Tire vibrations on a wet road are slightly lower than those on a dry road. A separate mechanism for wet pavement is acceleration noise, produced when water droplets are thrown away or when they hit the ground or the car body.

2.4 Tire-Pavement Noise Test Procedures

The relative contributions to noise generation of the four types of sound sources vary with the type of tire, road surface and vehicle speed (Nelson and Phillips, 1994; Sandberg and Ejsmont, 2002). To evaluate the noise reduction effect of different measures, reliable sound measurements are necessary. Several standard measure methods have been used to measure tire-pavement noise. Detailed procedures are depicted in the existing contributions (ISO, 1997; ISO, 2001; Sandberg, 2007). All methods can be categorized into three main groups: wayside, source noise measurements and nearfield acoustic holography.

2.4.1 Wayside Noise Measurement

Wayside noise measurement is a far field noise measurement. The location of receivers is a fixed distance (commonly 7.5 or 15 m) from the pavement. As most measurements are taken at the side of the pavement, this method is technically termed wayside noise measurement. There are three common types of wayside testing: statistical pass-by test, controlled pass-by test and time-averaged test.

2.4.1.1 Statistical Pass-By Test

Statistical pass-by (SPB) methods utilize a random sample of typical vehicles measured one at a time (ISO, 1997). The maximum sound pressure level is captured for each passby vehicle using a sound measurement system such as a sound level meter (SLM).

The instrument is located 7.5m from the central line of the travel lane (see Figure 2.14). A statistically significant sample of light and heavy vehicles must be collected. The data is used to compute a Statistical Pass-by Index (SPBI) which can be used to compare various pavements. Details of the international standard SPB measurement method are specified by ISO (1997). SPB method accounts for all aspects of traffic noise at the sideline of the highway including engine, exhaust and aerodynamic noise. The method also takes into account the variation that occurs across vehicles of the same type. However, the measurement is not tightly controlled since random vehicles are measured for each site. In some cases a paired site method is used, where identical vehicles are measured for each site. For SPB measurements the traffic stream must be such that only a single vehicle passes through the measurement site at a time. The measurement site must be selected to avoid background noise, reflections, or terrain that might affect the measurement. In general, the background noise levels must be 10 dB(A) less than the measured vehicle noise.

2.4.1.2 Controlled Pass-By Test

For controlled pass-by (CPB) measurements the same measurement setup as SPB is used. For CPB relatively few selected vehicles are driven at a controlled speed past the measurement location. In some cases, to emphasize tire-pavement noise the vehicle may coast past the measurement point. No standards currently exist in the U.S. for CPB but

the European Union is currently developing a method for EU Standardization and possibly for ISO, based on a French national standard (F119).

The CPB method takes less time than the SPB method but does not account for the variation that might occur in vehicles of the same type. The method has the same site limitations as SPB and requires a light traffic density making it more suited to test track conditions.

2.4.1.3 Time-Averaged Test

For conditions of heavy traffic density, neither SPB nor CPB can be used to evaluate tire-pavement noise because vehicle pass-bys are not sufficiently isolated. For such applications, investigators have used methods of measuring time-averaged traffic noise. For time-averaged measurements, sound pressure is averaged and converted to the equivalent noise level.

2.4.2 Source Noise Measurement

Opposed to wayside noise measurements, source noise measurement is a near field measurement. Commonly, the receiver location is very close to noise source (less than 1m). Source noise measurement is of increasing interest, particularly for those who wish to design and build quieter pavements. Currently, there are two techniques to measure tire-pavement noise: close-proximity (CPX) and onboard sound intensity (OBSI). CPX is archived as a draft international standard ISO 11819-2 in EU (ISO, 2001). OBSI measurement method is in the process of being standardized in USA (ASTM, 2009).

2.4.2.1 Close proximity Methods (CPX Method)

CPX methods were developed to focus the measurement on tire-pavement noise. The measurement procedures are described in ISO/CD 11819-2. The microphones are fixed on a trailer near the tire (see Figure 2.15).

In the trailer, the hood covers the microphone to reduce wind noise and reflect noise from other traffic. Microphones are accurately fixed in the same place relative to tires so that the recorded sound is generated by the same noise sources, i.e 200 mm from the side wall of the tire, 200 mm from the wheel axis and 100 mm above the road surface, as shown in Figure 2.16. To eliminate the test uncertainties from test tires, ISO standard specifies that two most commonly reference test tires used in the CPX test. They are Avon/Copper type ZV1(size 185/60 R15), and Dunlop type SP Arctic (size 185R14) (see Figure 2.17).

Furthermore, to focus the research on pavement perspectives, some researchers replace the above rib test tires with smooth tires. Cesbron et al. (2009) performed a CPX test for a Michelin slick tire rolling on six different pavement surfaces. Tire-pavement noise was measured by the CPX method with a PIARC smooth tire on a replica of an ISO 10844 surface (Sandberg, 2002)

2.4.2.2 Onboard Sound Intensity Method (OBSI Method)

OBSI is a sound intensity test method. Sound intensity describes the flow of sound energy from a sound source. Unlike sound level test, sound intensity measurements only capture the sound produced by the noise source under measurement, eliminating the interruption from other sound sources. OBSI standard (ASTM, 2009) provides a satisfactory method to meet all tire-pavement noise measuring needs for researchers.

OBSI test system is similar to CPX test system (see Figure 2.18). The system measures the sound intensity at defined locations near the tire-pavement interface using phase matched microphones wearing wind screens (see Figure 2.19). ASTM OBSI standard draft (ASTM, 2009) specifies that OBSI test tire is the standard reference test tire (SRTT) P225/60R16-97S radial standard (ASTM F 2493-06) made with a rubber compound that has a low sensitivity to temperature.

In conclusion, the CPX and OBSI methods are similar since they both fix the microphones in a position to test the noise source in the tire-pavement contact patch, and collect the data from rolling tires. However, there are still some important differences as shown Table 2.2.

2.4.3 Nearfield Acoustic Holography

In addition to the above mentioned standard testing methods, several more advanced testing methods have been proposed for research on noise localization (Morgan et al., 2006; Hendricx and Mancosu, 1999). The popular method proved to be applicable for tire-pavement noise research is nearfield acoustic holography.

Acoustic holography is a process to perform a spatial transformation of sound fields. The nearfield acoustic holography testing method is consisted of two steps. In the first step, the sound pressure is measured in the points of a plane grid in the near field of the source. It could completely describe the sound field in the tested plane (see Figure 2.20). The tested data is then transformed into frequency domain by discrete Fourier transform. In the last step, an inverse two-dimensional Fourier transform is applied to calculate the spatial pressure distribution in the chosen plane. Very briefly its overall principle can be

described as in Figure 2.21. As such, acoustic holography provides an accurate three-dimensional characterization of the sound field and the source.

Several configurations are found in literature. Bolton and Kim (2003) used nearfield acoustic holography procedure to visualize the sound field radiated by a tire rolling on a drum. Tanaka (2004) used a stationary microphone array to identify the tire-pavement noise of a vehicle coasting by. The standard spatial transform method requires that measurements are taken under steady-state conditions. The obtained source distributions are then an average over a relatively long measurement time. In case a source is varying in time, non-stationary spatial transform methods have been developed which calculate a source distribution at discrete time distances. These methods are known as time domain acoustic holography methods and have been applied in tire-pavement noise studies.

2.5 Tire-Pavement Noise Modeling

To analyze the complex noise generation mechanisms from tire-pavement interaction, a number of models have been developed to simulate tire-pavement noise interaction dynamics for years. However, to our best knowledge, there is no model capable of associating simultaneously the tire structure dynamics with the resulting structural noise radiation and aerodynamic noise to date. Instead, each model is proposed for a specific application such that simplification can be made in the modeling process. An overview of these existing tire-pavement noise models are presented as following:

2.5.1 Overview of Tire-Pavement Noise modeling

According to the modeling methodologies, the existing tire-pavement noise models can be classified as statistical models, hybrid models and deterministic models:

2.5.1.1 Statistical Models

The statistical model is based on the idea of correlating sound pressure levels with parameters which are assumed to characterize the tire-pavement interaction. Statistical models are generally used to predict the far field tire-pavement noise of a passenger car from intrinsic characteristics of the road. The principle of statistical models is to build a correlation function between measured noise levels and parameters which are assumed to be able to characterize the generation mechanisms of the tire-pavement noise based on experimental data statistical analysis. Most statistical models can be found in road design applications.

A popular statistical model is SPERON model (Beckenbauer et al., 2008). SPERON statistical model is based on the assumption of non-coherent sound sources whose intensities are linearly superimposed and can predict sound pressure levels of pass-by tire-pavement noise. This method agrees with the prerequisites of a multiple regression defined as

$$p^2_{coast-by} = p^2_{vibr} + p^2_{airflow} + p^2_{cavity} + p^2_{aerodyn} \qquad \textbf{(2.3)}$$

$$p^2_{vibr} = aF_c^2 \Gamma^{\alpha_1} B^{\alpha_2} S^{\alpha_3} \qquad \textbf{(2.4)}$$

$$p^2_{airflow} = b(F_c^2 \Gamma^{-1.5} S^{-2})^{\beta_1} B^{\alpha_2} V^4 \qquad \textbf{(2.5)}$$

$$p^2_{cavity} = cG_{pattern}^{r_1} \qquad \textbf{(2.6)}$$

$$p^2_{aerodyn} = dV^{\delta_1} \qquad \textbf{(2.7)}$$

where p_{vibr}^2 is a component that represents the mechanically excited sound source which is driven by contact forces; $p_{airflow}^2$ is a component which is related to air flow within the tire-pavement contact path; p_{cavity}^2 is tire interior cavity resonances; $p_{aerodyn}^2$ represents residual effects of the air flow noise sources around the car body; a, b, c, d are regression coefficients; $\alpha_1, \alpha_2, \alpha_3, b_1, r_1, \delta_1$ are exponents; F_c is tire-pavement contact force (N) ; Γ is tire pavement contact air flow resistance (Pa s/m); B is tire width (m); S is tire tread stiffness (N/m); $G_{pattern}$ is spectral power of the tread pattern variation; and V is driving speed (m/s).

The SPERON model is a rather research oriented product. A comprehensive database and an extensive description of the road and tire are provided for the pass-by noise evaluation. This model can handle road surface and light vehicle tire types not used for its construction. It has been used for the development of new pavement. The only disadvantage in this model is that noise predictions are limited to road pavement with no acoustic absorption.

2.5.1.2 Hybrid Models

As previously mentioned, statistical models do not account for the whole variety of tire-pavement interaction, since the analyzed data is limited by test conditions. Therefore, hybrid models have been developed that could express noise levels as a function of parameters which describe tire-pavement interaction. For instance, Clapp (1985) developed a hybrid model to relate contact forces to noise levels. For this, tire deformation is estimated by modeling the penetration of roughness peaks into an elastic half space.

35

2.5.1.3 Deterministic Models

Deterministic models are used to describe the physical processes involved in the generation and radiation of tire-pavement noise. This type of model requires detailed physical information of tire and air properties and thus is most suitable for tire and pavement design application to reduce noise generation. In the past decades, there are three main research groups to make continuous contributions to the numerical simulation of tire-pavement noise in the past twenty years, which are led respectively by A. P. Dowling from Cambridge University, Wolfgang Kropp from Chalmers University of Technology, and J. S. Bolton from Purdue University. Their main contributions are summarized in the following subsections

Models by A. P. Dowling Group

O'Boy and Dowling (2009) proposed a multilayer bending orthotropic plate tire analytical model, in which sidewalls and air pressure were considered to simulate tire dynamic behavior when the tire was rolling at one speed across road surface. The proposed model incorporates the material properties of each layer, which may be provided without experimental validation for a particular tire belt package. The noise propagation is governed by linear Helmholtz equation, and solved by boundary element method (BEM). Horn effect is numerically characterized in the simulation based on their previous contributions (Graf, 2002; Graf, Kuo, Dowling and Graham, 2002). The model was validated by experimental data. Numerical and experimental comparisons illustrated that the model can effectively simulate radial vibration mechanism. However, due to the neglect of stick-slip action as the tread block vibrates tangentially upon exiting contact

patch, large errors between predicted and experimental result at the positions to the rear of the tire.

Models by Wolfgang Kropp Group

As a kind of spectral finite element method, wideguide Finite Element Method (WFEM) was used to develop tire dynamic model, in which a tire was simulated by orthotropic single-layer shell element, and was regarded as a wideguide in the circumferential direction. This method significantly reduces the computational cost compared to traditional finite element models, and is then extended to study tire noise generation (Wolfgang, 2012). The noise propagation is governed by linear Helmholtz equation, and solved by boundary element method (BEM). Furthermore, in order to study turbulence noise effect, Conte (2008) used the turbulence model to study the near field turbulence effect of tire-pavement noise by commercial software FLUID software. The main disadvantage of this approach is its incapability to consider the effect of tire structure vibration due to the variation of pavement groove.

Models by J. S. Bolton Group

A single-layer bend plate orthotropic finite element model was developed using the commercial finite element software ANSYS, in which tire dynamic behaviors were employed to calculate sound pressure level in far fields by commercial BEM code SYSNOISE (Yum, 2003; Kim, 2005; Kim, 2007). The proposed model was first used to analyze the surface reflection effect of tire-pavement noise (Kim and Bolton, 2004). It was found that the second radiation mode above 700 Hz results in significant amplification of sound from the contact patch area. Then, the influence of tire size and

shape on sound radiation in the mid-frequency region was studied (Kim, Hong and Bolton, 2007). An optimization of the sound radiation was performed by modification of the tire structure and shape.

A lot of useful information was obtained from the above analyses. However, due to the limitation of coupling between ANSYS and BEM, the proposed model cannot consider tire rotation in the simulation. Therefore, the model does not study the effect of tangential vibration and aerodynamic mechanisms on tire-pavement noise at the rolling state.

Other Studies

Besides the work form three main groups, contributions from other studies are summarized below.

Brinkmeier et al. (2008) developed a finite element model to simulate the dynamic behavior of a stationary rolling tire in ground contact by using an arbitrary Lagrange-Eulerian formulation (ALE). The Helmholtz equation was employed to describe noise radiation in the far field, and numerical methods were used to solve for tire-pavement noise. However, the model is not validated by experimental data, and thus cannot be evaluated effectively. Similarly, Koishi et al. (2011) used ABQAUS to simulate steady state tire dynamics in ALE formulation, and built an acoustic model to simulate sound propagation. However, it is theoretically similar to the Brinkmeier's model (Brinkmeier et al., 2008), and is not clearly validated.

Tsujiuchi et al. (2002) used measurement modal analysis data rather than tire dynamic simulation as noise source. The sound radiation is simulated by commercial BEM code LMS. The analyzed modal data are inputted into the developed BEM acoustic model to

simulate sound radiation from tire surface. The results illustrate that this model can effectively simulate sound radiation. However, since tire vibration data need to be tested manually, this approach has a large limitation in tire noise research and application.

Guisset and Augusztinovicz (1999) developed a tire noise prediction model by combining a structural transient finite element approach (ABAQUS) with a radiation model based on acoustic infinite element technology (SYSNOISE). It is focused on tire vibrations, thus the aerodynamic mechanisms are left aside. It is theoretically similar to the Bolton's model (Kim and Bolton, 2007).

Plotkin and Stusnick (1981) attempted to more or less completely model the tire-pavement noise generation and propagation by combing a lot of sub-models. Their work aims to combine a lot of sub-models together to be a complete model. However, most effective computational models today are not present in the sub-models and the complete model is also suffered from insufficient validations.

De Roo and Gerretsen (2000) developed a comprehensive mathematical simulation model for the excitation and radiation of tire-pavement noise, which combines two partially independent noise excitation models, and a fully elaborated radiation and propagation model. The goals of the model include: (1) description and prediction of the influence of road surface characteristics on tire-pavement noise emission; (2) study of the influence of tire parameters on tire-pavement noise emission and development of design concepts for tire noise.

The above models are simplified to some extent for their specific applications. This kind of physical tire-pavement noise models is typically composed of a tire-pavement

interaction model and a noise radiation model. These two different sub-models are discussed more in detail below.

2.5.2 Tire-Pavement Interaction Modeling

The modeling of tire-pavement interaction is a complex process. It normally includes two different sub-models, namely tire model and pavement model. These two sub-models interact with each other through contact modeling mechanisms.

2.5.3 Tire Modeling

Accurate tire modeling is a key to tire-pavement interaction modeling analysis. However, tire modeling is difficult due to its structural and material complexity. As the important issue of vehicle dynamics research, in the past decades, tire dynamics has been widely researched (Badalamenti and Doyle, 1988; Kung, 1990; Eichler, 1996; Larsson et al., 2002; Pinnington, 2002; Pinnington and Briscoe, 2002; Brinkmeier et al., 2004). Mathematical models are abstracted from the complex tire dynamic structure. These models in the existing literatures can be classified into analytical models and numerical models.

(1) Analytical Models

Tire dynamics is originally modelled as a simple mathematical model to analyze the vibration of static tires (Gong, 1993). Badalamenti and Doyle (1988) developed single-point contact model to analyze the vertical vibration characters of tire, where the model is represented by a spring and damper in parallel. In the single-point contact model, the contact point is restricted to lie directly beneath the wheel axle. To overcome the above

restriction, a flexible ring model was developed by Gong (1993), which was also used to research tire characteristics in the tire rolling state (see Figure 2.22).

In this model, sidewall is simulated by the springs, where the radial and tangential direction springs represent radial and tangential sidewall stiffness, respectively. Gong (1993) defined the motion equation of the flexible ring model as

$$\rho h \ddot{u}_r + \lambda \dot{u}_r + \frac{EI}{R^4}(\frac{\partial^4 u_r}{\partial \theta^4} - \frac{\partial^3 u_\theta}{\partial \theta^3}) + \frac{Eh}{R^2}(u_r + \frac{\partial u_\theta}{\partial \theta}) + \frac{p_0}{R}(u_r - \frac{\partial^4 u_r}{\partial \theta^4} + 2\frac{\partial u_\theta}{\partial \theta}) + k_r u_r = f_r \quad \textbf{(2.8)}$$

$$\rho h \ddot{u}_\theta + \lambda \dot{u}_\theta - \frac{Eh}{R^2}(\frac{\partial^2 u_\theta}{\partial \theta^2} + \frac{\partial u_r}{\partial \theta}) + \frac{EI}{R^4}(\frac{\partial^3 u_r}{\partial \theta^3} - \frac{\partial^2 u_\theta}{\partial \theta^2}) + \frac{p_0}{R}(u_\theta - \frac{\partial^2 u_\theta}{\partial \theta^2} - 2\frac{\partial u_r}{\partial \theta}) + k_\theta u_\theta = f_\theta \quad \textbf{(2.9)}$$

where

h : Ring thickness (m)

R : Ring radius (m)

u_r : Ring radial displacement (m)

u_θ : Ring tangential displacement (m)

E : Young's modulus (N/m^2)

k_r : Sidewall radial stiffness (N/m^2)

k_θ : Sidewall tangential stiffness (N/m^2)

ρ : Ring density (kg/m^3)

λ : Damping coefficient (Ns/m)

$I = h^3/12$: Area inertia moment per unit width (kg/s)

p_0: Air pressure (Pa)

f_r: Distributed forces per unit width in the radial direction (N/m)

f_θ: Distributed forces per unit width in the radial direction (N/m)

A similar equation of flexible ring model can be found in the literature (Eichler, 1996). This model effectively simulates tire dynamics in the radial and tangential direction, but does not consider the displacement variation in the ring tread width. It only uses some parameters to simulate the real tire made of many materials. Eichler (1996) proposed a three-dimensional flexible ring model, where several rings are coupled by stiffness to simulate the ring tread band displacement variation. However, these flexible ring models have two common disadvantages: First, it is only valid for dynamic responses in the frequency range of 0-300 Hz. Second, it is difficult to determine the material properties required for the model.

To model the tire dynamic properties above 300 Hz, Kropp (1989) proposed an orthotropic plate model, where the tire belt is modelled as a finite plate with different tangential and lateral properties (Kropp, 1989). Pinnington and Briscoe (2002) used a one-dimensional wave equation to describe tire dynamics. The tire belt is modelled as a Timoshenko beam (see Figure 2.23), to analyze the high frequency vibration from the tire belt shear and rotational effects. However, Pinnington and Briscoe (2002) did not consider the effect of tire sidewall. Pinnington (2002) subsequently extended the model with sidewall dynamics, where the sidewall is presented in two parts:

(1) Below the ring frequency (about 400 Hz) of the sidewall there is a "static" model of a pressurized inextensible curved membrane under tension (see Figure 2.24(a)).

(2) Above the ring frequency, there is a "dynamic model" of a beam transmitting tension, bending and compression wave (see Figure 2.24(b)).

Considering that no analytical models in the existing literatures are appropriate for the modelling of radial and tangential vibrations at high frequencies with local deformation, Larsson and Kropp (2002) proposed a double-layer tire model (see Figure 2.25). The double layers are made of isotropic thick plates with tension on an elastic bed, and coupled with different thicknesses and material properties, respectively. A plate represents the unfolded tire above the spring frequency. The bedding consists of individual springs in tangential, radial and lateral directions.

(2) Numerical Models

Analytical models are useful to study the dynamic behavior of tires, but unfortunately they tend to be restricted to regular geometries and simple boundary conditions. They could not determine material parameters in the tire modelling, nor describe the complex contact between tire and pavement. Therefore, they are not suitable for the tire and pavement texture design process. Since the numerical finite-element method can effectively describe the physical structure of the tire and the complex contact between tire and pavement, it is effective to analyze the material properties of tire and pavement texture influencing the tire vibration. Numerical modelling allows the desired level of accuracy required and the associated computational time requirement to be managed simultaneously, and the entire designs to be constructed, refined and optimized. Numerical tire models have been developed in the past dozens of years (Richard, 1991; Takagi and Takanari, 1991). Richard (1991) proposed a finite element smooth tire model

below about 400 Hz, where the basic structural elements consist of isotropic rubber with a three-node triangular section and cord layers with a two-node linear section. Taking into account the tire structural symmetry, the tire is modelled by meshing only half of the section to save computation time and effort (see Figure 2.26).

Kung (1990) chose non-linear laminated shell elements with membrane and bending stiffness for modelling tire. The modes (0-250 Hz) are simulated and compared to measurements. The frequencies at which the natural modes occur are about the same as measured. However, the amplitude of the frequency response shows significant deviations from measured values. The contact with road pavement is not considered. Takagi and Takanari (1991) used plane finite elements to develop a tire model in the frequency range 0-250 Hz, which considers tire pressure, patch deformation and tire rotation. Compound linear material characteristics are used to account for different material layers. At last, the results are compared to measurements. Unfortunately, there were large difference between computed and measured values.

Recently, Brinkmeier et al. (2004) used the arbitrary Lagrange–Eulerian (ALE) formulation to determine the complex eigenvalues and modes of a stationary rolling tire in ground contact, which is depicted in Figure 2.27. In this methodology, the rotation of the tire is accounted for by letting the material flow through the mesh and the deformation of the tire due to the tire-pavement contact is accounted for by a deformation of the (non-rotating) mesh. This approach also saves computation effort and time, but its main shortcoming is that commercial finite element packages such as ADINA and ANAYSIS do not provide finite element code for arbitrary Lagrange–Eulerian formulation to build solid model.

44

Furthermore, A Wideguide Finite Element Method (WFEM) approach has been proposed in which the tire is regarded as a wideguide in the circumferential direction (Nilsson, 2004). A conventional finite element method is used to model the cross-section of the waveguide. Then, a wave equation is used to describe the wave propagation in the circumferential direction. The main advantage of this approach is the low computation cost incurred.

More recently, Wang (2009) and Wang (2011) developed a three-solid multi-layer tire model by commercial finite element code. A tire is modeled as a composite structure including rubber and reinforcement. Wang (2009) proposed a static three-solid truck rib tire model using Lagrangian formulation (as shown in Figure 2.28), which was solved by ADINA commercial finite element code. The model was used to evaluate the stress distribution on contact patch at the static state. Furthermore, Wang (2011) developed a steady three-dimensional rolling truck tire model using an Arbitrary Lagrangian Eulerian (ALE) formulation, which was solved by ABAQUS commercial finite element code (as shown in Figure 2.29). It was used to evaluate the mechanisms of load distribution on contact patch under various tire loading and rolling conditions. The predicted results have illustrated that the three-solid tire model can accurately evaluate the contact stress between tire and pavement. However, due to the lack of researches on tire dynamics by three-solid materials, three-solid tire model cannot be effectively evaluated for tire dynamic simulation.

2.5.4 Pavement Modeling

Sandberg and Ejsmont (2002) divided tire-pavement noise generation mechanisms into two groups: mechanical and aero-dynamical mechanisms. They are coupled together to

function as noise sources. As input stimuli to these mechanisms, a reliable prediction of vertical, longitudinal and lateral stresses distribution on tire-pavement contact area is of importance. In the past decades, conventional pavement analytical approaches have always assumed that contact vertical pressure is equal to tire inflation pressure uniformly distributed on the contact surface between tire and pavement (Yoder, 1994). To date, this assumption is still prevalently used in many empirical pavement design procedures. In addition, it is frequently assumed in pavement design analyses that tire load is stationary (Huang, 1993; AASHTO, 1996).

The assumptions of uniform contact stress distribution and stationary tire are inappropriate for pavement design and pavement performance prediction. These assumptions ignore the fact that localized tire-pavement contact stresses could influence the development of pavement ruts and in the initiation and propagation mechanisms of cracking in pavements. Experimentally, Lippmann (1985) noted that vertical contact stress distribution at the tire-pavement contact interface is non-uniform and this finding was further verified by De Beer et al. (1997). However, these studies were based on static loading conditions and could not adequately describe the real traffic conditions where vehicles are moving (i.e. tires are rolling).

Compared to the numerous experimental studies on static tire-pavement contact, relatively few experiments were conducted for a rolling tire loading on pavement surface (De Beer, 1994; De Beer et al., 1997; Douglas et al., 2000; Douglas, 2009). De Beer (1994) investigated experimentally the contact stress distributions developed when a smooth Goodyear truck tire was rolling on a pavement surface at a speed of 8 km/h under different wheel loads. It was found that the behavior of the contact stress distributions of

the rolling tire may differ significantly to that of the static tire, and speeds have little effect on the contact stress distribution of rolling tires. De Beer et al. (1997) further surmised that vertical stress profiles for pneumatic tires could be either an "n-shape" or an "m-shape" (as illustrated in Figure 2.30), depending on the type of tire (passenger car or truck), loading conditions and pavement material type and surface properties.

Experimental efforts to study tire-pavement contact stresses often consume a lot of time and are very costly. This leads researches to explore the use of numerical methods to model tire-pavement interaction. In past decades, pavement or contact modeling has been widely developed to mathematically describe tire-pavement interaction (Moore et al., 1988; Myers, 2000; Drakos, 2003; Wang, 2009; Wang 2011). In order to analyze effects of tire-pavement interaction on top-down cracking and instability rutting, Myers (2000) and Drakos (2003) numerically developed three-layers pavement systems, namely asphalt concrete, base and subgrade (as shown in Figure 2.30). The models can effectively analyze the stress distribution in the pavement layers.

On the other hand, some researches (Brinkmeier et al., 2004) focus on the contact problems between tire and pavement. Since contact occurs between pavement surface and tire, only pavement surface needs to be modeled. Originally, in the analytical model, spring and damping elements are used to simulate horizontal friction and vertical stress on pavement. Since analytical method is unable to completely simulate the complex structure, the numerical method is developed to simulate pavement surface by shell elements with infinite stiffness (Moore et al., 1988; Ong and Fwa, 2007; Fwa and Ong, 2008). Ong and Fwa (2007) simulated a numerical smooth pavement surface to analyze hydroplaning between smooth tire and smooth pavement. Moore et al. (1988) effectively

developed a numerical grooved pavement surface to research tire dynamics with pavement textures.

2.5.5 Sound Propagation Modeling

Sound dynamics problem has been widely investigated by many researchers and engineers owing to its practical engineering value. In the early days, research was mostly based on analytical and experimental studies. However, in the last few decades, with the fast development of computer technology, numerical methods have been feasible to solve the sound aerodynamics problems. Sound propagation is a very complex process. Since sound aerodynamics will vary with propagation environment, till now, there does not exist a unique method that will provide reliable sound propagation information. Many different models have been developed to describe sound dynamics in the given areas. They can generally be classified into near-field models and far-field models.

(1) Near-field Models

Taking into account ventilation around noise sources, sound propagation in near field can be effectively described by nonlinear second order partial differential equations models, including direct numerical simulation model, turbulence model and large eddy model (Chung, 2002). The complete Navier-Stokes Equations are applied, and the direct numerical simulation (DNS) model is considered as the most exact technology for sound radiation simulation (Wilcox, 2006; Seo et al., 2008). For an arbitrary volume V enclosed by a surface S with outer normal vector n, the Navier-Stokes equations can be expressed as

$$\frac{d}{dt}\int_{V}\rho dV + \int_{s}\rho(u-b)\bullet ndS = 0 \qquad\qquad (2.10)$$

$$\frac{d}{dt}\int_{V}\rho u dV + \int_{s}\rho u(u-b)\bullet ndS = \int_{s}P\bullet ndS + \int_{V}fdV \qquad\qquad (2.11)$$

$$\frac{d}{dt}\int_{V}\rho(e+\frac{1}{2}\|u\|^{2})dV + \int_{s}\rho(e+\frac{1}{2}\|u\|^{2})(u-b)\bullet ndS$$
$$= -\int_{s}q\bullet ndS - \int_{s}(P\bullet u)\bullet ndS + \int_{V}f\bullet udV \qquad\qquad (2.12)$$

where u is the fluid velocity of volume V; ρ is the fluid density of volume V; b is the velocity of the control surface S; P is the stress on the control surface S; e is the internal energy per unit of mass. For a material control volume in the Lagrangian system, we have $u\bullet n = b\bullet n$. For a fixed control volume in Eulerian system, we have $b=0$.

Mankbadi et al. (1998) used DNS model to solve a supersonic jets problem described by compressible Navier-Stokes equations (Mankbadi et al., 1998; Wendt, 2009). Seo et al. (2008) researched a direct numerical simulation procedure for cavitating flow noise. Although DNS can accurately simulate noise propagation, the discretized equations must be solved on extremely fine grids. As a result, it has a very high computation cost. Wilcox (2006) analyzes the resolution requirement of DNS and predict that the number of grid points required to fully resolve three dimensional flows is approximately proportional to $Re^{\frac{9}{4}}$ (Reynold number). For turbulence flow with Re more than 2,000, the number of the grid points to simulate this flow must be more than 20 million. Therefore, DNS is hard to solve practical complex problems due to its high computation cost.

Since air turbulence should be described by random fluctuations, statistical methods rather than deterministic methods, turbulence models, also called Reynolds average Navier-Stokes (RANS) methods, have been studied widely in the past, where time averaging of variable is carried out in order to separate the mean quantities from fluctuation. The instantaneous velocity, $u_i(x,t)$, can be expressed as the sum of a mean , $\overline{u}_i(x)$, and a fluctuating part, $u'_i(x,t)$, so that

$$u_i(x,t) = \overline{u}_i(x) + u'_i(x,t) \tag{2.13}$$

The mean quantity $U_i(x)$ is defined by

$$\overline{u}_i(x) = \frac{1}{T} \int_t^{t+T} u_i(x,t)dt \ , \ T_1 \leq T \leq T_2 \tag{2.14}$$

where T is the time period, T_1 is the maximum period of velocity fluctuations, and T_2 is the time scale characteristic of the slow variations in the flow.

When the time (Reynolds) averaging is applied to the incompressible N-S equations, one obtains the well-known RANS equations expressed as

$$\frac{\partial \overline{u}_i(x)}{\partial x_i} = 0 \ , \ \frac{\partial u'_i(x,t)}{\partial x_i} = 0 \tag{2.15}$$

$$\frac{\partial}{\partial t}(\rho \overline{u}_i) + \frac{\partial}{\partial x_j}(\rho \overline{u}_i \overline{u}_j) = -\frac{\partial \overline{p}}{\partial x_i} + \frac{\partial}{\partial x_j}(v \frac{\partial \overline{u}_i}{\partial x_j}) + \frac{\partial}{\partial x_j}(-\rho \overline{u'_i u'_j}) \tag{2.16}$$

where $\overline{p}$ is the mean stress and v is the dynamic viscosity of fluid.

50

In the RANS model, large and small scales of turbulence can be modelled on average so that fine refinements necessary for DNS are not required. They are generally used to research time independent incompressible flows. However, since sound aerodynamic problems are highly time dependent, they cannot be effectively solved by the RANS equations.

As a trade-off between DNS and RANS, large eddy simulation (LES) is the perfectly suitable method to research sound propagation problems in the near field (Wagner et al., 2007). In LES, every variable, $\phi(x,t)$, is split into resolvable large scale part (grid scale), $\overline{\phi}(x,t)$, and unresolvable small scale part (subgrid scale) , $\phi'(x,t)$, by spatial filtering operation,

$$\phi(x,t) = \overline{\phi}(x,t) + \phi'(x,t) \tag{2.17}$$

The spatial filtering operation on variable $\phi(x,t)$ to yield the filtered variable $\phi'(x,t)$ is defined by

$$\overline{\phi}(x,t) = \iiint_{R^3} G(x - \xi; \Delta)\phi(\xi,t)d\xi \tag{2.18}$$

where

$$G(x - \xi; \Delta) = \begin{cases} 1/\Delta^3, & |x_i - \xi_i| < \Delta x_i / 2 \\ 0 & \text{otherwise} \end{cases} \tag{2.19}$$

In Eq (2.13), Δ is filtered width, normally equal to mesh length.

Applying this filtering operation to incompressible flow, one obtains the following filtered N-S equations,

$$\frac{\partial \overline{u}_i}{\partial x_i} = 0 \tag{2.20}$$

$$\frac{\partial \rho \overline{u}_i}{\partial x_i} + \frac{\partial \rho \overline{u_i u_j}}{\partial x_j} = -\frac{\partial \overline{p}}{\partial x_i} + v \frac{\partial^2 \overline{u}_i}{\partial x_j \partial x_j} \tag{2.21}$$

$$\tau_{ij}^R = \rho(\overline{u_i u_j} - \overline{u}_i \overline{u}_j) \tag{2.22}$$

where $\overline{u}_i$ is the filtered velocity, and $\overline{p}$ is the filtered stress.

The above equation can be rewritten as

$$\frac{\partial \rho \overline{u}_i}{\partial x_i} + \frac{\partial \rho \overline{u}_i \overline{u}_j}{\partial x_j} = -\frac{\partial \overline{p}}{\partial x_i} + v \frac{\partial^2 \overline{u}_i}{\partial x_j \partial x_j} - \frac{\partial \rho \tau_{ij}^R}{\partial x_j} \tag{2.23}$$

The effect of small scales will appear through the residual stresses, τ_{ij}^R, which must be modelled by the SGS model (Chung, 2002). Large scales are computed and small scales are more easily modelled than in RANS. Since the large-scale turbulence is to be computed, the mesh refinements required are much more than in RANS, but less than in DNS because the small-scale turbulence is modelled.

Computational time and accuracy are the most important two aspects in numerical simulation. The higher the computation accuracy, the more computational time is required. The comparison between computational cost and accuracy in these three turbulence models are shown in Table 2.3.

(2) Far-field Models

In contrast to near-field modelling, sound simulation in the far-field does not need to consider the turbulence effect in the aerodynamic area, but focus on acoustic propagation. In acoustic far-field modelling, some reasonable approximations are allowed to achieve effective solutions with less computational cost. The existing approximate mathematical models to describe the characteristics of sound radiation include Lighthill acoustic analogy equation and Helmholtz equation (Chung, 2002; Brinkmeler et al., 2008; O'Boy and Dowling, 2009).

The Lighthill acoustic analogy equation is a vorticity mode acoustics model. It is proposed by Lighthill (1952) to simulate aerodynamic sound in the far field. Considering acoustic variable ϕ, pressure p and density ρ, as the sum of variable perturbation ϕ' and variable constant reference state ϕ_0, Lighthill rewrote N-S equations to derive the well-known Lighthill acoustic analogy equations,

$$(\frac{1}{c^2}\frac{\partial^2}{\partial t^2} - \nabla^2)[c^2(\rho - \rho_0)] = \frac{\partial^2 T_{ij}}{\partial x_i \partial x_j}$$ (2.24)

where T_{ij} is the Lighthill stress tensor given by

$$T_{ij} = \rho u_i u_j + ((p - p_0) - c^2(\rho - \rho_0))\delta_{ij} - \tau_{ij}$$ (2.25)

In the Lighthill acoustic analogy equations, the analysis aerodynamic acoustics is splitted into two steps. The first step deals with sound source generated by fluid flow in any real continuous medium. The second step is to analyze sound propagation in a acoustic medium at rest, exerted by external fluctuating sources which are a function of T_{ij}, known from the first step. The wave operator of Lighthill's analogy is limited to constant flow

53

conditions outside the source zone. No variation of density, speed of sound and Mach number is allowed.

Helmholtz equation is a pressure mode acoustic model defined by Eq (2.22). It has been applied to calculate sound propagation in tire-pavement noise simulation. Brinkmeler (2008) used weighted residual technique to derive the weak formulation of Helmholtz equation. This weak formulation is numerically solved by the infinite element method to calculate sound propagation. O'Boy and Dowling (2009) used Green's function to analytically solve Helmholtz equation to derive sound pressure levels in the observer position.

$$\nabla^2 p + \left(\frac{w}{c}\right)^2 p = 0 \qquad\qquad (2.26)$$

2.6 Research Needs and Work Scope

Based on the extensive literature review provided in this chapter, it is noted that a lot of contributions have been made to understand the generation mechanisms of tire- pavement interaction noise and provide the methods to reduce tire-pavement noise. However, they are mainly originated from experimental studies. On the other hand, although experimental studies can generate empirical relationships between the noise generated and various factors of tire-pavement interaction, they do not provide detailed engineering information (such as spatial, temporal and frequency distributions of sound pressure, contours of sound pressure, etc.) for an in-depth understanding of the mechanisms of tire-pavement noise generation. They also cannot be applied to tire and pavement types not

covered by the test conditions, nor to operating conditions and circumstances different from the experimental tests.

Based on the review, the following areas have been identified as the work scope for the present research:

1. To propose a fully-interactive near-field tire pavement noise generation-propagation model. It can be validated by experimental data from standard test methods like CPX and OBSI.

2. To evaluate the impact of pavement properties. The main research work is to develop a numerical model to analyze the effect of pavement texture and friction to tire-pavement noise.

3. To extend the numerical model to research vehicle cornering effect on tire-pavement noise.

4. To apply the proposed numerical model to perform parametric analyses on factors that may affect tire-pavement noise, and to predict tire-pavement noise likely to be generated under different vehicle operating conditions.

To focus on the modeling of interaction between tire and pavement, smooth pavement surface is first researched in this thesis by considering the PIARC smooth tire (PIARC, 2004). The proposed tire-pavement noise model is simulated by finite element methods. The data to validate the proposed model are those measured by the standard near field test method, namely CPX. The following are some assumptions made in the tire-pavement noise simulation in this research:

- The tire rolling motion along pavement is described as a combination of pure pavement horizontal translation with respect to tire and pure tire rotation around the tire axle to save computation effort used to simulate the noise radiation model.

- The wind noise influence is not considered in this research project, as the hood and wind screener is used against wind noise in the CPX and OBSI test methods.

- Constant atmosphere temperature is used in tire-pavement noise simulation in this thesis.

Table 2.1 Coefficients between tire-pavement noise and speed by Equation 2.1

Source	A	B	Remark
Ejsmont (1982)	98.2-1.95B	27…46	Passenger car tires
Steven and Pauls (1990)	26.2	32.9	Porous AC
	27.3	33.5	Porous AC
	23.4	37.3	ISO-S
	24.4	36.9	SMA
	24.6	37.2	Surface dressing
	21.9	39.9	PCC
	27.9	35.5	AC
	27.1	36.7	Asphalt
Ivannikov et al (1998)	7.1	37.6	Average of 10 truck tires, ISO surface
	11.8	36.3	Average of 10 truck tires, SMA surface
	10.7	36.8	Average of 10 truck tires, porous surface

SMA: Stone Mastic Asphalt; AC: Asphalt Concrete;
PCC: Portland Cement Concrete

Table 2.2 Differences between OBSI and CPX Methods

	Differences between OBSI and CPX Methods
1	The OBSI uses dual-microphones to measure sound intensity. The CPX method uses single microphones to measure sound pressure. OBSI could use the data from two microphones to classify the direction of sound sources.
2	Although the two methods accurately fix the microphone position, the positions specified for microphone are different. It means that the generation mechanisms will play different roles in sound tested by the two methods.
3	CPX methods use a hood to prevent the interference from other noise sources. It is not used in OBSI method.
4	OBSI method is widely used in US, while CPX method is more commonly used in other parts of the world.

Table 2.3 Comparison between Computational Cost and Accuracy in DNS, RANS and LES Turbulence Models

Turbulence Model	Computational Cost	Computational Accuracy
DNS	High	High
RANS	Low	Low
LES	Middle	Middle
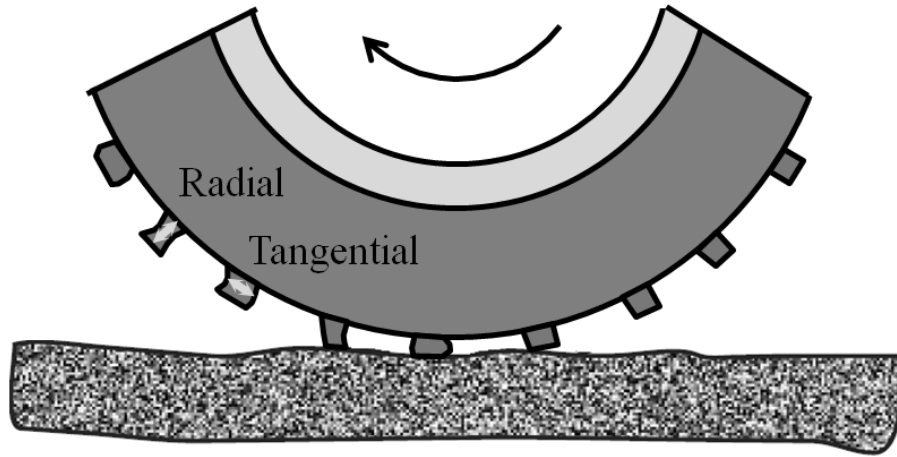
Figure 2.1 Radial and tangential vibration noise generation mechanism
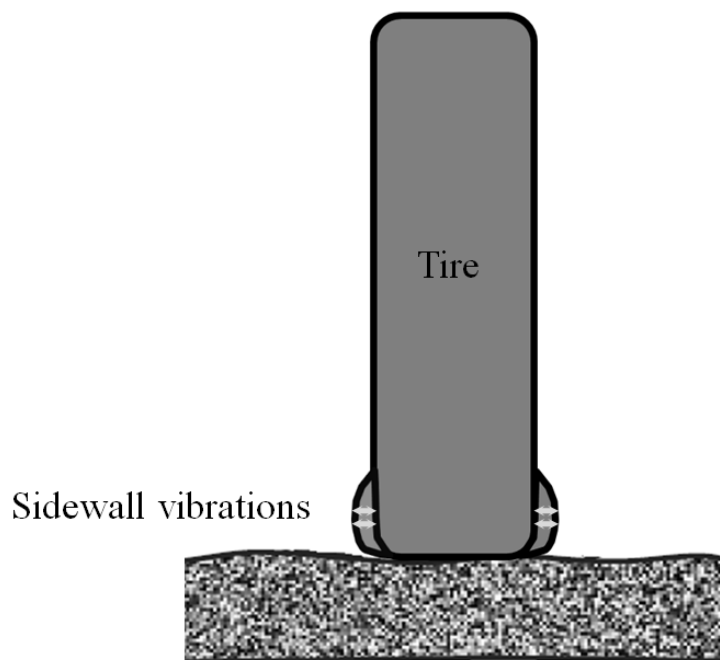
Figure 2.2 Sidewall vibration noise generation mechanism

Figure 2.3 Stick-slip noise generation mechanism
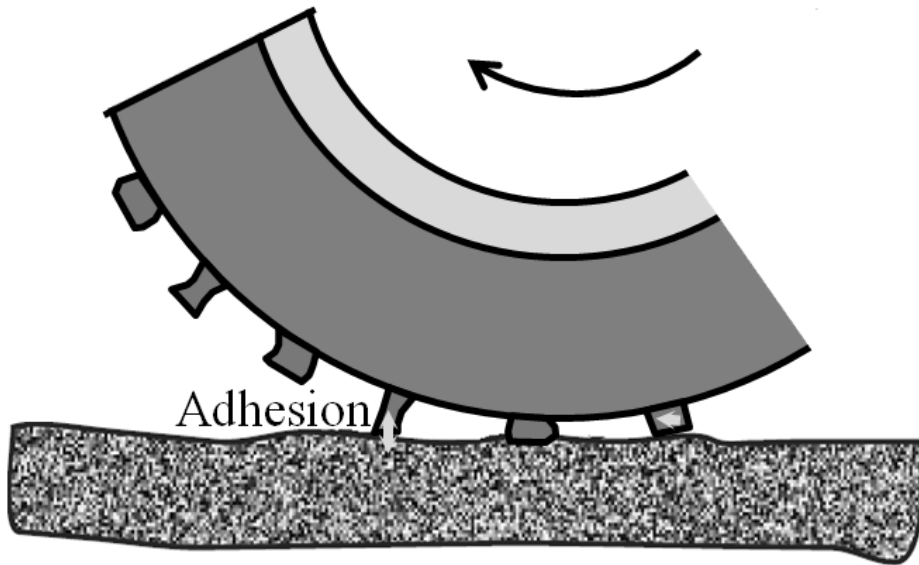
Figure 2.4 Adhesion stick-snap noise generation mechanism
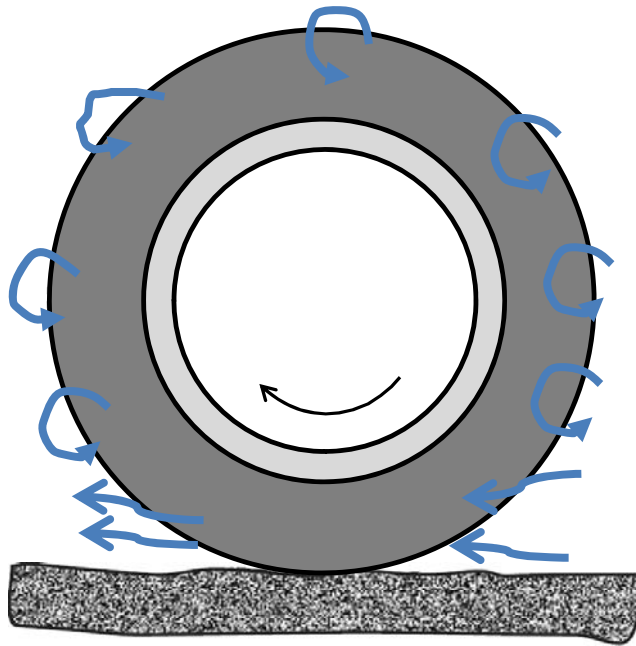
Figure 2.5 Turbulence air flow around a rolling tire
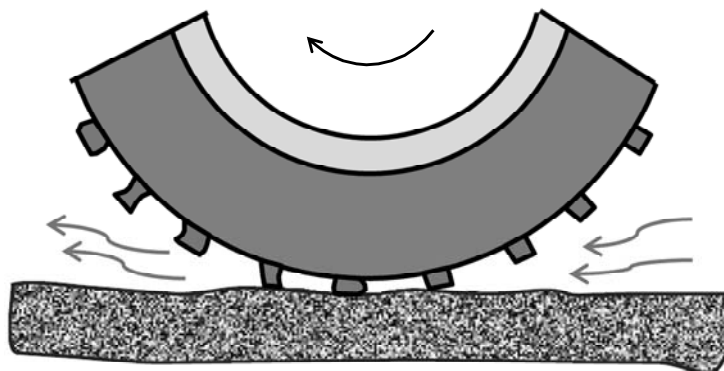
Figure 2.6 Air-pumping noise generation mechanism
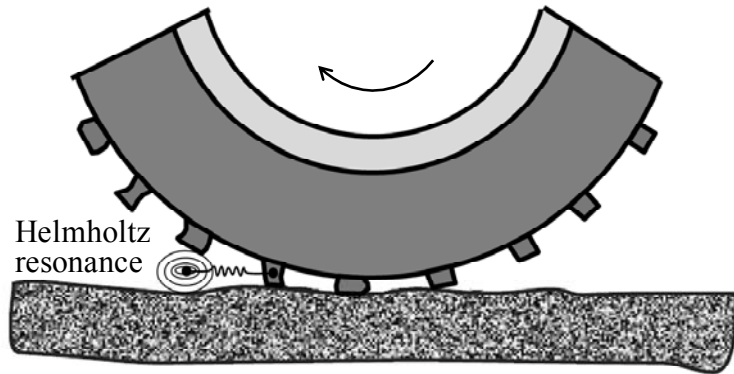
Figure 2.7 Air resonant radiation noise generation mechanism
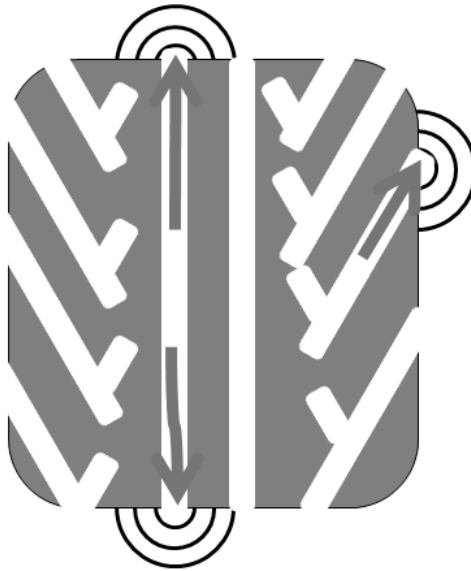
Figure 2.8 Pipe resonance noise generation mechanism
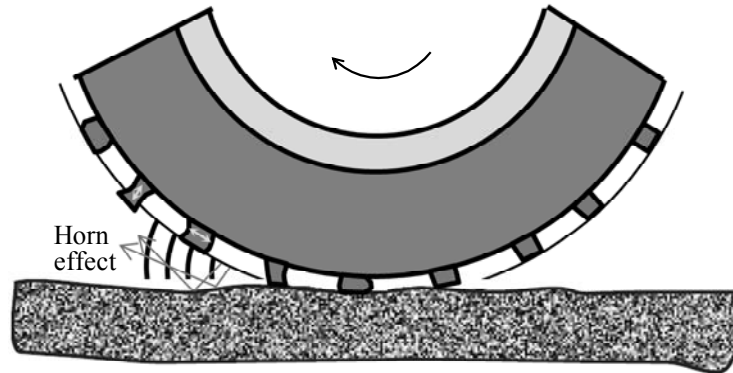
Figure 2.9 Horn effects noise generation mechanism

Changes in the Tread Pattern	Effect On:			
	A-Weighted Sound level	Frequency Spectrum		
		Level of tread impact fundamental freq.	Level of air resonance frequencies	Level of highest frequencies (4-16 khz)
Increase of groove width 2→9 mm	↑	↑	↑	↓
9→12 mm	↓	↓	●	↓
Decrease of groove angle (relative to rolling dir) 90→70°	↓	↓	↓	●
70→0°	●	↓	●	●
Addition of symmetrically diagonal grooves	●	●	●	↓
Addition of circumferential grooves to a transverse groove pattern	↓	●	↓	↓
Addition of microslots	↓ ●	↓	●	●
Opening of pocket type grooves	↓	●	↓	↓
Matching of curvilinear grooves to trailing instead of leading edge	↓	↓	●	●

↑ Increase; ↓ Decrease; ● No influence

Figure 2.10 Influence of tread pattern variation on tire-pavement noise (Ejsmont and Sandberg, 1984)
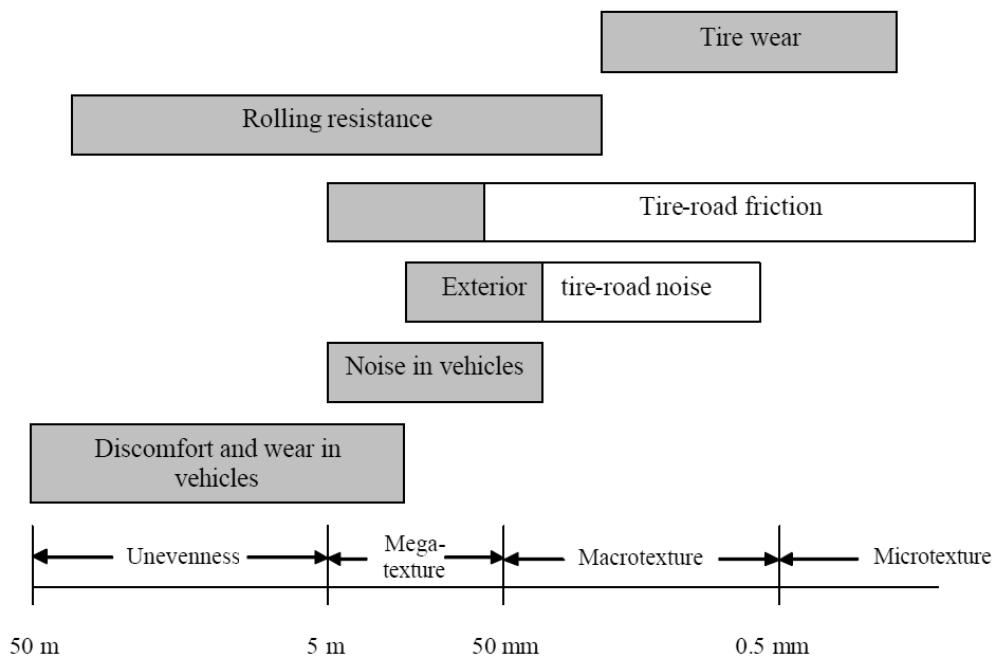
Figure 2.11 Effect of ranges of texture on tire-pavement interaction
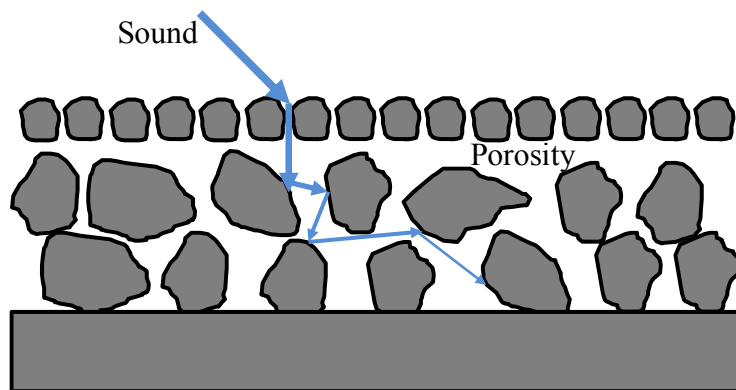
Figure 2.12. Sound absorption in the porous pavement

(a)	(b)	(c)
(d)	(e)	(f)
(g)	(h)	(i)
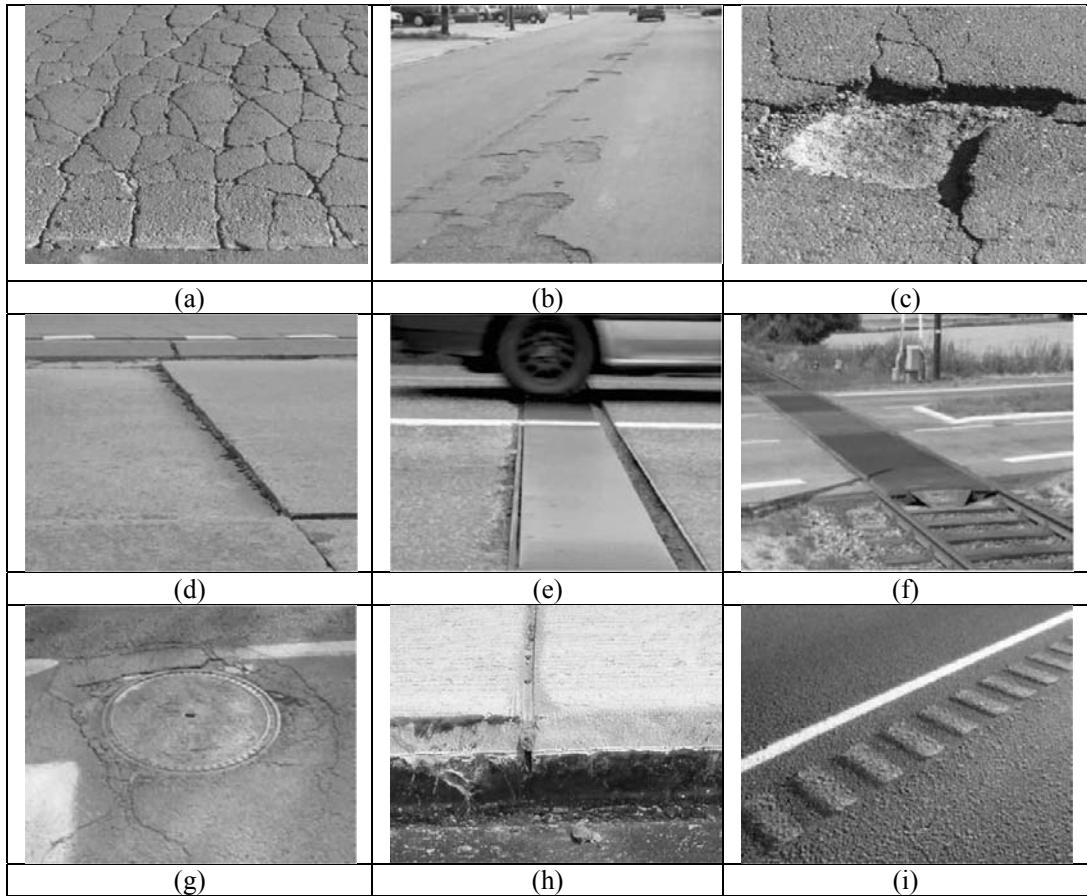
Figure 2.13 Pavement surface discontinuities
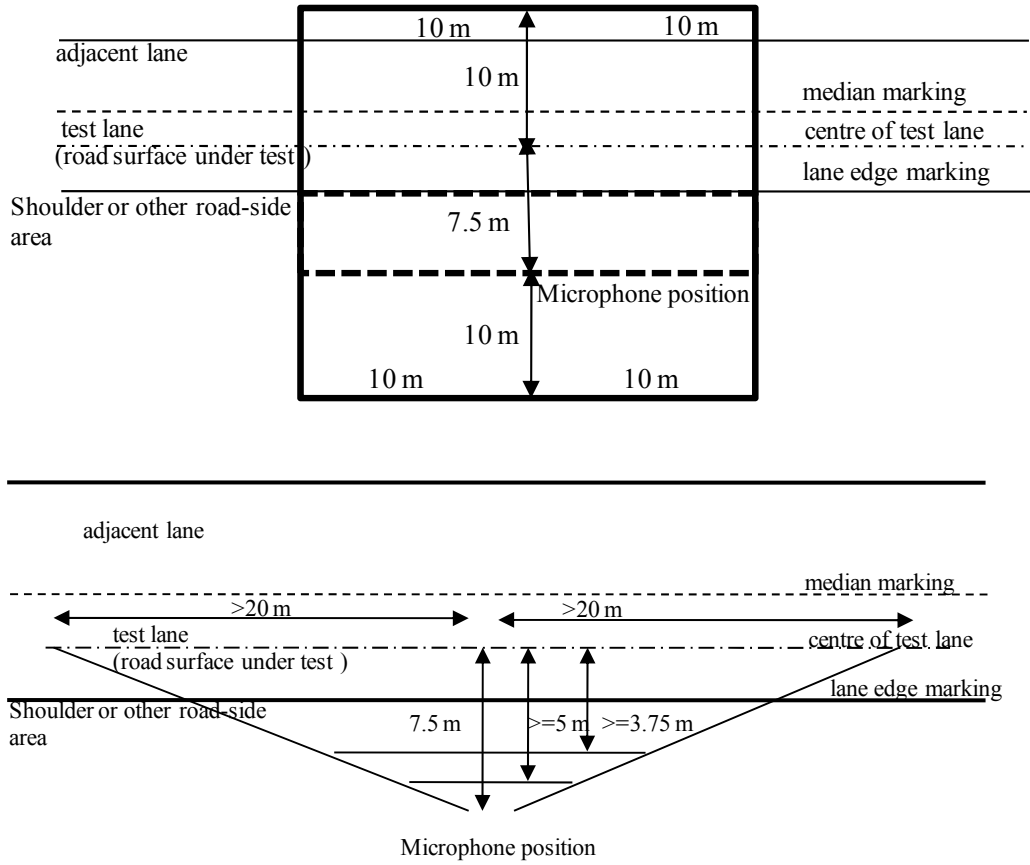
Figure 2.14 Measurement layout for statistical pass-by measurement (ISO, 1997)

Figure 2.15 CPX trailer measurement equipment (Roo et al., 2009)

Lateral View

Direction of Travel

100 mm

Tire Patch Contact with pavement

Top View

Center line of the Tire

200 mm

Microphone 2

Microphone 1

200 mm
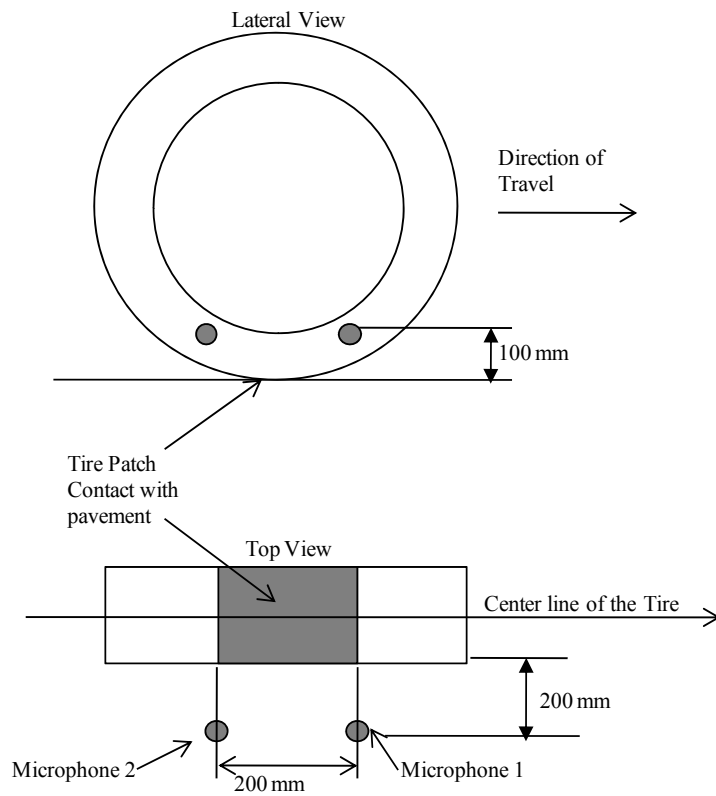
Figure 2.16 Microphone positions of CPX measurement system

67

Figure 2.17 CPX reference test tires (Avon/Copper and Dunlop) (Roo et al., 2009)

Figure 2.18 Onboard sound intensity measurement system (ASTM, 2009)
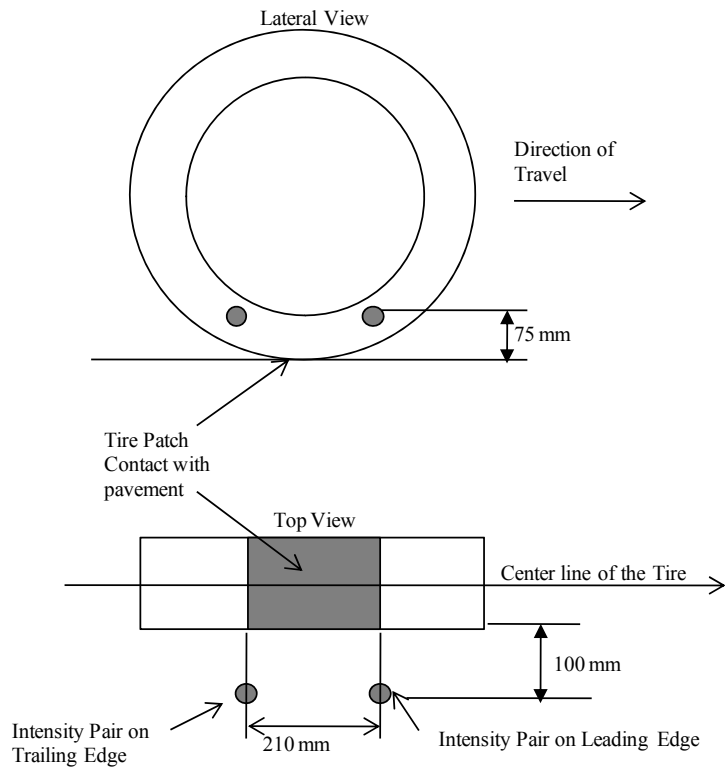
Figure 2.19 Microphone positions of OBSI measurement system

Figure 2.20 Microphone array positioning for tire noise measurement on a moving vehicle (Rasmussen and Gade, 1996)
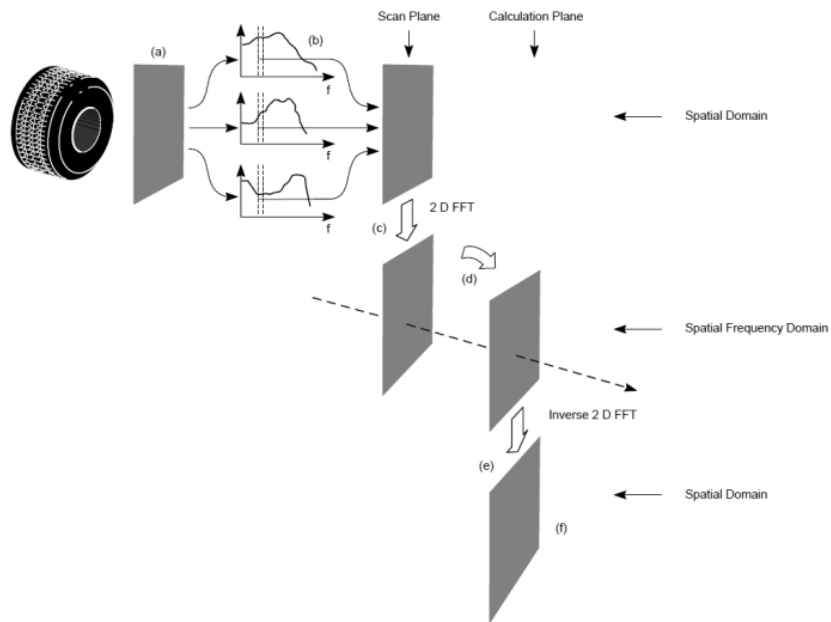
Figure 2.21 Overall principle of STSF; (a) measurement of cross-spectra in the scan plane; (b) calculation for one temporal frequency at a time; (c) 2D-spatial Fourier transformation; (d) transformation of simple wave types to other planes; (e) inverse 2D-spatial Fourier transformation; (f) to obtain the sound field in the new plane (Rasmussen and Gade, 1996)
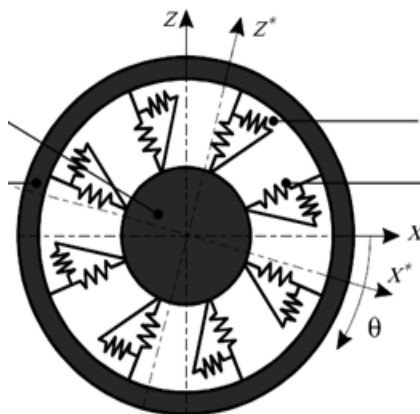
Figure 2.22 Flexible ring tire model
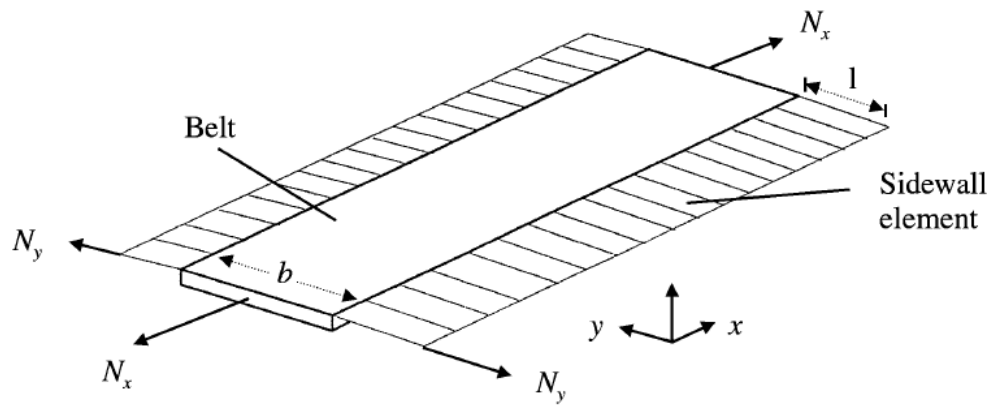
Figure 2.23 Belt and sidewall model (Pinnington and Briscoe, 2002)
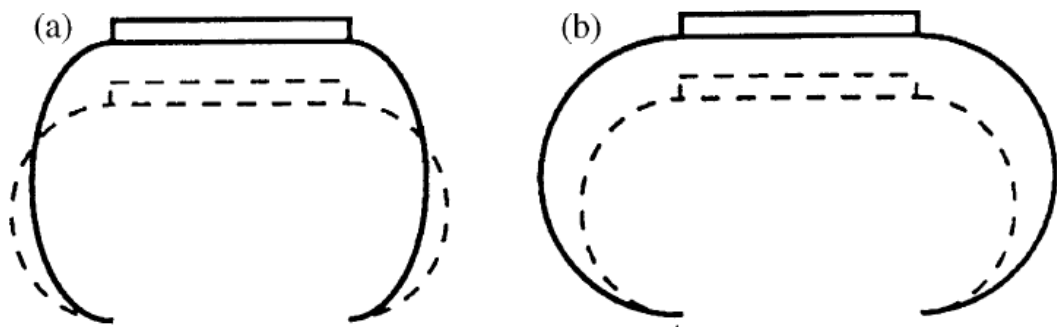
Figure 2.24 Cross-sectional deformation patterns of (a) bending, (b) stretching (Pinnington, 2002)
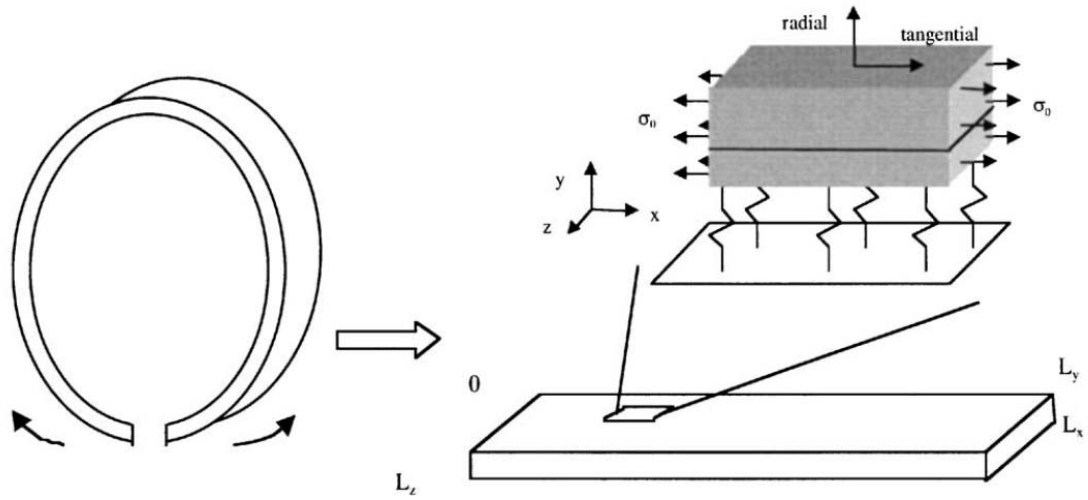
Figure 2.25 Double-layer plate tire model (Larsson and Kropp, 2002)
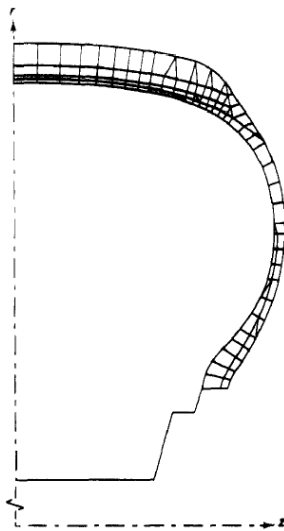
Figure 2.26 Finite element mesh for the tire section (Richard, 1991)
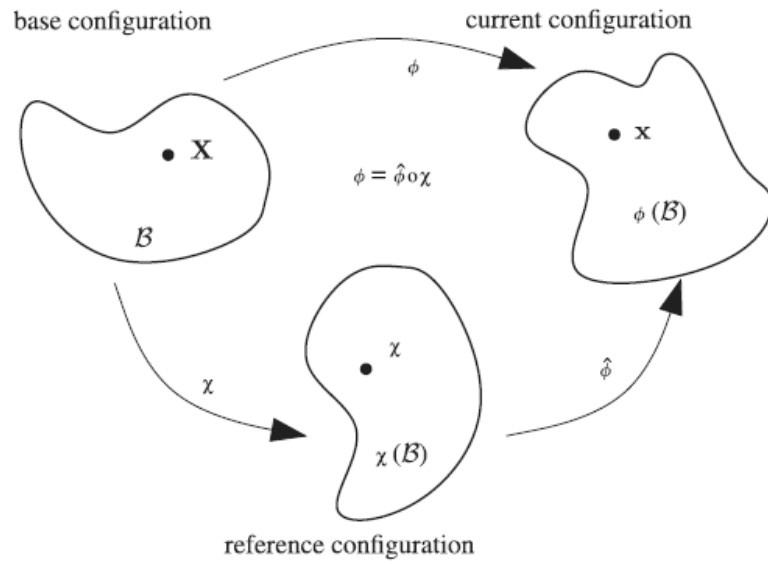
Figure 2.27 ALE reconfiguration decomposition of tire motion
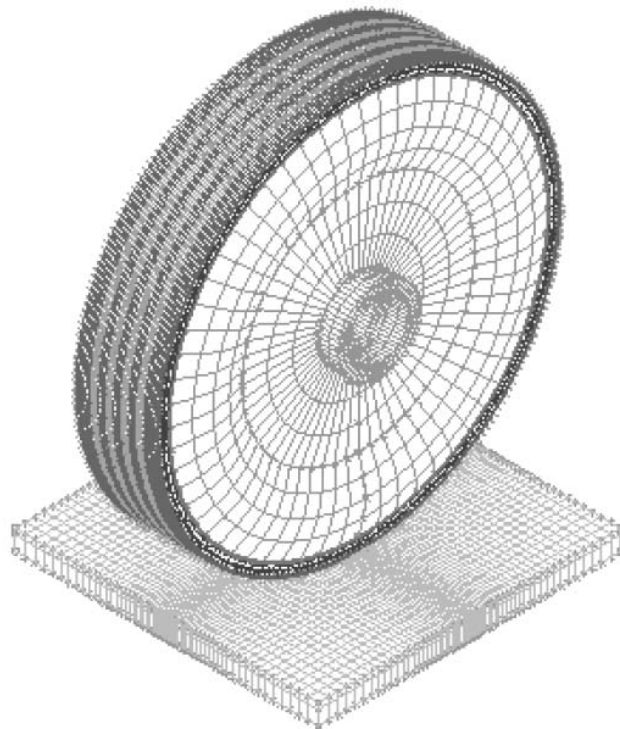
Figure 2.28 Static three solid tire-pavement interaction model (Wang, 2009)

| (a) Cross-section | (b) who tire model |
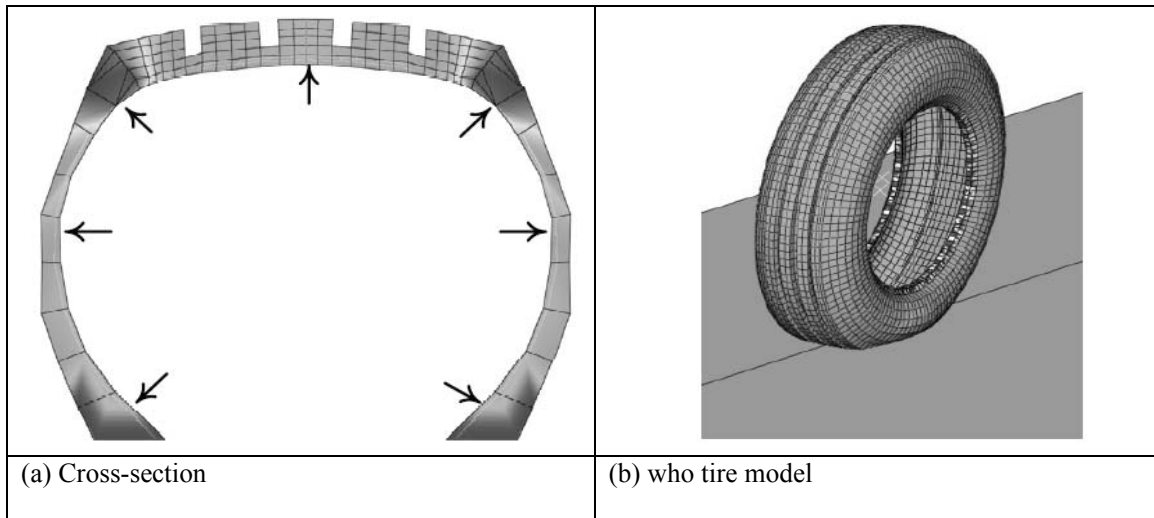
Figure 2.29 Rolling tire-pavement interaction model (Wang, 2011)
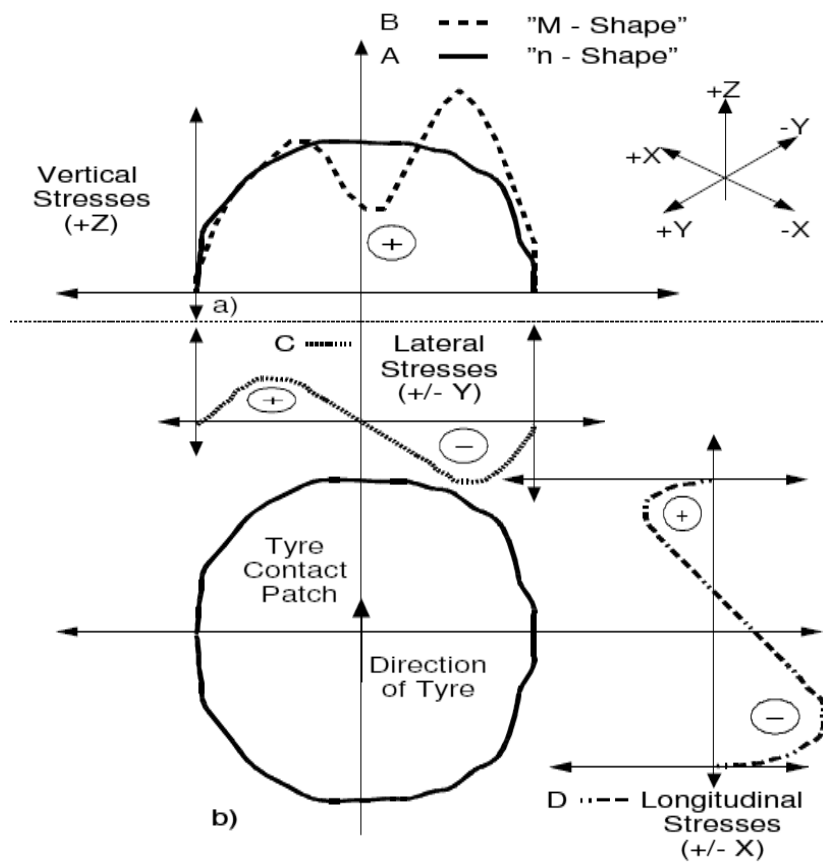
Figure 2.30 Basic three-dimensional contact stresses and basic shapes on the rolling tire from experimental observations (De Beer et al., 1997)

| (a) Thin asphalt pavement | (b) Thick asphalt pavement |
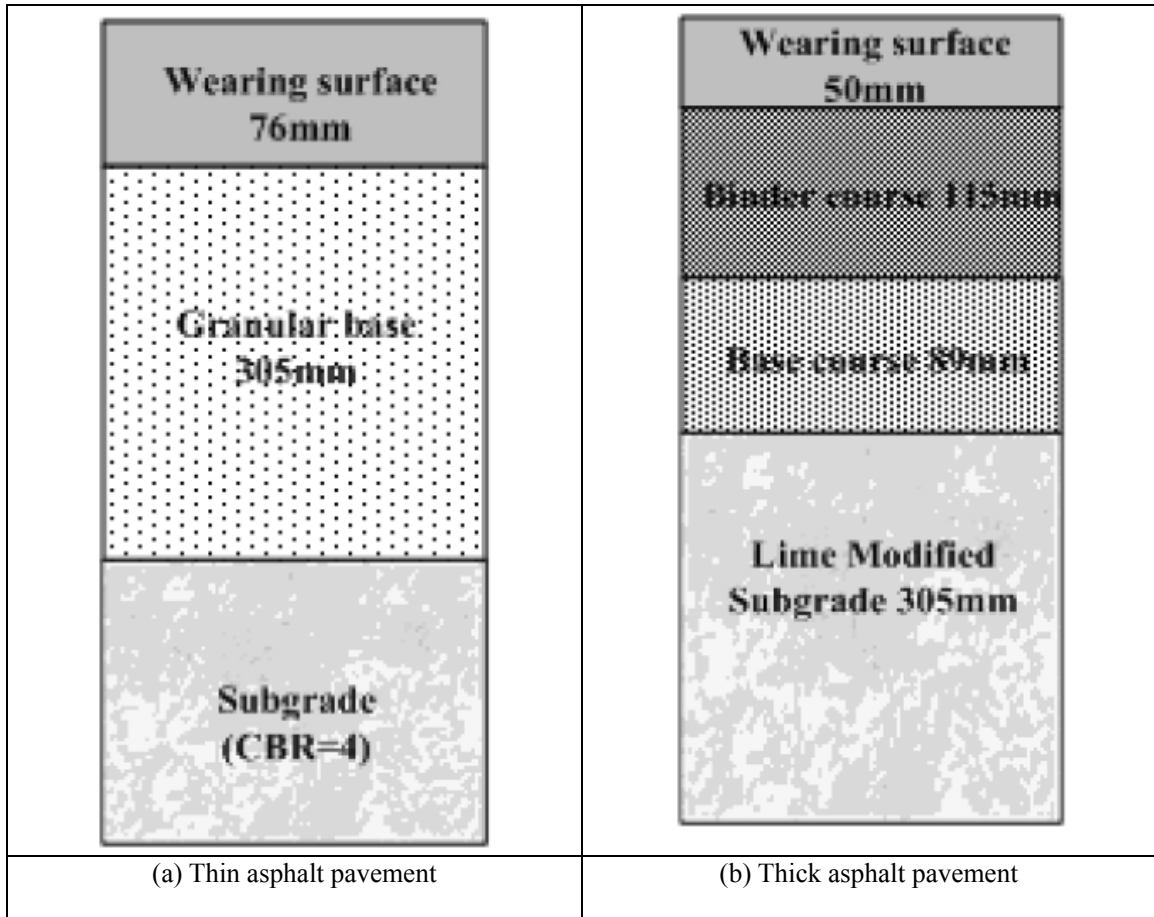
Figure 2.31 Cross sections of asphalt pavement

CHAPTER 3 Numerical Modeling of Dynamic Tire and Pavement Interaction

3.1 Introduction

For tire-pavement noise, the dominant noise generation mechanism is tire structure dynamics caused by interaction between tire and pavement. In order to study the effect of dynamic tire on tire-pavement noise, it is desirable to have models available by which tire structure dynamics can be simulated as a function of tire and pavement interaction properties, tire dynamic characteristics, and so on. In this chapter, we develop a dynamic tire and pavement interaction model. Tire dynamics is simulated by means of the widely used thin shell element, which had been proven by researchers (Kropp, 1989; O' Boy and Dowling, 2009) as an effective means to model tire vibration. The model developed in this chapter shall be used for the tire-pavement noise modeling analysis in the next chapter.

3.2 Pneumatic Tire

The modeling of rolling tire is perhaps the most important component of the tire-pavement interaction modeling and has a direct influence on the accuracy of computed contact stress distribution. In this thesis, the PIARC smooth tire shown in Figure 3.1 (a) is used. The main dimensions of PIARC smooth tire is shown in Figure 3.1 (b). The PIARC smooth tire is radially constructed with the sidewall capped with single-ply polyester, and a three-ply tread (one polyester and two steel belts). The tire properties are obtained from PIARC tire specification (PIARC, 2004).

3.3   Concept of Rolling Tire and Pavement Interaction Modeling

The rolling tire and pavement interaction modeling is a very complex process, which includes rolling tire modeling, pavement surface modeling, and rolling tire and pavement contact modeling. The rolling tire and pavement models interact with one another through the contact modeling mechanism. These sub-models allow the determination of the tire-pavement contact patch area and the stresses developed at the tire-pavement interface, as shown in Figure 3.2.

Four steps are taken to model the rolling tire and pavement interaction as explained below.

Step 1: Tire modeling

Dynamic rolling tire modeling is first developed to focus the modeling on the effect of different pavement textures on noise generation, PIARC smooth tire is considered in the present research. The tire material input parameters can be classified into three types: tire mass, tire damping ratio and tire stiffness. Tire stiffness includes tread circumference elastic modulus, tread cross-section elastic modulus, tread shear modulus, tread Poisson's ratio, sidewall circumference elastic modulus, sidewall cross-section elastic modulus, sidewall shear modulus, and sidewall Poisson's ratio.

Step 2: Pavement surface modeling

In this thesis, since contact occurs between pavement surface and tire, only the pavement surface needs to be modelled by shell elements as a massless rigid body. The pavement input parameters includes pavement mass and pavement stiffness.

Step 3: Rolling tire and pavement contact modeling

The tire and pavement contact is modelled using 3-dimentional finite element method. The contact property between tire and pavement is described by friction coefficient in this thesis. In the modeling of complex contact problems, the following shows the general features of the problems:

1) The points of contact surface are not known priori.

2) Friction can be modeled according to a pre-selected friction law.

3) Double-sided contacts are permitted.

4) Both sticking and sliding can be modeled.

Step 4: Parameter calibration

Tire property specifications provided by manufactures do not give the structural parameters of the tire model. These structural parameters have to be calibrated using actual measured structural response of tires under load.

3.4 Tire and Pavement Interaction Dynamic Numerical Modeling

3.4.1 Modeling Approach

3.4.1.1 Tire and Pavement Interaction

Shown in Figure 3.3 is a tire with its center fixed on the point O. A Lagrange frame of reference XYZ (see Figure 3.3) is used in the proposed model to analyze the dynamics of a tire moving horizontally at velocity v with a rolling angular velocity w.

The angular velocity w acting on the point O is transferred to tire tread by tire sidewall. The air pressure p' is uniformly acting on the internal surface of tire sidewall and tread. In the same time, the pavement moves horizontally with velocity $v = w \cdot \bar{r}$ and vertically with wheel load p, where $\bar{r}$ is the tire radius. The horizontal friction force f is loaded on the tire due to the relative motion between tire and pavement with speed v. The local frame of reference θxr attached on the tire tread rotates with the tire tread. The complete tire and pavement interaction model mechanism is show in Figure 3.4.

3.4.1.2 Tire Construction

A typical tire carcass consists of rubber, plies and reinforcing belts. The ply and belt are made up of flexible filaments of a high modulus cord and a matrix of rubber. In addition to the carcass rubber, a tire has tread and sidewall rubber. In steel belted radial tires such as passenger tire, the tread band forms a relatively rigid flat band. Since the tire thickness is small compared to the modal wavelength of the highest frequency of interest, transverse shear deflections of tire can be neglected in tire dynamics. Every layer of tire could be described by orthotropic material according to physical behavior and measure results (Yum and Bolton, 2007; Kropp, 1989; Pinnington and Briscoe, 2002; Muggleton, Mace, and Brennan, 2003). This kind of material has been widely used in tire dynamic simulation with an acceptable accuracy.

A tire has a multi-layer non-homogeneous and orthotropic structure. Compared with those in a single-ply system where laminated would generally twist, bend and stretch when subjected to a tensile load, the relations between stresses and strains in a multi-ply system are more complicated. Theoretically, multi-layer simulation can effectively predict the influence of a small design change on the tire response. However, practical

simulation revealed several shortcomings of multi-layer simulation. First, this method requires a lot of computation time in general. Wang (2009) used multi-layer materials to simulate the contact stress between truck tire and pavement by commercial finite element software ADINA. It took about 180 minutes CPU time per step for tire-pavement interaction, which is too long for tire-pavement noise simulation. Second, this method has a high requirement for detailed tire structure and parameter information. Multi-layer simulation is rarely used to study tire structure dynamics since the detailed tire material and structure information is usually unavailable in most cases. Third, the multi-layer FEM tire model is hardly converged due to the combination of complicated multi-layer structure and continuous rolling dynamics.

Nowadays, the limit factor for accuracy of the dynamic tire model is often appropriate input data rather than deficiencies in the model (Sabiniarz, 2011). The equivalent single layer tire simulation can avoid the above disadvantages, and has been widely used in tire dynamic simulation and tire-pavement noise simulation in the existing simulations (Yum and Bolton, 2007; Sabiniarz, 2011; Pinnington and Briscoe, 2002).Thus, a single-layer orthotropic model is used in this research to simulate tire dynamics.

3.4.2 Tire Numerical Modeling

The three dimensional stress-strain (σ - ε) relation in a single-layered ply can be expressed as

$$\sigma = [C]\varepsilon \qquad\qquad \textbf{(3.1)}$$

where

$$\sigma = \begin{bmatrix} \sigma_a \\ \sigma_b \\ \sigma_c \\ \sigma_{ac} \\ \sigma_{ab} \\ \sigma_{bc} \end{bmatrix}, \text{ and } \varepsilon = \begin{bmatrix} \varepsilon_a \\ \varepsilon_b \\ \varepsilon_c \\ \varepsilon_{ab} \\ \varepsilon_{bc} \\ \varepsilon_{ca} \end{bmatrix} = \begin{bmatrix} \dfrac{\partial u}{\partial a} \\ \dfrac{\partial v}{\partial b} \\ \dfrac{\partial w}{\partial c} \\ \dfrac{\partial u}{\partial b} + \dfrac{\partial v}{\partial a} \\ \dfrac{\partial v}{\partial c} + \dfrac{\partial w}{\partial b} \\ \dfrac{\partial w}{\partial a} + \dfrac{\partial u}{\partial c} \end{bmatrix}$$

with point displacement $[u(a,b,c) \quad v(a,b,c) \quad w(a,b,c)]^T$ in local axes system with orthogonal material axes a, b and c, as shown in Figure 3.5.

The element stress-strain matrix in local axes system (see Figure 3.5) for an anisotropic material can be derived as:

$$[C] = \begin{bmatrix} 1/E_a & -v_{ab}/E_b & -v_{ac}/E_c & 0 & 0 & 0 \\ -v_{ba}/E_b & 1/E_b & -v_{bc}/E_c & 0 & 0 & 0 \\ -v_{ca}/E_a & -v_{ca}/E_a & 1/E_c & 0 & 0 & 0 \\ 0 & 0 & 0 & 1/G_{ab} & 0 & 0 \\ 0 & 0 & 0 & 0 & 1/G_{bc} & 0 \\ 0 & 0 & 0 & 0 & 0 & 1/G_{ac} \end{bmatrix} \tag{3.2}$$

where E_i is Young's modulus, G_{ij} is shear modulus and v is Poisson's ratio. The symmetric relationship between Young's modulus and Poisson ratio is:

$$\frac{v_{ji}}{E_i} = \frac{v_{ij}}{E_j}, \quad i, j = a, b, c \tag{3.3}$$

81

In order to calculate the inverse [C], the following constraints are necessary so that the stress-strain matrix is positive-definite:

$$\left| v_{ji} \right| = \left(\frac{E_i}{E_j} \right)^{1/2} , \quad i, j = a, b, c \tag{3.4}$$

$$v_{ab} v_{bc} v_{ac} \frac{E_a}{E_c} < 0.5(1 - v_{ab}^2 \frac{E_a}{E_b} - v_{bc}^2 \frac{E_b}{E_c} - v_{ac}^2 \frac{E_a}{E_c}) \leq 0.5 \tag{3.5}$$

Using the thin shell approximation (neglecting transverse shear deformation), the simpler form for stress-strain matrix Equation 3.2 can be shown below:

$$[C] = \begin{bmatrix} 1/E_a & -v_{ab}/E_b & 0 \\ -v_{ba}/E_a & 1/E_b & 0 \\ 0 & 0 & 1/G_{ab} \end{bmatrix} \tag{3.6}$$

By inverting the matrix [C], one can express stress as a function of strain as shown:

$$[Q] = \begin{bmatrix} Q_{11} & Q_{12} & 0 \\ Q_{12} & Q_{22} & 0 \\ 0 & 0 & Q_{66} \end{bmatrix} \tag{3.7}$$

and

$$\begin{aligned} Q_{11} &= E_a / (1 - v_{ab} v_{ba}) \\ Q_{12} &= v_{ab} E_b / (1 - v_{ab} v_{ba}) \\ Q_{22} &= E_b / (1 - v_{ab} v_{ba}) \\ Q_{66} &= G_{ab} \end{aligned} \tag{3.8}$$

where the cord directions labeled by a and the direction perpendicular to the cord labeled by b form an axis system referred to as the principal material directions of a ply.

Since, in general, the ply loading direction on the tire does not coincide with the principle

material direction, it is necessary to employ the equations governing the transformation of second order tensor.

$$\left\{ \begin{array}{c} \sigma_a \\ \sigma_a \\ \tau_{ab} \end{array} \right\} = [T] \left\{ \begin{array}{c} \sigma_\theta \\ \sigma_x \\ \tau_{\theta x} \end{array} \right\} \tag{3.9}$$

where

$$[T] = \begin{bmatrix} m^2 & n^2 & 2mn \\ n^2 & m^2 & -2mn \\ -mn & mn & (m^2 - n^2) \end{bmatrix} \tag{3.10}$$

where m=cos θ, n=sin θ.

Substituting Equation 3.10 into Equation 3.6, we can obtain stress-strain matrix in the local principle material direction:

$$\left\{ \begin{array}{c} \sigma_\theta \\ \sigma_x \\ \tau_{\theta x} \end{array} \right\} = [T]^{-1}[Q][T] \left\{ \begin{array}{c} \varepsilon_\theta \\ \varepsilon_x \\ \varepsilon_{\theta x} \end{array} \right\} = [\overline{Q}] \left\{ \begin{array}{c} \varepsilon_\theta \\ \varepsilon_x \\ \varepsilon_{\theta x} \end{array} \right\} = \begin{bmatrix} \overline{Q}_{11} & \overline{Q}_{12} & 0 \\ \overline{Q}_{12} & \overline{Q}_{22} & 0 \\ 0 & 0 & \overline{Q}_{66} \end{bmatrix} \left\{ \begin{array}{c} \varepsilon_\theta \\ \varepsilon_x \\ \varepsilon_{\theta x} \end{array} \right\} \tag{3.11}$$

where

$$\begin{aligned}
\overline{Q}_{11} &= Q_{11}m^4 + 2(Q_{12} + 2Q_{66})n^2m^2 + Q_{22}n^4 \\
\overline{Q}_{12} &= (Q_{11} + Q_{22} - 4Q_{66})n^2m^2 + Q_{12}(n^4 + m^4) \\
\overline{Q}_{22} &= Q_{11}n^4 + 2(Q_{12} + 2Q_{66})n^2m^2 + Q_{22}m^4 \\
\overline{Q}_{16} &= (Q_{11} - Q_{12} - 2Q_{66})nm^3 + (Q_{12} - Q_{22} + 2Q_{66})n^3m \\
\overline{Q}_{26} &= (Q_{11} - Q_{12} - 2Q_{66})n^3m + (Q_{12} - Q_{22} + 2Q_{66})nm^3 \\
\overline{Q}_{66} &= (Q_{11} + Q_{22} - 2Q_{12} - 2Q_{66})n^2m^2 + Q_{66}(n^4 + m^4)
\end{aligned} \tag{3.12}$$

A tire is composed of several plies at various cord angles bonded together in a prescribed stacking sequence. The relations connecting stresses and strains in a multi-ply system are

complicated compared to a single-ply system where laminates would generally twist and bend, as well as stretch, when subjected to a tensile load.

The classical thin laminated shell theory assumes that a cross section originally straight and perpendicular to the reference surface of the shell remains straight and perpendicular to the reference surface in the deformed state. Under these assumptions, the strains at any point in a shell can be related to the displacements and curvatures of the reference surface.

Consider a carcass ply composed of N ply, see Figure 3.6. For the k-th ply, Equation 3.11 can be written by

$$
\left\{
\begin{array}{c}
\sigma_\theta \\
\sigma_x \\
\tau_{\theta x}
\end{array}
\right\}_k
= [\overline{Q}]_k
\left\{
\begin{array}{c}
\varepsilon_\theta \\
\varepsilon_x \\
\varepsilon_{\theta x}
\end{array}
\right\}
\tag{3.13}
$$

where all matrices must have the subscript k for the orientation of the particular ply with respect to the shell coordinate and its unique $\overline{Q}$. Based on these assumptions, the components of the displacement for the shell can be represented as the translations and rotations of the linear element. For the case with no transverse shear deformation, the stress-strain relations become

$$
\left\{
\begin{array}{c}
\sigma_\theta \\
\sigma_x \\
\tau_{\theta x}
\end{array}
\right\}_k
= [\overline{Q}]_k
\left\{
\begin{array}{c}
\varepsilon_{\theta_0} + x_\theta z \\
\varepsilon_{x_0} + x_x z \\
\varepsilon_{\theta x_0} + x_{\theta x} z
\end{array}
\right\}
\tag{3.14}
$$

where ε_i are the middle surface strains, x_i is the shell curvatures. The thermal and hydrothermal strains are ignored.

84

It is convenient to deal with resultant forces and moments acting on a shell cross-section rather than on individual stress components because the tire carcass consists of several layers. It is assumed that the stresses are linearly distributed through the thickness of each layer in a thin elastic laminated shell. Thus, the use of equivalent stress and moment resultants eliminates the variations with respect to the thickness and makes it possible to apply a two-dimensional theory instead of a three-dimensional theory.

Stress and moment resultants can be formulated in terms of the middle surface strains and curvatures by integrating Equation 3.14 over each lamina and summing the resulting expressions over N laminas

$$
\begin{Bmatrix} N_\theta \\ N_x \\ N_{\theta x} \end{Bmatrix} = \sum_{k=1}^{n} \int_{h_{k-1}}^{h_k} \begin{Bmatrix} \sigma_\theta \\ \sigma_x \\ \tau_{\theta x} \end{Bmatrix}_k dz
$$

$$
= \sum_{k=1}^{n} \left\{ [\overline{Q}]_k \begin{Bmatrix} \varepsilon_{\theta_0} \\ \varepsilon_{x_0} \\ \varepsilon_{\theta x_0} \end{Bmatrix} \int_{h_{k-1}}^{h_k} dz + [\overline{Q}]_k \begin{Bmatrix} x_\theta \\ x_x \\ x_{\theta x} \end{Bmatrix} \int_{h_{k-1}}^{h_k} z dz \right\}
$$

$$
= [A][\varepsilon_0] + [B][x]
$$

(3.15)

By the same operation as above, the moment resultants can be found

$$
\begin{Bmatrix} M_\theta \\ M_x \\ M_{\theta x} \end{Bmatrix} = \sum_{k=1}^{n} \int_{h_{k-1}}^{h_k} \begin{Bmatrix} \sigma_\theta \\ \sigma_x \\ \tau_{\theta x} \end{Bmatrix}_k z dz
$$

$$
= \sum_{k=1}^{n} \left\{ [\overline{Q}]_k \begin{Bmatrix} \varepsilon_{\theta_0} \\ \varepsilon_{x_0} \\ \varepsilon_{\theta x_0} \end{Bmatrix} \int_{h_{k-1}}^{h_k} z dz + [\overline{Q}]_k \begin{Bmatrix} x_\theta \\ x_x \\ x_{\theta x} \end{Bmatrix} \int_{h_{k-1}}^{h_k} z^2 dz \right\}
$$

$$
= [B][\varepsilon_0] + [D][x]
$$

(3.16)

85

Thus, the shell constitutive equations are:

$$\begin{Bmatrix} N_\theta \\ N_x \\ N_{\theta x} \\ M_\theta \\ M_x \\ M_{\theta x} \end{Bmatrix} = \begin{bmatrix} A_{11} & A_{12} & A_{16} & B_{11} & B_{12} & B_{16} \\ A_{21} & A_{22} & A_{26} & B_{21} & B_{22} & B_{26} \\ A_{61} & A_{62} & A_{66} & B_{61} & B_{62} & B_{66} \\ B_{11} & B_{12} & B_{16} & D_{11} & D_{12} & D_{16} \\ B_{21} & B_{22} & B_{26} & D_{21} & D_{22} & D_{26} \\ B_{61} & B_{62} & B_{66} & D_{61} & D_{62} & D_{66} \end{bmatrix} \begin{Bmatrix} \varepsilon_{\theta_0} \\ \varepsilon_{x_0} \\ \varepsilon_{\theta x_0} \\ x_\theta \\ x_x \\ x_{\theta x} \end{Bmatrix} \qquad \textbf{(3.17)}$$

where the value of the individual elements of the sub-matrices can be calculated in terms of the transformed reduced stiffness matrix as follows:

$$A_{ij} = \sum_{k=1}^{n} [\overline{Q_{ij}}]_k (h_k - h_{k-1}) \ (i,j = 1,2,6) \qquad \textbf{(3.18)}$$

$$B_{ij} = \frac{1}{2} \sum_{k=1}^{n} [\overline{Q_{ij}}]_k (h_k^2 - h_{k-1}^2) \ (i,j = 1,2,6) \qquad \textbf{(3.19)}$$

$$D_{ij} = \frac{1}{3} \sum_{k=1}^{n} [\overline{Q_{ij}}]_k (h_k^3 - h_{k-1}^3) \ (i,j = 1,2,6) \qquad \textbf{(3.20)}$$

$$E_x = \dfrac{\begin{vmatrix} A_{11} & A_{12} & A_{16} & B_{11} & B_{12} & B_{16} \\ A_{21} & A_{22} & A_{26} & B_{21} & B_{22} & B_{26} \\ A_{61} & A_{62} & A_{66} & B_{61} & B_{62} & B_{66} \\ B_{11} & B_{12} & B_{16} & D_{11} & D_{12} & D_{16} \\ B_{21} & B_{22} & B_{26} & D_{21} & D_{22} & D_{26} \\ B_{61} & B_{62} & B_{66} & D_{61} & D_{62} & D_{66} \end{vmatrix}}{\begin{vmatrix} A_{22} & A_{26} & B_{12} & B_{22} & B_{26} \\ A_{26} & A_{66} & B_{16} & B_{26} & B_{66} \\ B_{12} & B_{16} & D_{11} & D_{12} & D_{16} \\ B_{22} & B_{26} & D_{12} & D_{22} & D_{26} \\ B_{26} & B_{66} & D_{16} & D_{26} & D_{66} \end{vmatrix}} \dfrac{1}{h} \tag{3.21}$$

$$E_y = \dfrac{\begin{vmatrix} A_{11} & A_{12} & A_{16} & B_{11} & B_{12} & B_{16} \\ A_{21} & A_{22} & A_{26} & B_{21} & B_{22} & B_{26} \\ A_{61} & A_{62} & A_{66} & B_{61} & B_{62} & B_{66} \\ B_{11} & B_{12} & B_{16} & D_{11} & D_{12} & D_{16} \\ B_{21} & B_{22} & B_{26} & D_{21} & D_{22} & D_{26} \\ B_{61} & B_{62} & B_{66} & D_{61} & D_{62} & D_{66} \end{vmatrix}}{\begin{vmatrix} A_{12} & A_{16} & B_{11} & B_{12} & B_{16} \\ A_{16} & A_{66} & B_{16} & B_{26} & B_{66} \\ B_{11} & B_{16} & D_{11} & D_{12} & D_{16} \\ B_{12} & B_{26} & D_{12} & D_{22} & D_{26} \\ B_{16} & B_{66} & D_{16} & D_{26} & D_{66} \end{vmatrix}} \dfrac{1}{h} \tag{3.22}$$

$$G_{xy} = \dfrac{\begin{vmatrix} A_{11} & A_{12} & A_{16} & B_{11} & B_{12} & B_{16} \\ A_{21} & A_{22} & A_{26} & B_{21} & B_{22} & B_{26} \\ A_{61} & A_{62} & A_{66} & B_{61} & B_{62} & B_{66} \\ B_{11} & B_{12} & B_{16} & D_{11} & D_{12} & D_{16} \\ B_{21} & B_{22} & B_{26} & D_{21} & D_{22} & D_{26} \\ B_{61} & B_{62} & B_{66} & D_{61} & D_{62} & D_{66} \end{vmatrix}}{\begin{vmatrix} A_{11} & A_{12} & B_{11} & B_{12} & B_{16} \\ A_{12} & A_{22} & B_{12} & B_{22} & B_{26} \\ B_{11} & B_{12} & D_{11} & D_{12} & D_{16} \\ B_{12} & B_{22} & D_{12} & D_{22} & D_{26} \\ B_{16} & B_{26} & D_{16} & D_{26} & D_{66} \end{vmatrix}} \dfrac{1}{h} \tag{3.23}$$

$$v_{xy} = \dfrac{-\begin{vmatrix} A_{12} & A_{26} & B_{12} & B_{22} & B_{26} \\ A_{16} & A_{66} & B_{16} & B_{26} & B_{66} \\ B_{11} & B_{16} & D_{11} & D_{12} & D_{16} \\ B_{12} & B_{26} & D_{12} & D_{22} & D_{26} \\ B_{16} & B_{66} & D_{16} & D_{26} & D_{66} \end{vmatrix}}{\begin{vmatrix} A_{22} & A_{26} & B_{12} & B_{22} & B_{26} \\ A_{26} & A_{66} & B_{16} & B_{26} & B_{66} \\ B_{12} & B_{16} & D_{11} & D_{12} & D_{16} \\ B_{22} & B_{26} & D_{12} & D_{22} & D_{26} \\ B_{26} & B_{66} & D_{16} & D_{26} & D_{66} \end{vmatrix}} \tag{3.24}$$

A total of 51 nodes for the tire in the meridional direction were used to model the tire cross-section. The other nodes were generated by rotating the basic 51 nodes trough 360° circumferentially in equal angular steps. The tire model has 80 divisions along the circumferential direction. The tire mesh design had a total of 8320 elements. The tire-pavement interaction model with mesh division is shown in Figure 3.7.

For the modeling of the pneumatic tire, three structural components, namely tire rim, tire sidewalls and tire tread, are considered. The tire rim is considered to be a rigid body. The tire sidewalls and treads are assumed to be orthotropic elastic materials with composite elastic properties. Their structural properties are characterized by the following parameters: elastic modulus, shear modulus, and Poisson's ratios. Figure 3.8 shows the meshes of these element groups, and the tire-pavement interaction model with the selected mesh division is shown in Figure 3.7.

3.4.3 Pavement Surface Modeling

Pavement surface is modelled as a rigid surface that does not deform under the action of the tire load, and fixed in all translational and rotational directions except translation in the transverse direction. Shell elements are used for flat surface modeling. Four-node

quadrilateral shape single shell elements are used to model plane pavement surface in the ADINA software (ADINA, 2009). Pavement material is assumed to be a massless rigid body. One shell element is sufficient to describe the surface dynamics of the smooth pavement.

3.4.4   Modeling of Tire-Pavement Interaction

The dynamic interaction between tire and pavement is a two-body contact problem. The complexity of contact phenomena is due to the fact that the vertical and tangential contact tractions at the interface are unknown a priori, and the actual contact area is also unknown. A general two-body Ω_i , $i = 1, 2$, contact is shown in Figure 3.9. S_u is the surface over which Dirichlet boundary conditions are specified and S_f the surface with Neumann boundary conditions. S^I is the surface area of body I that can come into contact with body J, and S^J the surface of body J that can potentially be in contact with S^J . Together S^I and S^J make a contact surface pair. ${}^tS_c$ is the actual contact area common to both S^I and S^J at the time of consideration.

The governing equations to describe the contact condition between tire and pavement at time t, which is obtained by virtual work principle, is (Baig, 2006)

$$
\begin{aligned}
&\sum_i \left\{ \int_{{}^tV} \rho_i \ddot{\mathbf{u}}_i \cdot \delta \mathbf{u}_i \mathrm{d}{}^tV \right\} + \sum_i \left\{ \int_{{}^tV} c_i \dot{\mathbf{u}}_i \cdot \delta \mathbf{u}_i \mathrm{d}{}^tV \right\} + \sum_i \left\{ \int_{{}^tV} {}^t\boldsymbol{\tau}_i \cdot \delta \mathbf{e}_i \mathrm{d}{}^tV \right\} = \\
&\sum_i \left\{ \int_{{}^tV} {}^t\mathbf{f}_i^{\mathrm{B}} \cdot \delta \mathbf{u}_i \mathrm{d}{}^tV + \int_{{}^tS_f} {}^t\mathbf{f}_i^{\mathrm{S}} \cdot \delta \mathbf{u}^S \mathrm{d}{}^tS \right\} + \int_{{}^tS_c} {}^t\mathbf{f}^{\mathrm{C}} \cdot (\delta \mathbf{u}^{\mathrm{P}} - \delta \mathbf{u}^{\mathrm{T}}) \mathrm{d}{}^tS
\end{aligned}
\tag{3.25}
$$

where, for pavement P and tire T with $i = \mathrm{P}$ or T , ρ_i is the density, c_i is the damping ratio, ${}^t\boldsymbol{\tau}_i$ is the stress tensor, $\delta \mathbf{e}_i$ is the strain corresponding to the virtual displacements

89

$\delta \mathbf{u}_i$, ${}^t \mathbf{f}_i^B$ is body forces per unit volume, ${}^t \mathbf{f}_i^S$ is surface force per unit area acted on ${}^t S_f$, ${}^t \mathbf{f}^C$ is surface force per unit area on contact surface ${}^t S_c$.

Since pavement is assumed to be massless rigid and body forces are ignored, we have

$$
\begin{aligned}
&\int_{{}^t V} \rho_P \ddot{\mathbf{u}}_P \cdot \delta \mathbf{u}_P \mathrm{d}^t V = 0 \\
&\int_{{}^t V} c_P \dot{\mathbf{u}}_P \cdot \delta \mathbf{u}_P \mathrm{d}^t V = 0 \\
&\int_{{}^t V} {}^t \boldsymbol{\tau}_P \cdot \delta \mathbf{e}_P d^t V = 0 \\
&\int_{{}^t V} {}^t \mathbf{f}_P^B \cdot \delta \mathbf{u}_P \mathrm{d}^t V = 0 \\
&\int_{{}^t V} {}^t \mathbf{f}_T^B \cdot \delta \mathbf{u}_T \mathrm{d}^t V = 0 \\
&\int_{{}^t S_f} {}^t \mathbf{f}_P^S \cdot \delta \mathbf{u}_P^S \mathrm{d}^t S - \int_{{}^t S_c} {}^t \mathbf{f}^C \cdot \delta \mathbf{u}_P \mathrm{d}^t S = 0
\end{aligned}
\tag{3.26}
$$

Therefore, Equation (3.25) can be rewritten as

$$
\begin{aligned}
&\int_{{}^t V} \rho_T \ddot{\mathbf{u}}_T \cdot \delta \mathbf{u}_T \mathrm{d}^t V + \int_{{}^t V} c_T \dot{\mathbf{u}}_T \cdot \delta \mathbf{u}_T \mathrm{d}^t V + \int_{{}^t V} {}^t \boldsymbol{\tau}_T \cdot \delta \mathbf{e}_T d^t V = \\
&+ \int_{{}^t S_f} {}^t \mathbf{f}_T^S \cdot \delta \mathbf{u}_T^S \mathrm{d}^t S - \int_{{}^t S_c} {}^t \mathbf{f}^C \cdot \delta \mathbf{u}^T \mathrm{d}^t S
\end{aligned}
\tag{3.27}
$$

Pavement surface interacts with rolling tire through the contact surface S_c. Contact behavior has a great effect on tire dynamic performance. The vector of contact force acting on S_c can be described as

$$
{}^t \mathbf{f}^C = \lambda \mathbf{n} + t \mathbf{s}
\tag{3.28}
$$

where $\mathbf{n}$ is a unit vector outward normal to contact surface S_C, $\mathbf{s}$ is a unit vector tangential to contact surface S_C. λ and t satisfy

$$
t = \tau u \lambda
\tag{3.29}
$$

90

$$\lambda = {}^{t}\mathbf{f}^{C} \cdot \mathbf{n} \tag{3.30}$$

$$t = {}^{t}\mathbf{f}^{C} \cdot \mathbf{s} \tag{3.31}$$

where u is the dynamic frictional coefficient, τ is a non-dimensional frictional variable with $|\tau| \leq 1$. $|\tau| < 1$ implies that there is no relative tangential displacement between tire and pavement on their contact patch.

A set of equations to govern the dynamic motion of rolling tire are originally obtained in local coordinate system $r\theta x$ by Soedel (1993). They are transformed into main coordinate systems XYZ. By using the principle of virtual work and including contact forces with pavement, we obtain a governing matrix equation of tire structure as follows:

$$^{t}\mathbf{M}(\rho_{\text{tire}})\ddot{\mathbf{u}} + {}^{t}\mathbf{C}(c_{\text{tire}})\dot{\mathbf{u}} + {}^{t}\mathbf{K}(k_{\text{tire}})\mathbf{u} = {}^{t}\mathbf{R} - {}^{t}\mathbf{F} \tag{3.32}$$

where $^{t}\mathbf{M}$ is a mass matrix function of tire density parameter ρ_{tyre}, $^{t}\mathbf{C}$ is a damping ratio matrix function of tire damping ratio parameters c_{tyre}, $^{t}\mathbf{K}$ is a stiffness matrix function of tire stiffness parameters k_{tyre}, $^{t}\mathbf{R}$ is external force vector and $^{t}\mathbf{F}$ is internal nodal force vector.

The dynamic equilibrium equation can be expressed in the frequency domain as:

$$[-w^{2}\,{}^{t}\mathbf{M}(\rho_{\text{tire}}) + jw\,{}^{t}\mathbf{C}(c_{\text{tire}}) + {}^{t}\mathbf{K}(k_{\text{tire}})]\{\mathbf{U}(w)\} = \{{}^{t}\mathbf{R}(w)\} - \{{}^{t}\mathbf{F}(w)\} \tag{3.33}$$

where w is phase frequency.

By setting $\mathbf{C}(c_{\text{tire}})$ and $\{{}^{t}\mathbf{R}(w)\} - \{{}^{t}\mathbf{F}(w)\}$ to be zero, the free undamped vibrating system for equation (3.30) can be described as:

$$[-\lambda \, ^{t}\mathbf{M}(\rho_{\text{tire}}) + \, ^{t}\mathbf{K}(k_{\text{tire}})]\{\text{U}(w)\} = 0 \tag{3.34}$$

Based on the modal superposition principle,

$$\{\text{U}\} = \sum_{i=1}^{n} \{\phi\}_{i} q_{i} = [\phi]\{q\} \tag{3.35}$$

where the modal matrix $[\phi]$ is defined as $[\{\phi\}_{1} \quad \{\phi\}_{2} \quad \cdots \quad \{\phi\}_{n}]$, and q_{i} is complex modal amplitudes.

The subspace iteration method (Bathe, 2006) is used to decouple the governing equation (3.29), which can be rewritten in the modal coordinate form:

$$\ddot{\mathbf{u}}_{i} + 2\varsigma_{i} w_{i} \dot{\mathbf{u}}_{i} + w_{i}^{2}\overline{\mathbf{u}}_{i} = \Phi_{i}^{\text{T}} \, ^{t}\mathbf{R} - \Phi_{i}^{\text{T}} \, ^{t}\mathbf{F} \tag{3.36}$$

where w_{i} is the eigenvalue for modal i, $\{\phi\}_{i}$ is modeshape for modal i and ς_{i} is the modal damping ratio.

3.5 Tire Parameters Identification

For tire and pavement interaction dynamic simulation, tire parameters mainly include tire mass, tire damping ratio and tire stiffness. Tire stiffness includes tread circumference elastic modulus, tread cross-section elastic modulus, tread shear modulus tread poisson's ratio, sidewall circumference elastic modulus, sidewall cross-section elastic modulus, sidewall shear modulus and sidewall poisson's ratio.

Tire mass and damping ratios are the key parameters for wave vibration and transmission on the tire surface. Tire mass could be obtained from the PIARC smooth tire specification (PIARC, 2004), approximately equal to 1200 kg/m^{3}. Tire damping ratio is difficult to

estimate. In the existing experiment literature (Kindt et al., 2009; Gong 1993; Kim et al., 2007), the damping ratio of the passenger tire is around 0.04, which is used in this simulation for all frequencies.

Tire stiffness is a major element in several noise-generation mechanisms such as roughness excitation and friction (Kropp, 1989). In order to identify the unknown tire stiffness parameters, genetic algorithms (GAs) are employed in this study. The hybrid GA-FEM strategy is illustrated in Figure 3.10.

In this hybrid strategy, an essential aspect in the parametric correction procedure is the estimation of initial population. To estimate the appropriate initial population, the approach described by Nettles (1994) is used to obtain the expected equivalent single-layer expected tire stiffness values from laminated tire materials. The PIARC smooth tire is radially constructed with the sidewall capped with single-ply polyester, and a three-ply tread (one polyester and two steel belts). The expected stiffness values of PIARC smooth tire is illustrated in Table 3.1. An initial population is randomly generated in the region of ±20% expected values. For the current investigation, the bounds on tire stiffness parameters were set at about ±90% of the expected values. The GA parameter is given in Table 3.2.

In order to identify these parameters, the calibration process should be performed to make the contact patch obtained from the simulation approximately the same as the actual footprint of a tire on a dry pavement under the same load in the static state. The tire governing equation (3.29) can be written as

$$ {}^{t}\mathbf{K}(k_{tyre})\mathbf{u} = {}^{t}\mathbf{R} - {}^{t}\mathbf{F} \tag{3.37} $$

93

The fitness function for the tire stiffness calibration can be described as:

$$\textbf{Objective: } \text{Min}\{\underset{i=1,\ldots,N}{\text{Max}} \{\text{Max} \left\{ \begin{array}{l} \left|[Se_i]^{1/2} - [Ss_i(k_{tyre})]^{1/2}\right| / [Se_i]^{1/2}, \\ \left|We_i - Ws_i(k_{tyre})\right| / We_i, \\ \left|Le_i - Ls_i(k_{tyre})\right| / Le_i \end{array} \right\} \}\} \qquad \textbf{(3.38)}$$

Subject to: Equation (3.34)

where Se_i is the experimental contact patch area in the load i, $Ss_i(k_{tyre})$ is the simulation contact patch area with tire stiffness parameters k_{tyre} in the load i. We_i is the experimental contact patch width in the load i, $Ws_i(k_{tyre})$ is the simulation contact patch width with tire stiffness parameters k_{tyre} in the load i. Le_i is the experimental contact patch length in the load i, $Ls_i(k_{tyre})$ is the simulation contact patch length with tire stiffness parameters k_{tyre} in the load i. N is the number of tire loads. In this work, three loads (3980 N, 2920 N and 1980 N) are used for the calibration process. The iteration process is terminated when the maximum fluctuation of computed results is less than 10%. The comparison between predicted and measured contact patch shapes is illustrated in Figure 3.11.

Finally, we obtain the calibrated tire stiffness parameters shown in Table 3.3. Table 3.4 illustrates the comparison between simulated and experiment contact footprints for those static wheel loads considered in the study.

Based on the above tire parameters, the low order mode eigenfrequencies are calculated based on Equation 3.30 and compared with experimental data of similar tires, as shown in

94

Figure 3.12. The corresponding three dimensional mode shapes of tire tread are depicted in Figure 3.13.

3.6 Summary

The dynamic FEM tire model developed in this chapter provides an accurate prediction of the tire dynamics behavior for tire-pavement noise. The model is theoretically based and is able to describe the dynamic behavior of the tire tread and sidewall.

Study of the different existing tire-road noise models highlighted the difficulty to obtain reasonable material properties for the models. The problem parameters for the proposed tire model have been discussed in detail. The known parameters are obtained based on the standard tire specification. The unknown parameters are estimated using a comprehensive FEM-GA strategy, where initial parameters are calculated based on the equivalent multi-layers plate method. The experimental footprint area is chosen as the fitness function in the genetic algorithm for parameters calibration. With the final calibrated parameters, tire footprint areas under different wheal loads could be obtained with less than 10 % error.

In order to evaluate the effectiveness of the proposed model, we make a comparison between our model and other existing typical models as shown in Table 3.5 (Kropp et al., 2012; Wang, 2009). Kropp et al. (2012) model can accurately tire dynamics by frequency domain method, but this model can only simulate linear properties. It cannot study nonlinear property effects like nonlinear material and nonlinear contact between tire and pavement. The time domain model proposed in this thesis can effectively simulate

nonlinear contact between tire and pavement. It can also be extended to consider nonlinear material in tire modeling conveniently.

Wang (2009) developed a tire-domain solid model to simulate tire-pavement contact stress, and used trial and error method to calibrate the tire materials. Although this method can accurately simulate the contact stress, it is hardly used to simulate tire dynamics in the literature due to very high computational cost. In contrast, though the simplified model in this thesis has relatively lower accuracy, it is feasible for tire pavement noise simulation, since this method has been widely applied to tire dynamic simulation in the literature. A heuristic algorithm is developed in this chapter to calibrate tire materials. It is more effective than trial and error method used by Wang (2009).

Table 3.1 Initial orthotropic elastic properties for tire tread and sidewalls

	Elastic Modulus(N/m^2)		Shear Modulus	Poisson's	Thickness
	Circumference	Cross-section	(N/m^2)	Ratio	(mm)
Sidewall	1.3E+08	2.6E+07	5.4E+07	0.35	10
Tread	1.0E+08	5.0E+07	2.2E+07	0.5	15

Table 3.2 Genetic algorithm parameters

Population size	Generation	Crossover probability	Mutation probability
80	1000	0.8	0.1

Table 3.3 Orthotropic elastic properties for tire tread and sidewalls

	Elastic Modulus(N/m^2)		Shear Modulus	Poisson's	Density	Thickness
	Circumference	Cross-section	(N/m^2)	Ratio	(Kg/m^3)	(mm)
Sidewall	1.5E+08	4.5E+07	1.5E+07	0.38	1200	10
Tread	1.0E+08	9.0E+07	2.5E+06	0.45	1200	15

Table 3.4 Comparison of contact area between experiment and simulation

Load(N)	Length(mm)		width(mm)		Area(mm²)		Maximm Error
	Experiment (Andrén and Jolkin 2003)	simulation	Experiment (Andrén and Jolkin 2003)	simulation	Experiment (Andrén and Jolkin 2003)	simulation	
1980	110	103	75	68	7800	7000	9%
2920	130	125	90	93	11000	9500	7%
3980	162	150	99	105	14000	13000	6%

Table 3.5 Comparison between methodology, Computation time and Material calibration method in the proposed model and existing models.

	Our model	Wang (2009)	Kropp et al. (2012)
Methodology	Time domain	Time domain	Frequency domain
Computation time	middle	high	low
Material calibration methods	YES	YES	No
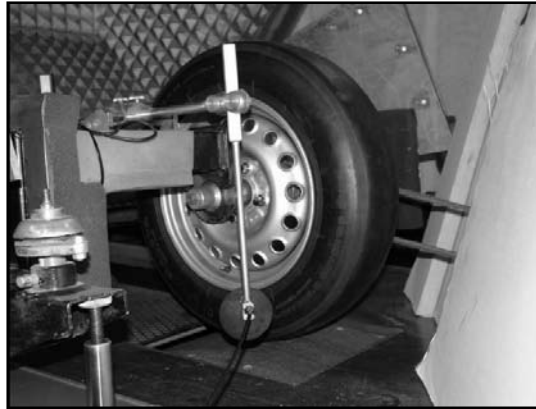
(a) Illustration of PIARC smooth tire
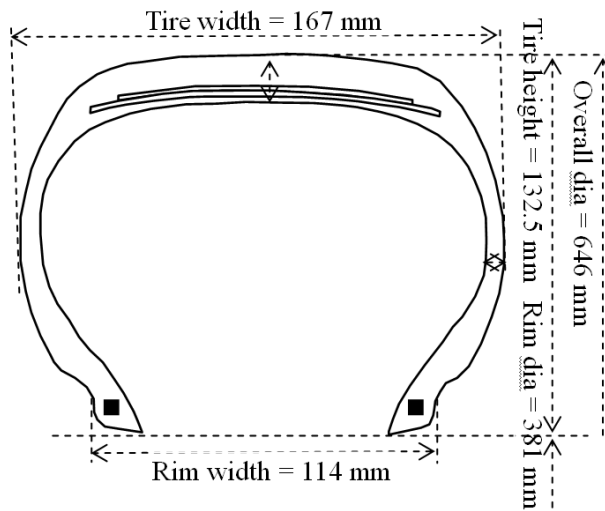
(b) Dimensions of cross-section

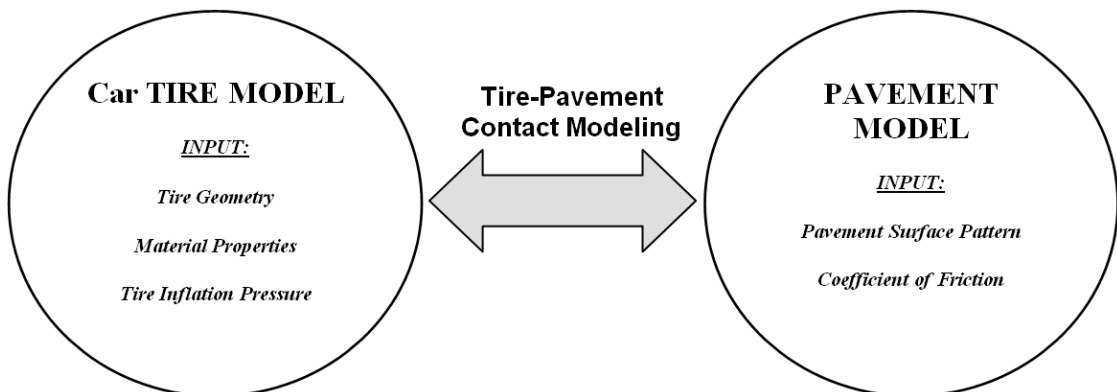**Figure 3.1 Main dimensions of PIARC smooth tire (PIARC, 2004)**

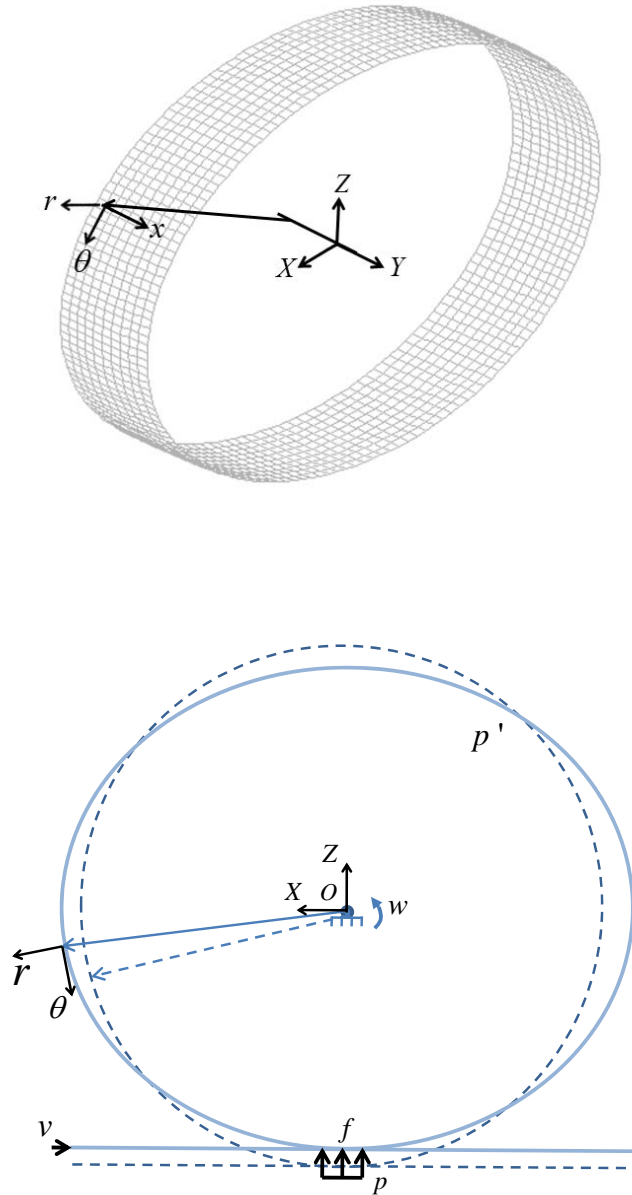**Figure 3.2. Key components of simulation model**

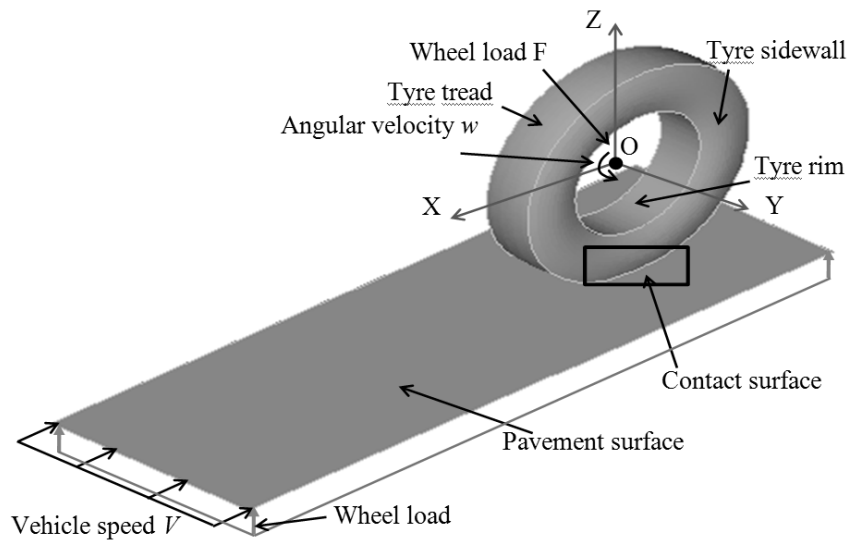**Figure 3.3 Model of shell element of tire tread**

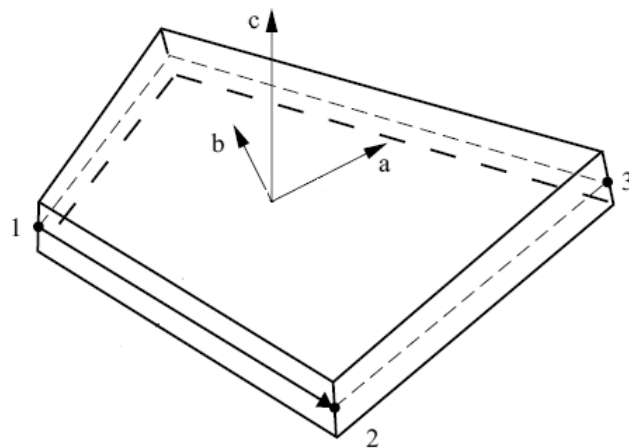**Figure 3.4. Complete tire and pavement interaction modelling mechanism**

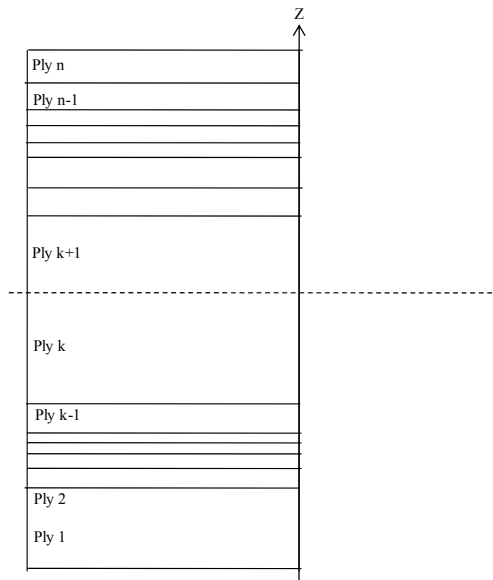**Figure 3.5 Definition of local axes system for shell elements**
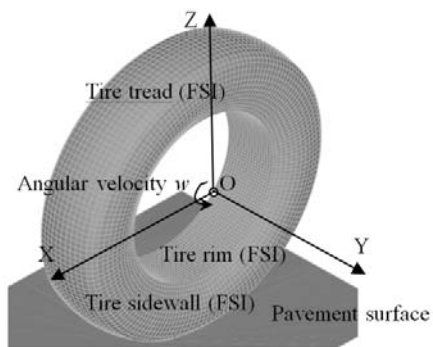
Figure 3.6 Cross section of a laminate
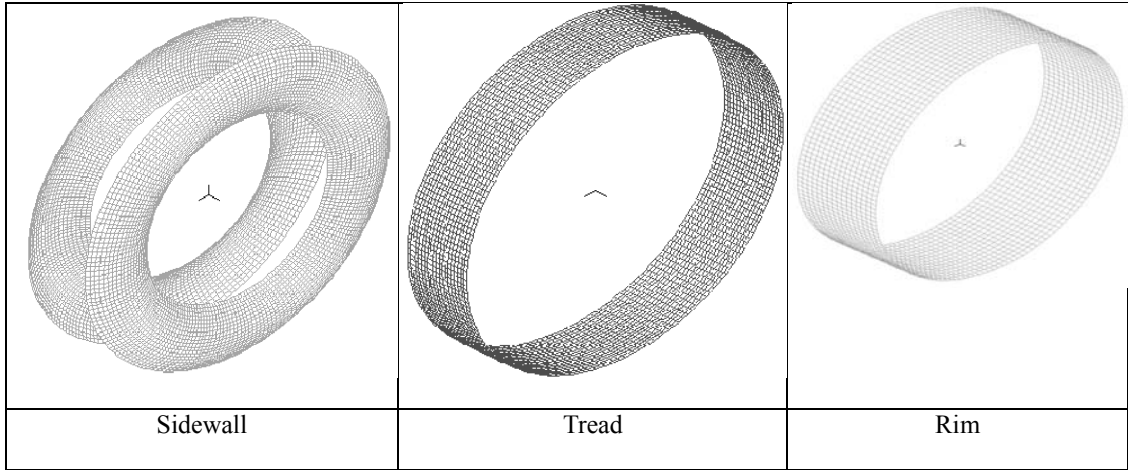

Figure 3.7 Tire pavement interaction geometry

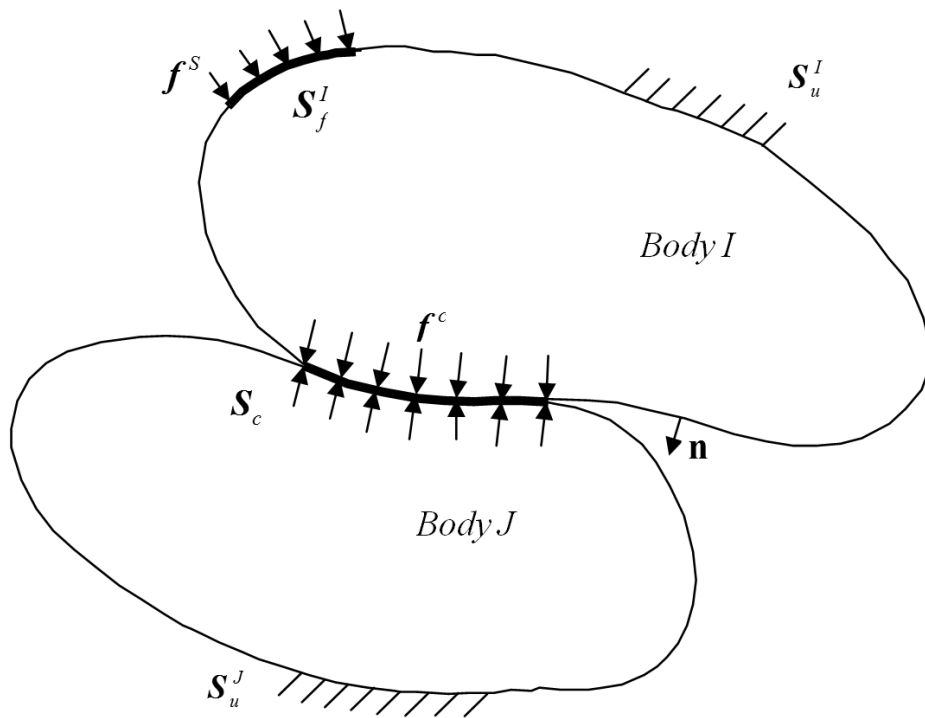| Sidewall | Tread | Rim |

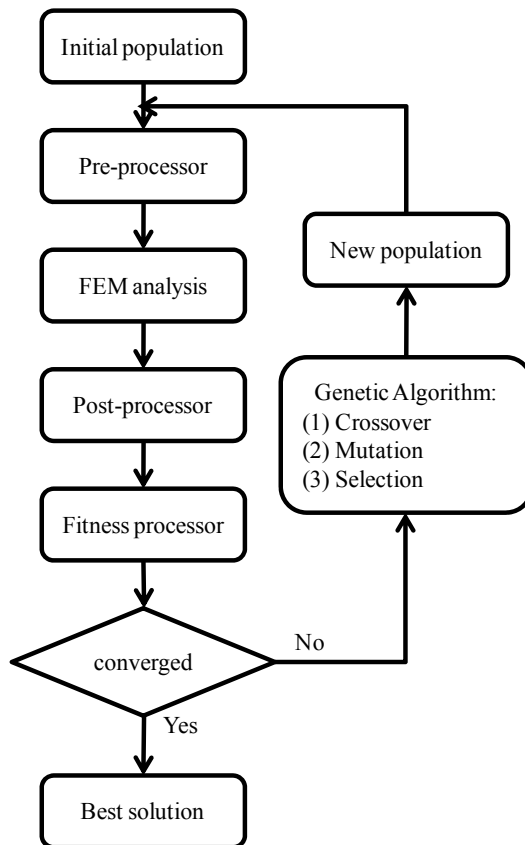**Figure 3.8 Meshes of tire element groups**

Figure 3.9 Two bodies contact
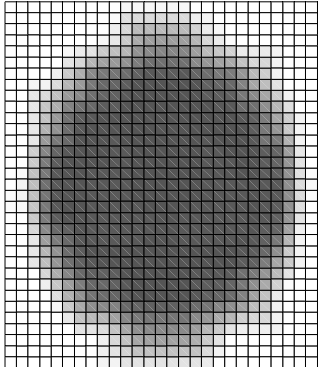
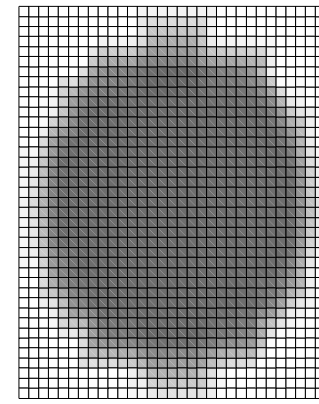**Figure 3.10 Framework of the hybrid GA-FEM strategy**
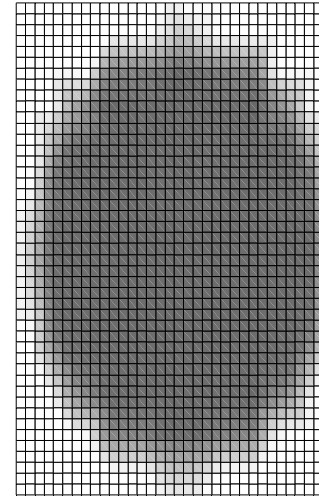
1980 N		
	(a) Simulation	(b) Experiment
2820 N		
	(a)Simulation	(b) Experiment
3980 N		
	(a) Simulation	(b) Experiment

Figure 3.11 Comparison of predicted and measured contact patch shapes

Figure 3.12 Comparison of calculated and measured eigenfrequencies along circumference

Mode (1,0) 93.6 Hz

Mode (2,0) 113.6 Hz

Mode (3,0) 126.7 Hz

Mode (4,0) 143.1 Hz

Mode (5,0) 161.5 Hz

Mode (6,0) 181.2 Hz

Figure 3.13 Calculated mode shapes of tire tread

CHAPTER 4   Development of Tire-Pavement Noise Model

4.1 Introduction

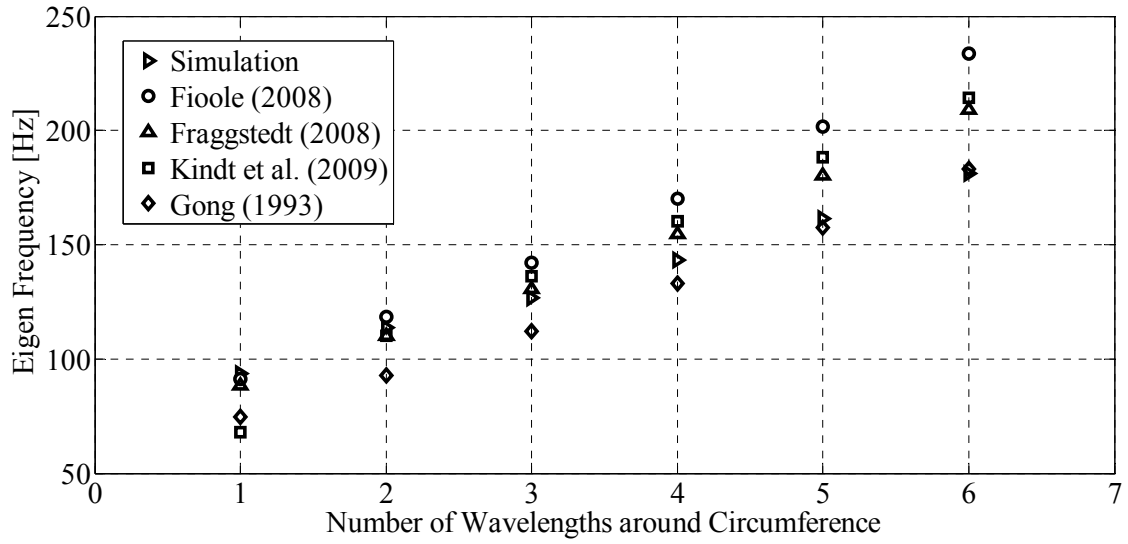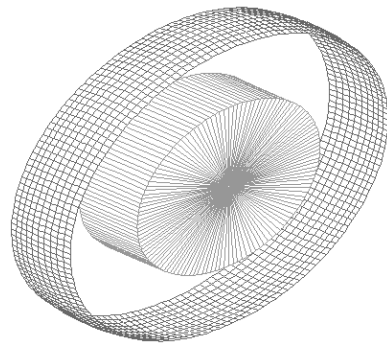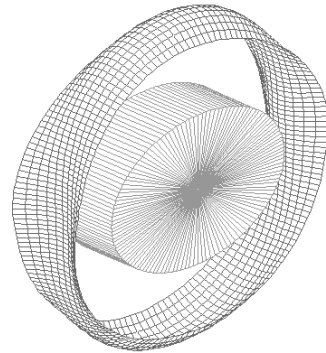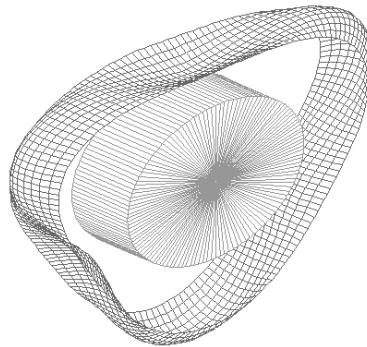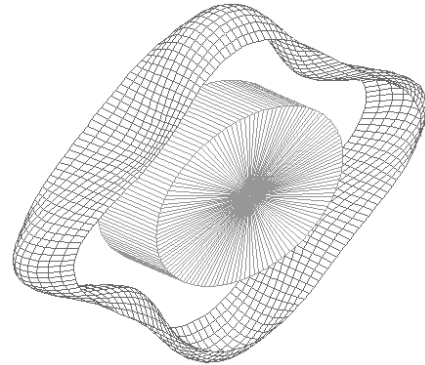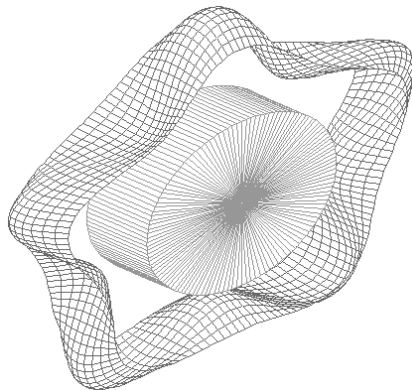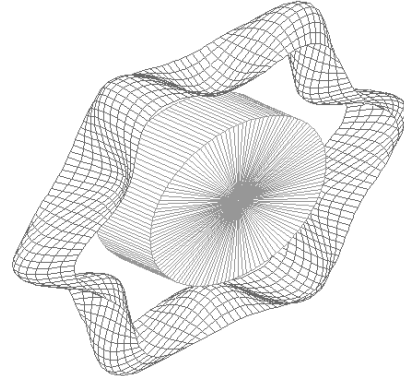The proposed tire-pavement noise model includes a tire-pavement interaction sub-model and the sound transmission sub-model. The tire-pavement interaction sub-model plays the role of noise source. It interacts with the sound transmission sub-model by a fluid-structure interface algorithm. Overall concept of tire-pavement noise modeling is described in Section 4.2 in detail. The tire-pavement interaction sub-model has been described and verified to be valid in Chapter 3. The sound transmission sub-model and fluid-structure interface will be proposed in this chapter. In Section 4.3, a sound transmission sub-model is developed based on theoretical analysis. In Section 4.4, a fluid structure interface algorithm is developed to couple the above two sub-models to form a tire-pavement noise model. In Section 4.5, an adaptive mesh procedure for the fluid component is introduced. In Section 4.6, the fluid structure interaction of the sound transmission sub-model is first validated by simulating noise from a revolving tire not in contact with road surface. In Section 4.7, the tire-pavement noise model is validated.

4.2 Overall Concept of Tire-Pavement Noise Modeling

In this research, the proposed tire-pavement noise model is composed of the tire-pavement interaction sub-model and the noise propagation sub-model. Rolling-tire Lagrange frame of reference is used in the three-dimensional tire-pavement interaction sub-model (see Figure 4.1), which is modelled as a smooth-plane pavement surface moving at a given speed V_X (m/s) toward the tire and a loaded tire rolling at a given angular velocity w_r (rad/s) (see Figure 4.2).

The tire rolling speed V_r is equal to the product of the angular velocity w_r and the effective rolling radius:

$$V_X = w_r r_e \tag{4.1}$$

where r_e is the tire radius, as shown in Figure 4.2. Slip point hub is normally located on the pavement surface. The longitudinal slip velocity V_{SX} is the difference between the pavement surface speed and rolling velocity of the tire:

$$V_{SX} = V_X - V_r \tag{4.2}$$

The Arbitrary-Lagrange-Euler (ALE) frame of reference is used in the three-dimensional noise propagation sub-model (see Figure 4.3), which is modelled as a half-sphere acoustic field around the rolling tire. The fluid of the sound radiation model is bounded by tire wall Γ_T, pavement wall Γ_P and hood wall Γ_H. The whole half-space of the sound radiation domain Ω is divided into an interior part Ω_i and an exterior part Ω_e by the boundary Γ. The external domain is used to prevent sound reflection on the hood boundary Γ_H. The pavement wall boundary Γ_P is considered as no-slip, where the fluid velocity vector $\mathbf{U}$ on the wall is prescribed to be zero. The pressure $\mathbf{P}$ gradient on the boundary Γ_H is set to be zero.

The two sub-models are coupled together by Fluid Structure Interface (FSI) in the tire-pavement noise model (see Figure 4.4). Air is modelled as a special from of 'fluid' in the analysis. A dynamic-state analysis is adopted. The proposed model is formulated to simulate the dynamic-state tire-pavement interaction, dynamic-state acoustic fluid around the tire, and FSI coupling.

At zero vehicle speed and a given load, the model calibrates the tire parameters by computing tire footprint to match the experimental footprint. The motion of rolling tire is simulated by applying a given speed to the pavement surface and a given angular velocity to tire. A zero speed is given to the air, since the wind noise is mostly avoided for a hood covering the tire or a windscreen enveloping the noise receiver in experimental studies. The noise simulation analysis is conducted in two stages. First, the noise pressure is collected on some sample frequency (20000 Hz in this study) from simulation results for a given speed. Second, noise sound pressure level is calculated. Before the noise simulation analysis, the adequacy of the air model boundary will be validated.

In the literature, the acoustic field has been modelled as either laminar or turbulent flows. The selection criterion is dependent on the Reynolds number (R) of the flow defined as

$$R = \frac{V_s t_w}{v} \tag{4.3}$$

where V_s = vehicle speed (m/s); t_w =water film thickness (m) and v =kinematic viscosity of fluid. The laminar flow is appropriate for modeling a flow at low vehicle speeds with $R < 500$, while the turbulent flow is used to model at high vehicle speeds with $R > 2000$. The flow between these two limits is transitional and may be either turbulent or laminar (ADINA, 2009).

The tire-fluid-pavement interaction problem is a two-way coupling problem. In the tire-pavement noise model, the fluid traction affects the structural deformations and solid displacement affects the flow pattern. For a given vehicle speed, the solution to the tire-pavement noise modeling problem is done by an iteration process.

Figure 4.1 depicts tire-pavement interaction sub-model with loads and boundary conditions. Figure 4.3 shows noise propagation sub-model with boundary. Their coupling mechanism is depicted in Figure 4.4, which is used in this study.

Noise data collected by CPX method on interaction of smooth tire and smooth pavement by past researchers are used to validate the model.

When calculating A-weighted sound pressure level, a frequency domain analysis of noise sample should be performed to add A-weighting frequency corrections. The data sampled in time domain is transformed into frequency domain by the discrete Fourier transformation method, as stated in the equations:

$$f_n = \frac{n}{N\Delta}, \; n = 0,1,\cdots,\frac{N}{2} \tag{4.4}$$

$$C_n = \sum_{k=0}^{N-1} c_k e^{2\pi ikn/N} \tag{4.5}$$

where Δ is the sampling interval, N is the sampling number.

Figure 4.5 shows the process to calculate A-weighting sound pressure level from noise sample in time domain, where the Power Spectral Density (PSD) can be estimated as:

$$P(0) = P(f_0) = \frac{1}{N^2}|C_0|^2 \tag{4.6a}$$

$$P(f_k) = \frac{1}{N^2}\left[|C_k|^2 + |C_{N-k}|^2\right] \quad k = 1,2,\cdots,(\frac{N}{2}-1) \tag{4.6b}$$

$$P(f_c) = P(f_{N/2}) = \frac{1}{N^2}|C_{N/2}|^2 \tag{4.6c}$$

4.3　Noise Propagation Modeling Approach

A complete set of the Navier-Stokes equations in the Eulerian system is applicable to describe the behaviour of sound transmission in an un-deformed computation domain. Since the fluid computation domain deals with deformed tire and tire tread vibration, the Eulerian system is no longer applicable to describe the sound transmission and an Arbitrary-Lagrangian-Eulerian (ALE) system is valid to simulate the fluid with deformation. It combines the advantages of both Lagrangian and Eulerian systems (see Figure 4.6).

In the ALE system, the Navier-Stokes equations discussed so far can be rewritten as (Zhang et al., 2003)

$$\frac{\partial}{\partial t}\int_V U dV + \oint_{\partial V}[(v-w)U-wG]dS = \int_V R dV \tag{4.7}$$

in which

$$U=\begin{bmatrix} \rho \\ \rho v \\ \rho E \\ \rho \varphi \\ 0 \end{bmatrix}, G=\begin{bmatrix} 0 \\ \tau \\ \tau v+k\nabla\theta \\ d_\varphi\nabla\varphi \\ d_\psi\nabla\psi \end{bmatrix}, R=\begin{bmatrix} 0 \\ f^B \\ f^B v+q^B \\ S_\varphi \\ 0 \end{bmatrix}$$

where τ is a stress tensor; v is velocity vector; w is moving mesh velocity vector; pressure; ρ is density; E is specific energy; internal energy; effective viscosity; second viscosity; f^B is specific rate of heat generation; φ represents any other variables

governed by convective-diffusive equations with d_φ and S_φ being its diffusion coefficient and source term, respectively, and ψ represents any other variables governed by the Laplace equations, with d_ψ being its diffusion coefficient. The variables that φ might represent are the turbulence kinetic energy K and the turbulence dissipation rate ε for the $K - \varepsilon$ turbulence model. The variable ψ represents the increment of fluid displacement for the moving boundary condition. The fluid body force f^B in this case includes the gravitational forces. For impressible flows, the density is assumed to be constant.

In the literature, fluid flows can be classified into turbulent and laminar flows. In fluid mechanics, the flows of practical relevance are almost always turbulent. Several turbulent models have been developed to replace the Navier-Stokes equations to simulate turbulent flows. Considering that the noise from tire rotation has Reynod number >2000 (Conte, 2008), turbulent flow simulation is assumed. Due to trade-off of computational effort and accuracy of tire-pavement noise numerical simulation, LES equations with standard sub-grid scale model is used in sound transmission simulation. It is suitable noise source simulation in the near field. In a three dimensional ALE coordinate system, the integral form of LES governing equations for an arbitrary moving cell with a volume of V(t) and a cell-face area of S(t), are given by

$$\frac{d}{dt} \iiint_{V(t)} \rho dV + \iint_{S(t)} \rho (\mathbf{U} - \mathbf{W}) \cdot \mathbf{d}S = 0 \tag{4.8}$$

$$\frac{d}{dt} \iiint_{V(t)} \rho \mathbf{U} dV + \iint_{S(t)} [\rho \mathbf{U}(\mathbf{U} - \mathbf{W}) - \sigma] \cdot \mathbf{d}S = \iiint_{V(t)} \mathbf{f}^B dV \tag{4.9}$$

where ρ is the air density, **U** is the flow velocity vector, **W** is the moving mesh velocity vector, $\mathbf{f}^{\mathrm{B}}$ is the air body force and σ is the total stress tensor,

$$\sigma = \mathbf{pI} - 2\mu\mathbf{e} - \lambda_1 \nabla \bullet \mathbf{UI} \tag{4.10}$$

where **p** is the pressure, **I** is unit matrix and λ_1 is the second viscosity, and normally supposed to be $-2/3\mu_0$ for air (Deardorff, 1970).

e is the strain tensor,

$$\mathbf{e} = \frac{1}{2}[\nabla\mathbf{U} + (\nabla\mathbf{U})^{\mathrm{T}}] \tag{4.11}$$

μ is the effective viscosity,

$$\mu = \mu_0 + \mu_t \tag{4.12}$$

μ_0 is the laminar viscosity and μ_t is the eddy viscosity given by

$$\mu_t = \sqrt{2}\rho C_{\mathrm{SGS}}^2 \Delta^2 \sqrt{\mathbf{e} \otimes \mathbf{e}} \tag{4.13}$$

where C_{SGS} is the dimensionless model constant set to be 0.10 as suggested by Deardorff (1970) for wall bounded flows, Δ is the element size.

In this simulation, air flow velocity from tire rotation is much smaller than sound wave velocity with Mach number Ma $\ll$ 1. Therefore, air flow could generally be treated as incompressible. However, when the sound wave simulation is to be included in the calculation, the compressibility must be considered in the Large Eddy Simulation (LES). A slight compressibility is suitable for such problems (Olson and Bathe, 1985), where the

air density only depends on pressure $\rho = \rho_0(1 + \mathbf{p}/\kappa)$ in which κ is the fluid bulk modulus of elasticity and ρ_0 is the reference density.

4.4 Coupling of Sub-Models

The coupling between the fluid sub-model (i.e. sound propagation sub-model) and the structure model (i.e. the tire-pavement sub-model) is made by fluid stress terms and structure displacement terms. At the fluid structure interface (FSI), the equilibrium conditions of displacement and stress are fulfilled. The two equations of the FSI are

$$\mathbf{d}_f = \mathbf{d}_s \tag{4.14}$$

$$\mathbf{n}.\boldsymbol{\tau}_f = \mathbf{n}.\boldsymbol{\tau}_s \tag{4.15}$$

where $\mathbf{d}_s$ and $\mathbf{d}_f$ are the displacements of the solid and fluid on FSI, respectively. $\boldsymbol{\tau}_s$ and $\boldsymbol{\tau}_f$ are the traction stresses of the solid and fluid on FSI, respectively.

The finite element equations of the coupled rolling tire and air noise system can therefore be expressed as

$$\mathbf{F}(\mathbf{X}) = \begin{bmatrix} \mathbf{F}_f(\mathbf{X}_f, \mathbf{d}_s) \\ \mathbf{F}_s(\mathbf{X}_s, \boldsymbol{\tau}_f) \end{bmatrix} = 0 \tag{4.16}$$

where $\mathbf{F}_f$ and $\mathbf{F}_s$ represent the system equations for the rolling tire and noise models respectively, and $\mathbf{X}_f$ and $\mathbf{X}_s$ are the fluid and solid nodal solution variables respectively. The iteration computing method is used to solve this problem. The noise equation and tire equation are solved individually by Newton method in succession using the latest

114

information provided from the other part of the coupled system in which the kth iteration can be described as

$$\mathbf{F}_f(\mathbf{X}_f^k, \mathbf{d}_s^{k-1}) = 0 \tag{4.17}$$

$$\mathbf{F}_s(\mathbf{X}_s^k, \boldsymbol{\tau}_f^k) = 0 \tag{4.18}$$

The convergence criteria are based on the values of computed stress and displacement. The stress criterion is defined as

$$r_\tau = \frac{\left\| \boldsymbol{\tau}_f^k - \boldsymbol{\tau}_f^{k-1} \right\|}{\left\| \boldsymbol{\tau}_f^k \right\|} \leq \varepsilon_\tau \tag{4.19}$$

and the displacement criterion is defined as

$$r_d = \frac{\left\| \mathbf{d}_s^k - \mathbf{d}_f^{k-1} \right\|}{\left\| \mathbf{d}_f^k \right\|} \leq \varepsilon_d \tag{4.20}$$

where r_τ and r_d are tolerances for stress and displacement convergence, respectively, which are both set as 0.1%. The maximum number of the FSI iteration is originally set as 15 considering computation cost. If FSI solution is not converged in the maximum FSI iteration number, but indicates a converging behavior, the maximum number could be increased for FSI solution convergence.

4.5 Convergence Analysis

The three dimensional sound domain is modeled using Four-node tetrahedral elements. LES is an expensive method to accurately solve these problems with multiple spatial and temporal scales. A major shortcoming of the ALE system is when tire undergoes large

deformation, the fluid mesh interacting with tire becomes so distorted that the iteration solution is not continued. Figure 4.7 shows a process that rolling tire tread compresses the fluid mesh on the pavement in the numerical model. The variation of the fluid element shape in this process is further illustrated in Figure 4.8. In this process, the fluid element shape undergoes large distortion after tire moves. The elements could overlap due to further deformation of tire tread (see Figure 4.9).

An adaptive procedure (Bathe and Zhang, 2009) to repair mesh distribution is available to obtain the relative accurate solution and decrease the computation complexity simultaneously. The criterion $C(F_e)$ of the adaptive mesh scheme is to determine the preferred element size h_{ep}. F_e are flow solution variables. The criterion can be calculated at time t_c that could be earlier than or the same as the restart time t_s. The criterion is applied to the entire fluid model. The criterion can be expressed as

$$C(F_e): \quad h_{ep} \max\{\min\{\|F_e\|, \frac{c}{h_{min}}\}, \frac{c}{h_{max}}\} = c \qquad \textbf{(4.21)}$$

where c is a constant, and F_e represents fluid solution variable like pressure gradient, velocity gradient, etc. h_{min} and h_{max} are the minimum and maximum element sizes allowed in the fluid mesh, respectively. The constant is determined by

$$c = \lambda_r \frac{1}{N_e} \sum_e h_e \|F_e\| \qquad \textbf{(4.22)}$$

116

where λ_r is a ratio factor used to control the mesh number in the sound propagation, h_e is the local element size, and N_e is the total number of elements in the sound propagation model.

In order to disentangle the numerical influences from those of the LES model, an adaptive mesh convergence analysis is performed under the condition of a sound plane wave source with the frequency 2500 Hz loaded on the internal boundaries Γ_T of the sound radiation model shown in Figure 4.3. Two collection points with coordinates (-0.1, 0.05, -0.31) and (-0.2, 0.29, -0.22) are chosen to monitor the pressure data. The first collection point is located in the area of contact patch, and the other one is located in the experiment microphone collection position (Sandberg and Ejsmont, 2002).The sound pressure levels at these two collection points are calculated by the equation

$$SPL = 20\log_{10}({p_{rms}}\Big/{2\times10^{-5}})\qquad\qquad\textbf{(4.23)}$$

in which p_{rms} is the root-mean-square pressure. The results are shown in Figure 4.10. It can be observed that the total mesh number seems to have little effect on the sound pressure level at Point 1. A possible reason is that the adaptive mesh strategy generates very high mesh density in the contact patch area, and it is sufficient to simulate the pressure wave propagation. In contrast, the sound pressure level at Point 2 is highly affected by the total mesh number of the sound propagation model. The relative error of the sound pressure level in the Micro-phone position (Point 2) is illustrated in Figure 4.11. The error is less than 5% when the mesh number of sound radiation model is larger than 160,000. It is difficult to obtain an accurate element number based on the algorithm (see

117

Equation 4.21), so we use a fluid mesh number range between 180000 to 220000 to obtain accurate solutions and avoid large mesh deformation. Figure 4.12 ilustrates that each analysis took about 150 hours of computation time on a computer of Intel Xeon E5645 with 6 cores. Since we have three computers of the same type for modeling, on average it took about 50 hours of computation time per computer to complete one analysis.

The benchmarking method proposed by Molares and Sobreira-Seoane (2008) is used to analyze the convergence rate of the proposed model in this research. Figure 4.13 shows the relative error against CPU-time. It illustrated a converge slope of almost -0.094 ($e_r \approx Ct^{-0.094}$).

Figure 4.14 illustrates the variation of mesh distribution on the cross-section of the sound transmission model obtained with the adaptive mesh strategy. The distribution of the initial 36,362 meshes is shown in Figure 4.14 (a), where the model contains the coarser elements. The final adaptively adjusted mesh is shown in Figure 4.14 (b).

The adaptive mesh is a function of the current model information and unknown adaptive parameters, which can be depicted as

$$\text{Adaptive mesh} = f(\text{current model information, input parameters}) \quad \textbf{(4.24)}$$

f is a nonlinear function. It can be solved by the adaptive mesh algorithm (see Equation 4.21).

Adaptive mesh is a time-consuming algorithm for the large-scale model in this research. The calculation time is strongly related to input parameters. Normally, it requires almost

118

one hour for one run of the adaptive mesh calculation. Inappropriate input parameters can result in several hours of computation time. In this thesis, an effective scheme was developed to obtain the effective adaptive meshes within acceptable time. In this scheme, Newton method is used as the core algorithm to solve this nonlinear problem.

In the algorithm, h_{ep} is the main parameter to determine the adaptive meshes, and h_{max} and h_{min} are secondary parameters to determine the adaptive meshes, which are originally set to be the values with 20% difference of h_{ep}. h_{ep} is regulated based on Newton algorithm in the iteration. Having obtained the data (N^{n-1}, h_{ep}^{n-1}) and (N^{n}, h_{ep}^{n}) where N^{i} is the adaptive mesh number in the ith iteration, h_{ep}^{n+1} is calculated as

$$h_{ep}^{n+1} = \frac{h_{ep}^{n} - h_{ep}^{n-1}}{N^{n} - N^{n-1}}(N^{n+1} - N^{n}) + h_{ep}^{n} \qquad \textbf{(4.25)}$$

where N^{n+1} is set to be 200,000 as the final adaptive mesh number. This simplified search process of adaptive mesh is illustrated in Figure 4.15. The search process is stoped when the adaptive mesh is in the range between 220,000 and 180,000.

4.6 Model parameters

4.6.1 Input Parameters

The input parameters can be classified into the following three types:

(1) Tire dynamic parameters - Tire load, tire pressure, tire velocity, tire angular velocity, friction coefficient

(2) Air property parameters - Air dynamic viscosity, air bulk modulus, air density

(3) Tire material parameters - Tire mass, tire damping ratio and tire stiffness. Tire stiffness includes tread circumference elastic modulus, tread cross-section elastic modulus, tread shear modulus, tread Poisson's ratio, sidewall circumference elastic modulus, sidewall cross-section elastic modulus, sidewall shear modulus, and sidewall Poisson's ratio.

4.6.2   Output Parameters

The time variation of noise pressures with sampling frequency of 50 kHz is the main output of the simulation analysis. By discrete Fourier transformation, the sound pressure level with frequency is obtained from time based noise data. It is further calculated with A-weighting correction to obtain A-weighting sound pressure level.

4.6.3   Determination of Input Parameters

The determination of the main input parameters is described in this section.

(1) Tire loading parameters

Tire load, tire pressure, tire velocity, tire angular velocity and friction coefficient are obtained experimentally. Table 4.1 gives the values used in the present simulation analysis of the tire (Sandberg and Ejsmont, 1990).

(2) Air property parameters

The air properties under constant temperature of 20 $^{\circ}C$ are used in the noise simulation as shown in Table 4.2 (Deardorff, 1970).

(3) Tire material parameters

Tire material parameters have been determined in the previous chapter.

4.7 Model Validation and Analysis

4.7.1 Validation of Sound Propagation Sub-Modeling

In order to validate the sound transmission model, rolling tire, as shown in Figure 4.16, is simulated as the noise source without the interference of pavement surface.

The noise data are obtained from the experiment by Ejsmont (2009) to validate the proposed sound transmission model. The experiment measured ventilation noise of a rolling PIARC smooth tire not in contact with road. Simulation data were collected by CPX standard test methods (see Figure 4.17), and the power spectrum density of the noise pressure level is calculated according to A-weighting scheme.

Since wind hood has a large influence on the acoustic free field conditions at frequencies below 500 Hz (Sandberg and Ejsmont, 1990), the reconstructed minimum noise frequency is chosen as

$$f_{\min} = 500\text{Hz} \qquad\qquad \textbf{(4.26)}$$

In this chapter, the variation of tire-pavement noise between 500 Hz and 2500 Hz, which covers the sensitive frequency range for human being, will be analyzed.

Figure 4.18 compares the power spectrum density of A-weighted SPL of the simulation results and experimental data for vehicle speeds of 30, 50 and 70 km/h. One can see that simulation results are in good agreement with the experimental results in all frequency bands. It can also be found that the turbulence noise level increases with tire rolling speed. The noise level increases by about 10 dB for a rolling speed increasing 20 km/h. It could be one of the dominant sources of tire noise in the high vehicle speed. Figure 4.19 shows

the turbulence flow velocity in the air field near tire. It is noted that turbulence flow is mainly originated from tire tread and sidewall in the simulation, and is uniformly distributed around tire.

4.7.2 Validation of Noise Prediction of Proposed Model

In order to understand the effect of different factors on tire-pavement noise generation, many experimental studies have been carried out with different experimental setups using PIARC smooth tire on smooth pavements in accordance with standard tire-pavement noise test procedures (Sandberg and Ejsmont, 1990). These experiments provide noise data to validate the tire-pavement noise computed by the numerical model developed. Simulation analysis is performed based on the experimental set-up by Sandberg and Ejsmont (2002) as illustrated in Table 4.1. The noise data is collected in the "Rear" microphone by the CPX standard measurement method (Sandberg and Ejsmont, 2002) (see Figure 4.17).

In the simulation, a static vertical load of 3000N is first applied to tire axle. In order to simulate tire dynamics, a further one revolution with angular velocity calculated by Equation 4.1 is added on tire hub. The tire tread dynamics at the speed 70 km/h on pavement are illustrated in Figure 4.20, which compared with experimental results by Périsse (2002), as shown in Figure 4.21. The acceleration of tyre element is coded by color. One can see that tire tread vibration varies along tire rolling on pavement. Main tyre vibration sources are located around tyre contact patch. Vibration intensity scales down with moving far from the contact patch. Since sound pressure amplitude is proportional to the noise source acceleration amplitude (O'boy and Dowling, 2009), it is

further predicted the tire tread elements generated more noise when located nearer to the contact patch in the simulation.

Figure 4.22 illustrates the sound pressure distribution pattern in selected time steps. It is observed that the noise pressure in the near field around tire varies with tire rotation. Most noise is found around the tire contact patch. This phenomenon is consistent with the analysis observed in Figure 4.20. Noise magnitude is higher at locations nearer to the tire contact patch.

Based on the above simulation conditions, the power spectrum density of the sound pressure levels are computationally determined with A-weighting in the "Rear" microphone position. The A-weighted one-third octave band sound pressure level frequency distributions are compared to experimental data (Sandberg and Ejsmont, 1990) as illustrated in Figure 4.23. It is shown that simulation results are in good agreement with the experimental measurements by the CPX standard test method.

In order to demonstrate the effectiveness of the proposed model, we compared the proposed model with the approaches in Yum et al. and O'boy (Yum et al., 2006; O' Boy and Dowling, 2009). Yum et al. studied the tire-pavement noise generation due to dynamic load. The calculated results are shown in Figure 4.24. It can be found that there is a 5 dB difference between numerical and measured values in the low frequency band less than 1000 Hz, which is similar to that of the proposed model in this thesis (see Figure 4.23). However, the difference increase to more than 15 dB in the high frequency band large than 1000 Hz. Clearly, the proposed model is much effective to simulate tire-pavement noise in the high frequency band by considering aerodynamic mechanisms in

the simulation. O'boy and Dowling (2009) studied rolling tire noise generation by a novel multilayer plates tire modeling method. The calculated results are illustrated in Figure 4.25. It can be seen that generally the new method significantly improves the predicted results in the low frequency band, which is better than the proposed model in this thesis. However, there is still a large error with more than 10 dB in the high frequency band, which is worse than the prediction by the proposed model in this thesis.

In order to refine the contribution to tire-pavement noise interaction emitted from the source region in the model, sound pressure level distribution on a horizontal cutting plane at distance of 100 mm above the tire bottom at the speed of 70 km/h is constructed. Figure 4.26 (a) shows the sound pressure level distribution on that cutting plane when the PIARC smooth tire rolls without contacting pavement. It can be observed that sound pressure level is higher at the leading and trailing edges than along tire sidewall. This indicates that tire rolling has a more significant impact on tire tread vibration. Figure 4.26(b) shows the sound pressure level distribution on that plane when the PIARC smooth tire rolls on pavement.

It is noted that the noise level is higher at the leading edge than trailing edge, as noted by previous experimental results (Sandberg and Ejsmont, 2002). Furthermore, comparing the difference between Figures 4-26 (a) and (b), it can be observed that noise levels in the presence of tire-pavement contact are much higher than that without contact. In the case where the smooth tire is rolling in air, sound pressure level tends to be more evenly distributed whereas for the case when the tire is rolling on pavement surface, sound pressure level near the tire-pavement contact patch tends to be higher.

124

Noise level increases by about 30 dB at the leading and trailing edges, and increases by about 27 dB at the sidewalls. Noise level difference at the leading and trailing edges is higher than at tire sidewalls probably due to stronger horn effect and noise sources at the leading and trailing edges, which are more important for tire pavement noise generation. The adhesive mechanisms and horn effect occur due to the presence of pavement surface and are not observed for a rolling tire in air. It is clear from the figures that the presence of pavement surface has a significant impact on the near-field sound pressure distributions.

In summary, the model allows the identification of various noise generation and propagation mechanisms. For the case of a smooth tire rolling on a plane pavement surface, specific mechanisms such as impact mechanisms (in terms of running deflection), adhesion mechanisms (stick-slip), air displacement mechanisms (in terms of air turbulence) and horn effect can be effectively studied, as illustrated in Table 4.3. The proposed model is able to produce better results than the current single mechanism models used in the literature (Brinkmeier et al., 2008; O' Boy and Dowling, 2009).

4.8 Summary

This chapter has presented the development of a three-dimensional finite element near-field tire-pavement noise simulation model. The simulation model makes use of fundamental structural mechanics and fluid dynamics theories to estimate the expected near-field sound pressure level (which could be in dB or dBA) caused by a rolling tire on a plane pavement surface. Unlike previous models which consider a limited number of noise mechanisms, the developed model takes into account multiple noise generation and propagation mechanisms, including structural vibration noise generation, aerodynamic

noise generation, horn effect and others. Simulation results from the model are compared against past experimental results obtained from the literature and the model was found capable of replicating the experimental data reported in past research. The ability of the model to identify key noise generation/propagation mechanisms and to perform parametric analyses on factors that may affect tire-pavement noise is further demonstrated, highlighting the potential of the numerical simulation approach to be a feasible and cost-effective means for future tire-pavement noise research.

Table 4.1 Values of tire loading parameters for simulation analysis

Velocity (km/h)	Inflation pressure(kPa)	Load (N)	Friction coefficient
50/70/90	190	3000	0.7

Table 4.2 Air property parameters for simulation analysis

	Dynamic Viscosity (Kg/ms)	Bulk Modulus (Pa)	Density (Kg/m^3)
Air (20 °C)	1.51E-005	142000	1.205

Table 4.3 Major Noise Generation and Propagation Mechanisms Covered by Various Studies in the Literature

Tire-Pavement Noise Mechanisms and Description					Mechanisms Used in References & Model					
					Reference					Developed Model
Mechanism				Description	Ref.1	Ref.2	Ref.3	Ref.4	Ref.5	
Generation mechanisms	Vibration (Structure-borne)	Impact mechanism	Tread impact	Impact of tire tread blocks or other pattern elements on road surfaces, causing radial and to some extent also tangential vibrations in the tire tread and belt, spreading to sidewalls.	✗	✗	✓	●	✓	*
			Texture impact	Impact of road surface texture on tire tread, causing radial and to some extent also tangential vibrations in the tire tread and belt, spreading to sidewalls.	✗	✗	✓	●	✓	*
			Running deflection	Occurs at leading and trailing edges giving tire belt/carcass vibrations.	✓	✓	✓	●	✓	✓
		Adhesion mechanism	Stick-slip	Tread element motions relative to road surface causing tangential type tire vibrations	✗	✗	✓	●	✓	✓
			Stick-snap	Rubber road adhesion, giving either radial or tangential vibrations	✗	✗	✓	●	✓	✗
	Aerodynamic (Air-borne)	Air displacement mechanism	Air turbulence	Due to tire displacing air when rolling on road	✗	✗	✗	✗	+	✓
			Air pumping	Due to air displacement into/out of cavities in or between tire tread and road surface	✗	✗	✗	●	+	*
			Pipe resonance	Air displacement in grooves in tread pattern amplified by resonance	✗	✗	✗	●	+	*
			Helmholtz resonance	Air displacement into/out of connected air cavities in tread pattern and road surface amplified by resonance	✓	✗	✗	●	+	*
Related propagation (amplification or reduction) mechanisms	Horn effect			Curved volume between tire leading and trailing edges and road surface constitute to an exponential horn used to amplify horn	✗	✓	✓	●	+	✓
	Acoustic impedance effect			Communicating voids in porous surfaces act like sound absorbing materials	✗	✗	✗	✗	✗	✗
				Same but affect sound propagation to a far field receiver	✗	✗	✗	✗	✗	✗
	Mechanical impedance effect			Road surface gives more or less reaction to tire block impacts depending on dynamic tire/road stiffness proportions	✗	✗	✗	✗	✗	*
				Same type vibrations may be transferred to road surface, possibly radiating as sound	✗	✗	✗	✗	✗	✗
	Tire resonance			Belt resonances (mechanical resonances in belt)	✗	✗	✓	●	✓	✓
				Torus cavity resonance (resonance in air column of tire)	✗	✗	✗	✗	✗	✗

Note:

Ref. 1: Brinkmeier et al. (2008); Ref. 2: O' Boy and Dowling (2009); Ref. 3: Guisset and Augusztinovicz (1999);

Ref. 4: Plotkin and Stusnick (1981); Ref. 5: De Roo and Gerretsen (2000);

✓ indicates mechanism is considered and modeled,

✖ indicates mechanism is not considered

• in Plotkin and Stusnick (1981) indicates that there was a lack of computational capability and validation experiments even though framework was proposed.

+ indicates the noise propagation model is two-dimensional and may not be totally appropriate.

* indicates potential ability to the model to consider these effects with modifications to the relevant sub-model. Not considered in this paper
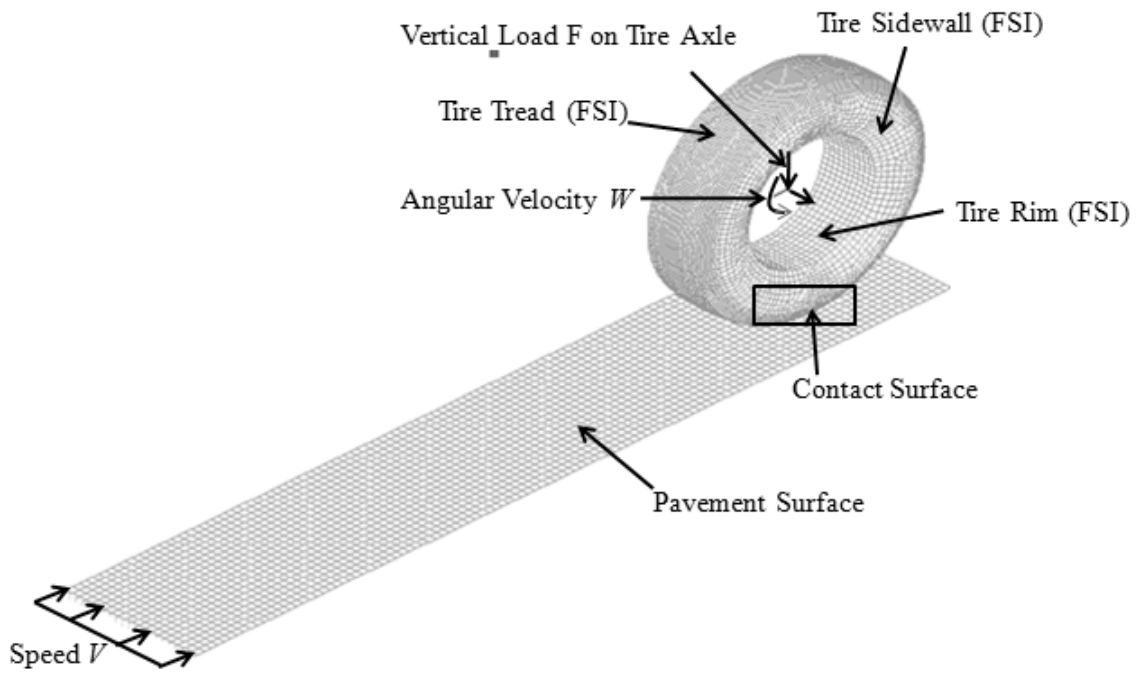
Figure 4.1 Tire-pavement Interaction Sub-Model
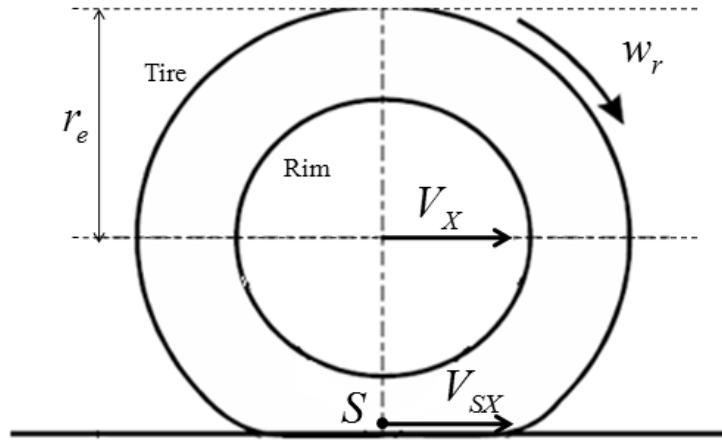
Figure 4.2 Kinetics of rolling tire
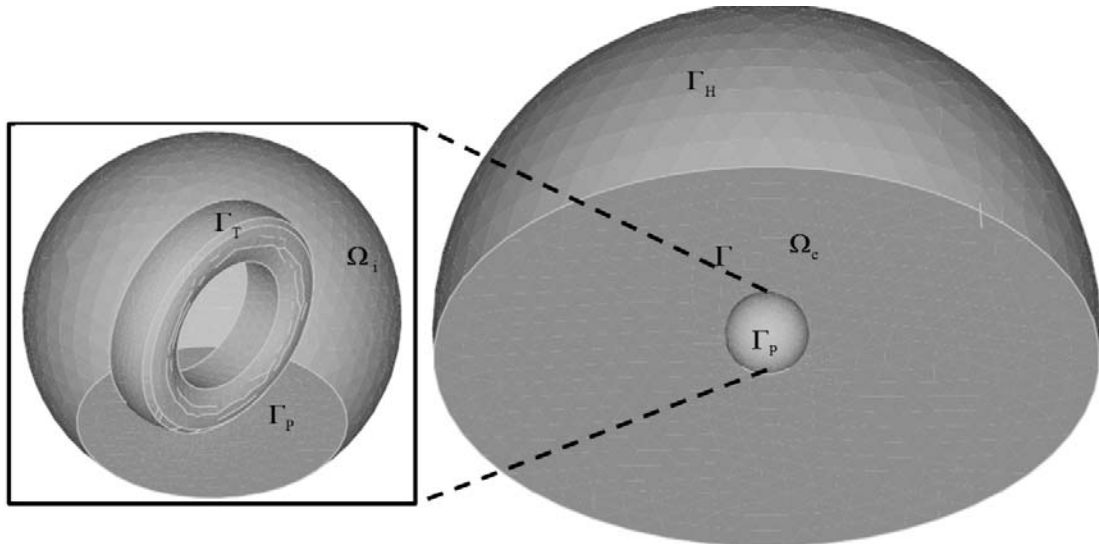
Figure 4.3 Noise Radiation Sub-Model
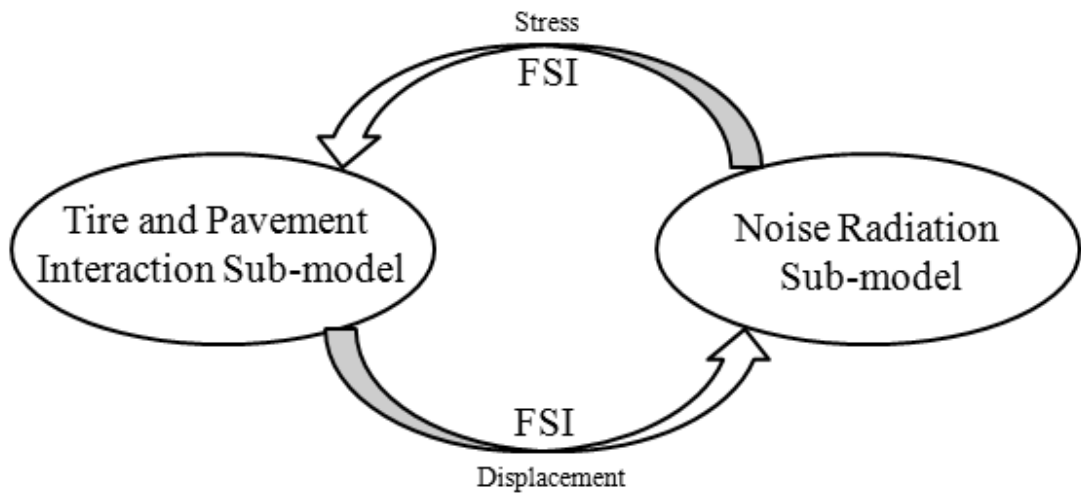
Figure 4.4 Tire-pavement Noise Model
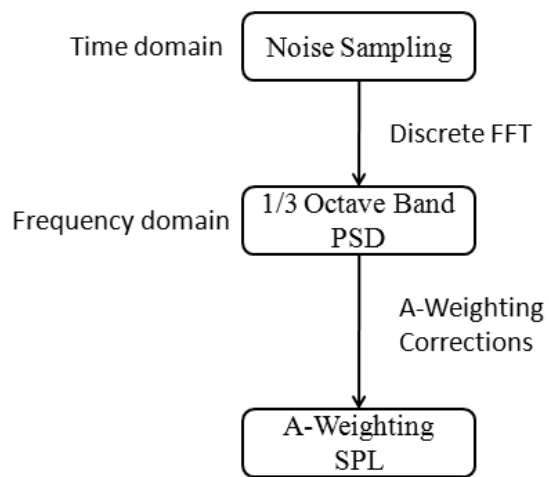
Figure 4.5: Calculation of A-Weighting SPL
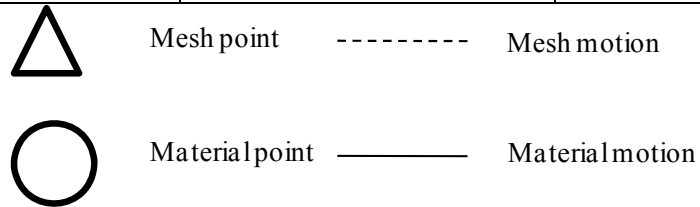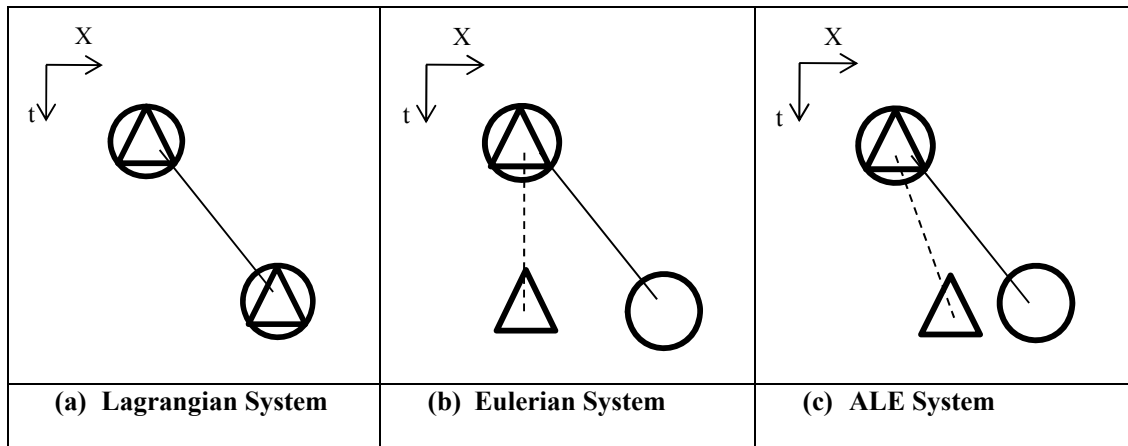
Figure 4.6 One Dimensional Material Motion in Lagrangian, Eulerian and ALE Systems
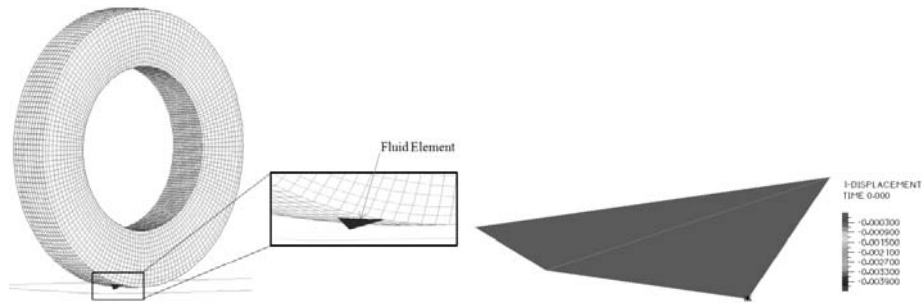
(a) Original mesh shape
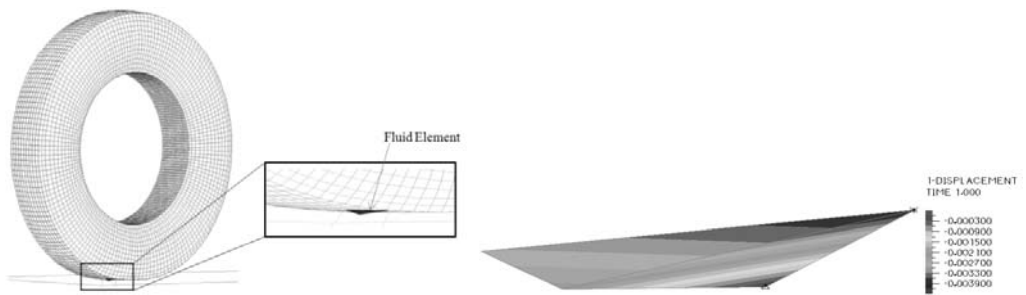
(b) Deformed mesh shape

Figure 4.7 Interaction between tire tread and fluid element
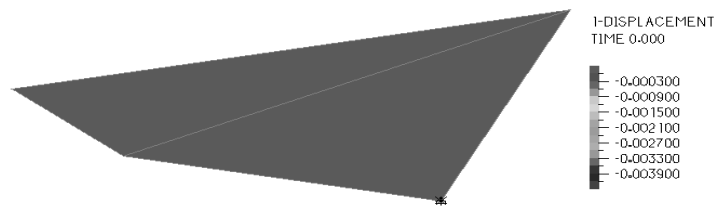
(a) Before Tire Moving
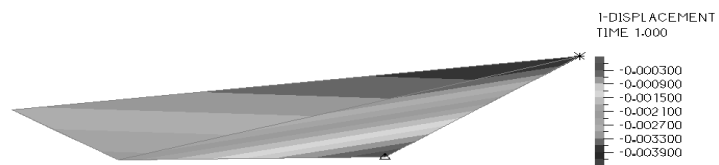
(b) After Tire Moving

Figure 4.8 Fluid Element Shape

134
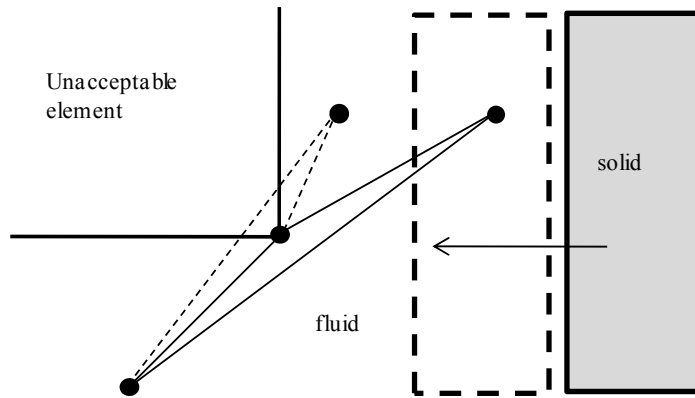
Figure 4.9 A typical case of reaching an unacceptable element
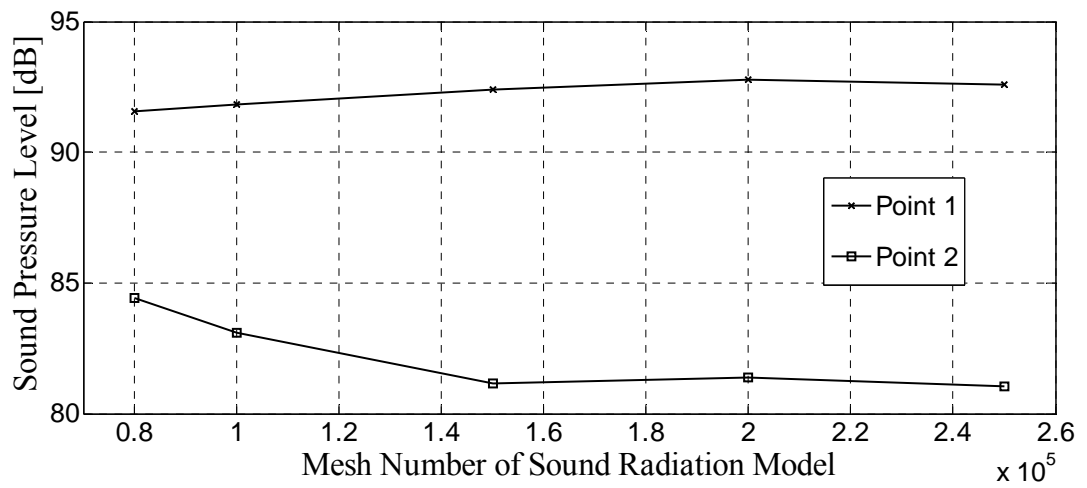
Figure 4.10 Adaptive mesh convergence analysis for sound radiation model
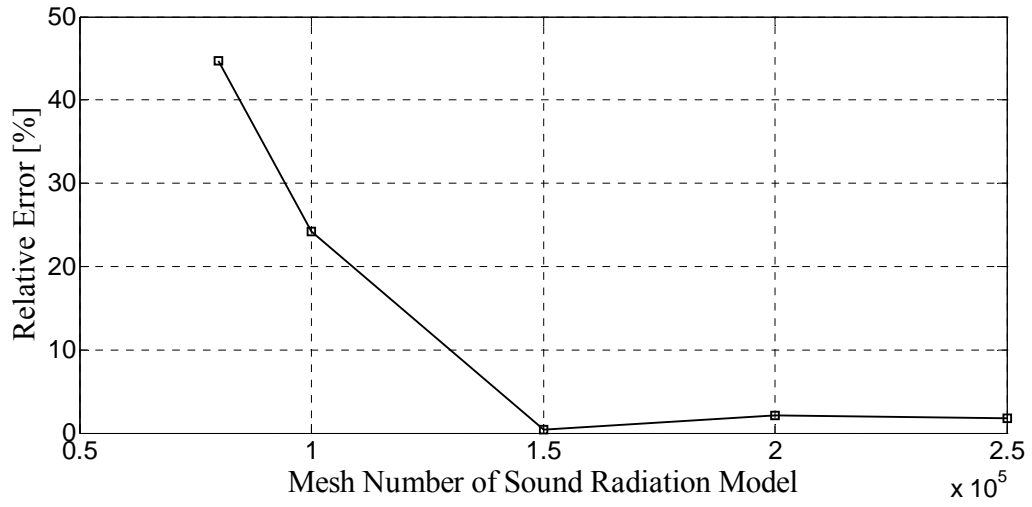
Figure 4.11 Relative error with mesh number of sound radiation model
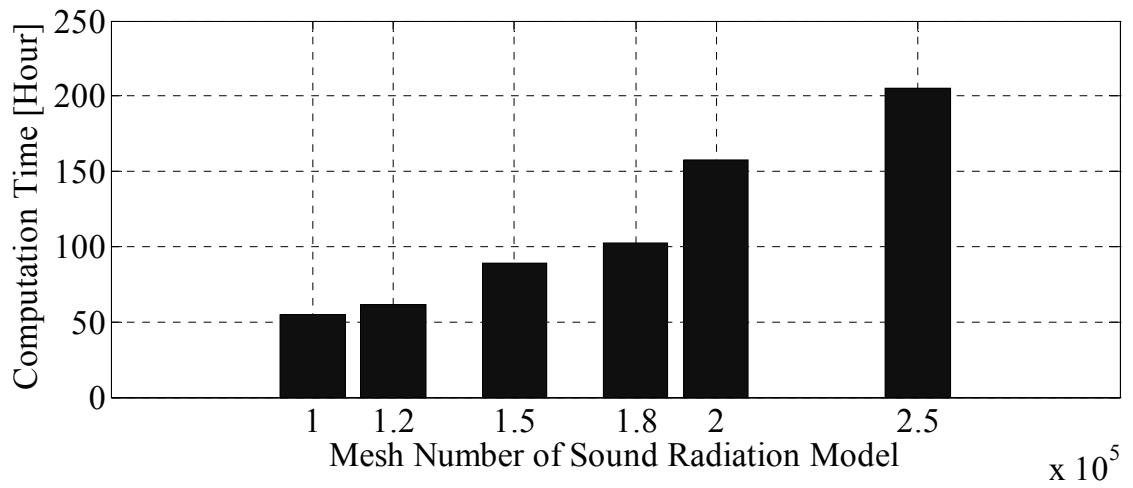
Figure 4.12 Computation time with mesh number of sound radiation model
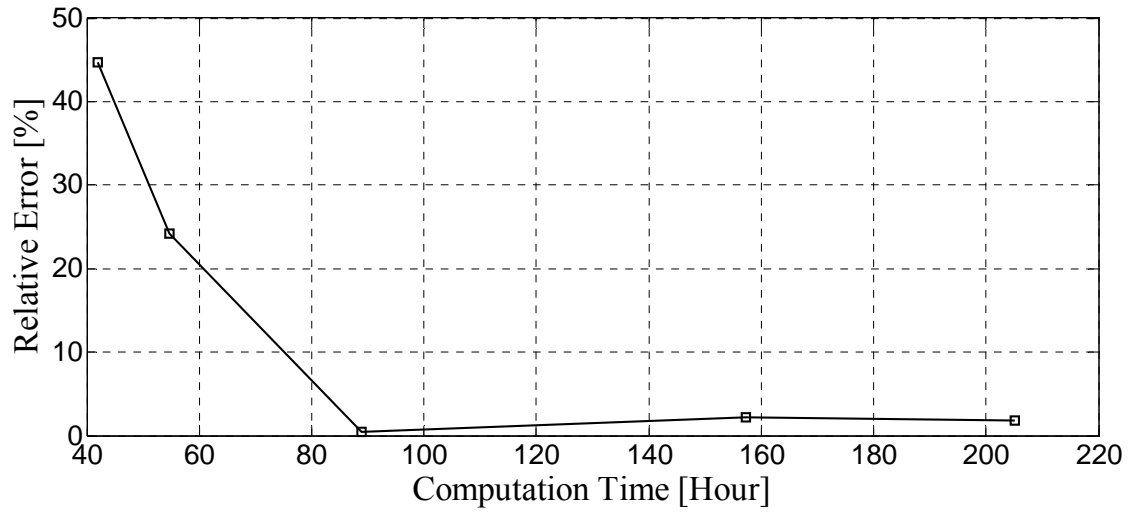
Figure 4.13 Relative error against CPU-time
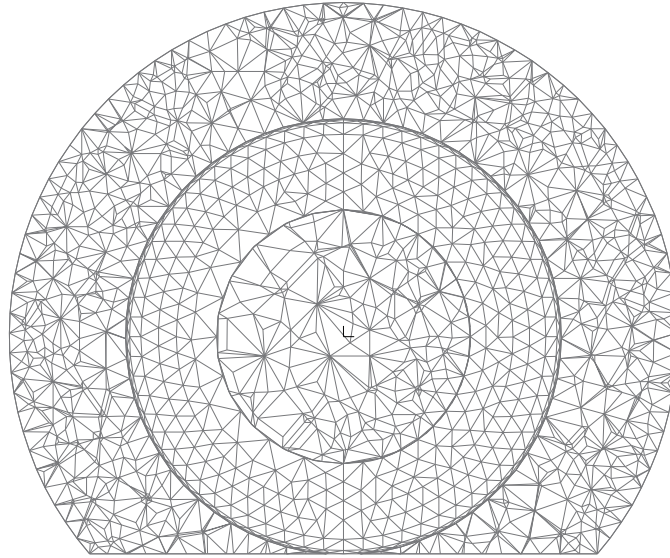
(a) Initial Mesh
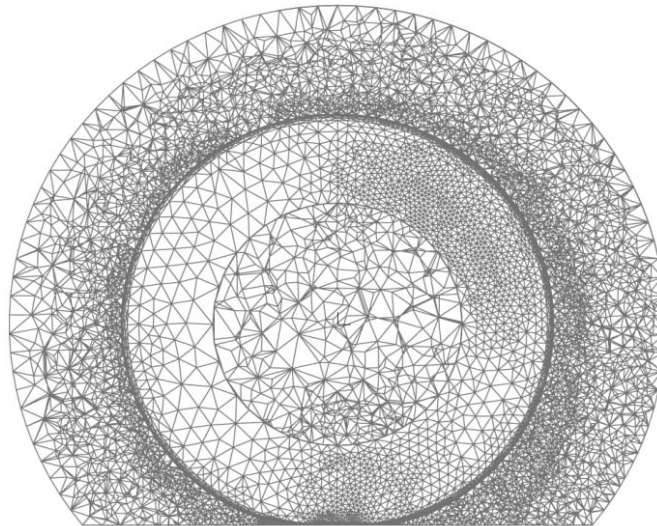
(b)Adaptively Reached Mesh
Figure 4.14 CFD mesh used for Sound Transmission Model
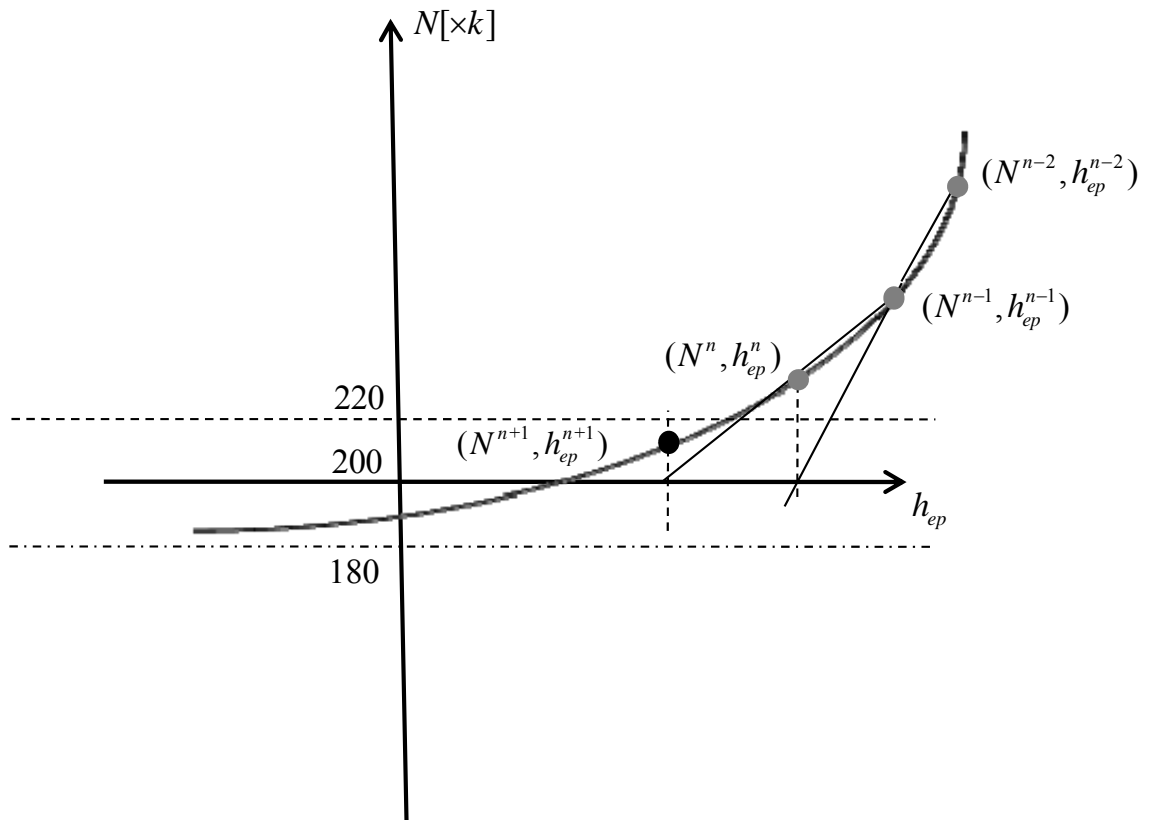
Figure 4.15 Search process sample for adaptive mesh
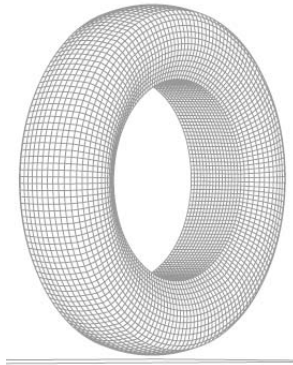
Figure 4.16 Rolling tire without contacting pavement surface sub-model
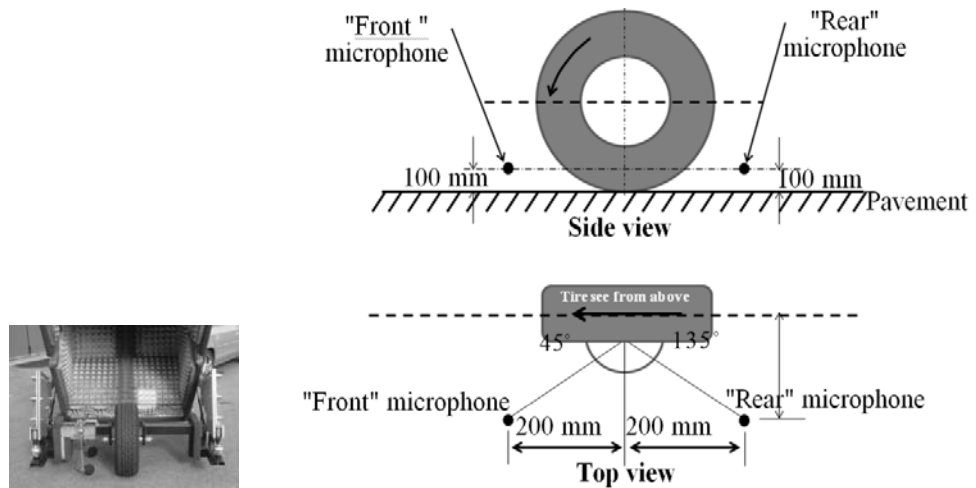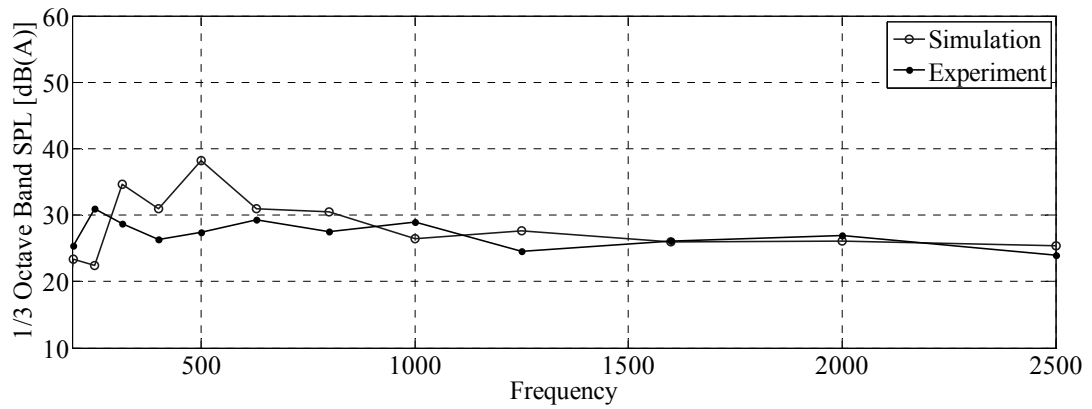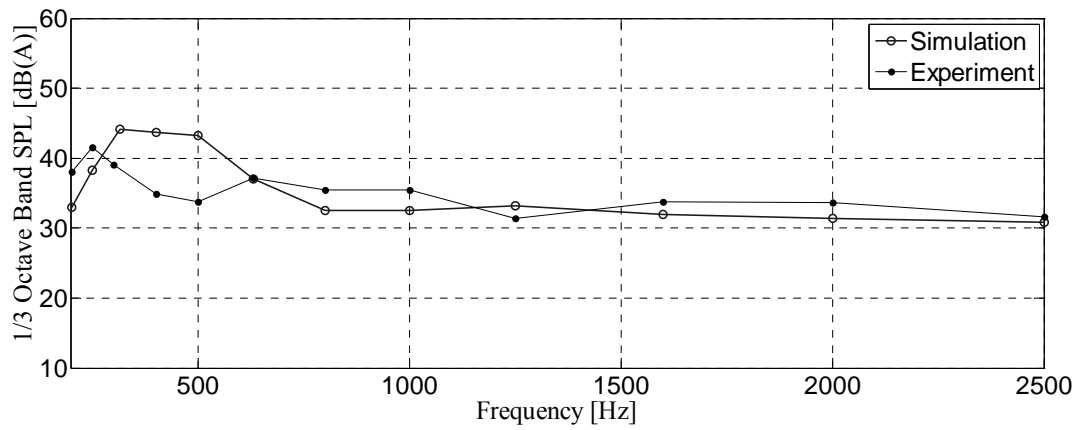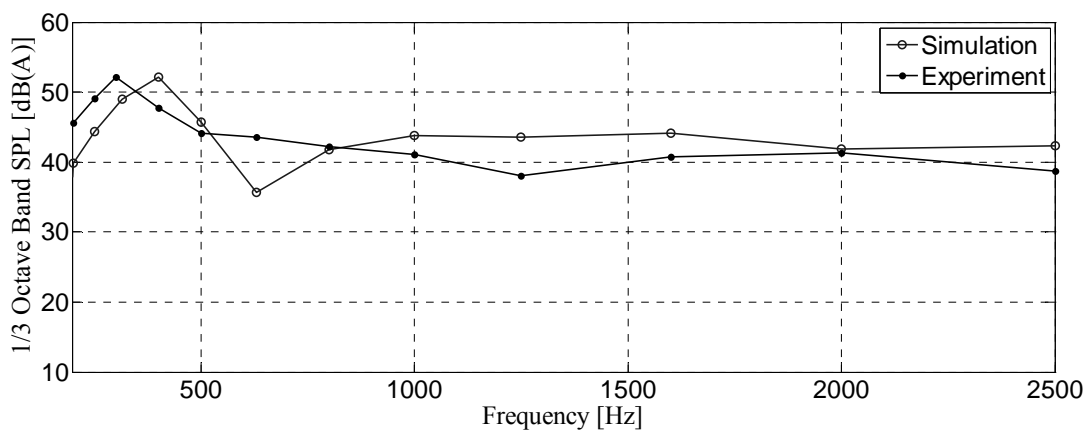

Figure 4.17 CPX standard test method (Sandberg and Ejsmont, 2002)

30 km/h

50 km/h

70 km/h

Figure 4.18 Comparison of power spectrum density of A-weighted noise level without pavement contact between Simulation and Experiment
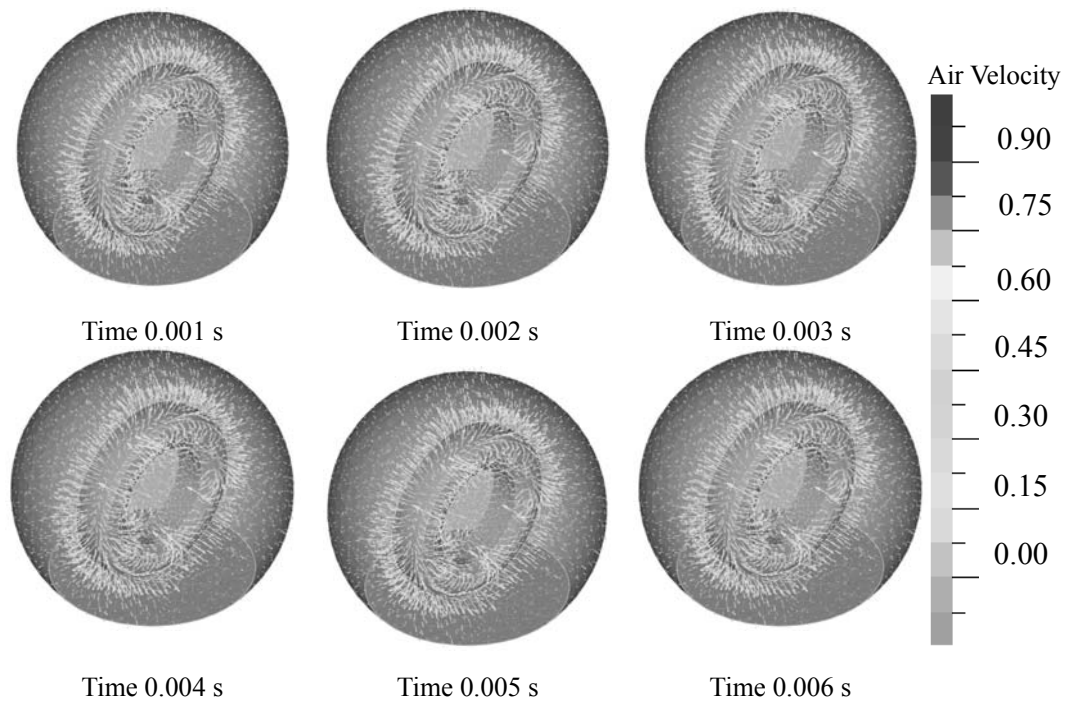
141

Time 0.001 s	Time 0.002 s	Time 0.003 s

Time 0.004 s	Time 0.005 s	Time 0.006 s

Figure 4.19 Turbulence flow in air field near tire

Time 0.001 s	Time 0.002 s	Time 0.003 s

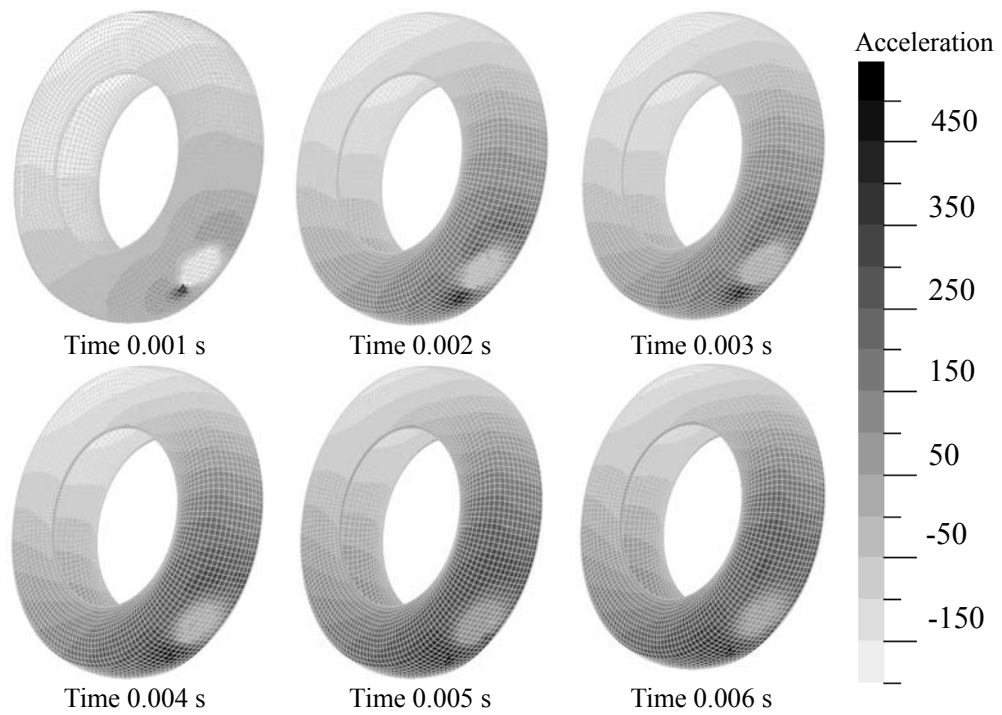|		
Time 0.004 s	Time 0.005 s	Time 0.006 s

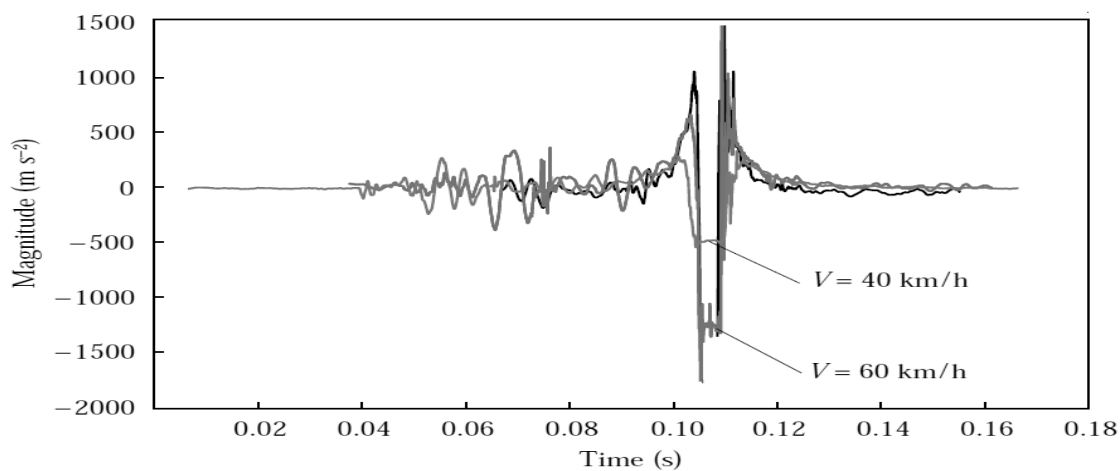**Figure 4.20Snapshots at discrete time steps of tire dynamics**

Figure 4.21 Experimental Calculated radial acceleration of tire tread in the vicinity of contact area (Périsse, 2002)
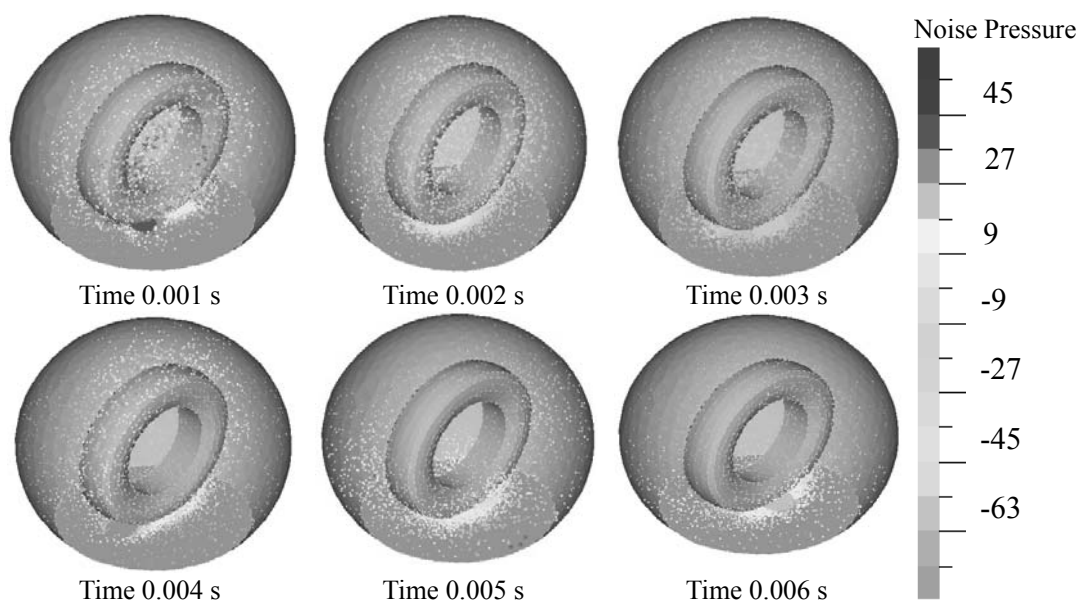

Time 0.001 s   Time 0.002 s   Time 0.003 s

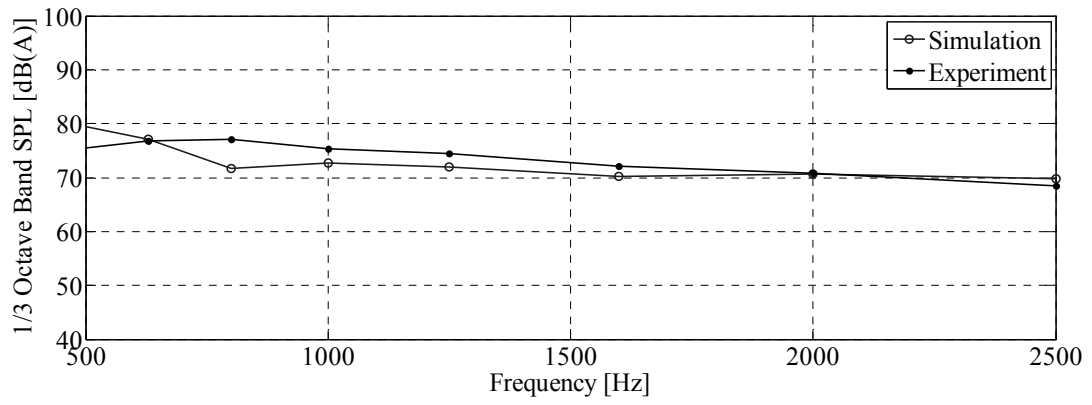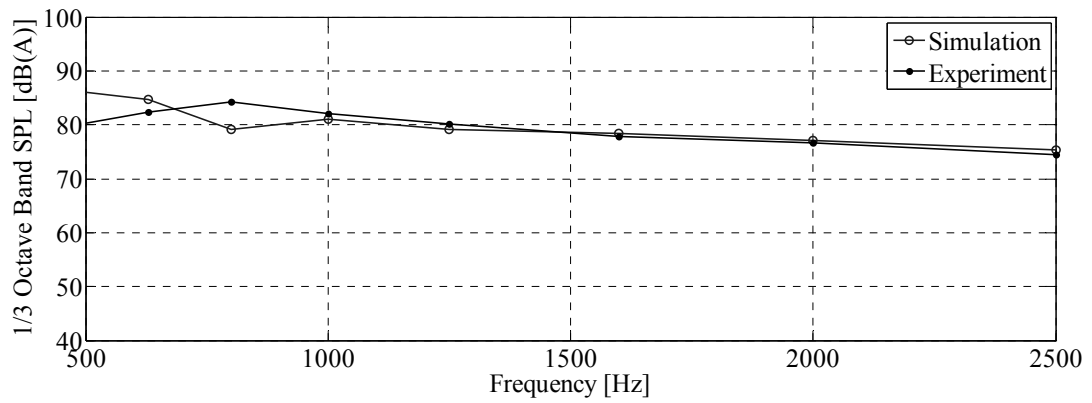Time 0.004 s   Time 0.005 s   Time 0.006 s

Figure 4.22 Sound pressure distribution pattern in simulation

(a) 50 km/h

(b) 70 km/h
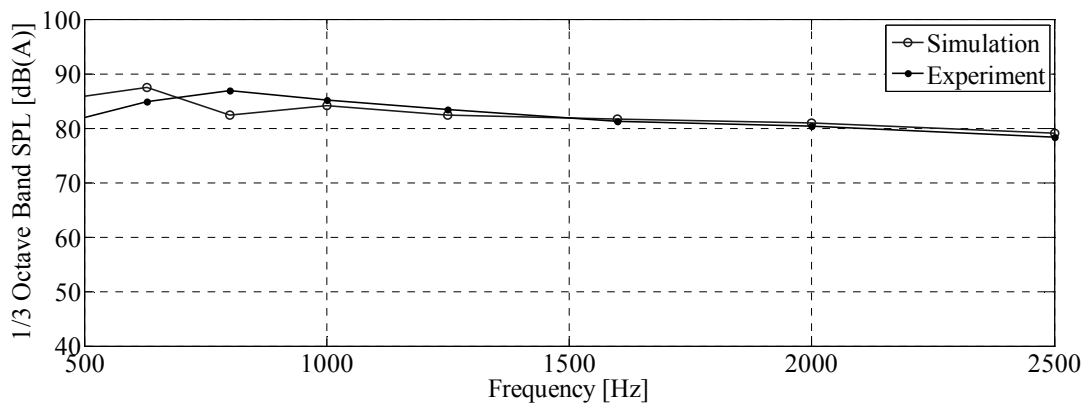
(c) 90 km/h

Figure 4.23 Comparison of A-weighted sound pressure level frequency distribution between simulation and measurement
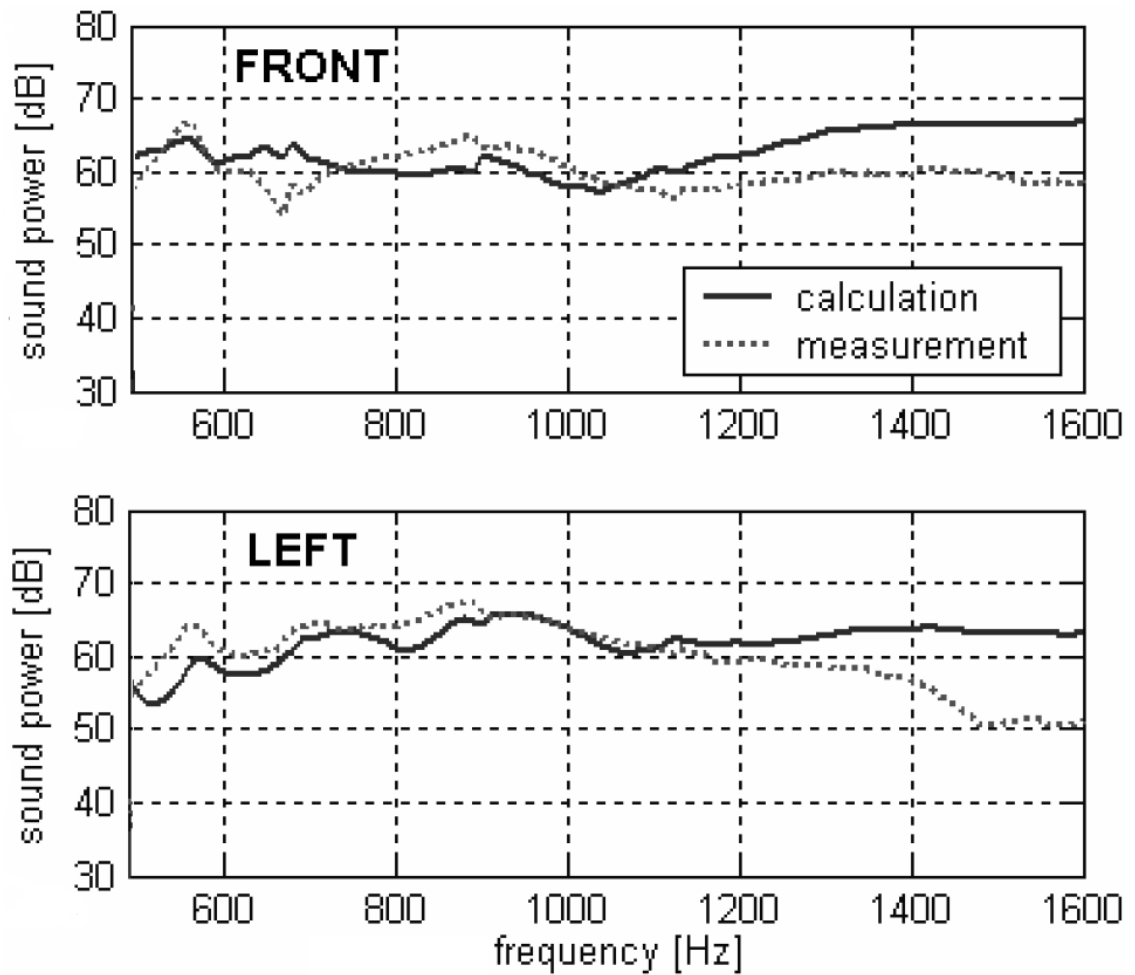
Figure 4.24 Measured and calculated radiated sound power (Yum et. al., 2006)
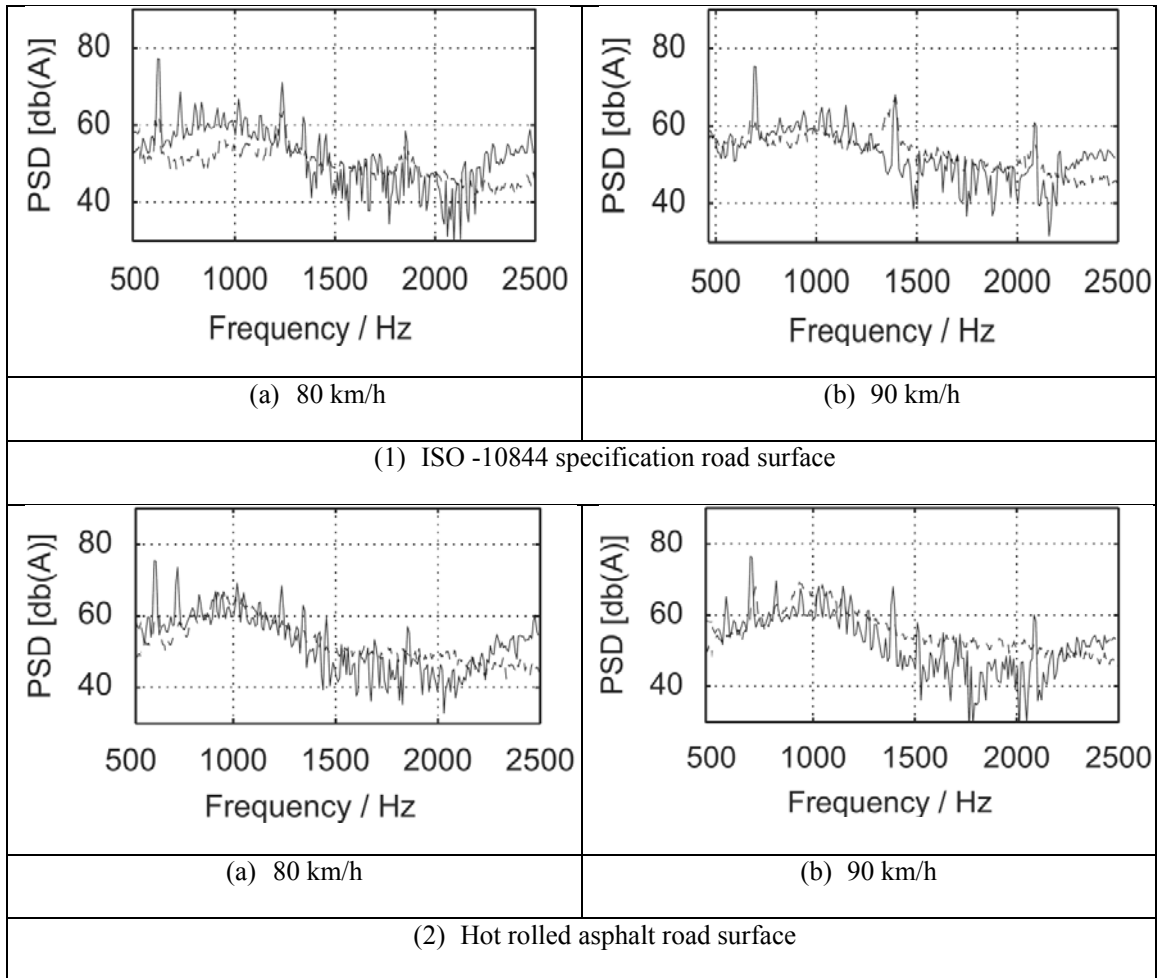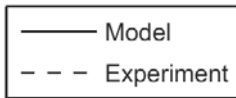
Figure 4.25 Measured and calculated A- weighting power spectral density at microphone position 4 (O'boy and Dowling, 2009)

(a) PIARC smooth tire rolls without contacting pavement

(b) PIARC smooth tire rolls on pavement
**Figure 4.26 Sound pressure level distribution on the horizontal plane at 100 mm
above the bottom of PIARC smooth tire at the speed of 70 km/h**

CHAPTER 5   INFLUENCE   OF   TIRE-PAVEMENT FRICTION ON TIRE-PAVEMENT NOISE

5.1 Introduction

In the past decades, the reduction of tire pavement noise has become a major issue in the process of pavement design. Tire-pavement 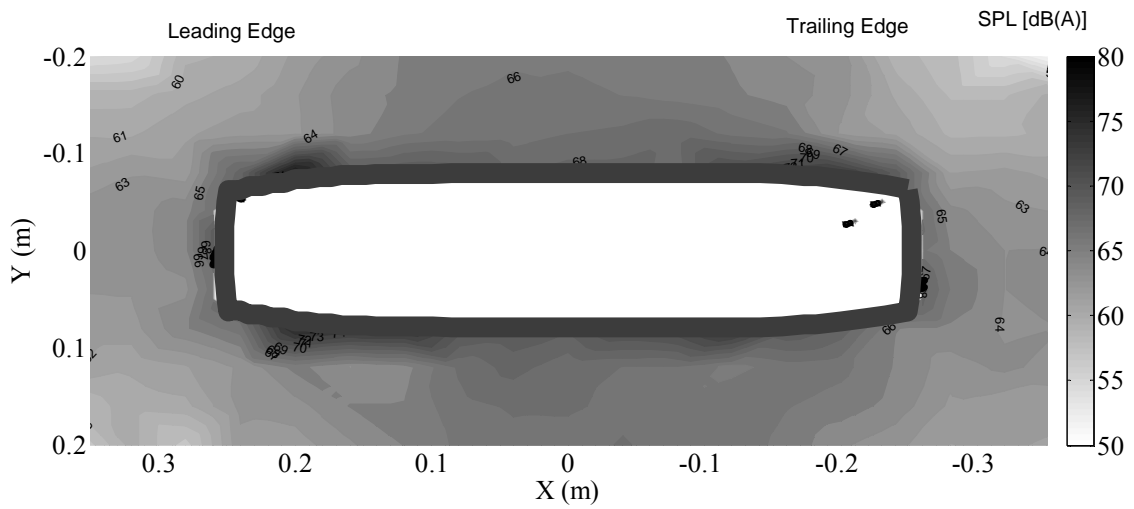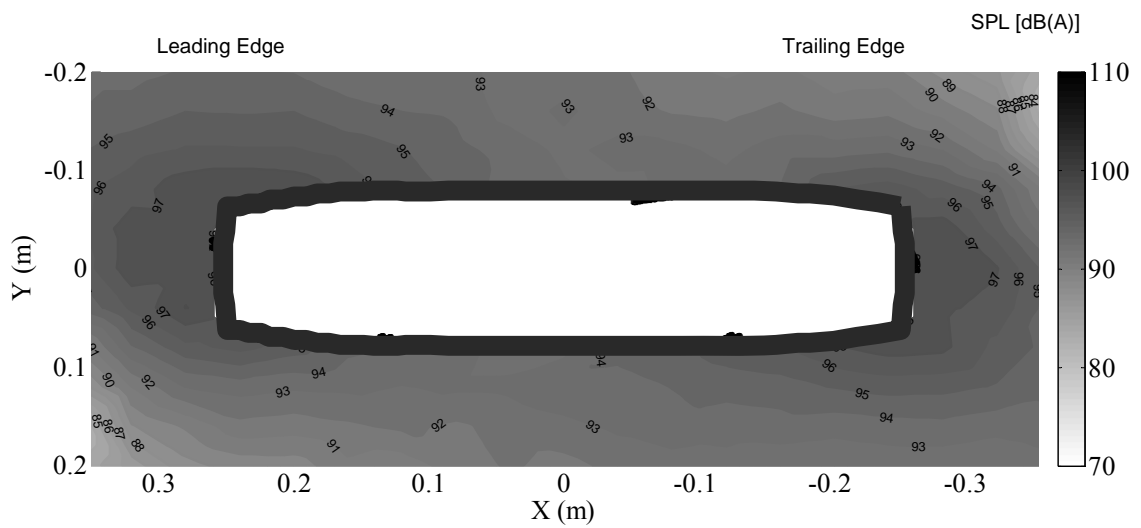noise is generated by complex mechanisms such as tire vibration, air turbulence and stick slip phenomena which are mainly resulted from tire and pavement interaction (Sandberg and Ejsmont 2002). Therefore, a valid description of tire-pavement contact interaction is of great significance for the study of these mechanisms.

When a tire rolls on a pavement, the interaction between tire and pavement generates vertical and tangential stresses at the contact patch, resulting in the vibration of tire belt which act as noise sources. In order to reduce noise generation from tire-pavement interaction, many researchers have studied tire-pavement contact interaction by the methods of experimental studies and mathematical modeling. Périsse (2002) experimentally tested tire belt radial vibration acceleration of a tire rolling on pavement. It was found that vibration acceleration decreased as tire belt moved away from the tire-pavement contact patch. The experimental results showed that the main noise sources were located around the tire contact patch area.

Cesborn et al.(2009) experimentally studied the effect of vertical contact force on noise generation of rolling tires and observed a linear influence of surface macro-texture on the vertical contact around 800 Hz, and consequently on the medium frequency noise levels via the vibrations transmitted to the tire. Other researchers have applied numerical

models to study the noise generation mechanics of tire-pavement interaction. Tire dynamics was originally modelled in a simple mathematical model to analyze the vibration of static tires (Gong 1993). Badalamenti and Doyle (1988) developed a single-point contact model to analyze the vertical vibration characters of tire, where the model was represented by a spring and damper in parallel. In the single-point contact model, the contact point was restricted to lie directly beneath the wheel axle. To overcome the above restriction, a flexible ring model was developed by Gong (1993), which is able to study tire characteristics in the tire rolling state.

Larsson and Kropp (2002) proposed a double-layer tire model. The double layers are made of isotropic thick plates with tension on an elastic bed, and coupled with different thicknesses and material properties. A plate represents the unfolded tire above the spring frequency. The bedding consists of individual springs in tangential, radial and lateral directions. The above models only focus on the study of tire structure dynamics.

Recently, many researchers have focused their interests on developing a comprehensive tire-pavement noise model. Brinkmeier et al. (2008) developed a finite element model to simulate the dynamic behavior of a stationary rolling tire with ground contact by using an arbitrary Lagrange-Eulerian formulation. Noise radiation was represented by Helmholtz equation in the far field, which was modelled by finite element method. He proposed an overall computational strategy using numerical methods to simulate of tire-pavement noise generation. O' boy and Dowling (2009) proposed a multilayer bending plate tire analytical model that considered sidewalls and air pressure in the simulation of tire dynamics of a tire rolling at one speed on road surface. Noise radiation was also represented by Helmholtz equation, but was modelled by boundary element method. In

149

all these models, only the normal contact stress was considered and tire-pavement friction force was not taken into account in the simulation.

The purpose of this chapter is to study the effect of tire-pavement friction on noise generation of a rolling tire. A three-dimensional finite element tire-pavement noise model considering tire-pavement friction is developed. In this model, tire dynamics is simulated by the theory of structure dynamics, and near-field sound transmission is simulated by the theory of aero-acoustics. The computed results are compared with experimental measurements and other numerical results to illustrate the capability of the model. Moreover, based on this model, simulation runs are performed to analyze the effect of tire-pavement friction on noise generation. Finally, some useful insights into tire noise generation mechanisms are obtained from the simulation results.

5.2 Tire-Pavement Friction Modeling

When a vehicle brakes or accelerates, tangential friction force develops at the tire-pavement contact and causes the stick and slip tire tread motions relative to the pavement surface. This stick and slip relative motion makes the tire vibrate tangentially to generate the squeal (a loud and offensive sound) dominated by a single frequency. The stick-slip behavior can be defined as follows:

Sliding: the gap between the contactor node and the target segment is closed; a compression force acts on the contactor node and the node kinematically slides along the target segments.

Sticking: as long as the tangential force on the contactor node that initiates sliding is less than the frictional capacity (equal to the normal force times the Coulomb friction coefficient), the contactor node sticks to the target segment.

The constraint function method is a regularizing technique which allows the treatment of the friction model without the need to differentiate between the stick and slip conditions. Two constrained functions are used to govern the contact behavior between tire and pavement

$$w_n(g,\lambda) = \frac{g+\lambda}{2} - \sqrt{\left(\frac{g-\lambda}{2}\right)^2 + \varepsilon_n} \qquad (5.1)$$

$$\tau + w_\tau(\dot{u},\tau) = \frac{2}{\pi}\arctan\left(\frac{\dot{u} - w_\tau(\dot{u},\tau)}{\varepsilon_\tau}\right) \qquad (5.2)$$

where g is the gap function given by

$$g = (\mathbf{x}^c - \mathbf{x}^t)\cdot\mathbf{n} \qquad (5.3)$$

$\mathbf{x}^c$ is a point on the tire surface and $\mathbf{x}^t$ is the point on the pavement surface satisfying

$$(\mathbf{x}^c - \mathbf{x}^t)\cdot\mathbf{s} = 0 \qquad (5.4)$$

ε_n and ε_τ are small, real and positive numbers.

The constrain equations (5.5) and (5.6) respectively describes the dynamic behavior of the vertical contact stress and horizontal contact stress. Multiplying equations (5.5) and (5.6) and integrating over the whole surface, the following constraint equation is obtained,

$$\int_{S_c}[\delta\lambda w_n(g,\lambda) + \delta\tau w_\tau(\dot{u},\tau)]dS_c = 0 \qquad (5.5)$$

The tire-pavement interaction problem is subject to the constraint equation (5.9), which is added to equation (3.27) to provide the contact conditions at the tire and pavement interaction interface.

Equation 5.5 can be described by Figure 5.1. It involves no inequalities, and is smooth and differentiable. The default value of ε_n is 1.0 x 10^{-12} is suitable for most applications and should rarely be modified (ADINA, 2009).

Equation 5.6 can be described by Figure 5.2. As is clear from this figure, the parameters determining the friction force include: (1) the friction variable τ ; (2) the vertical contact stress; and (3) the dynamic friction coefficient. It is noted that this method can be used to approximate the rigid stick-slip transition.

5.3 Influence of Tire-Pavement Friction on Tire Contact Stress Distribution

In order to study the relationship between tire dynamics and non-uniform interfacial pressure between tire tread and pavement, tire and pavement interaction dynamics is simulated and analyzed under different conditions of slip ratios, which is expressed as

$$S = (1 - \frac{wr}{v}) * 100\% \tag{5.6}$$

where w is the wheel angular velocity; r is the radius of the deformed wheel; v is the vehicle velocity. Depending on the value of S, three different rolling states of tire can be defined. When $S = 0$, the tire runs in the free rolling state. When $S > 0$, tire runs in the braking force state. When $S < 0$, tire runs in the driving force state.

Figure 5.3 shows the three-dimensional contact stress predicted from the proposed tire-pavement interaction model in the static loading condition. The vertical stress is distributed non-uniformly in the contact patch area, especially at the edge of the contact patch due to the bending stress in the sidewall. It is clearly illustrated that the vertical and transverse contact stresses have a convex shape along the contact length, while longitudinal contact stress have a reversed pattern with backward stresses in the front half and forward stresses in the rear half. The distribution patterns of the predicted vertical and longitudinal contact stresses are consistent with the patterns of the predicted contact stress by Wang (2011).

Figure 5.4 shows the contact vertical, transverse and longitudinal stress pattern distribution along contact central line. It is illustrated that vertical stress is non-uniformly distributed along central longitudinal contact line. There is a maximum vertical stress in the middle of the contact area. The longitudinal stress is non-uniformly distributed along central longitudinal contact line. The maximum longitudinal stress is located in the leading area in the contact area. The transverse stress is non-uniformly distributed along central transverse contact line. The maximum transverse stress is located in the intermediate area. The numerical results are further compared with experimental results. It can be found that the predicted central line pattern has a good agreement with the measured results (as shown in Figure 5.5) by Liu et al. (2010). The maximum measured vertical stress is about 548 kPa, and maximum predicted vertical stress is about 465 kPa. The relative error about the maximum vertical stress is about 14 %. The maximum measured longitudinal stress is 152 kpa, and the predicted maximum longitudinal stress is about 128 kpa. The relative error about the maximum longitudinal stress is about 15 %.

153

As shown in Figure 5.6, the free rolling angular velocity for the vehicle speed of 10 km/h was found equal to 8.35 rad/s. Transverse contact force is always equal to zero in the straight moving state in the various angular velocities. Consistent with the experimental findings reported by Tielking and Roberts and the numerical findings reported by Wang (2011), the analysis results shows that angular velocity has an influence on longitudinal contact stress, but is not significant.

Figure 5.7 shows the predicted longitudinal contact forces with the vertical loads 2000 N and 4000 N under different angular velocity. It can be seen that the longitudinal contact force increases with tire load increasing. The error of longitudinal contact forces between 2000 N and 4000 N is equal to zero at the state of free rolling. The error increases with the angular velocity varying far from the free rolling state until the maximum error 1000 N is achieved. The effect of angular velocity to longitudinal contact force will vary with tire load. It can be found from Figure 5.7 that under the condition of tire load with 2000 N, the peak longitudinal contact force is arrived at the angular velocity with 10 rad/s. The angular velocity increases to 12 rad/s to arrive at the peak longitudinal contact force under the condition of tire load with 4000 N.

Under the simulation conditions of Table 5.1, tire-pavement interaction in the three different rolling states can be simulated based on the calibrated model. Three-dimensional contact stress profiles are shown in Figure 5.8 to Figure 5.10. The contact area in the simulation is about $1.60 \times 10^4 \text{mm}^2$. It has an error of 6% compared with the experimental contact area of $1.70 \times 10^4 \text{mm}^2$ tested by Andrén and Jolkin (2003). To illustrate the variation of contact stress, we alternatively compare the contact stresses

along the circumference of tire predicted by tire model, as shown in Figure 5.11 and Figure 5.12 as described in the next paragraph.

Experimental works by Tielking and Roberts (1987) indicated that vehicle speed had almost no effect on vertical contact stress, and static vertical contact stresses were approximately equal to dynamic rolling vertical contact stress. The computed results in Figure 5.11 show that the vertical force distributions along longitudinal direction almost do not change with rolling state. The only tiny variation with slip ratio occurred in the trailing part of the contact patch. Thus, the computed results from the simulation model are consistent with the finding from experimental observations by Tielking and Roberts (1987). The computed results in Figure 5.12 show the longitudinal traction force distributions along tire circumference. It can be clearly observed that the longitudinal traction force distribution in the tire longitudinal direction of tire varies significantly with rolling state. The maximum traction force occurs in the acceleration state. The traction force is also found to increase with decreasing slip ratio.

5.4 Simulation Results and Analysis of Tire-Pavement Noise

To study the influence of tire-pavement friction on tire-pavement noise generation, Sandberg and Ejsmont (2002) carried out a comprehensive experiment according to standard friction and noise test procedures. The dry friction coefficient and tire pavement noise were measured with PIARC smooth tire. The experiment provides noise friction correlation data suitable for validation of the model developed in the present research to study the effect of friction on tire-pavement noise. Figure 5.13 plots the experimental data and computed results that are used for validation analysis in this thesis.

To analyze the effect of friction on tire-pavement noise, friction coefficients between 0.65 and 1.05 were used in the simulation for the vehicle speed of 70 km/h. Figure 5.14 shows the computed A-weighted sound pressure level frequency distribution for different values of friction coefficients. The overall noise levels for different friction coefficients are further analyzed and presented in Figure 5.15. It is found that the simulation results fell within 95 % confidence limits of the experimental results. This indicates that the model produces results consistent with experimental results, as shown in Figure 5.15. The noise error increases with higher friction coefficient. The reason for higher noise error in the higher friction coefficient could be because pavement texture as a key contribution of tire- pavement noise generation is not considered in this analysis.

To further analyze the noise and friction relationship, a statistic analysis of simulation results in the low frequency (< 800 Hz) and high frequency (>1200 Hz) range is carried out, as shown in Figure 5.16 and Figure 5.17. It can be seen that the low frequency noise generation mechanisms appear to be weakly correlated to friction coefficient. The high frequency noise generation mechanisms have a significant linear relationship with friction coefficient. In contrast, the noise level in low frequency band is much higher than in the high frequency band, more than 6 dB on average. Due to the weak friction to noise correlation in the low frequency band, it is believed that tire-pavement noise cannot be directly controlled by changing the friction between tire and pavement.

Figure 5.18 illustrates the difference of sound pressure level with friction (0.7) and without friction at the microphone position. It can be seen that friction has an obvious effect to tire-pavement noise generation in the whole freqquency band. Specially, the major effect of friction to tire-pavement noise is located in the frequency band from 500

Hz to 1000 Hz. The overall sound pressure level wih friction is 91 dB(A), and the overall sound pressure level without friction is 87 dB(A). Thus, the overall noise level increases by 4 dB due to friction effect. In order to refine the contribution of tire-pavement noise interaction emitted from source region in the model, the sound pressure level distribution on a horizontal cutting plane at the distance of 100 mm above the tire bottom is constructed at the speed of 70 km/h. The distribution construction is under the condition of both with and without friction and is based on the simulation results including the microphone positions. Figure 5.19 shows the overall sound pressure level distribution on that cutting plane with friction and without friction. It can be seen that friction will cause more noise generation in the environment. In order to make a clear comparison, the noise levels of four different locations (as shown in Figure 5.19) are obtained and shown in Table 5.2. It can be found that the noise level in the leading edge of tire is the same as that in the rear edge of tire when tire interacts with pavement without friction. Whereas, the noise level in the leading edge is larger than that in the rear edge when tire interacts with pavement with friction coefficient 0.7. In summary, more noise is made in the direction of the leading area of tire due to the effect of friction.

5.5 Summary

Based on the developed model in the last chapter, an analysis is performed in this chapter to evaluate the impact of surface friction on tire-pavement noise generation. First, the tire-pavement contact model is validated by comparing predicted and measured vertical and longitudinal stress distribution within tire-pavement contact patch for different slip ratios. The comparison shows that the contact model can describe with reasonable accuracy the contact behavior, and the transition between stick and slip state. Next, the

validated model is used to analyze the effect of friction coefficient on tire-pavement noise. The predicted results illustrate that friction coefficient has a different effect on tire pavement noise in the low and high frequency bands. It has a significant correlation with noise generation in the high frequency band. However, the correlation is weak in the low frequency band. This suggests that only tire-pavement noise in the high frequency range can be controlled by changing the friction between tire and pavement.

Table 5.1. Simulation conditions of interfacial pressure between tire and pavement

Vehicle velocity (km/h)	Inflation pressure (kpa)	Vertical load (N)	Friction coefficient
40	200	4980	0.20

Table 5.2 Computed tire-pavement noise at the chosen locations by simulation model

Location (see Figure 6.11)	Noise Level [dB(A)]	
	Without friction	With friction
Point 1	90	95
Point 2	90	93
Point 3	90	92
Point 4	87	91
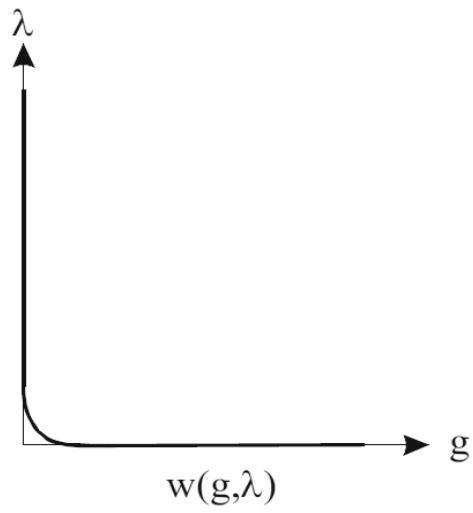
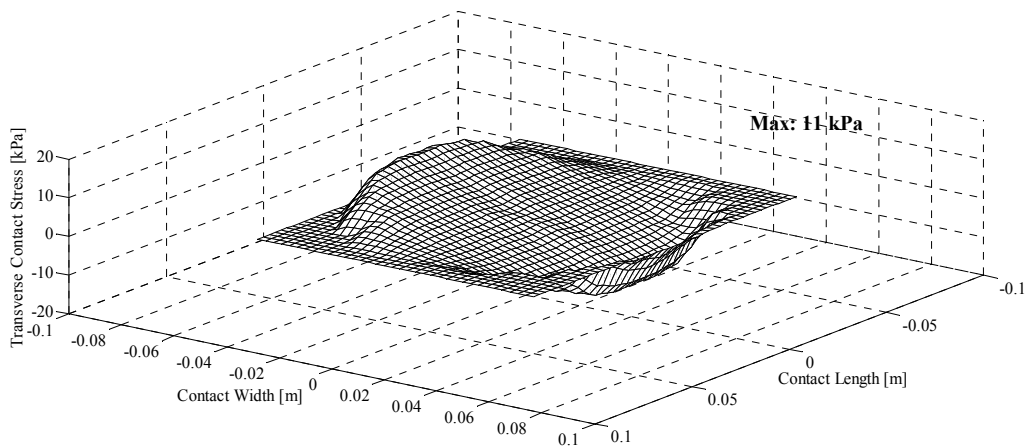**Figure 5.1 Constraint function for normal contact**
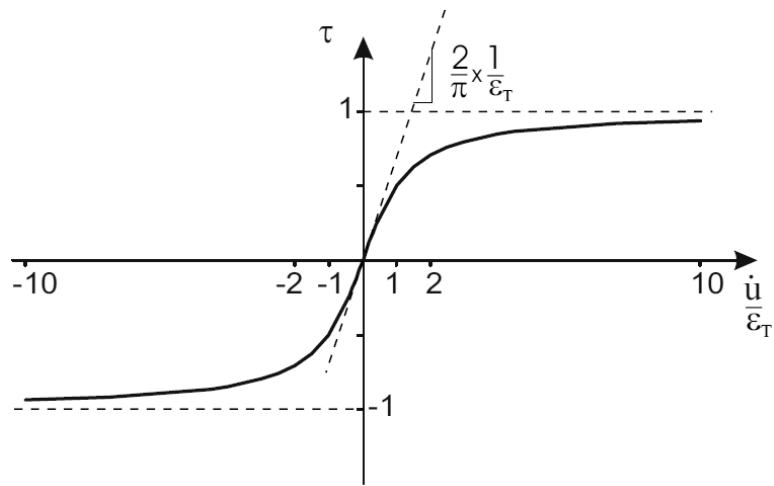
Figure 5.2 Friction contact constraint function
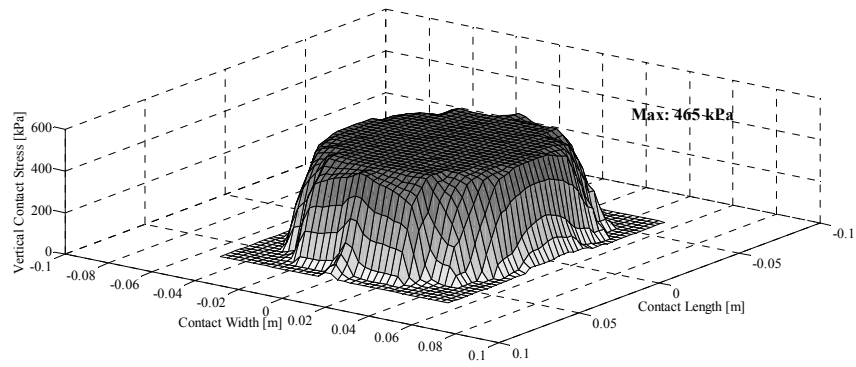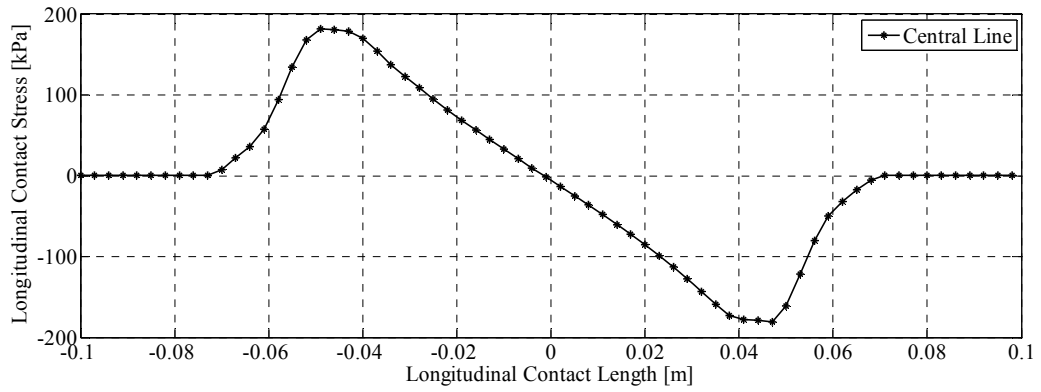
(a) Vertical stress
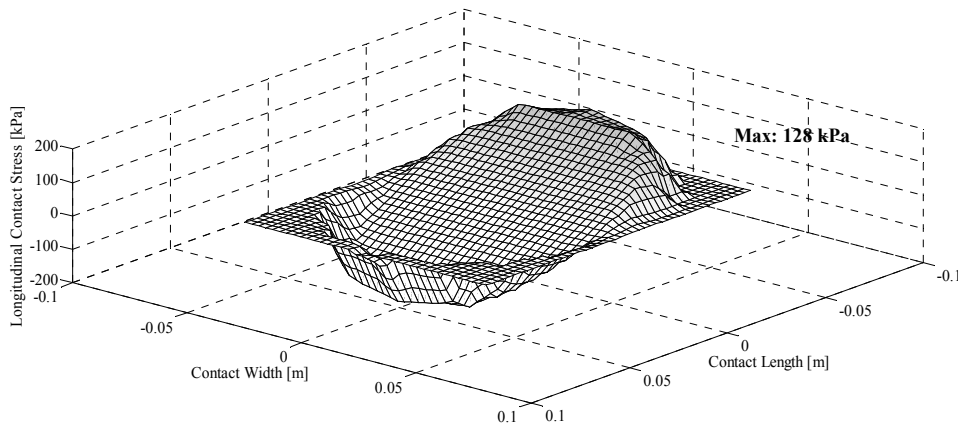
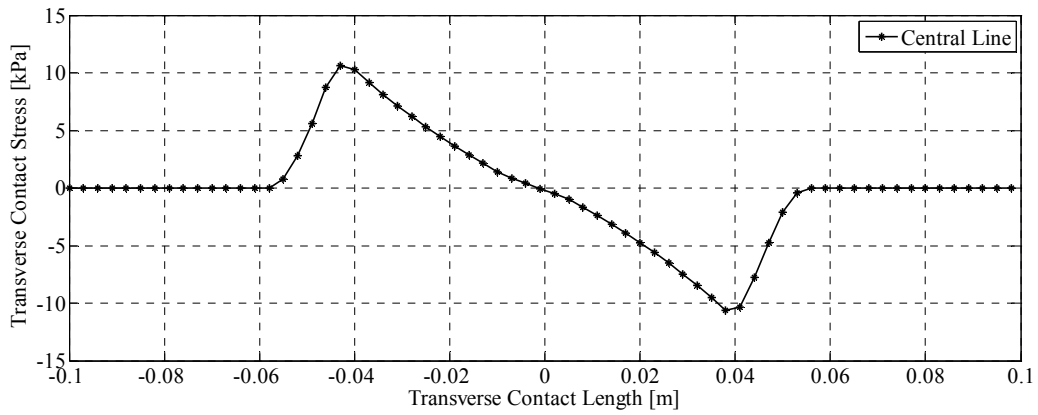(b) Longitudinal stress

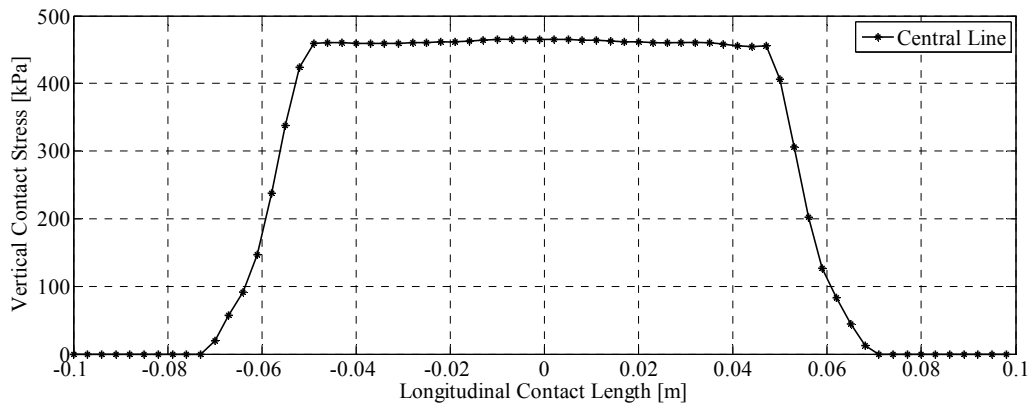(b) Transverse stress

Figure 5.3 Tire-pavement contact stress distributions at static loading condition

(a) Longitudinal stress

(b) Transverse stress

(c) Vertical stress

Figure 5.4 Predicted contact stress distributions along contact length at static loading condition
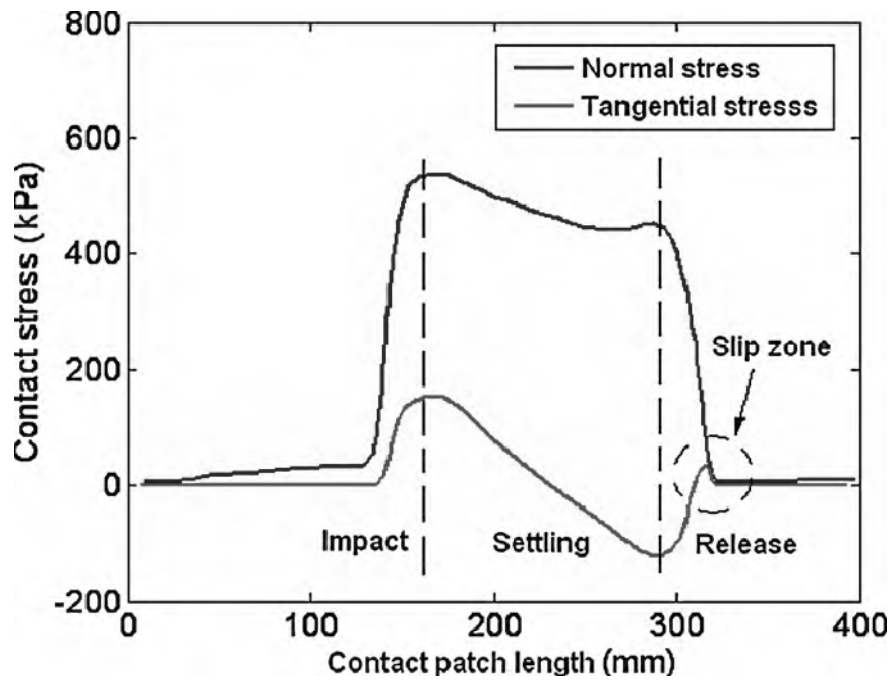
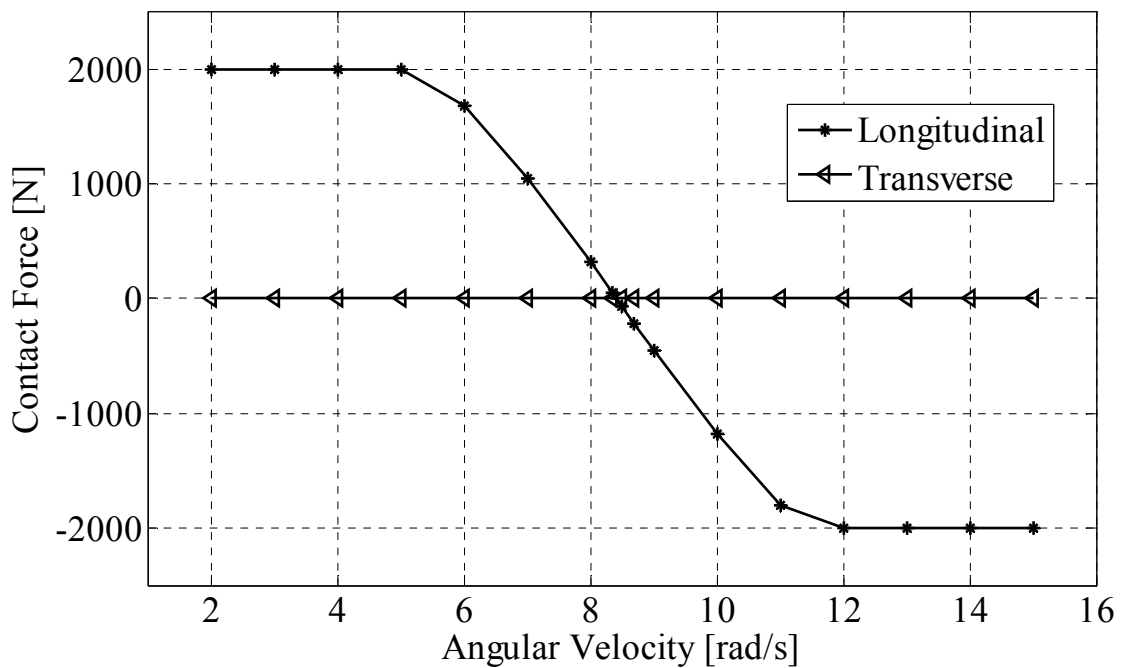**Figure 5.5 Measured contact stress distribution (Liu et. al, 2010)**

Figure 5.6 Predicted Contact force at various angular velocity at a constant vehicle speed (10km/h)
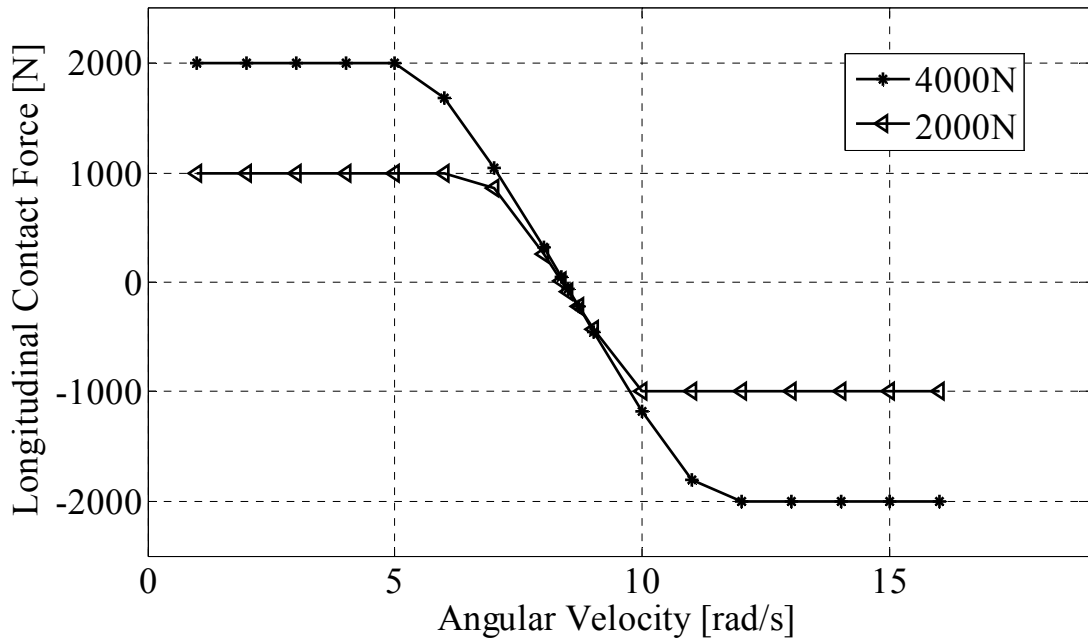
163

Figure 5.7 Predicted longitudinal contact forces under different loads and angular velocity at a constant vehicle speed (10km/h)
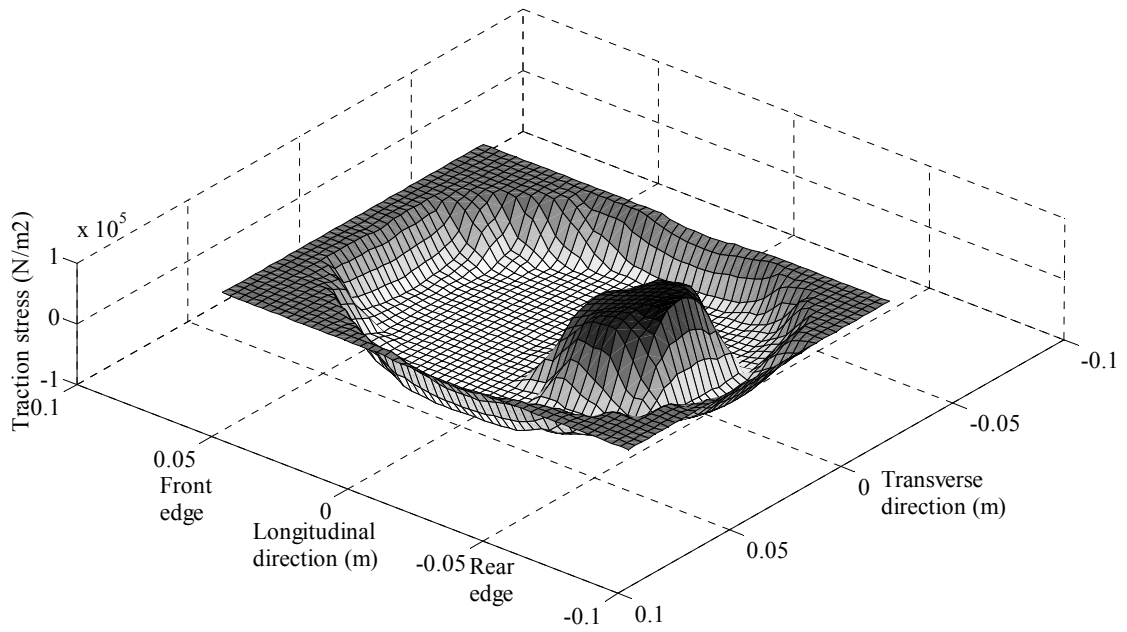
(a) Traction force
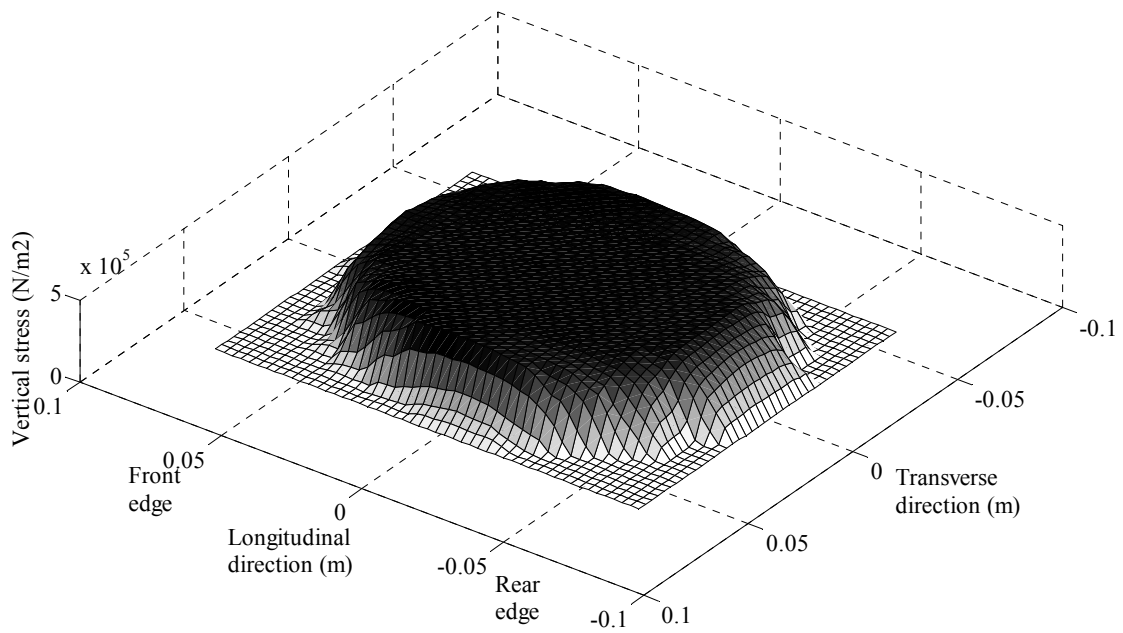
(b) Vertical stress

Figure 5.8 Tire-pavement contact distributions under slip ratio = -0.4 for driving force state
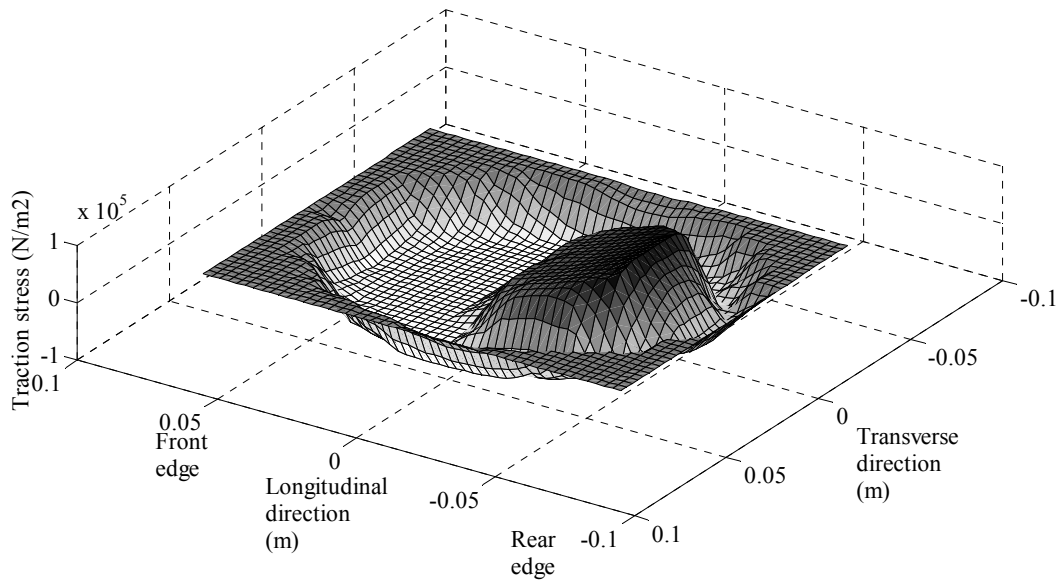
(a) Traction force
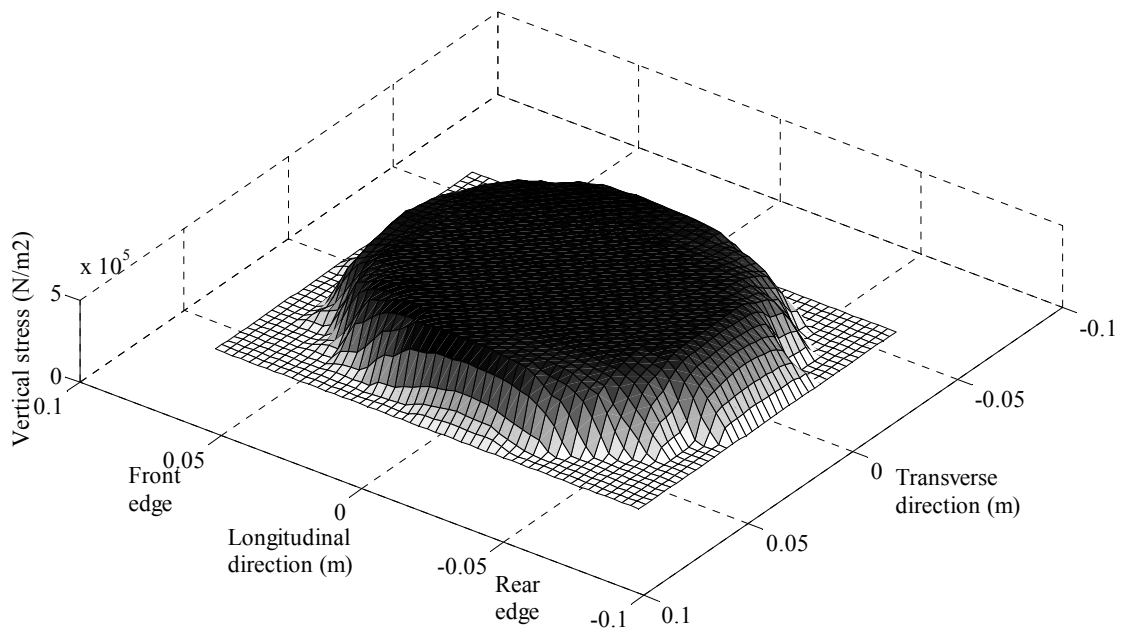
(b) Vertical stress

Figure 5.9. Tire-pavement contact distributions under slip ratio = 0 for free rolling state

166
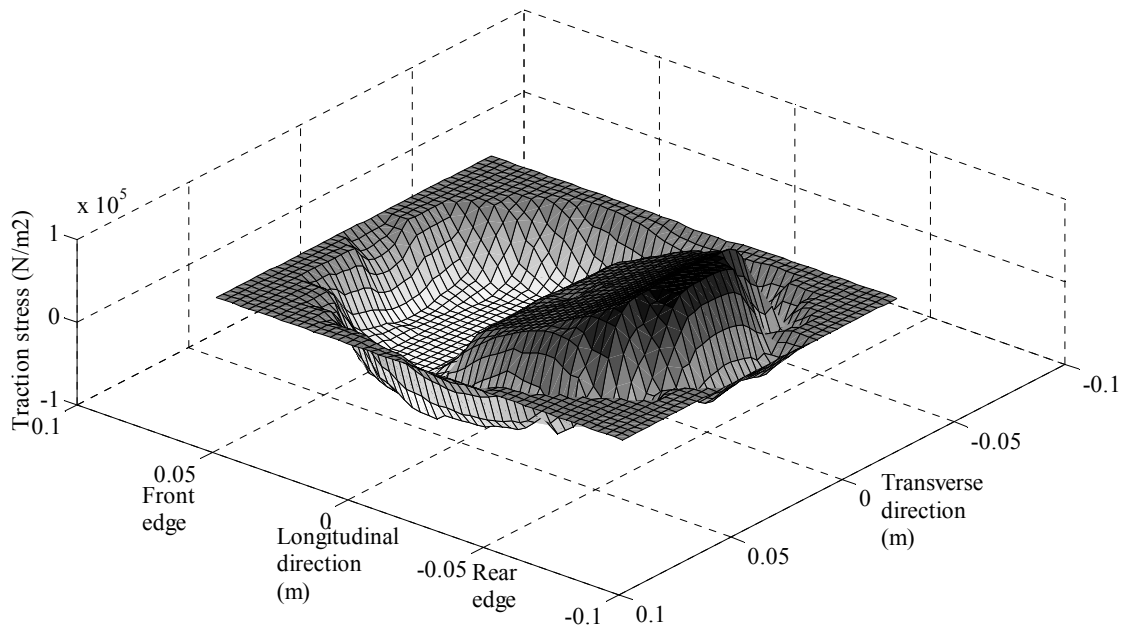
(a) Traction force
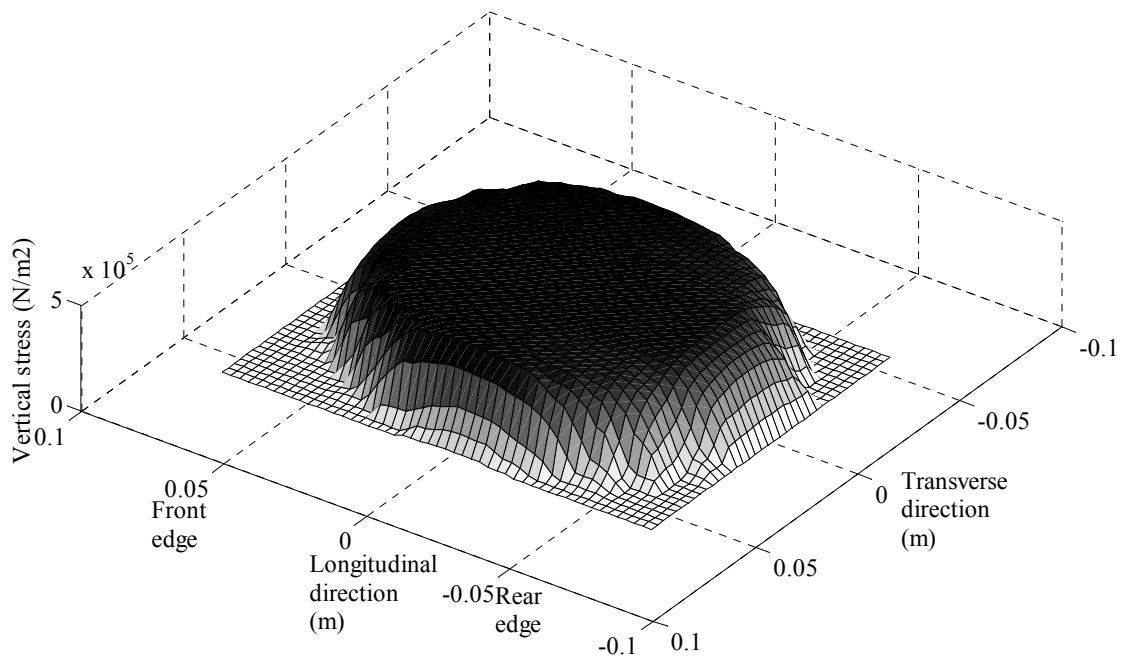
(b) Vertical stress

Figure 5.10. Tire-pavement contact distributions under slip ratio = 0.4 for breaking state
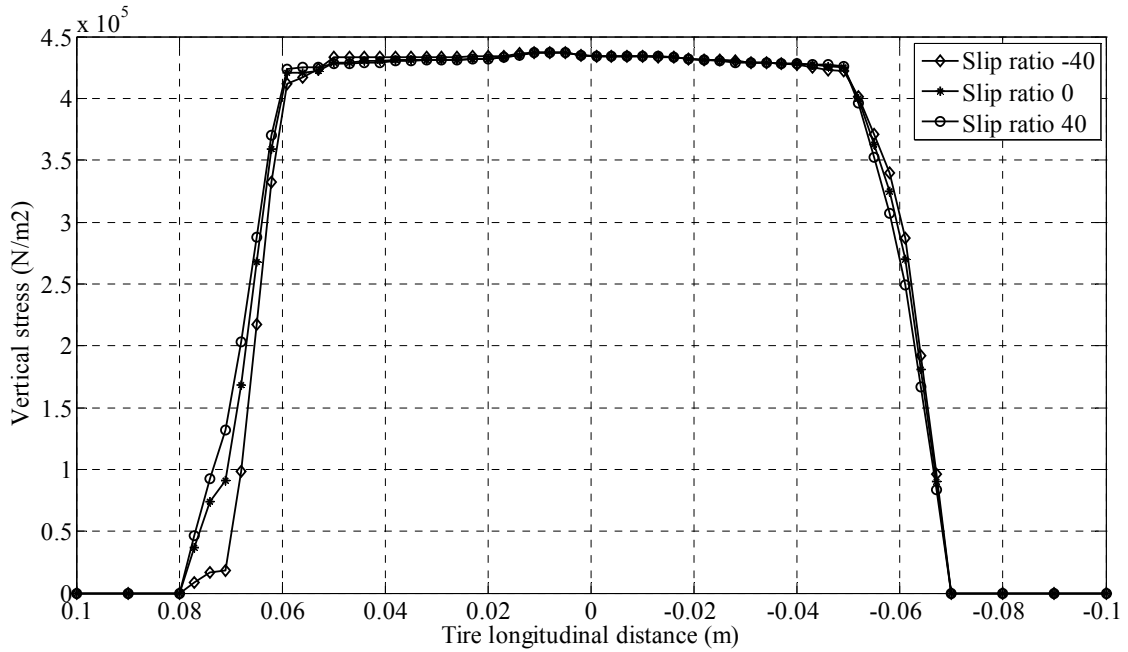
Figure 5.11 Comparison of predicted vertical contact stresses in different slip ratios
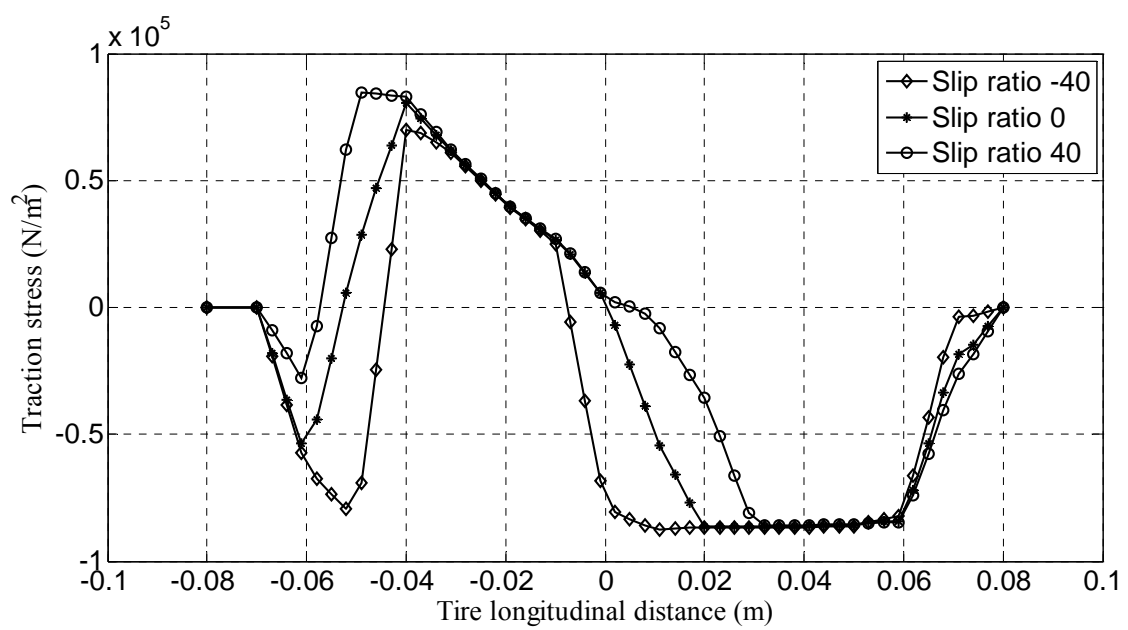
Figure 5.12 Comparison of predicted longitudinal traction force in different slip ratios

168
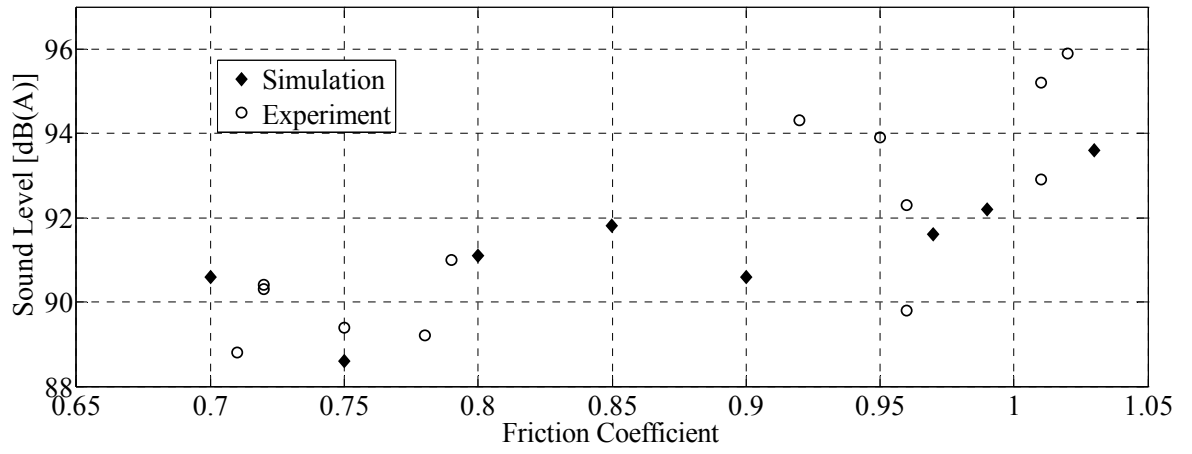
Figure 5.13 Experiment and simulation overall noise level
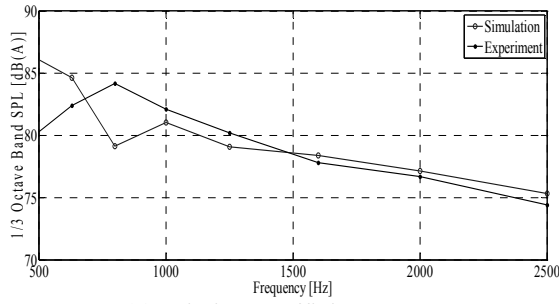
(a) Friction coefficient 0.70
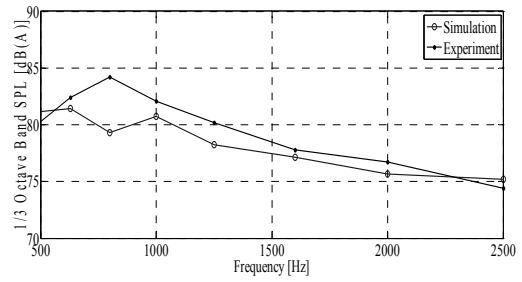
(b) Friction coefficient 0.75
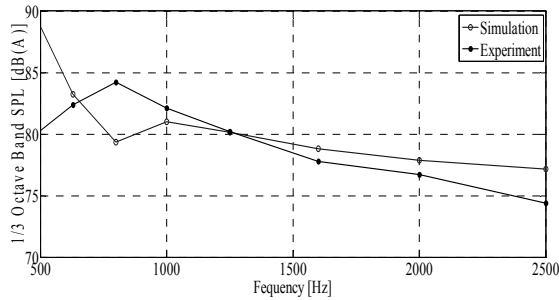
(c) Friction coefficient 0.80
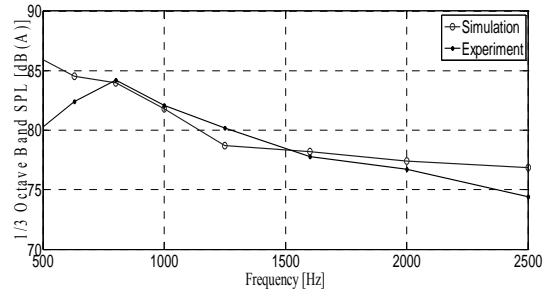
(d) Friction coefficient 0.85
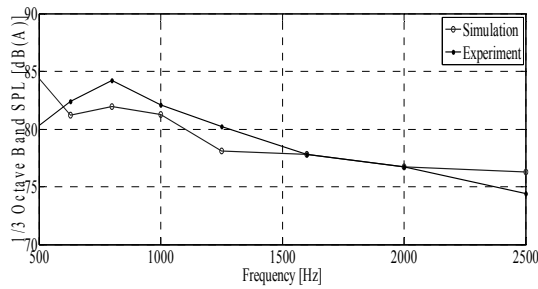
(e) Friction coefficient 0.90
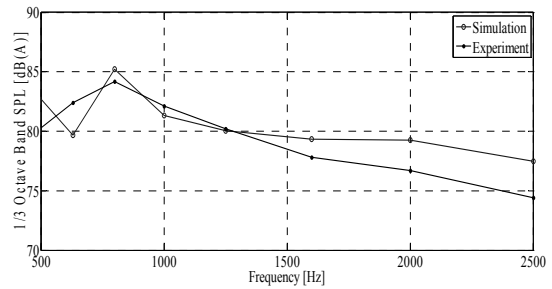
(f) Friction coefficient 0.97
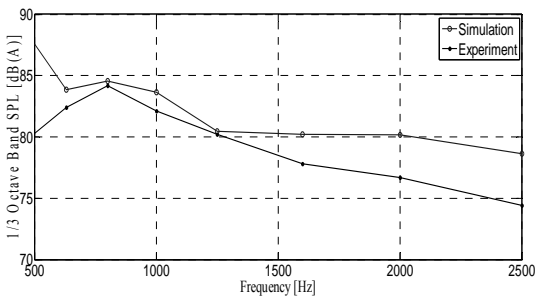
(g) Friction coefficient 0.99
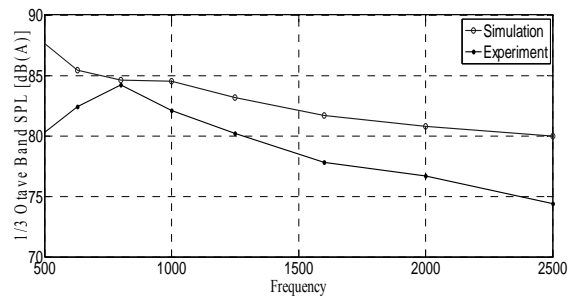
(h) Friction coefficient 1.03

Figure 5.14 Simulation A-weighted sound pressure level frequency distribution in the different friction coefficients

170
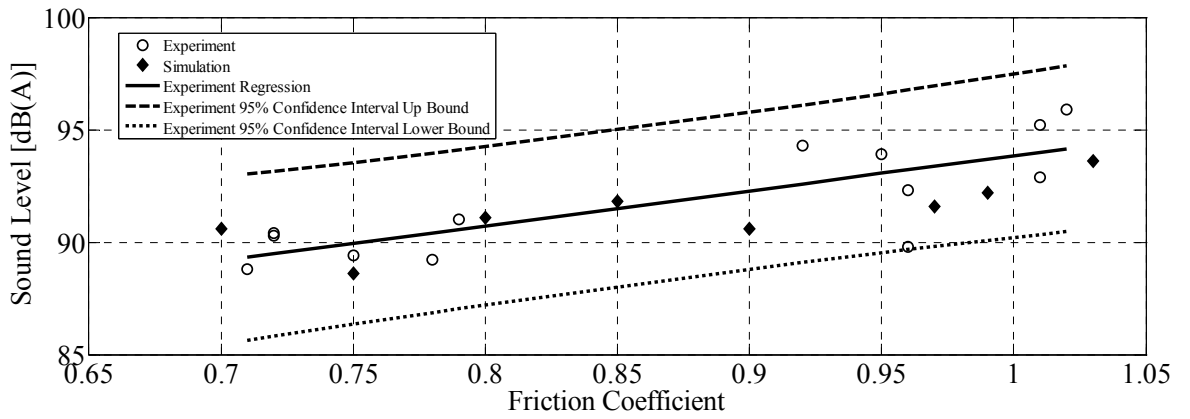
Figure 5.15 Comparison of noise friction correlation between simulation and measurement
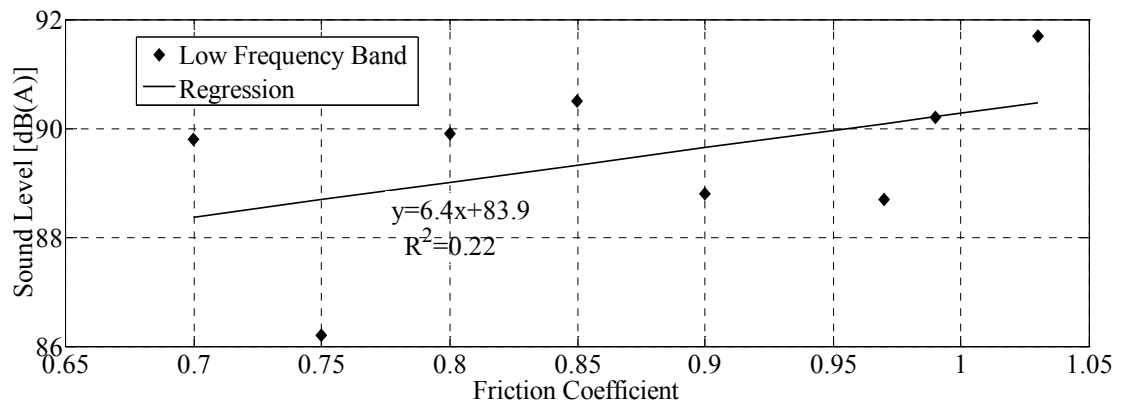
Figure 5.16 Simulation noise friction correlation in the low frequency band

171
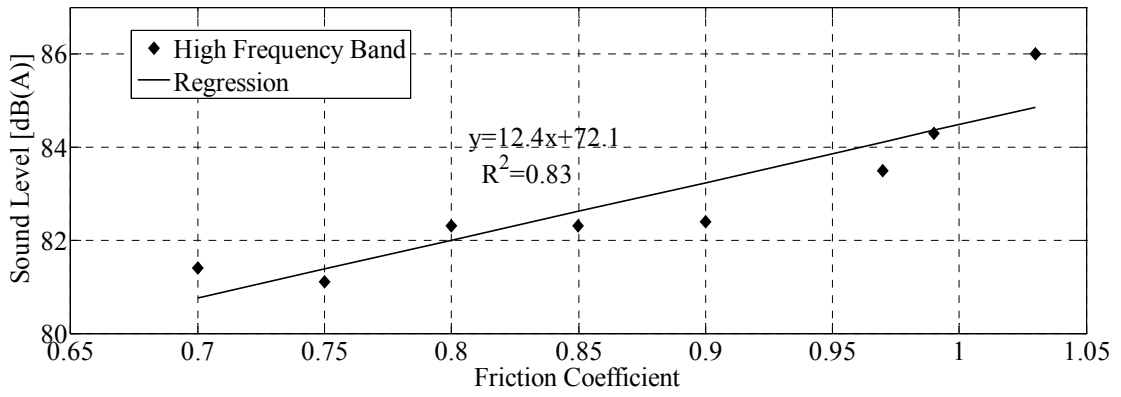
Figure 5.17 Simulation noise friction correlation in the high frequency band
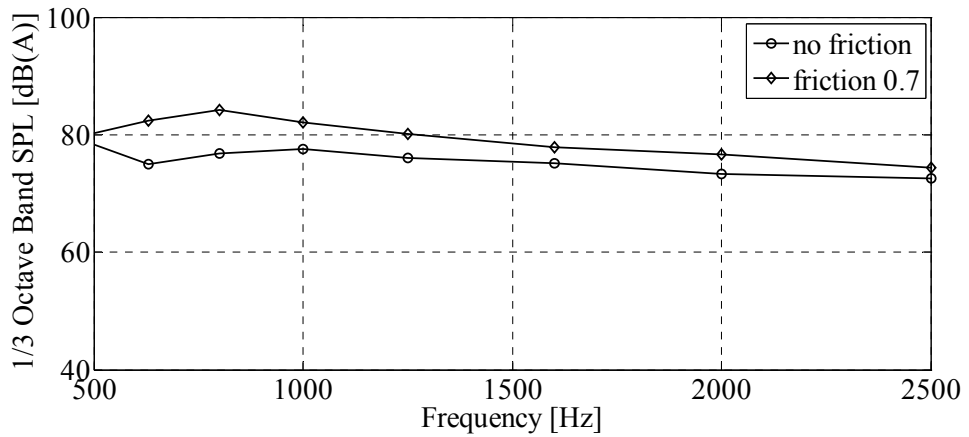
Figure 5.18 Predicted Sound pressure level without friction and with friction
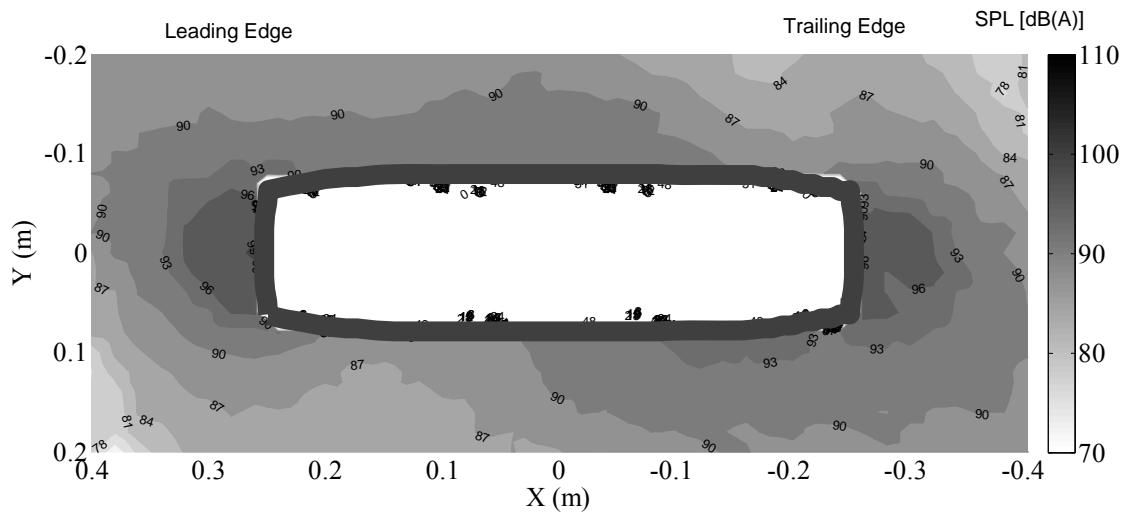
(a) PIARC smooth tire rolls without friction
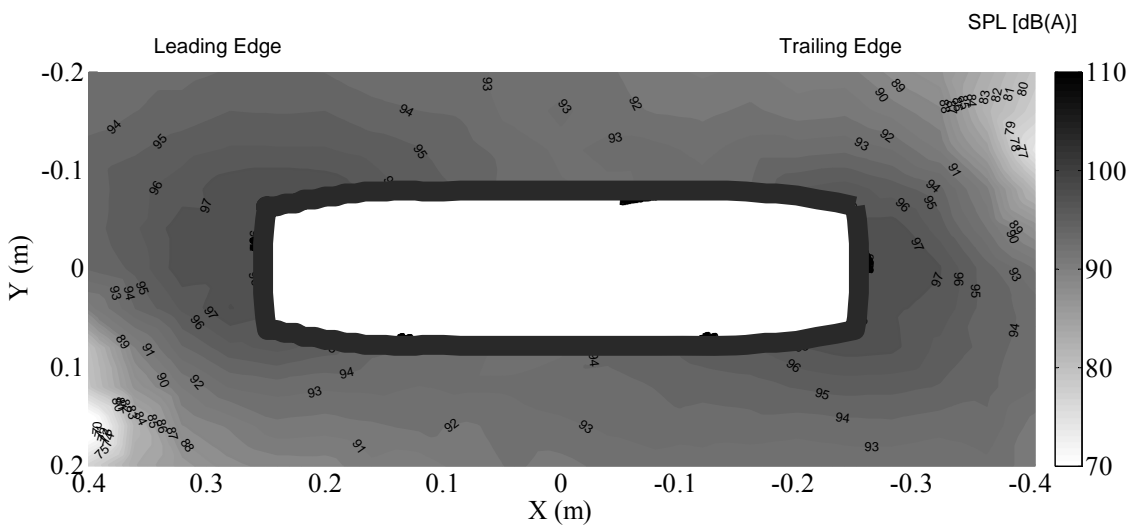
(b) PIARC smooth tire rolls with friction 0.7
Figure 5.19 Sound pressure level distribution on the horizontal plane at 100 mm above the bottom of PIARC smooth tire at the speed of 70 km/h

CHAPTER 6   ANALYSIS OF TIRE-PAVEMENT NOISE

IN VEHICLE CORNERING MOVEMENT

6.1 Introduction

During vehicle cornering movements, due to the constantly changing direction of the tire and the presence of radial forces, the state of tire-pavement contact stresses is different from that in straight road operations. Several researchers have studied cornering tire dynamics by the methods of experimental studies and mathematical modelling. Tönük and Ünlüsoy (2001) developed a detailed finite element model to prediction tire cornering force characteristics. Vil'ke and Dvornikov (1998) studied the steady-state cornering without slipping using a novel analytical model where the tire surface is represented by the deformed surface. Kozhevnikov (2011) proposed an analytical model capable of simulating complex dynamic processes to investigate the steady-state cornering of a wheel with slipping. All these models focus on the effect of cornering on tire-pavement interaction. However, no numerical research so far has been performed to study the effect of tire cornering on tire-pavement noise.

In this chapter, the tire-pavement noise simulation model developed in this research is employed to examine analytically the effect of tire cornering on tire-pavement noise. The theoretical development of the three-dimensional finite element near-field tire-pavement noise simulation model is first described. A numerical example is presented to demonstrate the capability of the proposed model to analyze tire-pavement noise generation during vehicle cornering actions.

6.2   Modeling development

A detailed description of the theoretical formulation and validation of the tire-pavement can be found in the previous chapters. In order to study the effect of the pavement radius on tire-pavement noise, some changes to the tire-pavement contact representation have to be made, as illustrated in Figure 6.1. Shown in Figure 6.1 is a tire with its center fixed on the point O. A Lagrange frame of reference XYZ (see Figure 6.1) is used in the proposed model to analyze the dynamics of a tire moving horizontally at velocity v with a rolling angular velocity w. The angular velocity w acting on the point O is transferred to tire tread by tire sidewall. The air pressure p' is uniformly acting on the inner surface of tire sidewall and tread. In the same time, the pavement, assumed to be rigid, moves horizontally with velocity $v = w \cdot \bar{r}$ and vertically with wheel load P, where $\bar{r}$ is the tire radius. The horizontal friction force f is loaded on tire due to the relative motion between tire and pavement. The local frame of reference θxr attached on the tire tread rotates with the tire tread.

To account for the horizontal friction force f, a relative cornering contact frame between tire and pavement is introduced into the tire-pavement interaction simulation. This has been effectively applied to experimentally study the effect of cornering on tire dynamics (Steen, 2010). Shown in Figure 6.1 (b) and (c) is a top view tire pavement interaction tire with its turning center located at O'. The pavement will move horizontally with angular velocity $w' = w \cdot \bar{r} / r'$, where r' is the pavement turning radius.

Figure 6.2 illustrates the cornering tire-pavement interaction model under their boundary conditions used in the simulation: vertical load and pavement angular velocity acting on the central point O' of pavement, and tire inflation pressure acting on the inner faces and

175

fluid-structure interface at the tread and sidewall surface of the tire (as shown Figure 6.1).

The pavement surface is assumed to be a rigid body. The detailed discussion for tire

materials and meshing has been done in Chapter 3, where 8320 elements are used in the

tire modeling. The adaptive mesh method is also used to calibrate the radiation model.

Having dynamic tire responses at time intervals of 0.00002 second on a computer of Intel

Xeon E5645 with 6 cores, the convergence of relative error against computation time is

demonstrated in Figure 6.3, which illustrated a converge slope of almost -0.092

($e_r \approx Ct^{-0.092}$).The convergence rate is the same as the straight moving tire-pavement

noise model in Chapter 4 (as shown in Figure 4.13). It is noted that CPU-time consumed

increases with the decrease of the relative error. The mesh number between 180000 to

220000 is used for noise radiation modeling to obtain accurate solutions and avoid large

mesh deformation.   The computation time as a function of fluid mesh number is

illustrated in Figure 6.4.

6.3   Determination of Effective Friction coefficient

By means of an unknown parameter identification strategy, as shown in Figure 6.5,

effective friction coefficient for a cornering movement can be obtained. The tolerance ε

of 3 dB is used in this iterative search (Sandberg and Ejsmont, 1986). The calibration

process is first performed to match the sound pressure level from the simulation

approximately to the experimental measured value for the case of a vehicle speed of 70

km/h with a wheel load of 3000N. In order to avoid local optima, three initial friction

coefficients are randomly chosen: 1.0, 0.75 and 0.55. The results of iterative search are

plotted in Figure 6.6. This plot shows the efficient friction coefficient is around 0.65.

Sandberg and Ejsmont (2002) illustrated that the range of friction coefficient tested by

PIARC smooth tire in the different kinds of pavements is from 0.7 to 1.0. In this research, 0.70 is chosen as the effective friction coefficient.

6.4 Tire-Pavement Contact Stress Analysis

Using the tire-pavement interaction model developed in this chapter, the tire-pavement contact stress distributions under three different driving states are determined. The three different driving states analyzed are: straight, right cornering and left cornering. The vehicle operating conditions chosen for the analysis are shown in Table 6.1.

Figure 6.7 shows the cornering forces that act on the tire during cornering at the different slip angles. The cornering force is induced on the tire due to the tread slip at the lateral direction when the vehicle is steering, which is parallel to the road surface and then increases non-linearly to its peak value at the slip angle of around 6°. When slip angle is large than 3.5^o, the transverse contact force is located within the 95% difference interval of the peak transverse contact force. This variation in cornering force due to slip angle is similar to the predicted results reported by Wang (2011), as shown in Figure 6.8, where the cornering force arrives at its peak value at the slip angle of around 5° and then stays relatively stable. The development trend of the cornering force has also a good agreement with the experimental results in the literatures (Wong, 1993).

Figure 6.9 illustrates the predicted cornering forces that act on the tire during cornering at a constant angle 3.5^o at the different rolling radius. We can see that the lateral contact force decreases with rolling radius increasing, and conversely, while the longitudinal contact force increases with rolling radius increasing. It implies that tangential force points in the direction of vehicle cornering with rolling radius decreasing. Figure 6.10

illustrates the predicted maximum contact stress at a constant angle 3.5° at the different rolling radius. It is illustrated that maximum lateral contact stress decrease with rolling radius increasing, and conversely, the maximum longitudinal contact stress increase with rolling radius increase.

Figure 6.11 presents the vertical and lateral stress distributions for three driving states. One can see that the stress distribution on the tire-pavement contact patch is reshaped from a rough ellipse (see Figure 5.8 and Figure 5.9) to a rough trapezoid (see Figure 6.11) due to the cornering action. The lateral stress on the contact patch points in the opposite direction of vehicle cornering. One of the shoulders becomes longer, and other grows shorter. When tire turns left, right shoulder becomes longer and left shoulder grows shorter. When tire turns right, right should becomes shorter and left shoulder grows longer. The vertical stress at the longer shoulder is higher than at the shorter shoulder. The above findings are in general agreement with the experimental results (see Figure 6.12) reported by Steen (2007).

6.5 Validation of Noise Prediction of Proposed Model

Since wind hood have a large influence on the acoustic free field conditions at frequencies below 500 Hz (Sandberg and Ejsmont 1991), the reconstructed minimum noise frequency is chosen as $f_{min} = 500\text{Hz}$. In this study, the variation of tire-pavement noise between 500 Hz and 2500 Hz is analyzed. This covers the sensitive frequency range for human beings.

Simulation analysis is performed based on the experimental study on the PIARC smooth tire by Ejsmont and Sandberg (1981). The noise data under different driving states (i.e.

straight driving, turning left, and turning right) were collected by the "rear" microphone according to the CPX standard measurement method (see Figure 6.13) at two vehicle speeds: 50 and 70 km/h.

From the simulation analysis using the proposed model developed in this study, the power spectrum density of the sound pressure levels at the "rear" microphone position are obtained, and the corresponding A-weighting values are computed. The A-weighting one-third octave band sound pressure level frequency distributions are plotted in Figure 6.14 along with the corresponding experimental data. By comparing the averaged numerical results with experiments, we can find that there is a good agreement in the all frequency band in the 50 km/h. In contrast, in the 70 km/h there is a relatively large SPL difference of 7 dB in the low frequency band.

Figure 6.15 compares the differences between the noise generated during right cornering and left cornering as obtained by the simulation of this research and the experimental results by Sandberg and Ejsmont (1981) for the vehicle speed of 70 km/h. There are two regions: a positive difference for low, and a negative for high frequencies. In general, there is a good agreement between the simulation and experimental results.

6.6 Analysis of Simulation Results

6.6.1 Near Field Distribution of Tire-Pavement Noise

The analysis in Figure 6.14 generates sound pressure in different frequency bands L_{Pi}. The overall sound pressure level L_P is calculated as,

$$L_P = 10 \log_{10} \sum_{i=1}^{N} 10^{L_{Pi}/10} \tag{6.1}$$

Figure 6.16 records the dBA computed for all the cases of cornering-speed combinations analyzed. It is illustrated from Figure 6.14 that the difference between the experiment and simulation in Figure 6.16 is mainly from SPL error in the low frequency. The existing literatures (Sandberg and Ejsmont, 2002) already illustrated that SPL in low frequency band is mainly affected by tire material properties. The material properties are influenced by tire cornering. It is possible reason why there is a large error in the low frequency band. Although there is a significant difference between simulation and experiment, simulation results illustrate a similar trend with experiment, at which the noise level is lower in straight driving than in the cornering, and more noise is generated in the "rear" microphone position in the tire right cornering state more than the tire left cornering state.

In order to refine the contribution to tire-pavement noise interaction emitted from source region in the model, the sound pressure level distribution on a horizontal cutting plane at the distance of 100 mm above the tire bottom is constructed for the speed of 70 km/h with straight driving and left cornering based on the simulation results, which includes the microphone positions. Figure 6.17 shows the overall sound pressure level distribution on that cutting plane. Compared with straight driving in Figure 6.17 (a), it can be observed that sound pressure level is higher at the right field than at the left field of the tire for left cornering. It indicates that left cornering will generate more noise in the right direction of tire due to lateral friction. In order to study the effect of velocity to tire-pavement noise, Figure 6.18 shows the overall sound pressure level distribution at vehicle speed of 50 km/h and 70 km/h. Table 6.2 further compare the noise levels of four

locations shown in Figure 6.11. The overall SPL has a 6dB increase when the vehicle speed increases from 50 km/h to 70 km/h.

6.6.2 Influence of Cornering Radius

The study covered the common range of passenger car cornering radius under the normal highway operating conditions. Figure 6.19 plots the variation of tire-pavement noise with vehicle speed 70 km/h for four different cornering radii, 65 m, 80 m, 100 m and 120 m. Figure 6.19 shows that lower tire-pavement noise was generated when vehicles travel on curves with larger radius. This result confirms the observed tire-pavement noise variation with cornering radius as recorded in experimental studies by researchers (Sandberg and Ejsmont, 1981).

6.7 Summary

This chapter extends the tire-pavement noise model proposed in the previous chapter to study tire-pavement noise generated by vehicles traveling on horizontal curves. The simulation process is first discussed, where a cornering force is applied on the contact patch of tire. An analysis was first performed to verify that the contact dynamics of cornering tires matched well with experimental data. The proposed model was next applied to simulate tire-pavement noise for different tire load parameters. The predicted results illustrate a good agreement with experimental data reported in past research. Further analysis was performed to show that cornering direction will influence tire-pavement noise in different frequency bands. Finally, a parameter analysis was performed to evaluate the effect of surface radius on tire-pavement noise. The simulated results illustrate that cornering force has different effects on tire-pavement noise in

different frequency bands, and that noise amplification increased as the cornering radius became sharper.

Compared to the existing models, the main contributions of the present approach include: (1) A fully three-dimensional numerical model is developed to simulate the effect of tire cornering on tire-pavement noise generation; and (2) The developed model can effectively predict the effect of cornering on tire-pavement noise.

Table 6.1 Simulation conditions of interfacial pressure between tire and pavement

Vehicle velocity (km/h)	Inflation pressure (kpa)	Vertical load (N)	Friction coefficient
70	190	3000	70

Table 6.2 Computed tire-pavement noise at the chosen locations by simulation model

Location (see Figure 6.11)	Noise Level [dB(A)]	
	Vehicle Speed 50 km/h	Vehicle Speed 70 km/h
Point 1	94	100
Point 2	96	104
Point 3	90	96
Point 4	92	98
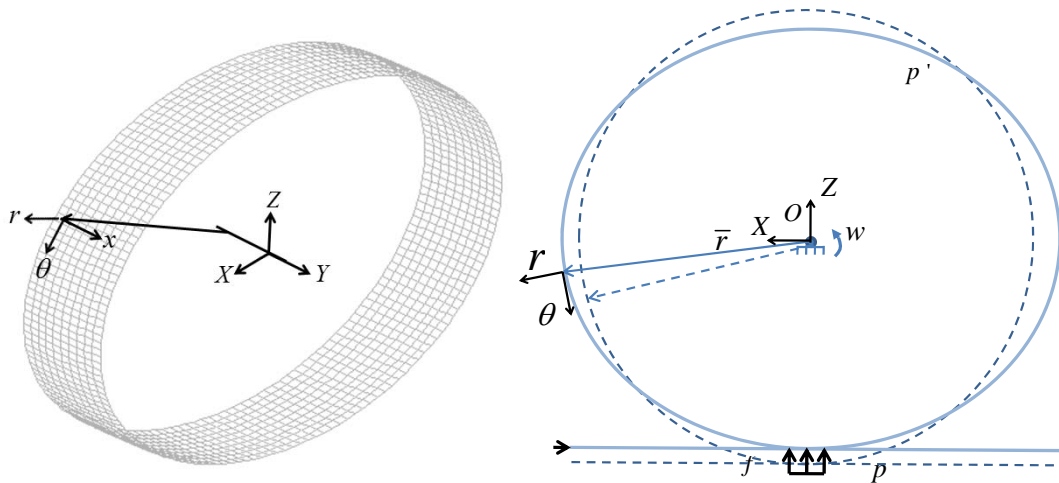
(a) Model of shell element of tire tread

Figure 6.1Framework of tire cornering on pavement
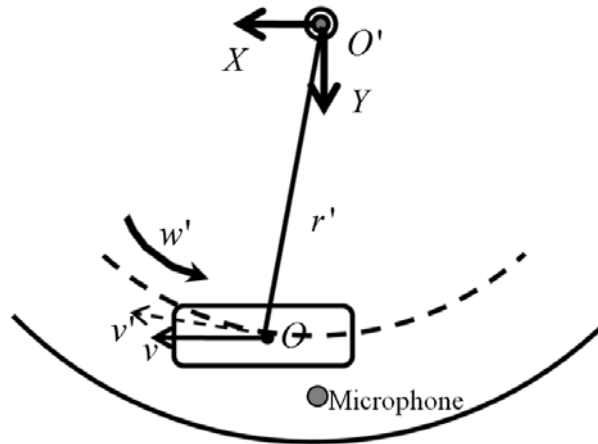
(b) Top-view of tire and pavement interaction for right turning
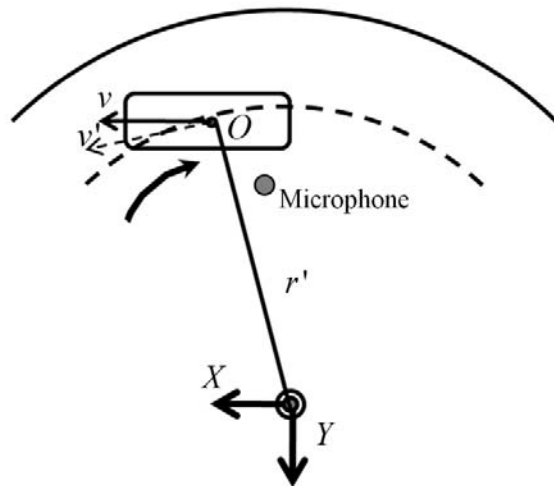
(c) Top-view of tire and pavement interaction for left turning

Figure 6.1 Framework of tire cornering on pavement (Continue)
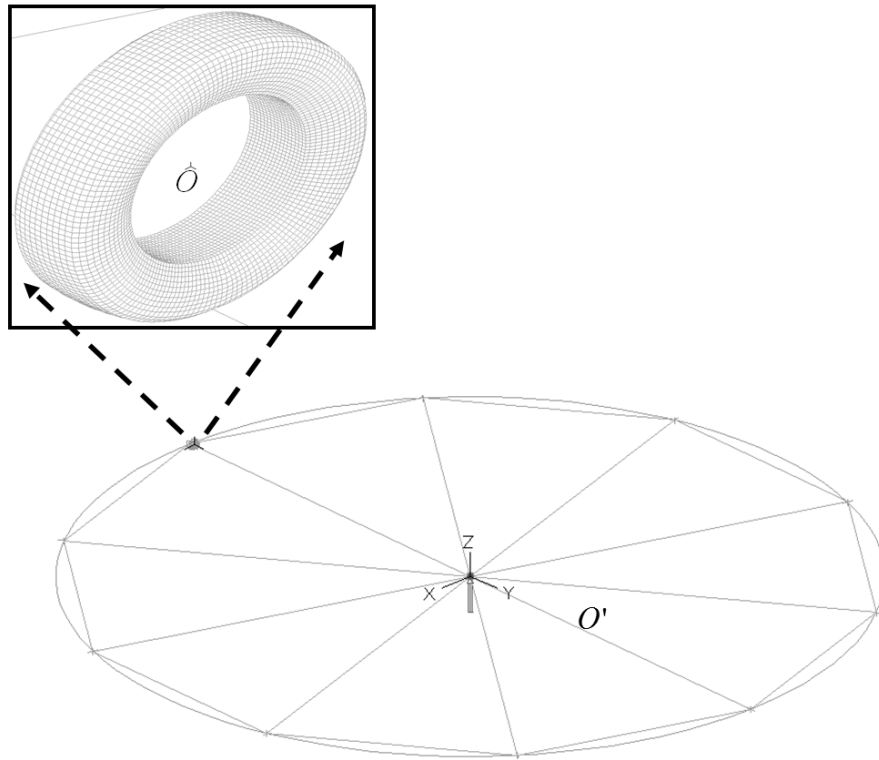
Figure 6.2 Cornering tire-pavement interaction model
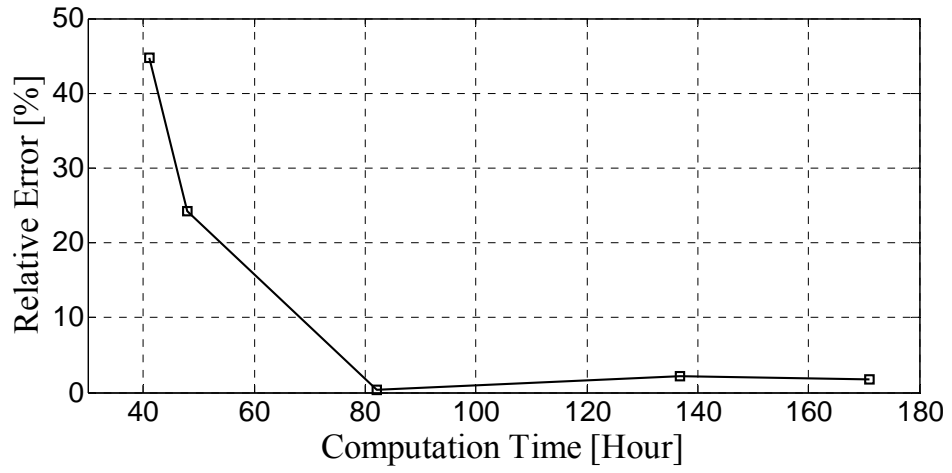
Figure 6.3 Relative error against CPU-time at the state of tire cornering
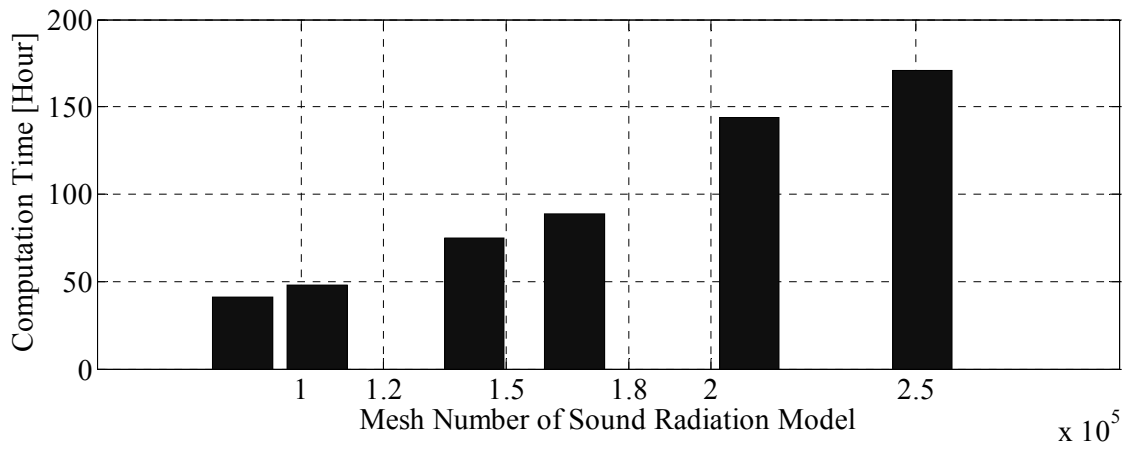
Figure 6.4 CPU-time against mesh number of sound radiation model at the state of tire cornering
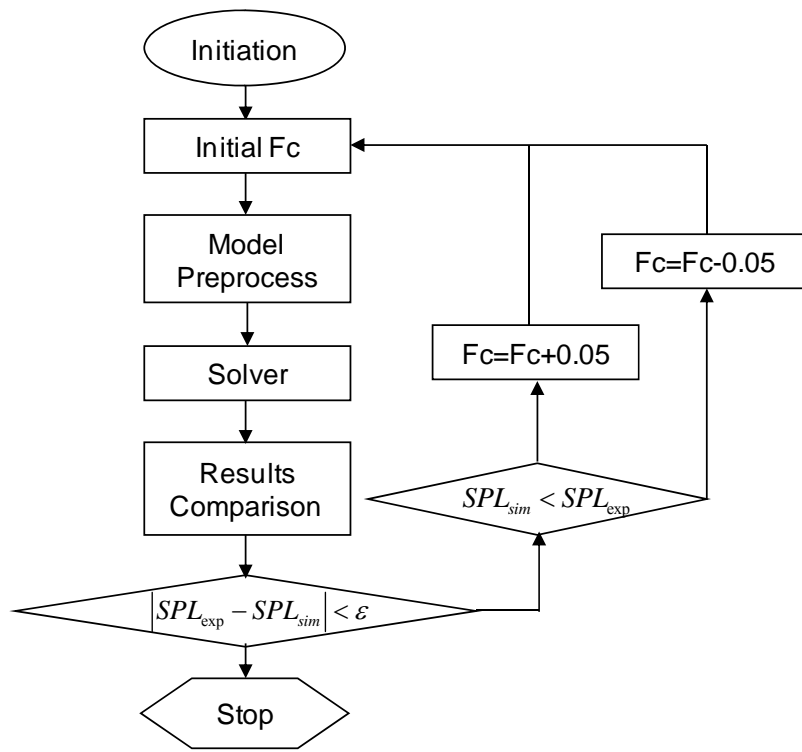
Figure 6.5 The framework of friction coefficient choice
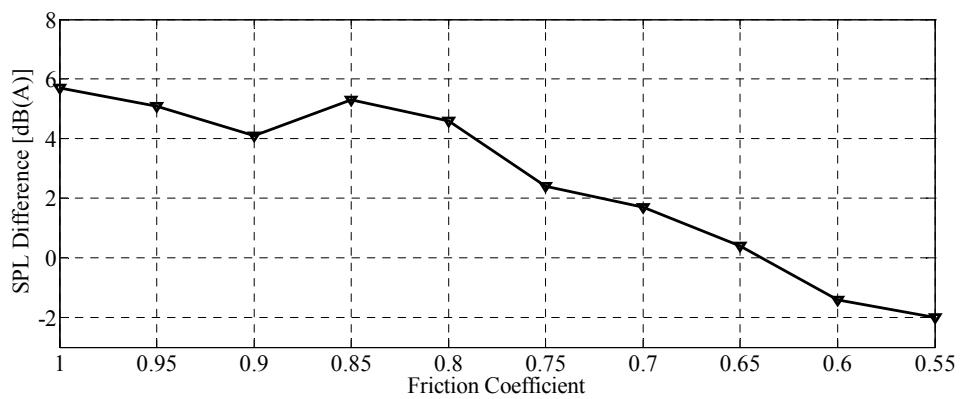
Figure 6.6 Noise difference between simulation and experiment with friction coefficient at speed 70 km/h
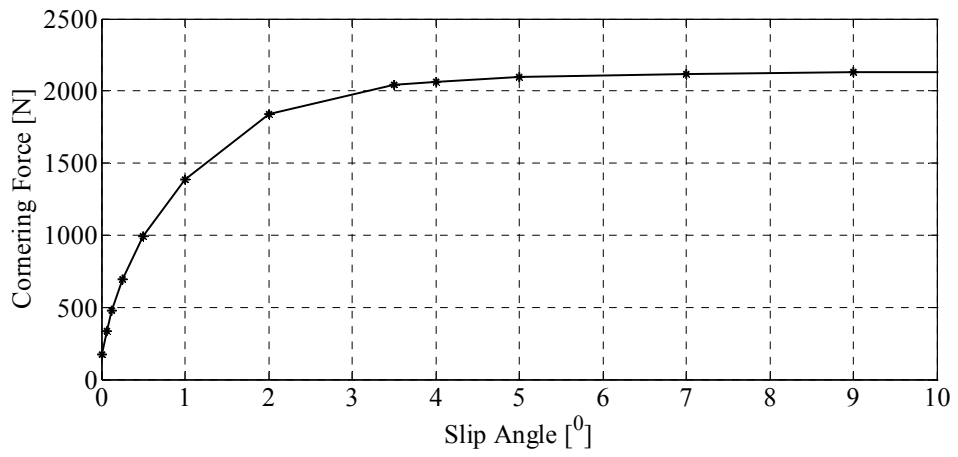
(1) Left cornering
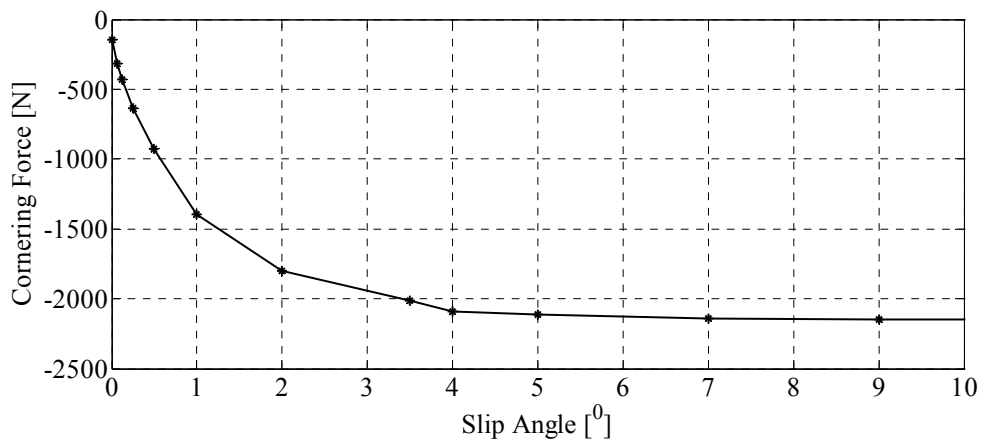
(2) Right cornering

Figure 6.7 Predicted transverse contact force with different slip angles at cornering state
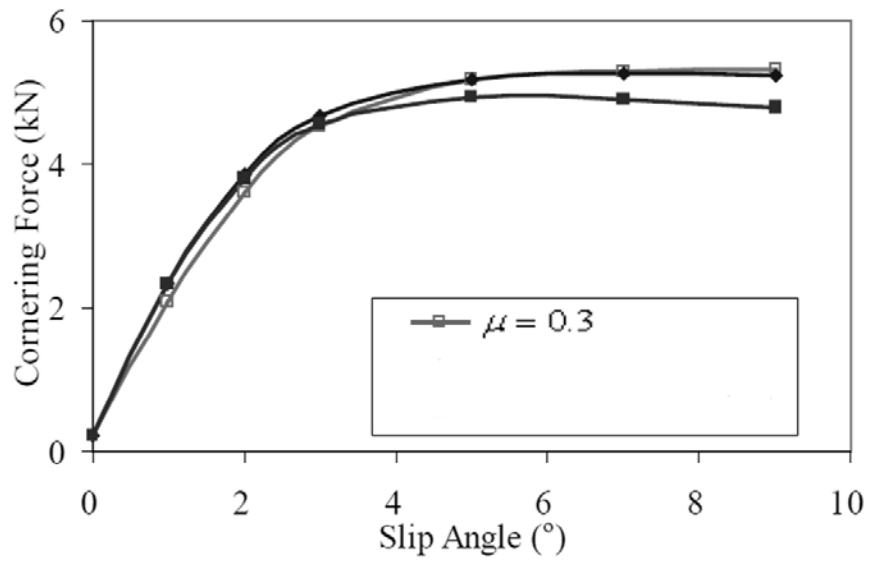
Figure 6.8 Predicted cornering force using different friction models by Wang (2011)
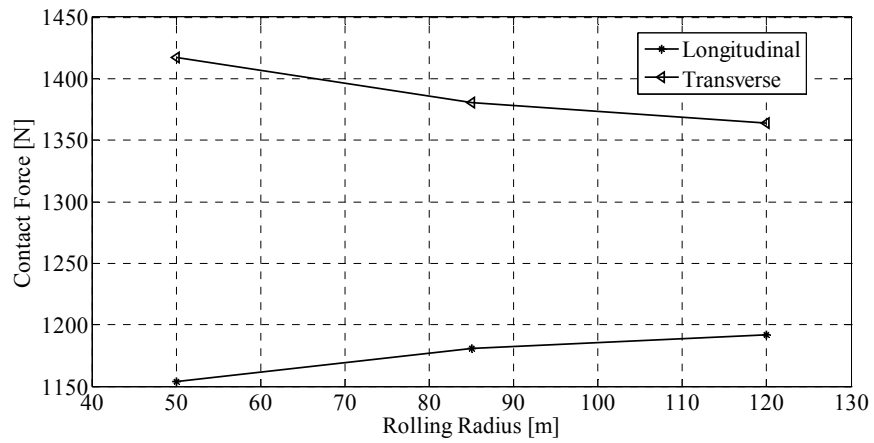
Figure 6.9 Predicted contact force with different rolling radius at a constant speed
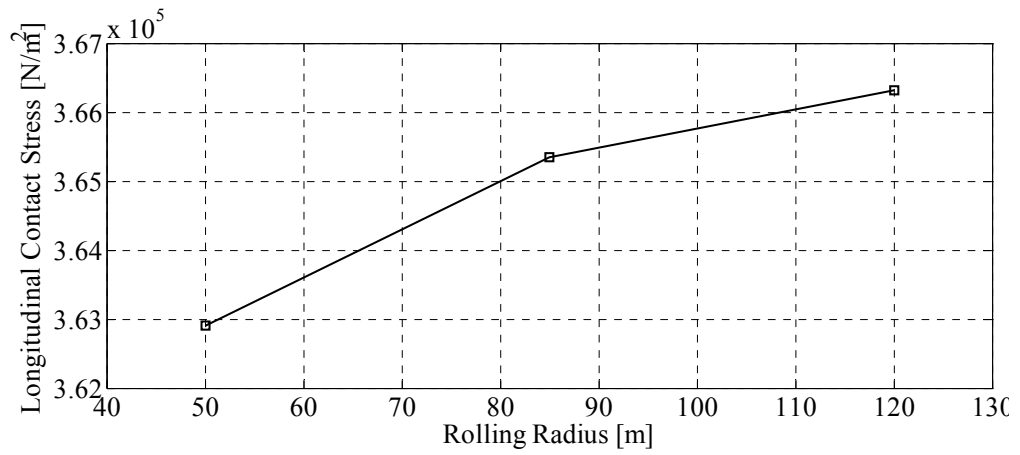
(a) Longitudinal stress
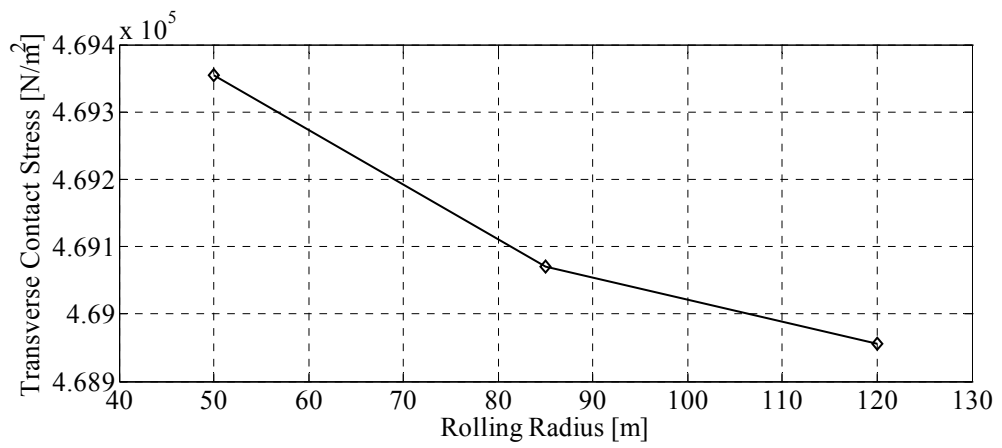
(b) Transverse Stress

Figure 6.10 Predicted Maximum stress with different rolling radius at a constant speed
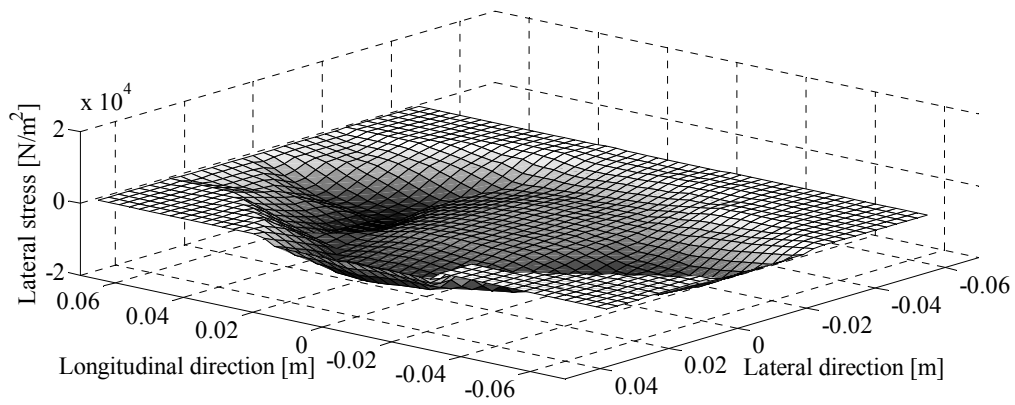
(a) Lateral stress distribution during left turn
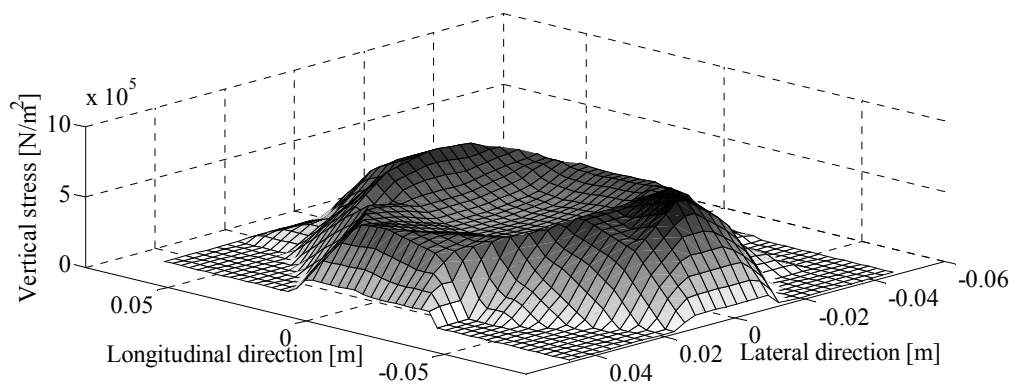
(b) Vertical stress distribution during left turn

Figure 6.11 Effect of cornering on contact stress from simulation

191
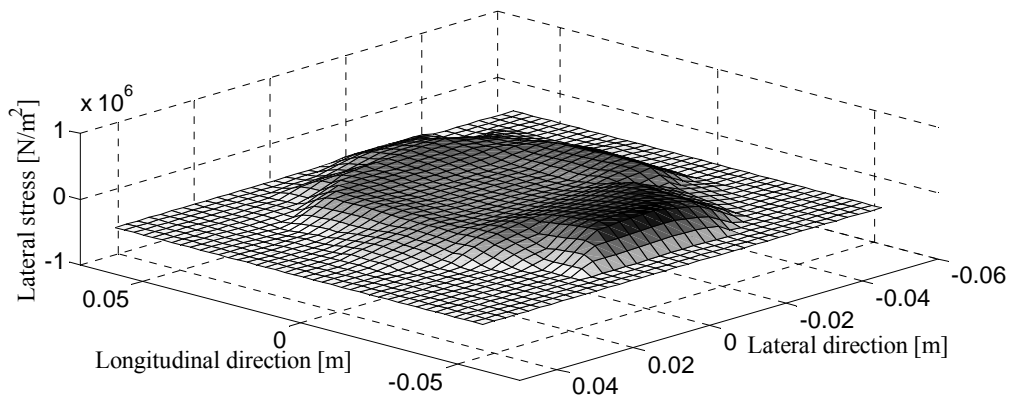
(a) Lateral stress distribution during right turn
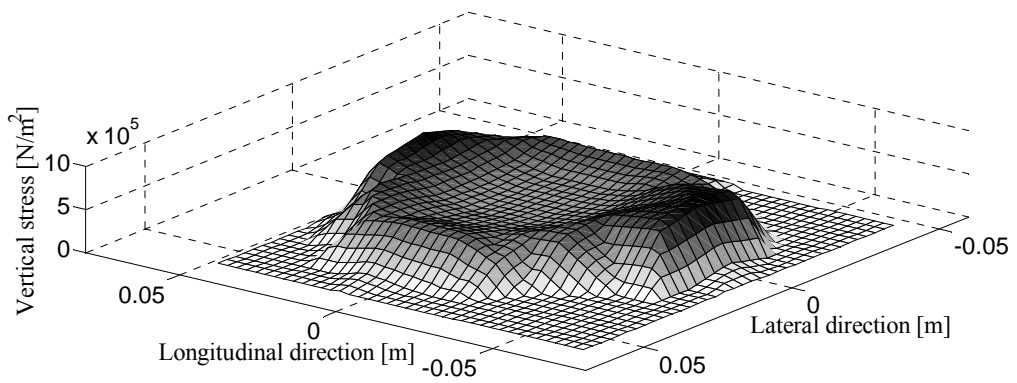
(b) Vertical stress distribution during right turn

Figure 6.11 Effect of cornering on contact stress from simulation (Continue)

Vertical stress	Lateral stress
(a) Left Turn	
Vertical stress	Lateral stress
(b) Right Turn	
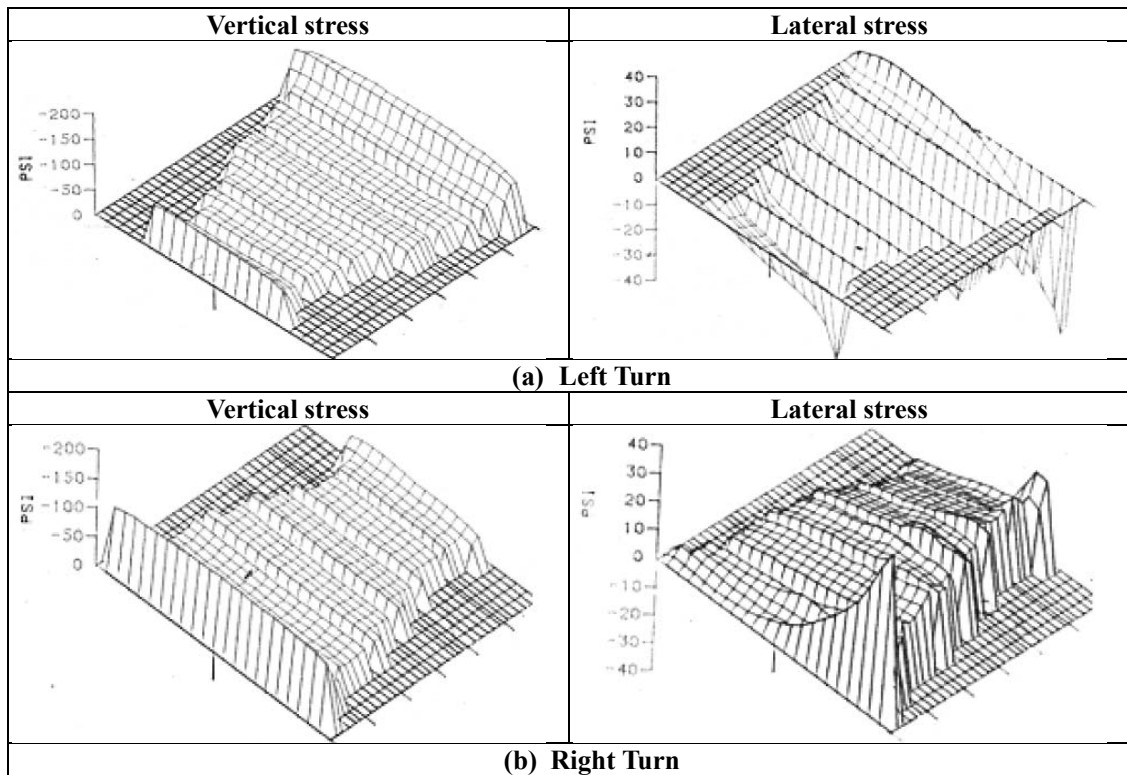
Figure 6.12 Effect of cornering on contact stress from experiment (Steen, 2007)
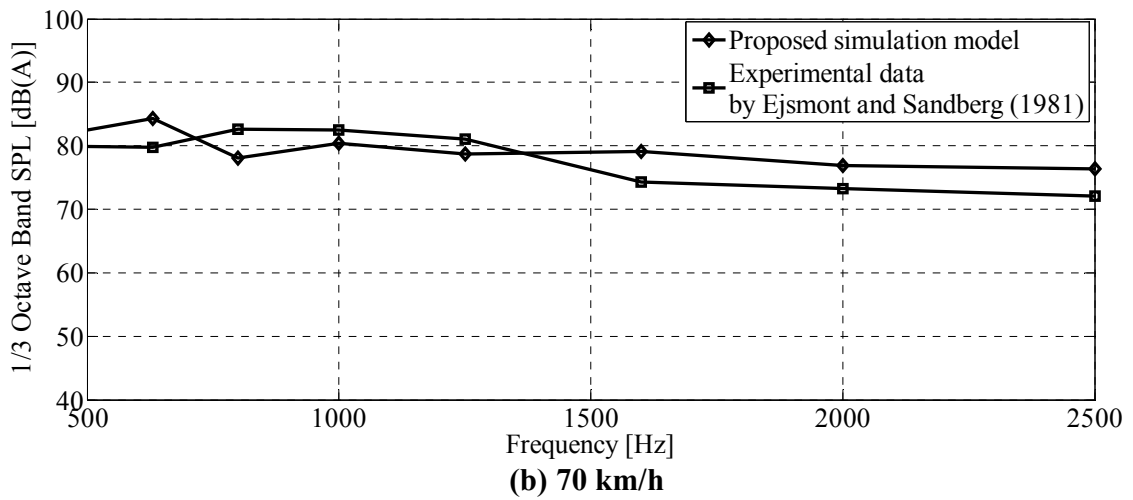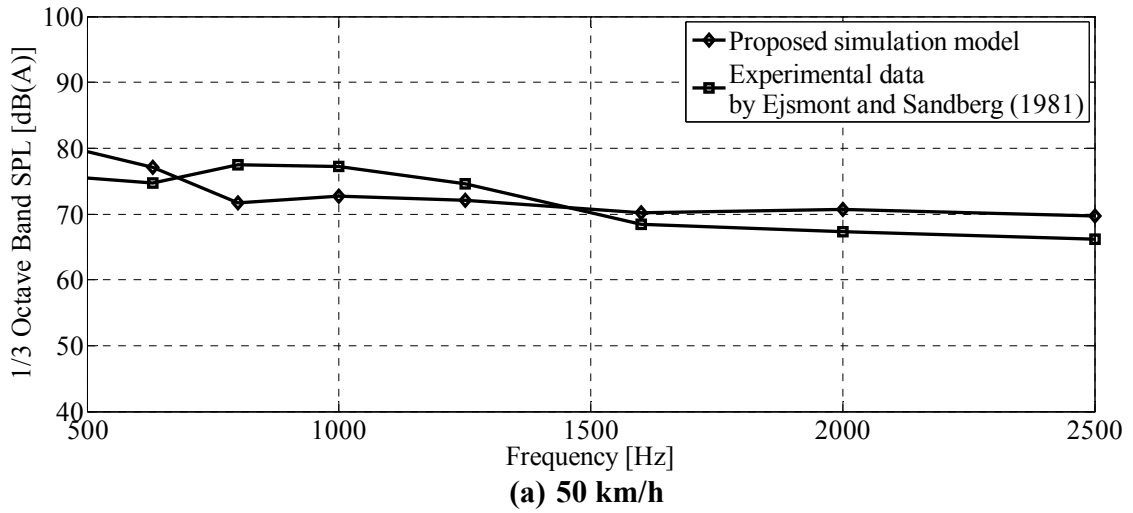
(a) 50 km/h

(b) 70 km/h

Figure 6.13 Comparison of A-weighted sound pressure level frequency distribution between simulation and measurement at the straight driving state

194
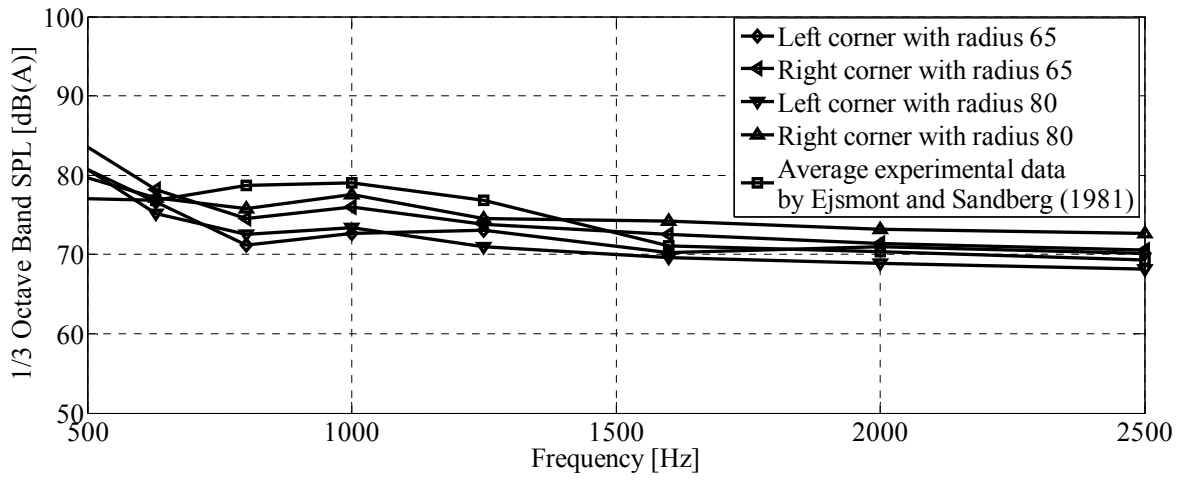
(a) 50 km/h
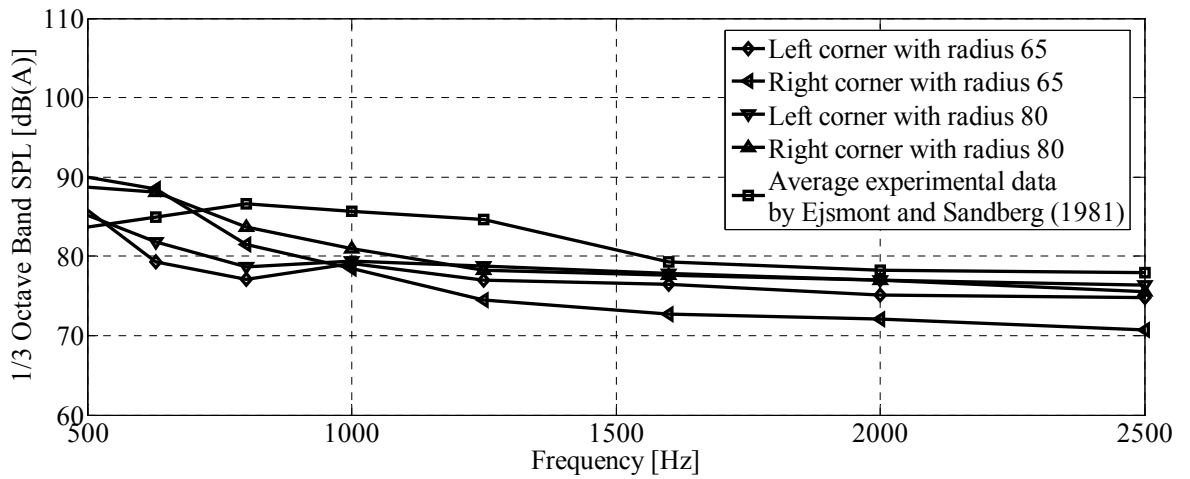
(b) 70 km/h

Figure 6.14 Comparison of A-weighted sound pressure level frequency distribution between simulation and measurement at the corner driving state
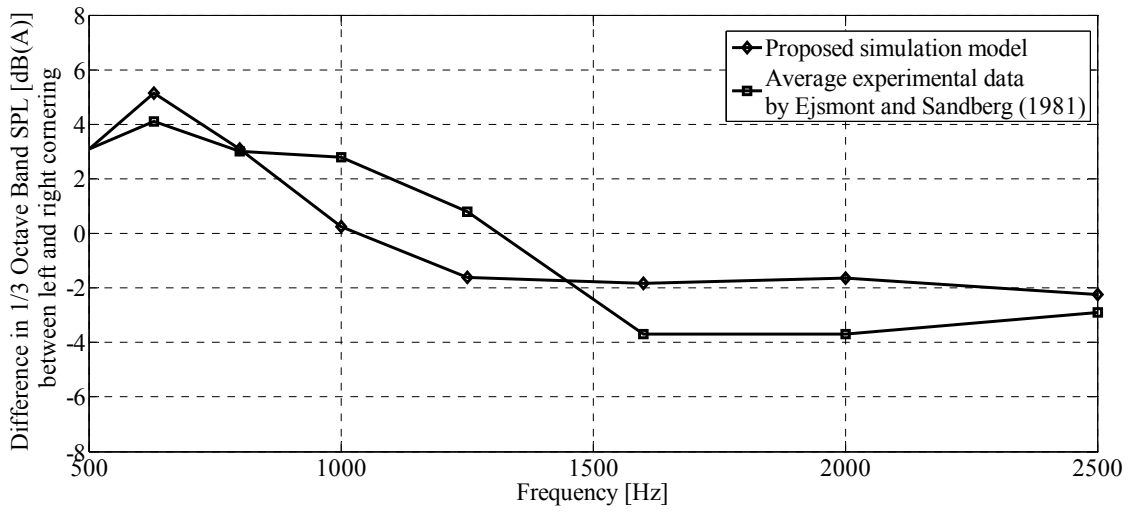
Figure 6.15 Difference in noise emission between right and left cornering at the vehicle speed 70 km/h

(a) 50 km/h

(b) 70 km/h
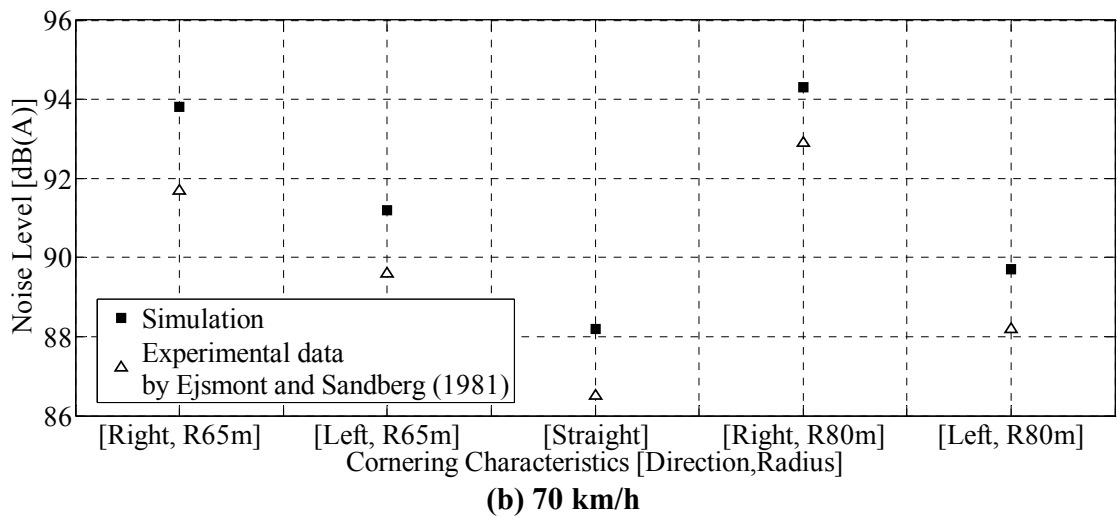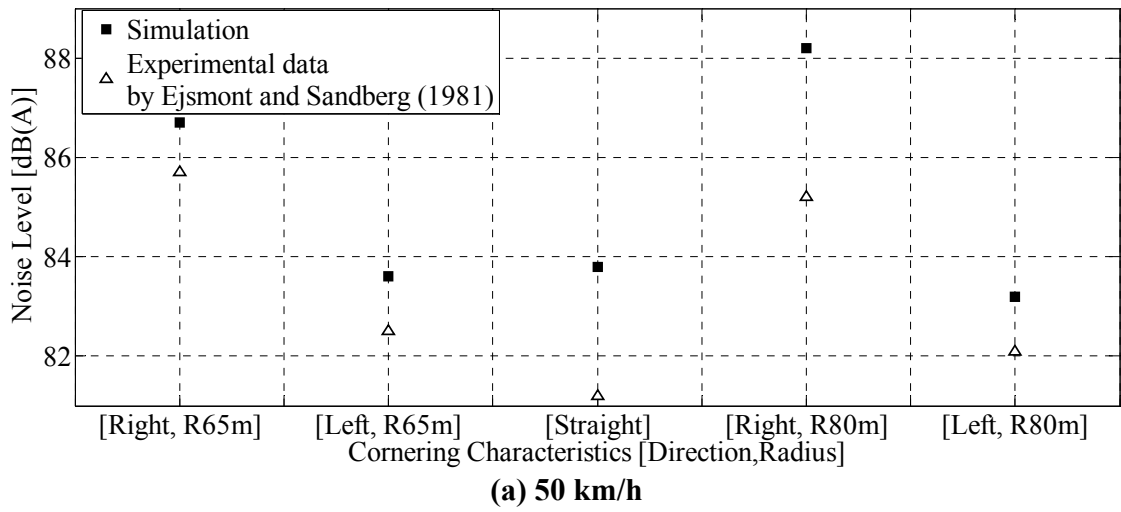
Figure 6.16 Validation of Model Computed dBA Values against Experimentally Measured Values
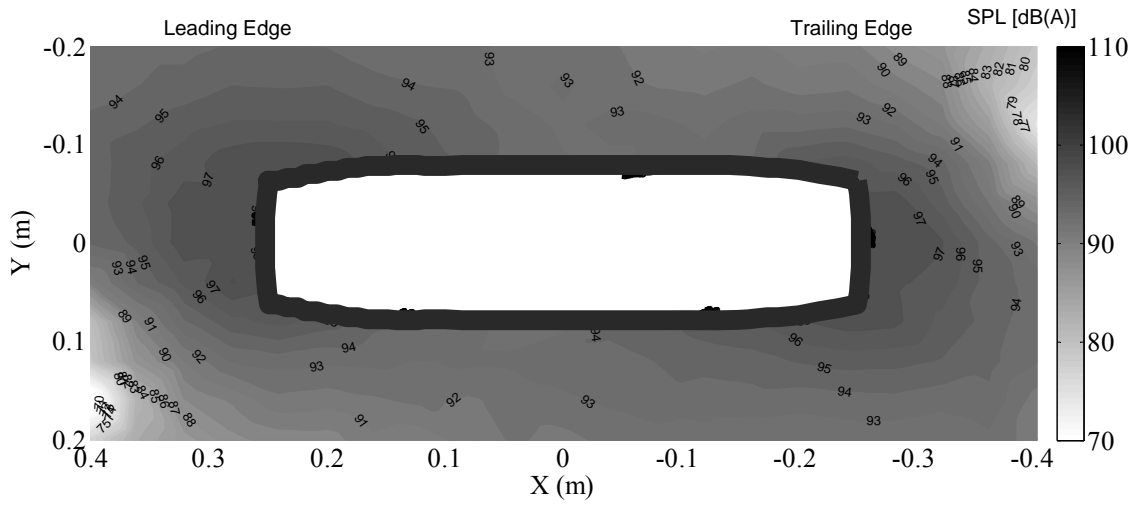
(a) Straight driving
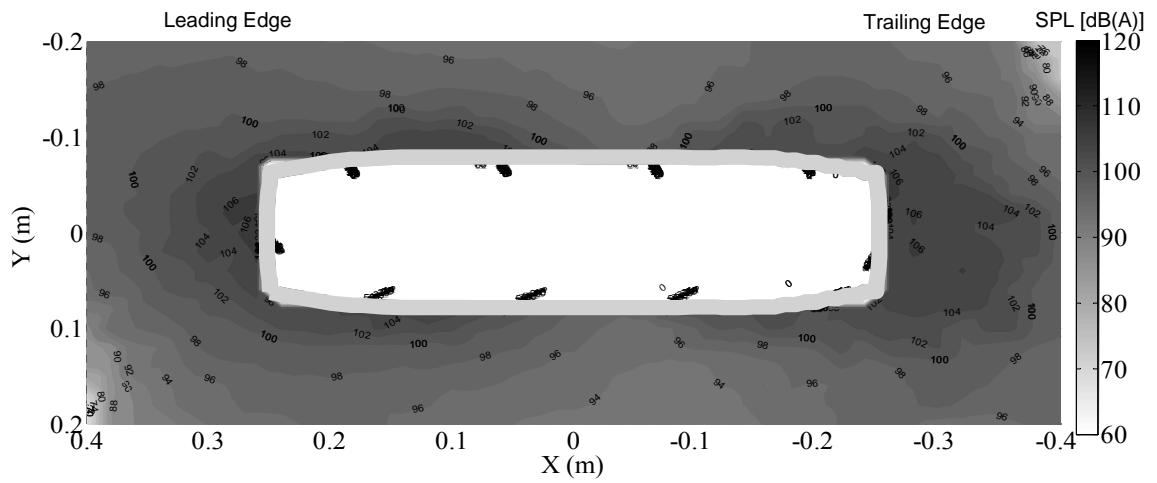
(b) Left cornering

Figure 6.17 Sound pressure level distribution on the horizontal plane at 100 mm above the bottom of PIARC tire at the speed of 70 km/h

198

(a) 50 km/h

(b) 70 km/h
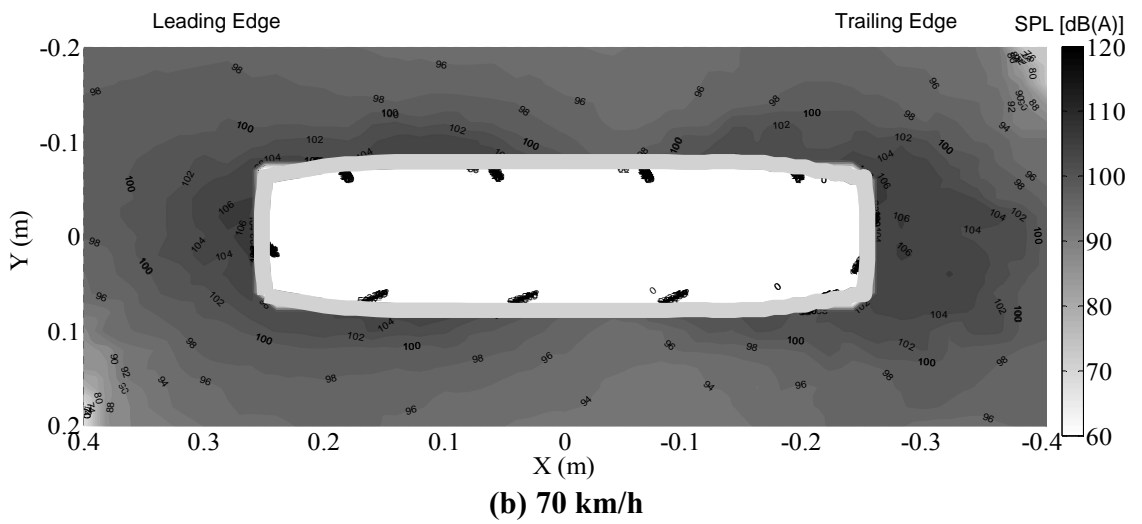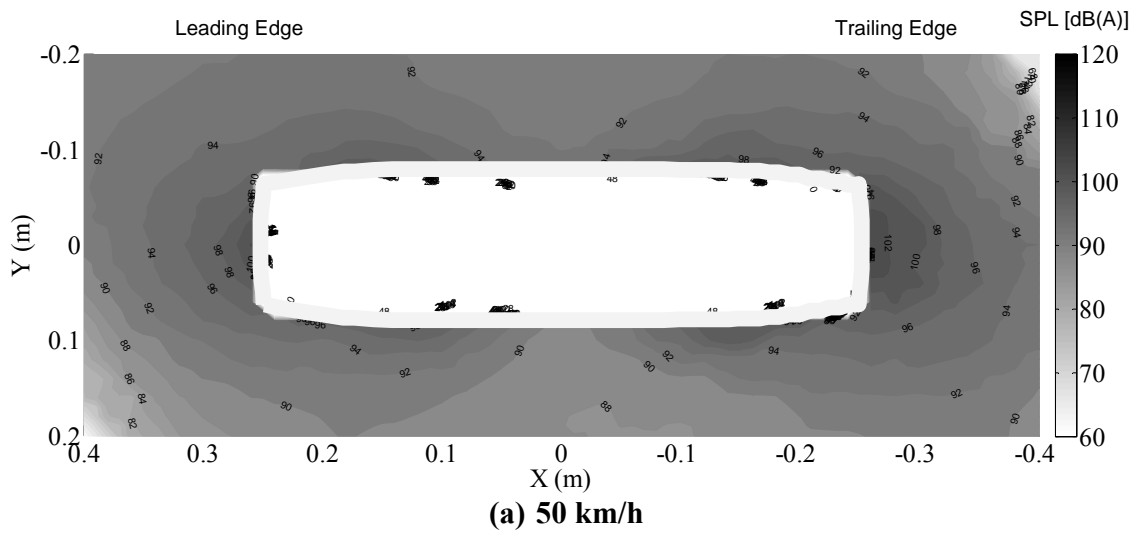
Figure 6.18 Sound pressure level distribution on the horizontal plane at 100 mm above the bottom of PIARC tire at the state of left cornering

199
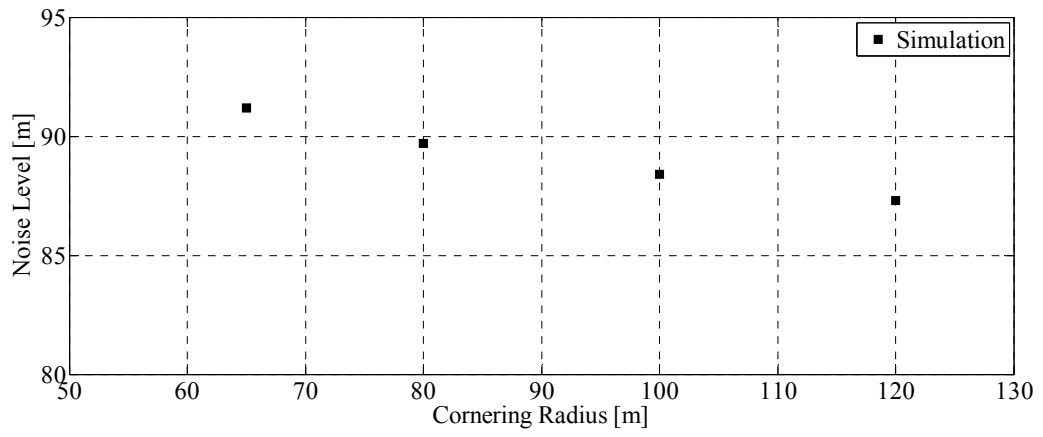
Figure 6.19 Effect of cornering radius to tire pavement noise

CHAPTER 7   FACTORS   INFLUENCING   TIRE-PAVEMENT NOISE

7.1   Introduction

The magnitude of tire-pavement noise is affected by a number of factors, including the type and size of tire (e.g. tire width, tire radius and tire rubber), tire tread pattern, vehicles speed, magnitude of wheel load, and pavement surface mixture type (e.g. dense graded, gap graded, and open graded) (Sandberg and Ejsmont, 2002; Sandberg, 2001 a). Among these factors, vehicle speed, wheel load and pavement surface mixture type are three that could be managed by transportation engineers in their effort to reduce traffic noise. For instance, limitation of vehicle speed and weight control of vehicle loading can be employed as traffic noise mitigation measures (Sandberg and Ejsmont, 2002). Similarly, suitable pavement surface mixtures can be designed to reduce tire-pavement noise to produce quiet pavement surfaces, such as the use of rubber asphalt mixes, open-grade friction courses, or porous asphalt and concrete mixtures (Putman and Amirkhanian, 2005; Donovan, 2011; Hall et al., 2009). The effect of tire size and tire tread pattern to tire-pavement noise has also been investigated by some empirical methods due to the tire complicated geometrical relations and its connection to other parameters like load, inflation pressure, thread pattern and speed class.

The chapter focuses on the effects of the magnitude of tire speed, wheel load and wheel width on tire-pavement noise. The three-dimensional finite-element simulation model developed in the previous chapters is employed to examine analytically these effects for vehicles travelling at different speeds. The theoretical development of the three-

dimensional finite element near-field tire-pavement noise simulation model is first described, followed by the application of the model to analyze tire-pavement noise generated at different vehicle speeds.

7.2 Numerical Implementation

To illustrate the capability of the proposed simulation model in Chapter 4 for evaluating the effect of wheel load at different vehicle speeds, tire-pavement noise was computed at four different vehicle speeds: 30, 50, 70 and 90 km/h for the case of a constant wheel load equal to 1,000N and 3,000 N respectively. Table 7.1 gives the tire loading values used in the simulation analysis of vehicle speed. For each speed, the inputted tire horizontal velocity v and angular velocity w (see Figure 3.3) satisfy the equation $v = w \cdot \bar{r}$ in the free rolling state, in which $\bar{r}$ is tire radius. This is followed by further analyses performed for four wheel load levels of 1,000, 2,000, 3,000 and 4,000 N at two wheel speeds of 30 and 70 km/h respectively. Table 7.2 gives the tire loading values used in the simulation analysis of wheel load.

In order to study the effect of tire width on tire-pavement noise, four tire width levels 180, 190, 200 and 210 mm are used in the analysis at the vehicle speed of 70 km/h. Figure 7.1 shows four tire models in which the tire width was modified without changing PIARC smooth tire tread radius. The total node number of 51, 53, 55 and 57 for the tire in the meridional direction are respectively used for the different tire width models as show in Figure 7.1. The tire model has 80 divisions along the circumferential direction. Thus, these four tires have 8320, 8640, 8960, and 9280 elements for mesh design respectively.

Table 7.3 gives the tire loading values used in the present simulation analysis of tire width.

The calibrated tire-pavement noise model in Chapter 4 will be applied to study the effect of these factors on tire-pavement noise generation, where approximately 200000 adaptive mesh elements are used for sound radiation modeling. Provided dynamic tire responses at time intervals of 0.00002 second, each analysis has been done on the computer of Intel Xeon E5645 with 6 cores.

The analysis generates sound pressure in different frequency bands L_{Pi}, the overall sound pressure level L_P is calculated as,

$$L_P = 10\log_{10}\sum_{i=1}^{N}10^{L_{Pi}/10}\tag{7.1}$$

Table 7.4 records the dBA computed tire-pavement noise for all the cases of wheel load-speed combinations analyzed.

7.3   Noise Vehicle Speed Influence on Tire Pavement Noise

Based on the results of simulation in this research, Figure 7.2 plots the trends of variation of tire-pavement noise with vehicle speed for two different wheel load levels, 1,000 N and 3,000 N. The trend curves in Figure 7.2 displays the following characteristics:

- When the wheel load is held constant, tire-pavement noise increases as the vehicle picks up its speed.

- Under a given wheel load, the rate of increase of tire-pavement noise with speed gradually falls as the vehicle speed increases.

- Comparison of the two trend curves indicates that a higher wheel load produces a higher tire-pavement noise at any given vehicle speed.

The above general trends are consistent with the experimental results measured by Iwao and Yamazaki (1996).

Based on past experimental studies of tire-pavement noise, researchers have suggested that the sound levels of tire-pavement noise are proportional to the logarithm of vehicle speed, and the tire-pavement noise and vehicle speed trend curve can be represented by the following the simple relationship,

$$L = A + B \cdot \log(V) \tag{7.2}$$

where L is the tire-pavement sound pressure level, A, B are speed coefficients, and V is vehicle speed in km/h. It is noted that the simulation model generated results also follow the suggested relationship closely, as shown below:

For wheel load of 1,000 N $\qquad L = 31.2 + 29.0 \cdot \log(V) \qquad R^2 = 0.93 \qquad$ **(7.3)**

For wheel load of 3,000 N $\qquad L = 35.9 + 28.5 \cdot \log(V) \qquad R^2 = 0.98 \qquad$ **(7.4)**

We can find that the correlation between vehicle speed and sound pressure level are not varied with wheel load.

In order to study the effect of vehicle speed to tire-pavement noise in different frequency bands, we make a difference of predicted sound pressure level between vehicle speed 90 km/h and 70 km/h with wheel load 3000N, as shown in Figure 7.3. We can find that vehicle speed generally has a same influence on tire-pavement noise generation in the whole frequency band from 500 Hz to 2500 Hz. There is an about 4 dB increase in sound

204

pressure level of whole frequency band when vehicle speed varies from 70 km/h to 90 km/h.

7.4 Wheel Load Influence on Tire Pavement

Based on the simulation model computed results as presented in Table 7.5, Figure 7.4 plots the variation in tire-pavement noise level with wheel load at two speed levels, namely at speeds of 30 km/h and 70 km/h. The wheel load was varied from 1000 N to 4000 N, representing approximately empty and fully-loaded passenger car respectively. The following observations can be made from Figure 7.4:

- For a given vehicle speed, higher tire-pavement noise was generated with vehicles with a higher wheel load. This result confirms the common trend of tire-pavement noise variation with vehicle speed as recorded in experimental studies by researchers (Konishi and Tomita, 1996; Iwao and Yamazaki, 1996).

- The magnitudes of tire-pavement noise increase with wheel load are summarized in Table 7.6. It is seen that the increases in tire-pavement noise per doubling of wheel load were as follows:

  For vehicle speed of 30 km/h, the tire-pavement noise increase was 2.4 dB(A) when wheel load increased from 1,000 N to 2,000 N; and it was 2.2 dB(A) when wheel load increased from 2,000 N to 4,000 N. At vehicle speed of 70 km/h, the corresponding tire-pavement noise increases were 1.7 and 2.0 dB(A). These results are in agreement with the experimental observations made in past studies as indicated in Table 7.6.

- Experimental works by past researchers indicated that wheel load influence was higher at low vehicle speeds than high speeds (Kim et al., 2007; Von, 1992). The

computed results presented in Figure 7.4 and Table 7.5 show that at the vehicle speed of 30 km/h, when the wheel load was raised from 1,000 N to 4,000 N, the tire-pavement noise increased from 75.2 to 79.8 dBA, giving a net increase of 4.6 dBA. At the vehicle speed of 70 km/h, the corresponding net increase was 3.7 dBA (changing from 84.1 to 87.8 dBA). Thus, the computed results from the simulation model are consistent with the finding made from experimental on-site observations in Table 7.5.

7.5 Tire Width Influence on Tire-Pavement Noise

In order to study the effect of tire width on tire-pavement noise, tire width ranges from 180 to 210 mm (see Figure 7.1) is used in simulation at the vehicle speed of 70 km/h. Figure 7.5 shows the computed A-weighted sound pressure level frequency distribution from 500 to 2500 Hz, which covers the most sensitive frequency range for human being. A comparison shows that in the low frequency band from 500 to 1000 Hz, the sound pressure level for the case of 180 mm tire width is obviously less than those of other tire widths.

The computed tire-pavement noise levels are plotted against different tire widths in Figure 7.6. It is illustrated that the noise increases with the increase in tire width from 180 mm to 200 mm. On average, the noise increase with width is 1.0 dB per 10 mm of tire width increase over the range of tire widths studies. The effect of tire width becomes insignificant when tire width is more than 200 mm. The rate of increase of tire-pavement noise decreases to 0.2 dB per 10 mm of tire width increase when tire widths increases from 200 mm to 210mm.

7.6 Summary

While experimental works are crucial and important in studying the magnitudes and characteristics of tire-pavement noise, theoretical and analytical models are useful in enhancing our understanding of the mechanisms of tire-pavement noise generation and our capability in predicting the magnitudes and characteristics of tire-pavement noise generated under different operating conditions. This chapter has presented an analytical simulation model for tire-pavement noise generated by passenger cars and demonstrated its applications in analyzing the impacts of wheel load and vehicle speed on tire-pavement noise.

The study covered the common range of passenger car wheel loads and vehicle speeds under the normal highway operating conditions. The wheel load range studied varied from 1,000 to 3,000 N, the wheel width range was from 180 to 210 mm, and the vehicle speed range was from 30 to 90 km/h. The computer simulation analysis produced results in good agreement with experimental data measured by past researchers. The following findings are obtained from the analysis in this chapter:

- Higher tire-pavement noise is generated at higher vehicle speeds.

- The rate of increase of tire-pavement noise with speed gradually falls as the vehicle speed increases.

- Higher tire-pavement noise is generated with vehicles with a higher wheel load.

- Wheel load influence is higher at low vehicle speeds than high speeds.

- Doubling of wheel load causes tire-pavement noise to increase by a magnitude of up to 2.5 dBA.

- Higher tire-pavement noise is generated with higher wheel width. The influence becomes lower with wheel width increase.

The analysis presented has demonstrated the ability of the proposed simulation model to perform parametric analyses on factors that may affect tire-pavement noise, and to predict tire-pavement noise likely to be generated under different vehicle operating conditions. The results suggest that the computer simulation model can serve as a useful analytical tool to study the problem of tire-pavement to improve our understanding of the various issues involved, and enhance our capability in formulating effective strategies to reduce tire-pavement noise.

Table 7.1 Values of tire loading parameters for vehicle speed analysis

Velocity (km/h)	Inflation pressure(kPa)	Load (N)	Friction coefficient
30/50/70/90	190	1000/3000	0.7

Table 7.2 Values of tire loading parameters for wheel load analysis

Velocity (km/h)	Inflation pressure(kPa)	Load (N)	Friction coefficient
30/70	190	1000/2000/3000/4000	0.7

Table 7.3 Values of tire loading parameters for tire width analysis

Velocity (km/h)	Inflation pressure(kPa)	Load (N)	Friction coefficient
70	190	3000	0.7

Table 7.4 Computed tire-pavement noise by simulation model

Wheel Load (N)	Sound Level (dBA)			
	Vehicle Speed 30 km/h	Vehicle Speed 50 km/h	Vehicle Speed 70 km/h	Vehicle Speed 90 km/h
1000	75.2	78.8	84.1	89.2
2000	77.6	--	85.8	--
3000	78.6	81.2	88.2	92.3
4000	79.8	--	87.8	--

Table 7.5 Influence of doubling wheel load on passenger car tire-pavement noise

Vehicle Speed	Change in dB(A)	
	Increase Load from 1000 N to 2000 N	Increase Load from 2000 N to 4000 N
30 km/h	2.4	2.2
70 km/h	1.7	2.0

Table 7.6 Past research on influence of doubling wheel load

Study	dB(A) Increase per Doubling of wheel Load
Konishi and Tomita (11)	2 dB(A)
Ejsmont and Taryma (14)	1 to 2 dB(A) with inflation pressure adjusted 0.7 to 1.5 dB(A) with inflation pressure not adjusted
Sandberg (2)	<2.5 dB(A)
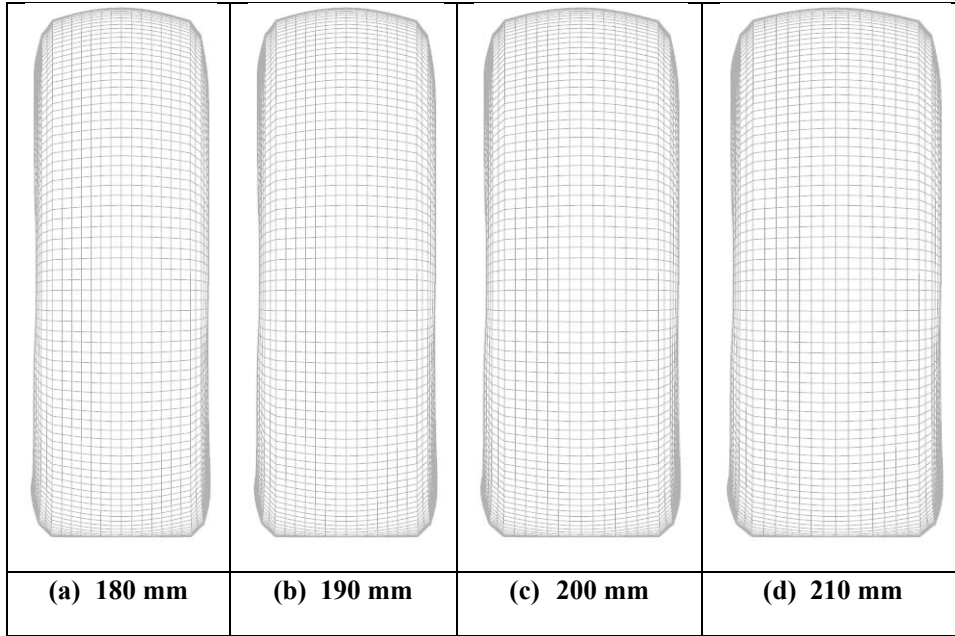
Figure 7.1 Wide based tire structure
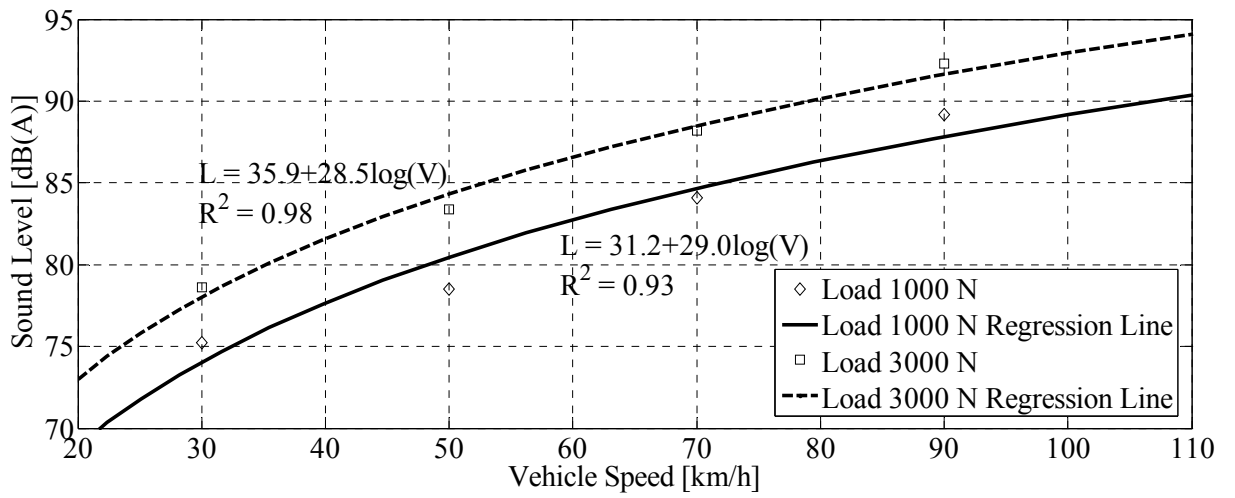
Figure 7.2 Variation of tire-pavement noise with vehicle speed at different wheel loads

211
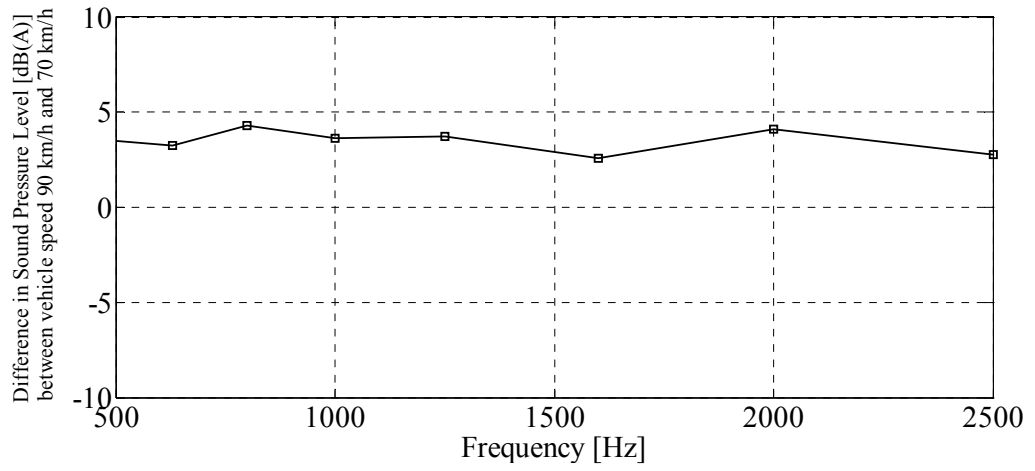
Figure 7.3 Difference in sound pressure level between vehicle speed 90 km/h and 70 km/h at wheel load 3000 N
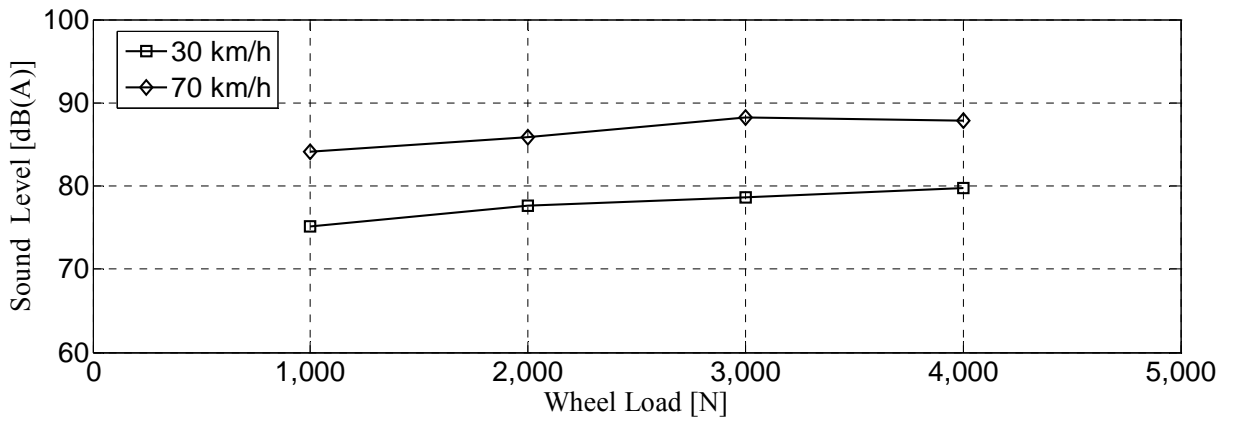
Figure 7.4 Effect of wheel load on tire-pavement noise
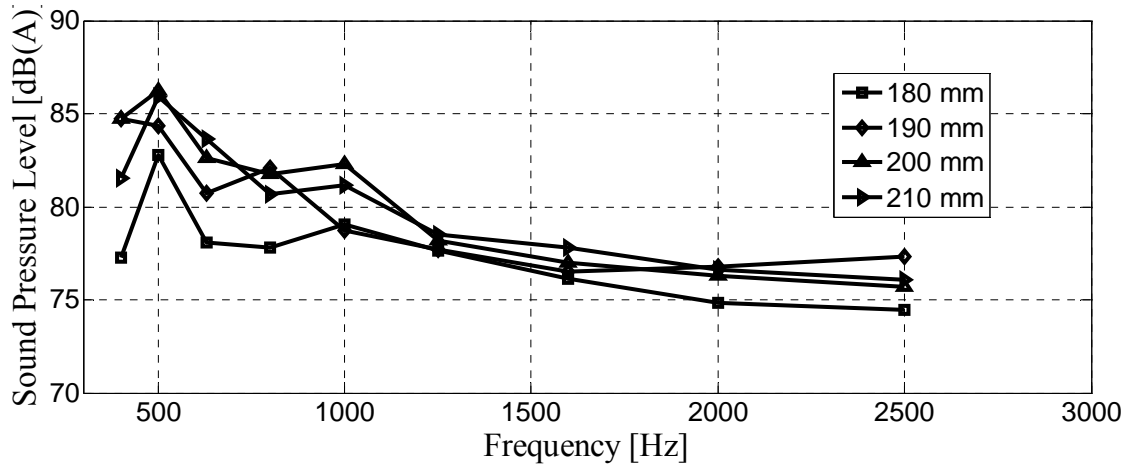
Figure 7.5 Effect of tire width on A-weighted sound pressure level frequency distribution
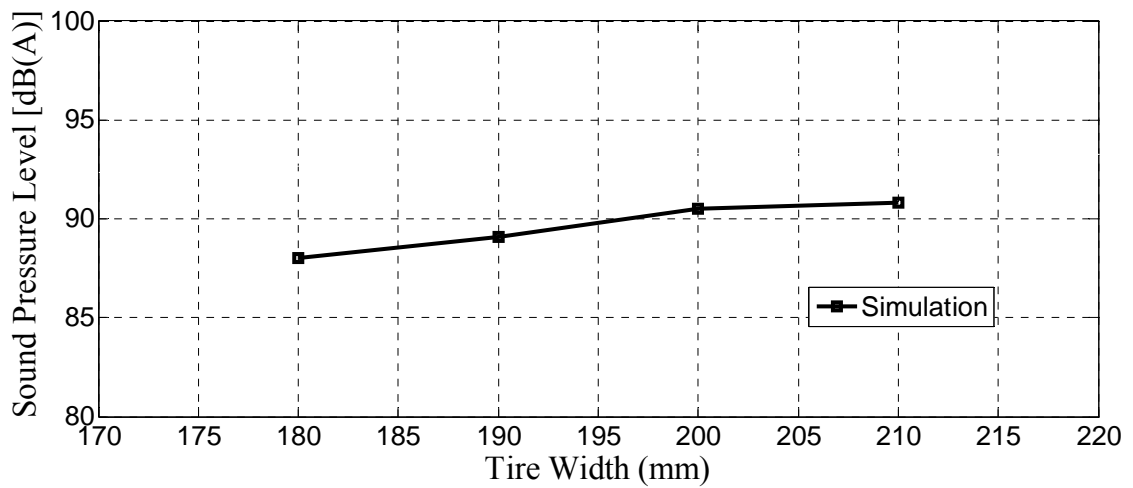
Figure 7.6 Effect of tire width on the overall tire-pavement noise

CHAPTER 8   Conclusion and Future Works

8.1   Formulation and Development of Tire-Pavement Noise Simulation Model

Traffic noise is a major concern for people due on its effect to our work efficiency and physical health. Traffic noise is mainly composed of engine noise, aerodynamic noise and tire-pavement noise. Tire-pavement noise is a main source of traffic noise in the normal speed range of road traffic. Taking into account the complex process of tire-pavement noise generation, computer simulation methods have been found useful to study the natural mechanisms of tire-pavement noise.

This research project proposed a general tire-pavement noise interaction simulation method to quantitatively analyze the effects of those factors related to pavement and transportation management on tire-pavement noise interaction. The tire-pavement noise model consists of a tire-pavement interaction sub-model and a noise transmission sub-model coupled by fluid-structure interface (FSI). There are several essential assumptions to model tire-pavement noise interaction:

   (1) The effects of wind noise are negligible;

   (2) The effects of tire rotation on the fluid interface are negligible;

   (3) Temperature is constant throughout the simulation;

For tire-pavement interaction modeling, interaction of smooth tire and smooth pavement has been simulated and validated against experimental data, in which the PIARC standard smooth tire is used. Restart analysis is run for the mesh adaption in the fluid model.

The noise transmission sub-model has been developed using the LES turbulence model. This turbulence model can be used effectively to simulate sound transmission in the air field near noise source. The air field is described by an arbitrary Lagrangian-Eulerian (ALE) formulation fully coupled to the rolling tire by Lagrangian formulations for fluid and structure interaction.

In the noise transmission modeling, an initial coarse mesh is used to avoid large element distortions in tire-pavement interaction. Then, a mesh adaption procedure is applied for the adaptive repair, coarsening and refining of meshes is used in this interaction analyses. This procedure combined with the restart analysis solves the complex tire-pavement interaction noise problems iteratively in the transient dynamic analysis. The mesh adaption criteria are the trade-off between accuracy of noise solution and computation effort. In addition, for accuracy of noise solution, mesh edge length in the transmission region should be less than one tenth of the shortest sound wavelength of interest.

To couple the noise transmission and tire-pavement interaction sub-models, fluid structure interfaces are specified in this rolling tire model corresponding to the interfaces specified in the noise transmission sub-model. The calculation is done based on an iterative computing method of two-way coupling.

Although the proposed FSI model in this thesis has high computation cost compared to the existing models, it can consider structure mechanical and aerodynamic mechanisms simultaneously. Since the contact algorithm is used for tire and pavement interaction, the effect of friction on tire-pavement noise can be effectively studied in this research. Furthermore, the proposed time-domain model can also be conveniently extended to

incorporate non-linear materials effect into the dynamic response calculation. Taking into account the limitations of frequency domain model to simulate the complicated nonlinear interaction between tire and pavement, and interaction between tire and air, the proposed tire-pavement noise simulation method in this thesis could be a potential method to comprehensively study tire-pavement noise mechanisms.

Throughout this research, tire-pavement noise modeling is performed using the commercial FEM software package ADINA 8.6.4. All post-process data are analyzed in MATLAB 10.0, and evaluated with experiment data obtained from by the CPX near field noise test method. The results illustrate that this tire-pavement noise interaction simulation method is able to quantitatively analyze the interaction among tire, pavement and air, and can be used to research the relationship between pavement factors and tire-pavement noise.

8.2 Analysis and Validation of Tire-Pavement Noise Simulation Model

8.2.1 Modeling of Dynamic Rolling Tire Moving on a Pavement Surface

A numerical model for computing tire-pavement contact stress of a smooth tire moving on a smooth pavement has been developed in this research. The PIARC smooth tire is the tire simulated in the numerical model. Through the use of finite-element simulation, it was found that the model can produce contact patches that are similar to that observed in experiments. The model was then applied to study the effect of three different rolling conditions (free-rolling, driving and braking) on the development of vertical contact and traction stresses. It was found that the simulation model can effectively predict the variation in contact stress distributions for the three rolling conditions.

8.2.2 Modeling of Tire-Air-Pavement Interaction to Predict Tire-Pavement Noise

After determining the tire-pavement interaction sub-model, the research focuses on the development of sound transmission sub-model and fluid structure-interaction algorithm. For noise transmission sub-model, the LES turbulence model was applied with the consideration of turbulence in the near field close to tire. The Arbitrary Lagragian Eulerien (ALE) system is used to describe the transmission of sound. The fluid structure interaction (FSI) algorithm is used to couple these two sub-models. The sound transmission sub-model is first validated by simulating sound transmission from a rolling tire without contacting pavement. Then, the tire-pavement noise model was further validated against the experiment data. The validation analysis concluded that the proposed tire-pavement noise model is effective in simulating noise propagation from tire-pavement interaction.

8.2.3 Effect of Tire Friction on Tire-Pavement Noise

The effect of tire friction on tire-pavement noise has been investigated experimentally by researchers. Past researches have recognized that the impact on noise generation is very complex. The exact noise level with friction variation is a function of tire type, speed and road surface. Tire-pavement noise is sensitive to tire friction for most tires. The sensitivity is different for different tires. It was found that the friction influence is higher at high frequency than at low frequency, especially for smooth tire. At low frequency, tire-pavement noise changes little with tire friction. At high frequency, tire-pavement noise increases with tire friction. In order to validate the relation between tire friction and tire-pavement noise, this research develops a numerical method and validate it against measured data. The simulation results for different tire friction were analyzed by

statistical method. The analysis concluded that it serves as a useful tool to research the complex relationship between tire-pavement friction and tire-pavement noise generation.

8.2.4 Effect of Vehicle Cornering on Tire-Pavement Noise

Past experimental studies have shown that side force generated during cornering of vehicles has a great influence on tire-pavement noise generation. This research presents an analytical simulation model for tire-pavement noise, with the aim to offer an analytical tool to optimize road geometric design for minimizing traffic noise. The computer simulation analysis produced results in good agreement with experimental results measured by past researchers. The analysis presented has demonstrated the ability of the proposed simulation model to perform parametric analyses of road geometric design that may affect tire-pavement noise.

8.2.5 Effects of Tire Load and Tire Width on Tire-Pavement Noise

This part of the study covered the common range of passenger car wheel loads, wheel widths and vehicle speeds under the normal highway operating conditions. The wheel load range studied varied from 1,000 to 4,000 N, The wheel width range was from 180 to 210 mm, and the vehicle speed range was from 30 to 90 km/h. The computer simulation analysis produced results in good agreement with experimental results measured by past researchers. The analysis shows that tire-pavement noise increases with vehicle speed. The increasing rate of tire-pavement noise gradually falls as vehicle speed increases. Higher tire-pavement noise is generated with vehicles with a higher wheel load, and the effect of wheel load on tire-pavement noise is stronger at low vehicle speeds than high speeds. Higher tire-pavement noise is generated with larger wheel width. The influence becomes lower as wheel width increases.

8.3 Recommendations for Future Works

There are several areas where further research could be done to improve the proposed simulation model as well as additional work needed to apply the proposed model to analyze other aspects of pavement performance.

8.3.1 Impact of Pavement Surface Texture on Tire-Pavement Noise

Cement concrete pavement (CCP) is frequently used on high volume streets and highways in USA and some European countries (Wayson, 1998). It has widely been recognized that CCP surface texture has a major influence on tire-pavement noise generation.

The surface texture properties of CCP, including grooving, should be considered. Two main groove properties (groove width, and groove spacing) are known to affect tire-pavement noise. These surface groove properties can be modelled using finite element mesh, and incorporated into the simulation model.

The effect of groove properties on tire-pavement noise generated can be studied by using different groove spacing, different groove widths, and different combinations of groove spacing and groove width.

8.3.2 Ribbed Tire Dynamics and Effect on Tire-Pavement Noise

Tire tread pattern is an important factor that affects tire-pavement noise generation. Past researches have shown that tire-pavement noise increased by patterning tire tread. However, these researches were mainly done based on experimental methods which are expensive and time consuming.

A numerical method is an indispensable alternative to thoroughly investigate tire-pavement noise generation. It has been illustrated in Section 2.1 that nine forms of tire patterns has been used on reference tires to analyze tire-pavement interaction noise. As a more common commercial tire pattern, rib pattern tire can be considered first. To numerically analyze the relation between rib pattern and tire-pavement noise, it requires developing a rib tire dynamic finite element model and validating them against measured data. Near field noise transmission sub-model which has been validated in this research can be used to couple the rib tire dynamic model by means of FSI algorithm to simulate noise propagation.

The effects of tire tread pattern can be studied by using several different tire groove patterns like longitudinal grooves, transverse grooves, and combined longitudinal and transverse grooves. The study can also include other parameters of tire tread pattern such as groove depth, groove number and groove width.

8.3.3   Effect of Vehicle Slip on Tire-Pavement Noise

Tire-pavement noise has mainly been investigated under the condition when tires are free rolling on the pavement. However, in actual driving, free rolling tire must overcome rolling resistances by creating a slip between the tire tread and the pavement surface.

It is known from past research that slip acting on a tire tends to increase tire-pavement noise. In the acceleration state, tire-pavement noise level is 5 dB higher than free rolling state (Sandberg and Ejsmont, 2002). There is a higher increase of noise at low speeds than at high speeds.

The investigation of the influence of tire slip on tire-pavement noise is not an easy task. Although some empirical methods have been proposed to solve the problem, the results were not satisfactory (Sandberg and Ejsmont, 2002). To study the effect of tire slip with different vehicle speeds on tire-pavement noise, a finite element approach can be adopted.

Initially, the effect of slip on tire-pavement noise can be studied by using variable slips with a constant vehicle speed in the acceleration or deceleration state. Next, the factor of vehicle speed can be considered. The effect of the combination of vehicle speed and slip can be studied in two ways: constant slip and variable vehicle speed, and variable slip and variable vehicle speed. The research results can be analyzed by statistical methods to numerically develop a relationship between tire slip and tire-pavement noise.

8.3.4 Improvement to the proposed tire-pavement noise modeling

The elastic orthotropic materials used in this research were based on the works of previous researchers. However, it is believed that a shell element with these parameters does not simulate with full accuracy the properties of a real tire composed of rubber and steel belt layers, especially in the low frequency domain. This problem could be solved by application of more realistic material parameters or introduction of a solid model with visco-elastic material parameters. Compared with ADINA finite element code, ABAQUS is more comprehensive in the nonlinear material simulation. It could be used to impose tire and pavement simulation with composite nonlinear materials. Furthermore, The ALE formulation for structure in ABQUS could more effectively simulate the interaction between structure and fluid.

On the other hand, although the ADINA finite element code can consider many important aspects in tire-pavement noise simulation by FSI, it requires significant computation time, resource and accuracy. Some other commercial numerical software like ANSYS and SYSNOISE could be used to improve the tire-pavement noise simulation. ANSYS is strong in traditional CFD simulation since FLUENT software code has been effectively merged with ANSYS. It could be used to strengthen the simulation of noise radiation in the CFD model. SYSNOISE is a powerful tool to predict the linear acoustic field generated inside and outside of a vibration structure. The program utilizes numerical methods based on the direct and indirect boundary element method and a pressure formulation for acoustic finite and infinite element modeling. It could be used to predict tire-pavement noise propagation in the far field with less computation time and source.

Reference

AASHTO (1996) AASHTO Guide for Design of Pavement Structures. American Association of State Highway and Transportation Officials. Washington D.C.

Andersson P.,W. Kropp (2009). Rapid tyre/road separation: An experimental study of adherence forces and noise generation, Wear,Vol. 266, No. 1-2, pp. 129-138

Andrén, P. and A. Jolkin (2003).Elastohydrodynamic aspects on the tyre-pavement contact at aquaplaning, VTI report 483A, Sweden.

ADINA R&D, Inc. (2009) ADINA 8.6 Manuals. ADINA R&D, Inc. Massachusetts, USA.

Anfosso-Ledee, F. and Y. Pichaud (2007). Temperature effect on tire-road noise, Applied Acoustics, Vol. 68, No. 1, pp. 1-16.

ASTM (2009). Standard Practice for Measurement of Tire/Pavement Noise Using the On-Board Sound Intensity (OBSI) Method, American Society for Testing and Materials, USA.

Badalamenti, J. M. and G. R. Doyle (1988). RADIAL-INTERRADIAL SPRING TIRE MODELS, Journal of Vibration Acoustics Stress and Reliability in Design-Transactions of the Asme, Vol. 110, No. 1, pp. 70-75.

Baig, M. A. I.(2006). A Consistent Segment Procedure for solution of 2D Contact problem with Large Displacement, PHD Thesis, Massachusetts Institute of Technology.

Bathe, K. J.(2006). Finite Element Procedures, Cambridge, MA: Klaus-Jürgen Bathe.

Bathe, K. J. and H. Zhang (2009). A mesh adaptivity procedure for CFD and fluid-structure interactions, Computers Structures, Vol. 87 (11-12), pp. 604-617.

Beckenbauer, T. P., Klein, J.-F. Hamet and W. Kropp (2008). Tire/road noise prediction: A comparison between the SPERoN and HyRoNe models - Part 1. Euronoise, Paris.

Bies, D. and C. Hansen (2009). Engineering Noise Control Theory and Practice. London, Taylor and Francis.

Bernhard, R. and Wayson, R. L. (2006). An Introductoin to Tire/Pavement Noise of Asphalt Pavement, Purdue University, USA.

Blab, R. (1999). Introducing Improved Loading Assumptions into Analytical Pavement Models Based on Measured Contact Stresses of Tires. Presented at the International Conference on Accelerated Pavement Testing.

Blundell, M. and D. Harty (2004). The Multibody Systems Approach to Vehicle Dynamics, SAE International and Elsevier.

Bolton, J.S., Kim, Y.J. (2003). Visualization of the tire vibration and sound radiation and modeling of tire vibration with an emphasis on wave propagation, Technical report, The Institute for Safe, Quiet and Durable Highways.

BRITE/EURAM project BE 3415 (1994). State-of-the art report on Surface properties of concrete roads in accordance with traffic safety and reduction of noise. November 1994.

Brinkmeier, M., U. Nackenhorst, O. von Estorff and S. Petersen (2004). Physically based modelling of tire rolling-noise by a finite element approach. Internoise 2004, Prague, Czech Republic.

Brinkmeier, M., U. Nackenhorst, O. von Estorff and S. Petersen (2008). A Finite Element Approach for the Simulation of Tire Rolling Noise. Journal of Sound and Vibration, Vol. 309, No. 1-2, pp. 20-39.

Cesbron, J., F. Anfosso-Ledee, D. Duhamel, H. P. Yin and D. Le Houedec (2009). Experimental study of tire/road contact forces in rolling conditions for noise prediction, Journal of Sound and Vibration, Vol. 320, No. 1-2, pp. 125-144.

Chung, T. J. (2002). Computational Fluid Dynamics, Cambridge University Press.

Clapp, T. G. (1985). Approximation and Analysis of Tire/pavement Contact Information Resulting from Road Surface Roughness, North Carolina State University, USA

Conte, F. (2008) Modélisation cfd du phenomena acoustique de pompage d'air dans un contact pneumatique/chaussée (Cfd modeling of acoustic phenomena pumping air into a tire/road contact), PHD Thesis, Institut national des sciences appliquées (Lyon), Université de soutenance

Deardorff, JW. (1970) A numerical study of three-dimensional channel flow at large Reynolds numbers, Journal of Fluid Mechanics, Vol. 41, pp.453–480.

De Beer, M. (1994) Measurement of Tire/Pavement Interface Stresses under Moving Wheel Loads. Final Report, Center for structural mechanics: University of Pretoria, South Africa.

De Beer, M., Fisher, M.C. and Jooste, F.J. (1997) Determination of Pneumatic Tire/Pavement Interface Contact Stresses under Moving Loads with Some Effects on Pavements with Thin Asphalt Surfacing Layers. Proceedings of the 8th International

Conference on Asphalt Pavements, International Society for Asphalt Pavements, 8–14 August, Seattle, Washington, pp. 179–227.

Doan, V. Q. (1996). Influence of Tire Construction and Tire Mold Profile on Coast-by Noise. Tire Technology International 1996, The Annual Review of Tire Materials and Tire Manufacturing Technology.

Donea, J.(1983). Arbitrary Lagrangian Eulerian methods. In: Computational Methods for Transient Analysis, V.I. North- Holland, Elsevier.

Donovan, P. R. (2011). Tire Noise Generation and Propagation over Porous and Non-Porous Asphalt Pavements. In TRB 90th Annual Meeting Compendium of Papers. DVD. Transportation Research Board of the National Academies, Washington DC.

Douglas, R.A. (2009) Tire/Road Contact Stresses Measured and Modeled in Three Coordinate Directions. NZ Transport Agency Research Report 384, Wellington, New Zealand.

Douglas, R. A., Woodward, W. D. H., and Woodside, A. R. (2000) Road Contact Stresses and Forces under Tires with Low Inflation Pressure, Canadian Journal of Civil Engineering, Vol. 27, pp. 1248-1258.

Drakos, C. A. (2003). Identification of Physical Model to Evaluate Rutting Performance of Asphalt Mixtures, PhD Thesis, University of Florida, USA.

Eichler, M. (1996). Ride comfort calculations with adaptive tire models. Proceedings of International Symposium on Advanced Vehicle Control, Aachen, Germany.

Ejsmont, Jerzy A., and Sandberg, Ulf. (1981).Cornering influence on tire/road noise, INTER-NOISE and NOISE-CON Congress and Conference Proceedings, InterNoise88, Avignon FRANCE, pp 1323-1738

Ejsmont, J. A. (1982). Comparison of Road and Laboratory Measurements and Influence of Some Tire Parameters on Generation of Sound, Swedish Road and Transport Research Institute, Sweden.

Ejsmont, J. A., S. Taryma (1982). Halas Open Samochodow Osobowych Poruszajacych Sie Posuchych Nawierzchniach asfaltowych I Betonowych. Ph.D Thesis, Technical university of Gdansk, Poland.

Ejsmont, J. A. and U. Sandberg (1984). Influence of tread pattern on tire/road noise, SAE Technical Paper Series, Vol. SAE Paper No. 841238 No.

Ejsmont, J. A. and P. Mioduszewski (2009). Certificatoin of vehicles used for tire/road noise evaluation by CPX method, Noise Control Engineering Journal, Vol.57(2), pp. 121-128.

Fioole, J.(2008). Experimental Modal Analysis of an Automobile Tire, Bachelor Project, Eindhoven University of Technology.

Fraggstedt, M.(2008). Vibrations, Damping and Power Dissipation in Car Tires, PhD Thesis, MWL, KTH.

Fujikawa, T., H. Koike, Y. Oshino and H. Tachibana (2005). Definition of road roughness parameters for tire vibration noise control, Applied Acoustics, Vol. 66, No. 5, pp. 501-512.

Fwa, T. F. and G. P. Ong (2008). Wet-Pavement Hydroplaning Risk and Skid Resistance: Analysis, Journal of Transportation Engineering, Vol. 134, No. 5, pp. 182-190.

Gagen, M. J. (1999). Novel acoustic sources from squeezed cavities in car tires, Journal of the Acoustical Society of America, Vol. 106, No. 2, pp. 794-801.

Gibbs, D., R. Iwasaki, R. Bernhard,J. Bledsoe, D. Carlson. (2005). Quiet Pavement Systems in Europe, Federal Highway Administration.

Gong, S. (1993). A study of in-plane dynamics of tires, PHD Thesis, Delft University of Technology, Holland.

Graf, R. A. G., C. Y. Kuo, A. P. Dowling and W. R. Graham (2002). On the horn effect of a tire/road interface, Part I: Experiment and computation, Journal of Sound and Vibration, Vol. 256, No. 3, pp. 417-431.

Graf, R. A. G., Tyre-road Interaction Noise, Ph. D. Thesis, Department of Engineering, University of Cambridge, 2002.

Hall, J. W., K. L. Smith and P. Littleton. (2009). Texturing of Concrete Pavements. NCHRP Report 634. National Cooperative Highway Research Program. Transportation Research Board of the National Academies, Washington D.C.

Hall, J. W., K. L. Smith and P. Littleton. (2009). Measuring Tire-Pavement Noise at the Source. NCHRP Report 630. National Cooperative Highway Research Program, Transportation Research Board of the National Academies, Washington D.C.

Hanson, D. I., R. S. James and C. NeSmith (2004). NCAT Report 04-02 - Tire/pavement noise study, National center for asphalt technology, USA.

Hayden, R. E. (1971). Roadside Noise from the Interaction of a Rolling Tire with the Road Surface, Proceedings of the Purdue Noise Control Conference, Purdue university, Indiana, USA.

Hendricx, W. and Mancosu, F. (1999).Experimental determination of the noise emitting parts of a rotating tire in the european research project TINO. In proceedings of the 1999 SAE Noise and Vibration Conference, Traverse City, USA, paper 1999-01-1732.

Howell, W.E., Perez, S.E. and Volger, W. A. (1985) Aircraft Tire Footprint Forces. Tire Pavement Interface, ASTM STP 929, Pottinger, M.G. and Yager, T.J. (eds), American Society for Testing and Materials, Philadelphia, pp 110-124.

Huang, Y. H. (1993) Pavement Analysis and Design. Prentice-Hall, Inc. Englewood Cliffs, New Jersey.

ISO (1997). Acoustic--Measurement of the influence of road surfaces on traffic noise--Part 1: Staistical Pass-By Method, International Orgnization for Standards Geneva, Switzerland.

ISO (2001). Acoustic--Measurement of the influence of road surfaces on traffic noise--Part 2: The Close Proximity Method, International Orgnization for Standards, Geneva, Switzerland.

Ivannikov, A., U. Haberkorn, H. Langenberg. (1998). Einflussgrössen auf Reifen/Fahrbahn Geräusche von Lkw bei unterschiedlichen Fahrbedingungen. Forschungsvereinigung Atomobiltechnik.

Iwao, K. and I. Yamazaki (1996). A Study on the Mechanism of Tire/Road Noise. JSAE Review, Vol. 17, pp 139-144.

Koishi et al. (2011). Radiation Noise Simulation of a Rolling Tire Excited by Tread Pattern. 2011 SIMULIA Customer Conference.

Kim, B. S., C. H. Chi and T. K. Lee (2007). A study on radial directional natural frequency and damping ratio in a vehicle tire, Vol.68, pp. 538-556.

Kindt, P., D. Berckmans, F. De Coninck, P. Sas and W. Desmet (2009). Experimental analysis of the structure-borne tire/road noise due to road discontinuities, Mechanical Systems and Signal Processing, Vol. 23, No. 8, pp. 2557-2574.

Kindt, P., P. Sas and W. Desmet (2009). Development and validation of a three-dimensional ring-based structural tire model, Journal of Sound and Vibration, Vol. 326, pp. 852-869.

Konishi, S., N. Tomita. (1996). Test Results of Load Inflation Relation, Informal Document of Bridgeston Corporation. Japan.

Kozhevnikov, I. F. (2011). The steady-state cornering of a wheel with a reinforced tire with slipping. ACTA MECHANICA, Vol. 217, No 3-4,pp 347-362

Kropp, W. (1989). Structure-borne sound on a smooth tire, Applied Acoustics, Vol. 26, pp. 181-192.

Kropp, W., K. Larsson and S. Barrelet (1998). The influence of belt and tread band stiffness on the tyre noise generation mechanisms, Proc. of the international Congress on Acoustics(ICA) 1998, USA.

Kropp, W., P. Sabiniarz, H. Brick, T. Beckenbauer (2012). On the sound radiation of a rolling tyre, Journal of Sound and Vibration, Vol. 331, No. 8, pp 1789–1805.

Kuijpers, A. and G. v. Blokland (2001). Tire/road noise models in the last two decades: a critical evaluation. Internoise 2001, Holland.

Kung, L. E. (1990). Radial vibrations of pneumatic radial tires, SAE Technical papers 900759.

Kuo, C. Y., R. A. G. Graf, A. P. Dowling and W. R. Graham (2002). On the horn effect of a tire/road interface, Part II: Asymptotic theories, Journal of Sound and Vibration, Vol. 256, No. 3, pp. 433-445.

Larsson, K., S. Barrelet and W. Kropp (2002). The modelling of the dynamic behaviour of tire tread blocks, Applied Acoustics, Vol. 63, No. 6, pp. 659-677.

Leeuwen, H. v., A. Kok and J. Reubsaet (2007). The Uncertainty of acoustical measurements on road surfaces using the CPX-method. INTER-NOISE 2007, Istanbul.

Lighthill, M. J. (1952). On sound generated aerodynamically: 1. General theory, Proc. Roy. Soc. A211, 1107.

Lippmann, S.A. (1985) Effects of Tire Structure and Operating Conditions on the Distribution of Stress between the Tread and the Road. Tire Pavement Interface, ASTM STP 929, Pottinger, M.G. and Yager, T.J. (eds), American Society for Testing and Materials, Philadelphia, pp. 91-109.

Liu, F., M.P.F. Sutcliffe and W.R. Graham (2010).Prediction of tread block forces for a free-rolling tyre in contact with a smooth road, Wear, Vol. 269, No. 9–10, pp. 672–683.

LMS (2000). SYSNOISE Rev 5.5: User Manual , LMS International.

Mankbadi, R. R., R. Hixon, S.-H. Shih and L. A. Povinelli (1998). Use of linearized Euler equations for supersonic jet noise prediction, AIAA Journal, Vol. 36, No. 2, pp. 140-147.

Milne, G. (2006). Your Home Technical Manual 2.7 Noise Control, Department of Climate Change and Energy Efficiency, Australia.

Molares, A. R. and M. A. Sobreira-Seoane (2008). Benchmarking for acoustic simulation software, euronoise 2008.

Moore, I. D., N. Purushothamant and B. S. Heatont (1988). Three-dimensional elastic finite element study of the skid resistance of grooved pavement, International Journal for Numerical Methods in Engineering, Vol. 26, No. 437-452.

Morgan, P.A. Phillips, S.M. and Watts, G.R. (2006). The localisation, quantification and propagation of noise from a rolling tire.Technical report, Transport Research Foundation, UK.

Muggleton, J.M., B.R. Mace, M.J. Brennan (2003).Vibrational response prediction of a pneumatic tyre using an orthotropic two-plate wave model.Journal of Sound and Vibration, Vol. 264(4), No. 929-950.

Myers, L. A. (2000). Development and Propagation of Surface-Initiated Longitudinal Wheel Path Cracks in Flexible Highway Pavements, PhD Thesis, University of Florida, USA.

Nelson, P. M. and S. Phillips (1994). Designing Porous Road Surfaces to Reduce Traffic Noise, TRL, Crow Thorne, England.

Nettles, A.T.(1994), Basic mechanics of laminated composite plates, NASA.

Nilsson, N. (1979). Possible method of reducing external tire noise. Proceedings of the international tire noise conference 1979, Stockholm,Sweden.

Nilsson, C.-M.(2004). Waveguide Finite Elements Applied on a Car Tire, PHD Thesis, Kungliga Tekniska högskolan, Sweden

O' Boy, D., and Dowling, A. (2009). Tire/road interaction noise- Numerical noise prediction of a patterned tire on a rough road surface, Journal of Sound and Vibration, Vol. 322, pp. 270-291

OECD (2002). OECD Guidelines towards Environmentally Sustainable Transport, Organisation for Economic Co-operation and Development, France.

Olson, L. G. and K. J. Bathe (1985). An infinite element for analysis of transient fluid—structure interactions, Engineering Computations, Vol2(4) , pp.319-329.

Ong, G. P. and T. F. Fwa (2007). Wet-Pavement Hydroplaning Risk and Skid Resistance: Modeling, Journal of Transportation Engineering, Vol. 133, No. 9, pp. 590-598.

Park, D. W. (2005) Effects of Non-Uniform Tire Contract Stresses on Pavement Response, ASCE Journal of Transportation Engineering, Vol. 131, No. 11, pp 873-879.

Périsse, J. (2002). A study of radial vibrations of a rolling tire for tire-road noise characterisation, Mechanical Systems and Signal Processing, Vol. 16, No. 6, pp. 1043-1058.

Pinnington, R. J. (2002). Radial force transmission to the hub from an unloaded stationary tire, Journal of Sound and Vibration, Vol. 253, No. 5, pp. 961-983.

Pinnington, R. J. and A. R. Briscoe (2002). A wave model for a pneumatic tire belt, Journal of Sound and Vibration, Vol. 253, No. 5, pp. 941-959.

PIARC (1995). International PIARC experiment to compare and harmonize texture and skid resistance measurements, Paris, World Road Association.

PIARC (2004). Specification for a Standard Test Tire for Friction Coefficient Measurement of a Pavement Surface: Smooth Test Tire, World Road Association.

Putman, B. J. and S. N. Amirkhanian (2005). Rubberized Asphalt Mixtures: A Novel Approach to Pavement Noise Reduction. In Urban Transport XI – Urban Transport and The Environment in the 21st Century, edited by C. A. Brebbia and L. C. Wadhwa, WIT Press, Southampton, U.K., pp. 541-549.

Rasmussen, P., Gade, S. (1996). Tire Noise Measurement on a Moving Vehicle, Brüel&Kjær, Denmark.

Rasmussen, R. O., R. J. Bernhard, U. Sandberg and E. P. Mun (2007). The little book of quieter pavements, U.S. Department of Transportatoin, USA.

Richard, T. L. (1991). Finite element analysis of structural-acoustic coupling in tyres, Journal of Sound and Vibration, Vol. 149, No. 2, pp. 235-243.

RMA (1971). Truck tire noise Washington, D.C., USA, Rubber Manufactures Association.

Ronneberger, D. (1982). Noise generation from rolling tires-sound amplification by the "horn effect". Internoise 1982, San Francisco.

Roo, F. d., J. Telman, G. v. Blokland, H. v. Leeuwen, J. Reubsaet and W. J. v. Vliet (2009). Uncertainty of Close-Proximity (CPX) tire-road noise measurements - Round Robin test results. 35th German Annual Conference on Acoustics, German.

Sabiniarz, P. (2011). Modelling the vibrations on a rolling tyre and their relation to exterior and interior noise. PhD thesis, Chalmers University of Technology, G·oteborg, Sweden.

Sabiniarz, P., W. Kropp (2010). A waveguide finite element aided analysis of the wave field on a stationary tyre, not in contact with the ground, Journal of Sound and Vibration, Vol. 329, No. 15, pp 3041-3064.

Sandberg, U., Ejsmont J. A. (1985).The Estimation of Background Noise in Trailers Used for Tire/Road Noise Measurements. Internal Report, Swedish Road and Traffic Research Institute, Linkoeping, Sweden.

Sandberg, U. and J. A. Ejsmont (1986). Development of Three Methods for Measurement of Tire/Road Noise Emission: Coast-By, Trailer and Laboratory Drum, Noise Control Engineering Journal, Vol. 27, No. 3, pp 68-88.

Sandberg, U. and J. A. Ejsmont (1990). Tire/road noise on rubberized asphalt and cement concrete surfaces in Sweden,

Sandberg, U. (2001a). Tire/Road Noise - Myths and Realities. Internoise 2001, Holland.

Sandberg, U. (2001b). Noise emissions of road vehicles effect of regulations, International Institute of Noise Control Engineering, Sweden.

Sandberg, U. and J. A. Ejsmont (2002). Tire/road noise reference book, Informex.

Sandberg, U. (2003). The Multi-Coincidence Peak around 1000 Hz in Tyre/Road Noise Spectra, Euronoise 2003.

Sandberg, U. (2007). Possibilities to Reduce Noise Emission from the Tire/Road Interaction with Emphasis on the Swedish, Swedish road and transport research institute, Swedish.

Seo, J. H., Y. J. Moon and B. R. Shin (2008). Prediction of cavitating flow noise by direct numerical simulation, Journal of Computational Physics, Vol. 227, No. 13, pp. 6511-6531.

Soedel, W. (1993). Vibrations of Shells and Plates, 3nd edition, Marcel Dekker Inc., NewYork

Steen., R. van der (2007). Tyre/road friction modeling Literature survey, Eindhoven University of Technology

Steen, R. van der. (2010). Enhanced friction modeling for steady-state rolling tires, PHD Thesis, Technische Universiteit Eindhoven, Eindhoven

Steven, H. (1989). Investigations on a measuring method for the tire-road noise of passenger car, A workshop on rolling noise generation, 10/ 11 October 1989, Berlin, Genmany.

Steven, H., H. Pauls (1990). Entwicklung eines Messverfahrens für das Reifen-Fahrbahn Gerausch. Report from FIGE, Herzogenrath, Germany

Steven, H., D., G. J. Kuppers, M. H. van Blokland, van Houten and R. van Loon. (2000). International Validation Test for the 'Close Proximity Method' (CPX). CD-ROM. M+P Raadgevende ingenieurs bv, Netherlands.

Takagi, R. and S. Takanari (1991). Tire structural parameter analysis for road noise using an accurate fem model, SAE Special Publications 911873.

Tanaka, T.(2004), Identification methods for tire/road noise during vehicle operating conditions with acoustic holography, In proceedings of the Internoise 2004 conference, Prague, Czech Republic, paper 588.

Tielking, J.T. and F.L Roberts(1987). Tire contact pressure and its effect on pavement strain, Journal of Transportation Engineering, Vol.11, pp.56-71.

Tönük, Ergin , and Ünlüsoy, Y.Samim. (2001). Prediction of automobile tire cornering force characteristics by finite element modeling and analysis, Comput. Struct. Vol. 79, No. 13, pp. 1219-1232.

Tsujiuchi, N.,T. Koizumi, Y. Maeda,T. (2002). Iwagase.An Investigation of Rolling Tire Noise Generated by Vibration,2002 IMAC-XX: Conference & Exposition on Structural Dynamics.

Vil'ke, V.G., and Dvornikov, M.V. (1998). The rolling of a wheel with a pneumatic tire on a plane. J. Appl. Math. Mech., Vol. 62, No 3, pp 359–369

Von, M. (1992). A. Aspects of a Standardized Measuring Method for the Acoustical Properties of Tires. Report MVM.90.3.1, M+P raadgevende ingenieurs b.v., Aalsmeer, The Netherlands.

Wagner, C., T. Huttl and P. Sagaut (2007). Large-Eddy Simulation for Acoustics, Cambridge, Cambridge University Press

Walker, J. C. and A. R. Williams (1979). The improvement of noise and traction due to road/tire interaction. Proceedings of international tire noise conference 1979, Stockholm,Sweden.

Wang, G. M. (2009). Effects of truck tire type and tire-pavement interaction on top-down cracking and instability rutting, PHD Thesis, University of Florida, USA.

Wang, H. (2011). Analysis of tire-pavement interaction and pavement responses using a decoupled modeling approach, PHD Thesis, University of Illinois at Urbana-Champaign, USA.

Wayson, R. L. (1998). Relationship between pavement surface texture and highway traffic noise, University of Central Florida, Florida.

Wendt, J. F. (2009). Computational Fluid Dynamics An Introduction, Belgium, Springer.

Wilcox, D. C. (2006). Turbulence Modeling for CFD, USA, Dcw Industries, Incorporated.

Wolf, A., B.-M. Schuh, W.D.H. Woodward, H. Akbulut (1992). Erfassung des Wissensstandes über Reifen-/Fahrbahngeräusche beim Nutzfahrzeug. Forschungsvereinigung Automobiltechnik e.V. -FAT-, Frankfurt/Main.

Wong, J.Y., (1993), Theory of Ground Vehicles, John Wiley & Sons, Inc., New York, NY

Yamazaki , S., Fujikawa, T. (1989). Indoor test procedure for evaluation of tire treadwear and influence of suspension alignment, Tire Science and Technology, TSTCA, 17(4), October-December, 1989.

Yoder, E. J. (1994). Principles of Pavement Design, Wiley and Sons, Inc.

Yum, K. and J. S. Bolton. (2003). Effect of Rotation on the Vibration Characteristics of Tires. Proceedings of Internoise.

Yum, K., K. Hong, J. S. Bolton (2006), Experimental relationship between tire structural wave propagation and sound radiation,Inter-noise 2006,Hawaii, USA.

Yum, K., K. Hong and J. S. Bolton (2007). Influence of Tire Size and Shape on Sound Radiation from a Tire in the Mid-Frequency Region. SAE 2007 Noise and Vibration Conference and Exhibition, St. Charles, IL, USA.

Zhang, H. , X. Zhang, S. Ji, Y. Guo, G. Ledezma, N. Elabbasi, H. deCougny (2003) Recent development of fluid–structure interaction capabilities in the ADINA system, Computers and Structures, Vol. 81, pp. 1071–1085